



THE UNIVERSITY OF QUEENSLAND  
AUSTRALIA

# **Dendrimeric Phosphorescent Iridium(III) Complexes for Organic Light-Emitting Diodes**

Steven Michael Russell

BAppSc (Hon)

*A thesis submitted for the degree of Doctor of Philosophy at  
The University of Queensland in 2018  
School of Chemistry and Molecular Biosciences*



## **Abstract**

Commercial interest in utilizing organic light-emitting diodes (OLEDs) as light-emitting elements in displays and lighting applications has soared in recent years. The slowly increasing market share of products utilizing OLED displays has been driven by consumer demand for displays featuring higher image quality than has been historically possible. Concurrently; interest in OLED lighting is continuing to grow thanks to their ability to achieve high efficiencies capable of significantly reducing the current consumption of global electrical energy production for lighting purposes of approximately 20 %.

The successful development of highly efficient OLEDs has largely been reliant upon employing phosphorescent iridium(III) complexes as emissive dopants. While these materials exhibit many advantageous properties such as photoluminescence quantum yields up to unitary, colour tunability across the visible spectrum and the ability to harvest both singlet and triplet excitons; they generally exhibit poor solubility in most solvents limiting their processability to the relatively expensive, wasteful and energy inefficient vacuum thermal evaporation.

For existing commercial products incorporating OLEDs, the high expense of processing is overcome by the large unit cost of the current products; smartphones and televisions. If OLEDs are to be successfully employed in lighting and other less expensive display technologies, vacuum thermal evaporation must be replaced with more cost effective processing techniques. Of the candidates for alternative processing techniques, fabrication from solution by spin-coating or ink-jet printing is particularly attractive. Not only to these solution processes have relatively low cost per unit, can be affordably scaled to large-area devices and can be implemented in roll-to-roll production.

It has been reported that solubility of phosphorescent iridium(III) complexes can be enhanced through functionalization with branched moieties to produce a class of materials referred to as dendrimers. As well as enhanced solubility, the dendrimers containing iridium(III) complexes display significantly less quenching by triplet-triplet annihilation in the neat solid resulting from increased interchromophore distance from the bulky dendrons. Poly(dendrimer)s, an extension upon dendrimers where a dendronized monomer is polymerized, have been reported with the capacity to improve solution processability and device performance of iridium(III) complexes

With the aim of developing solution processable phosphorescent poly(dendrimer)s to produce higher efficiency OLEDs, the initial targets synthesized herein were designed to improve our understanding of structural variations on poly(dendrimer) properties. The two green-emitting poly(dendrimer)s, **PD<sub>B</sub>** and **PD<sub>C</sub>**, were designed to be equivalent to two

previously reported poly(dendrimer)s, **L1** and **L2**, but with an additional phenyl moiety lengthening the tether between the emissive pendant and the polymer backbone.

The solution photoluminescence quantum yields of **PD<sub>B</sub>** and **PD<sub>C</sub>** were found to be  $55 \pm 6 \%$  and  $56 \pm 6 \%$ , respectively. Compared to the photoluminescence quantum yields of  $65 \pm 7 \%$  and  $72 \pm 7 \%$  observed with **L1** and **L2**, respectively; the introduction of an additional phenyl moiety to length the tether results in an increase in non-radiative decay via inter-chain interchromophore interactions.

OLEDs featuring solution processed emissive layers containing **PD<sub>C</sub>** were observed to have very high external quantum efficiencies relative to the film photoluminescence quantum yield. With the hero device reaching an impressive external quantum yield of 19 % at  $100 \text{ cd/m}^2$ , it is believed that **PD<sub>C</sub>** undergoes significant preferential alignment during deposition from solution which allows for a greatly enhanced outcoupling efficiency. These results coincide well with the analogous literature poly(dendrimer) **L2** which was also found to produce the same enhanced outcoupling efficiency.

With the development of green-emitting poly(dendrimer)s showing interesting properties, the next targets described herein were designed to investigate whether dendrimers and poly(dendrimer)s provide equivalent benefits to red-emitting iridium(III) complexes. A series of four structurally interrelated dendrimers, as well as a poly(dendrimer), were designed and synthesized toward this goal.

The homoleptic dendrimers, **Hom1** and **Hom2**, were found to have impressive solution photoluminescence quantum yields of  $74 \pm 7 \%$  and  $86 \pm 9 \%$ , respectively. The heteroleptic dendrimers, **Het1** and **Het2**, were found to have high solution photoluminescence quantum yields of  $66 \pm 7 \%$  and  $61 \pm 6 \%$ , respectively. The poly(dendrimer), **PD<sub>C</sub>R**, was designed by replacing the ancillary ligand of **PD<sub>C</sub>** with the red-emissive ligand of the dendrimers and was found to have a solution photoluminescence quantum yield of  $72 \pm 7 \%$ .

Preliminary red-emitting OLEDs have been fabricated using the four dendrimers and the poly(dendrimer) as dopants. At present the highest external quantum efficiency has been achieved by **Hom2** with of  $11.0 \pm 0.4 \%$  at  $8.4 \pm 5.5 \text{ cd/m}^2$  with CIE 1931 coordinates of (0.66, 0.34) and a maximum luminance of  $6000 \text{ cd/m}^2$ . The **PD<sub>C</sub>R** was observed to achieve a similar external quantum efficiency of  $10.0 \pm 0.2 \%$  at  $5.2 \pm 2.6 \text{ cd/m}^2$  with CIE 1931 coordinates of (0.66, 0.34). It is known that these devices are still below the values expected and significant optimization is still required.

## **Declaration by author**

This thesis is composed of my original work, and contains no material previously published or written by another person except where due reference has been made in the text. I have clearly stated the contribution by others to jointly-authored works that I have included in my thesis.

I have clearly stated the contribution of others to my thesis as a whole, including statistical assistance, survey design, data analysis, significant technical procedures, professional editorial advice, financial support and any other original research work used or reported in my thesis. The content of my thesis is the result of work I have carried out since the commencement of my higher degree by research candidature and does not include a substantial part of work that has been submitted to qualify for the award of any other degree or diploma in any university or other tertiary institution. I have clearly stated which parts of my thesis, if any, have been submitted to qualify for another award.

I acknowledge that an electronic copy of my thesis must be lodged with the University Library and, subject to the policy and procedures of The University of Queensland, the thesis be made available for research and study in accordance with the Copyright Act 1968 unless a period of embargo has been approved by the Dean of the Graduate School.

I acknowledge that copyright of all material contained in my thesis resides with the copyright holder(s) of that material. Where appropriate I have obtained copyright permission from the copyright holder to reproduce material in this thesis and have sought permission from co-authors for any jointly authored works included in the thesis.

### **Publications during candidature**

No publications included

### **Publications included in this thesis**

No publications included

### **Submitted manuscripts included in this thesis**

No manuscripts submitted for publication

### **Other publications during candidature**

Conference Abstract: Russell, S. M., Brewer, A., Jansen-van Vuuren, R. D., Burn, P. L. Dendronized Red-emitting Iridium(III) complexes for Solution Processed Organic Light-Emitting Diodes. Presented at: MRS Spring Meeting 2018. 2-6 April 2018. Pheonix, Arizona, USA.

### **Contributions by others to the thesis**

Prof. Paul L. Burn – Project inception and contributed towards molecular design. As both the primary supervisor of my degree and project (90 % share of load) Paul contributed greatly by providing guidance as well as revision of the final draft thesis.

Dr Shih-Chun (Lawrence) Lo – Secondary supervisor (10 % share of load). Provided considerable guidance throughout my project.

Dr Ross D. Jansen-van Vuuren – Contributed greatly in instructing me in conducting laboratory work and organic synthesis. Due to our projects having materials in common we both synthesized and shared **2.2**.

Dr Fatemeh Maasoumi – Performed the PLQY and TCSPC measurements on **PD<sub>B</sub>** and **PD<sub>C</sub>**. Fabricated, tested and interpreted the results of OLEDs containing **PD<sub>C</sub>**.

Dr Anthony Brewer – Performed the film PLQY and TCSPC measurements on materials discussed in chapters 3 and 4. Fabricated, tested and interpreted the results of OLEDs using materials discussed in chapters 3 and 4.

Dr Paul E. Shaw – Provided instruction on the collection and interpretation of photophysical data (PLQY and PL lifetime)

Dr Graham McFarlane – Collected ESI-MS data for various compounds synthesized during the project.

Dr Peter Josh and Dr Amanda Nouwens– Collected ESI-MS data for various compounds synthesized during the project.

Dr Dani M. Stoltzfus – Collected all PESA data included within this thesis.

A. Prof Jack K. Clegg, Mr Aidan Brock and Mr Jacob Whittaker – Collection of single crystal X-ray data and provided instruction on solving the obtained structures.

Mr Michael Nefedov – Performed all elemental microanalysis measurements.

**Statement of parts of the thesis submitted to qualify for the award of another degree**

None

**Research Involving Human or Animal Subjects**

No animal or human subjects were involved in this research



## **Acknowledgements**

Organisations:

Part of this research was undertaken on the MX1 and MX2 beamlines of the Australian Synchrotron, Clayton, Victoria, Australia. We thank the Australian Synchrotron for travel support and their staff for assistance.

This work was performed in part at the Queensland node of the Australian National Fabrication Facility. A company established under the National Collaborative Research Infrastructure Strategy to provide nano and microfabrication facilities for Australia's researchers.

Individuals:

I wish to begin by thanking my principle supervisor, Paul L. Burn; without whom my research project and doctorate would not have been possible. Not only did Paul give me the opportunity to undertake my PhD studies at the University of Queensland; he also leant me support and guidance to perservere each time I almost threw in the towel. Beyond giving me the opportunity and supporting me at my worst; he was also an irreplaceable source of guidance and support.

I would also like to thank my co-supervisor, Shih-Chun (Lawrence) Lo, for his support and guidance. Lawrence assisted me greatly early in my studies as I transitioned into working in an organic chemistry laboratory. Throughout my project he was always available to provide his wisdom and knowledge on any problems that I encountered.

Beyond my supervisors, a special thanks must go to Ross Jansen-Van Vuuren who took me under his wing and taught me most of the organic chemistry skills I lacked. Ross spent a great deal of his precious time to support and guide me during my first three years. He is both a great friend and mentor and I sincerely appreciate everything he has done for me.

With so many group members passing through COPE over my nearly five year tenure as a student it would be a Herculean task to thank everyone individually. As such I would like to begin by thanking every member of COPE, past and present, both for their assistance and support as well as for making COPE what it is. There are, however, individuals who deserve special mention as they have played a large role in the success of my studies. In no particular order I would like to thank these individuals: Paul Shaw for taking the time to teach me all things spectroscopy as well as for all the pleasant conversations and quiet encouragement; Robert Wawrzinek for his knowledgeable advice in the lab and the many great conversations we had, he is both a great chemist and friend; Shenqiang Fan for his

wealth of sage advice, generous support and being a model chemist; Andy Clulow for the many enlightening discussions we had as office-neighbours, you were always both gregarious and wise; Sarah McGregor who started her honours roughly when I began my PhD, it has been a tough road where we have both had ups and downs, I survived the journey at least in part thanks to our chats here and there; Kinitra Hutchinson for the many times when our overlapping sense of humour gave me a good chuckle and the motivation to push through the day; Ajeesh Chandrasekaran and Wei (Larry) Jiang for their comradeship as fellow PhD students having provided me with advice, support and friendship; Joshua May for a friendship based on common interests and for being an incredible source of knowledge that rivals anyone I have ever met; Alex Loch for being who the person who he is, it is impossible not to like Alex, and his motivation and determination is inspiring; Ilene Allison for always providing a bright smile and honest emotions; Van Mai for being a great friend, and someone whose passion for reading and self-betterment is truly inspiring; Fatemeh (Pegah) Maasoumi both for her assistance with helping me on the OLED side of things and for her support when I encountered some rough patches; Anthony Brewer for his cheerful assistance with my understanding of OLEDs as well as helping me improve my presentation for MRS; Ardalan Armin for the many reassuring discussions we had as well as for all the knowledge I gained from listening to your passionate explanations; Safa Shoaee, Aren Yazmaciyan and Khalid Muhieddine for the numerous discussions which helped both motivate and teach me; Rob Borthwick, George Vamvounis, David Gendron and Jenny Donaghey for being friendly and helpful post-docs in the chemistry laboratory. Additionally I would like to thank Xin, Ajay, Mike, Vincent, Mujeeb, Kristen, Ebinazar, Ravi, Martin, Soniya, Renjie, Yuan and Hellen for their friendliness and assistance over the years. I would also like to thank Rob Kembery for his assistance with all things related to paperwork and communication with others outside the school as well as the cordial banter we often exchanged. I have tried to include everyone from COPE who had influenced me over the course of my PhD studies and I apologize if I have missed anyone. The truth is that COPE was full of many remarkable individuals who were also always keen to lend a hand when others were in need and I sincerely appreciate all the experiences you have provided me.

I would like to thank my doctorate committee chair, Jack Clegg, who made time available to aid me with any concerns. I also must thank Jack, along with his group members Aidan Brock and Jacob Whittaker, for their assistance in collecting and modelling the single-crystal X-ray diffraction data for my materials. They were always willing to assist me whenever I had questions and it was greatly appreciated.

I also appreciate the assistance Evan Moore provided me when I was having difficulties with the TCSPC fluorometer and for his time on my confirmation committee. Additionally, I would like to thank Ian Gentle for his time on my confirmation committee.

With instrumentation being such a large part of our research I would like to thank various technicians for their assistance. I am extremely grateful to Tri Le for training me in conducting NMR experiments as well as his continued support throughout my studies. Thank you also for the discussions and your great sense of humour. I would like to thank Javaid Khan and Peter Josh for their assistance with GPC and ESI-MS, respectively. Your help and friendly chats were greatly appreciated.

Beyond the academic front, I would like to move on to thanking my mother, Lea Russell. It is not an understatement to say that without my mother none of my PhD studies would have been possible. Not only was she the sole financial support for a great deal of my candidature, she was also probably my greatest pillar of support. Thank you for believing in me Mum; as well as for all your support and sacrifices over the years.

I also greatly appreciate the support provided by my father, Greg Russell. As a stout believer in my being able to achieve anything, this support over the past few years has been invaluable.

Finally, I would like to thank my dearest friends for their unending support and encouragement; Dylan Daley, Rebekka Muller, Benjamin Rohweder and Tomas Wood. You have all been alongside me through thick and thin. I hope you understand how appreciative I am of your friendship.

### **Financial support**

This research was supported by an Australian Government Research Training Program Scholarship.

## **Keywords**

Dendrimer, macromolecule, polymer, phosphorescence, organic, synthesis, iridium, emitting, diode, OLED

## **Australian and New Zealand Standard Research Classifications (ANZSRC)**

ANZSRC code: 030503, Organic Chemical Synthesis 60 %

ANZSRC code: 030303, Optical Properties of Materials 30 %

ANZSRC code: 030207, Transition Metal Chemistry 10 %

## **Fields of Research (FoR) Classification**

FoR code: 0305, Organic Chemistry, 50 %

FoR code: 0303, Macromolecular and Materials Chemistry, 40 %

FoR code: 0306 Physical Chemistry (incl. Structural), 10 %

# Contents

---

<b>Abstract</b>	<b>i</b>
<b>Declaration by author</b>	<b>iii</b>
<b>Publications during candidature</b>	<b>iv</b>
<b>Contributions by others to the thesis</b>	<b>v</b>
<b>Acknowledgements</b>	<b>vii</b>
<b>Keywords and research classification</b>	<b>x</b>
<b>Contents</b>	<b>xi</b>
<b>List of Figures, schemes and tables</b>	<b>xv</b>
<b>List of abbreviations and symbols</b>	<b>xxiv</b>
<b>Chapter 1: Introduction</b>	<b>1</b>
1.1 Motivation	1
1.1.1 Lighting technologies	1
1.1.2 Improved general lighting	2
1.1.3 Improved displays	3
1.2 Organic light-emitting diodes	
1.2.1 OLED architecture and working principles	4
1.2.2 Frontier orbitals of organic semiconductors	6
1.2.3 OLED efficiencies	8
1.3 Organic emissive chromophores	10
1.3.1 Photoluminescence	10
1.3.2 Electroluminescence	11
1.3.3 Phosphorescent iridium(III) complexes	14

1.3.4	Light-emitting polymers	16
1.3.5	Dendrimers	19
1.3.6	Poly(dendrimer)s	22
<b>Chapter 2: Synthesis and Properties of Green-Emitting Iridium(III) Poly(dendrimer)s</b>		<b>28</b>
2.1	Design rationale	28
2.2	Synthesis	30
2.2.1	Brominated ligands	30
2.2.2	Tether	31
2.2.3	Dendrons	35
2.2.4	Dendronized ligand	36
2.2.5	Complexation and monomer synthesis	36
2.2.6	Polymerization	38
2.3	Properties	41
2.3.1	Photophysical	41
2.3.2	Device performance	45
2.3.3	Comparison of <b>L2</b> and <b>PDc</b>	50
2.4	Summary	51
<b>Chapter 3: Synthesis of Red-Emitting Dendrimers and Poly(dendrimer)s containing Iridium(III) Complexes</b>		<b>52</b>
3.1	Initial Targets	52
3.1.1	Design rationale	52
3.1.2	Synthesis	54
3.1.2.1	Friedeländer quinoline synthesis	55
3.1.2.2	Buchwald-Hartwig amination	57
3.1.3	Summary	60
3.2	Re-evaluated targets	60
3.2.1	Design rationale	60
3.2.1.1	Homoleptic dendrimers	60
3.2.1.2	Heteroleptic dendrimers	62
3.2.2	Possible isomers of re-evaluated targets	64
3.2.3	Synthesis	66
3.2.3.1	Synthesis of ligands	67
3.2.3.2	Synthesis of <b>Hom1</b> ; Complexation	70

3.2.3.3	Synthesis of <b>Hom1</b> ; Bromination	73
3.2.3.4	Synthesis of <b>Hom1</b> ; Buchwald-Hartwig amination	75
3.2.3.5	Synthesis of <b>Hom2</b> ; Complexation	80
3.2.3.6	Synthesis of <b>Hom2</b> ; Buchwald-Hartwig amination	82
3.2.3.7	Synthesis of <b>Het1</b> ; Complexation	84
3.2.3.8	Synthesis of <b>Het1</b> ; Buchwald-Hartwig amination	88
3.2.3.9	Synthesis of <b>Het2</b> ; Complexation	89
3.2.3.10	Synthesis of <b>Het2</b> ; Buchwald-Hartwig amination	94
3.2.3.11	Iridium(III) complex purification discussion	99
3.3	Re-evaluated poly(dendrimer)	100
3.3.1	Design rationale	100
3.3.2	Synthesis	101
3.3.2.1	Complexation	101
3.3.2.2	Synthesis of the monomer	103
3.3.2.3	Polymerization	104
3.3.3	Isomerism determination by <sup>1</sup> H NMR	106
3.3.3.1	Possible isomers	106
3.3.3.2	Geometry of Ir(III) complexes within <b>PDcR</b>	107
3.3.3.3	Techniques to determine geometry	111
3.4	Summary	117
<b>Chapter 4: Properties of Red-Emitting Dendrimers and Poly(dendrimer)s containing Iridium(III) Complexes</b>		<b>118</b>
4.1.	Introduction	118
4.2.	Thermal analysis	118
4.2.1.	Thermal gravimetric analysis	119
4.2.2.	Differential scanning calorimetry	120
4.2.3.	Summary of thermal properties	122
4.3.	Investigation of photophysical properties	123
4.3.1.	UV/Vis absorption and photoluminescence spectroscopy	123
4.3.2.	Solution absorption and photoluminescence spectroscopy	123
4.3.3.	Film UV/Vis absorption spectroscopy	125
4.3.4.	Film photoluminescence spectroscopy	127
4.3.5.	Film photoluminescence spectroscopy: Quantum yields	129

4.3.6. Photoluminescence spectroscopy: emission lifetimes	132
4.3.7. Discussion	135
4.3.8. Photoluminescence spectroscopy: emission versus excitation	138
4.3.9. Summary	145
4.4. Electrochemistry	145
4.5. Device performance	148
4.6. Summary	154
<b>Chapter 5: Experimental</b>	<b>156</b>
4.7. General experimental	156
4.8. Synthetic procedures	160
<b>Chapter 5: Conclusions and Future Outlook</b>	<b>204</b>
<b>References</b>	<b>210</b>



# List of Figures, Schemes and Tables

---

## List of Figures

Figure 1.1	Simplified diagram of a bottom-emitting organic light emitting diode.	5
Figure 1.2	Schematic of the general structure of a multilayer OLED.	6
Figure 1.3	Simple visual representation of the spin statistics	12
Figure 1.4	Visualization of photoluminescence using a simplified Jablonski diagram	13
Figure 1.5	Doublet emission diagram	13
Figure 1.6	Examples of homoleptic and heteroleptic phosphorescent iridium(III) complexes	15
Figure 1.7	General structures of conjugated polymer systems	17
Figure 1.8	Generic structures and literature example of the three types of polymers incorporating phosphorescent complexes	18
Figure 1.9	Examples of two non-conjugated iridium(III) complex containing polymers	19
Figure 1.10	The general structure and example of a second generation dendrimer	20
Figure 1.11	Structures of example phenylene-based dendrimers containing iridium(III) complexes	21
Figure 1.12	Structures of example carbazole and triarylamine-based dendrimers containing phosphorescent iridium(III) complexes	22
Figure 1.13	General synthetic pathway for grafting-onto, grafting-from and grafting-through (macromonomer) methodologies	24

Figure 1.14	A series of phosphorescent iridium(III) complex containing poly(dendrimer)s reported by Burn <i>et al</i>	25
Figure 1.15	The structure of carbazole-based poly(dendrimer), <b>L2</b>	26
Figure 2.1	Structures of to the biphenyl-dendronized literature poly(dendrimer)s	29
Figure 2.2	Structures of previously reported poly(dendrimer)s	30
Figure 2.3	Normalized Absorption and Excitation Spectra of <b>PD<sub>B</sub></b>	41
Figure 2.4	Normalized TCSPC Decay Profiles of <b>PD<sub>C</sub></b>	42
Figure 2.5	Structure of commercial materials used in devices	46
Figure 2.6	Characteristics of devices utilizing <b>PD<sub>C</sub></b>	47
Figure 2.7	Comparison between the photoluminescence and electroluminescence of <b>PD<sub>C</sub></b>	48
Figure 3.1	Structure of a red-emitting iridium(III) complex	53
Figure 3.2	Structural relationship of previously reported green-emitting carbazoly-dendronized poly(dendrimer)s and the analogous <b>IT1</b> and <b>IT2</b>	54
Figure 3.3	Red-emitting, homoleptic iridium(III) carbazoly-dendrimers; <b>Hom1</b> and <b>Hom2</b>	61
Figure 3.4	The small molecule iridium(III) complexes comprising the analogous emissive centre to <b>Hom1</b> and <b>Hom2</b> ; <b>[Ir(tm<sub>q</sub>)<sub>3</sub>]</b> and <b>[Ir(tp<sub>q</sub>)<sub>3</sub>]</b> , respectively. <b>[Ir(tm<sub>q</sub>)<sub>3</sub>]</b> is synthesized in this work while <b>[Ir(tp<sub>q</sub>)<sub>3</sub>]</b> has been previously reported	62
Figure 3.5	Red-emitting, heteroleptic iridium(III) carbazoly-dendrimers; <b>Het1</b> and <b>Het2</b>	63
Figure 3.6	Structural comparison of target red-emitting dendrimers.	64

Figure 3.7	Possible isomers of the homoleptic and heteroleptic iridium(III) complex containing dendrimers	65
Figure 3.8	Structure of the ligands, <b>3.3</b> , <b>3.4</b> and <b>3.5</b> , within their asymmetric unit cell as determined by single-crystal X-ray diffraction experiments	68
Figure 3.9	Structure of <b>[Ir(tmq)<sub>3</sub>]</b> as determined by single-crystal X-ray diffraction	71
Figure 3.10	Structure of the homoleptic bromide-functionalized iridium(III) complex	74
Figure 3.11	Suspected side products formed during Buchwald-Hartwig amination of <b>3.6</b> . These are intermediates or deactivated intermediates within the synthesis of <b>Hom1</b>	75
Figure 3.12	Gel permeation chromatogram of <b>Hom1</b> . The mixture appears as a single non-disperse peak	77
Figure 3.13	<sup>1</sup> H NMR investigation of isomerism in <b>Hom1</b> : The thiophenyl proton alpha to the Ir-C bond (H <sub>α</sub> ) are examined as diagnostic peaks.	78
Figure 3.14	Structures of the major and minor isomers of <b>3.6</b> and <b>Hom1</b>	79
Figure 3.15	Structure of the homoleptic 4-bromophenyl-functionalized iridium(III) complexes, <b>3.7</b> , as determined by single-crystal X-ray diffraction experiments.	81
Figure 3.16	Proton NMR signals indicating that <b>3.8</b> is a mixture of two heteroleptic iridium(III) complexes.	85
Figure 3.17	Possible geometric isomers of <b>3.8</b>	86
Figure 3.18	Structure of the heteroleptic bromide-functionalized iridium(III) complex, <b>3.8</b>	87
Figure 3.19	Structures of the geometric isomers of <b>Het1</b> synthesized from <b>3.8</b>	89
Figure 3.20	Proton NMR signals indicating that <b>3.9</b> is a mixture of two heteroleptic iridium(III) complexes.	91
Figure 3.21	Possible geometric isomers of <b>3.9</b> .	91

Figure 3.22	Structure of the heteroleptic bromide-functionalized iridium(III) complex, <b>3.9</b>	92
Figure 3.23	Structure of <b>Het2</b> as determined by single-crystal X-ray diffraction experiments	96
Figure 3.24	Comparison of the Ir-Ir distance in crystals of <b>3.9</b> and <b>Het2</b> .	98
Figure 3.25	Gel permeation chromatography traces of the red-emitting dendrimers	100
Figure 3.26	Reported green-emitting poly(dendrimer) containing iridium(III) complex ( <b>L2</b> ) and the proposed red-emitting poly(dendrimer ( <b>PDcR</b> )	101
Figure 3.27	Possible ligand combinations formed during the reaction in Scheme 3.12	102
Figure 3.28	Gel-permeation chromatogram of <b>PDcR</b>	105
Figure 3.29	Potential isomers of the iridium(III) complexes within <b>PDcR</b> and its intermediates	107
Figure 3.30	Significant aromatic <sup>1</sup> H NMR (500 MHz, CDCl <sub>3</sub> ) signals of <b>3.10</b> relating to geometry identification.	108
Figure 3.31	A depiction of how the quinoline impinges upon only one 2-phenylpyridine in the iridium(III) complex of <b>3.10</b> ( <i>facial</i> ) observed from two angles	111
Figure 3.32	All possible geometries for the ligands of <b>3.10</b>	112
Figure 3.33	1D NOESY spectra	114
Figure 3.34	2D-NOESY of <b>3.10</b>	116
Figure 4.1	Thermal gravimetric analyses	119
Figure 4.2	Differential scanning calorimetry plots	121
Figure 4.3	Comparison of UV/Vis absorption and photoluminescence spectra	124

Figure 4.4	UV/Visible absorbance spectra of red-emitting dendrimers	126
Figure 4.5	UV/Visible absorbance spectra of red-emitting poly(dendrimer), <b>PDcR</b>	127
Figure 4.6	Photoluminescence spectra of dendrimers	128
Figure 4.7	Photoluminescence spectra of poly(dendrimer)	129
Figure 4.8	Structural relationship of target red-emitting dendrimers	131
Figure 4.9	TCSPC decays of the red-emitting dendrimers	133
Figure 4.10	TCSPC decays of the red-emitting poly(dendrimer)	134
Figure 4.11	Structure of the related green-emissive iridium(III) complex containing dendrimer, <b>L3</b>	135
Figure 4.12	Structures of the related red-emitting ( <b>PDcR</b> ) and green-emitting ( <b>L2</b> ) poly(dendrimer)s	137
Figure 4.13	Comparison of the absorption and excitation spectra of <b>[Ir(tmq)<sub>3</sub>]</b> in degassed toluene.	139
Figure 4.14	Comparison of the absorption and excitation spectra of dendrimers	140
Figure 4.15	Comparison of the absorption and excitation spectra of <b>PDcR</b>	141
Figure 4.16	Emission versus excitation contour plot of <b>[Ir(tmq)<sub>3</sub>]</b> in solution (toluene)	142
Figure 4.17	Emission versus excitation contour plots of the four red-emitting dendrimers	143
Figure 4.18	Emission versus excitation contour plots of <b>PDcR</b> in solution (toluene)	144
Figure 4.19	Cyclic voltammograms of red-emitting iridium(III) complexes versus Fc/Fc <sup>+</sup> redox couple	146
Figure 4.20	Typical device characteristics for OLEDs using <b>Hom1</b> or <b>Hom2</b> as the emissive dopant	149

Figure 4.21	Typical device characteristics for OLEDs using <b>Het1</b> or <b>Het2</b> as the emissive dopant	150
Figure 4.22	Comparison of the blend photoluminescence and electroluminescence spectra of the red-emitting dendrimers	151
Figure 4.23	Typical device characteristics for OLEDs using <b>PDcR</b> as the emissive dopant	152
Figure 6.1	Structure of proposed poly(dendrimer)s with branched tether moieties. The branched tethers are shown in red	208

## List of schemes

Scheme 2.1	Synthetic scheme of brominated ligands	31
Scheme 2.2	Synthetic methods of <b>2.3</b> and <b>2.4</b> attempted	32
Scheme 2.3	Synthetic scheme of lengthened tether.	35
Scheme 2.4	Synthesis scheme of first generation biphenyl-dendron.	35
Scheme 2.5	Synthesis scheme of first generation carbazoyl-dendron	36
Scheme 2.6	Synthetic scheme of dendronized ligands	36
Scheme 2.7	Synthetic scheme of cyclometallated complex	37
Scheme 2.8	Synthetic scheme of monomer	38
Scheme 2.9	Polymerization synthetic scheme	38
Scheme 3.1	Generic synthetic pathway attempted to give <b>3.4</b> with details of each attempted reaction condition are in Table 3.1	55

Scheme 3.2	Buchwald-Hartwig amination to give singly and doubly dendronized ligand	58
Scheme 3.3	Cyclometallation of dendronized ligand	59
Scheme 3.4	Cyclometallation of <b>3.4</b>	59
Scheme 3.5	One-pot cyclometallation of iridium(III) by <b>3.4</b> or the singly dendronized ligand	60
Scheme 3.6	Synthesis of ligands for red-emitting iridium(III) complexes.	67
Scheme 3.7	One-pot synthesis of <b>[Ir(tmq)<sub>3</sub>]</b>	70
Scheme 3.8	Bromination of <b>[Ir(tmq)<sub>3</sub>]</b> to give <b>3.6</b>	73
Scheme 3.9	Coupling of carbazolyl-dendron ( <b>2.11</b> ) to the brominated homoleptic iridium(III) core ( <b>3.6</b> ) by Buchwald-Hartwig amination	76
Scheme 3.10	One-pot synthesis of 4-bromophenyl-functionalized iridium(III) complex, <b>3.7</b>	80
Scheme 3.11	Buchwald-Hartwig amination to examine reactivity of the 4-bromophenyl position at 80°C	83
Scheme 3.12	Coupling of carbazolyl-dendron ( <b>2.11</b> ) to the brominated homoleptic iridium(III) core ( <b>3.7</b> )	83
Scheme 3.13	Two-step heteroleptic complexation	84
Scheme 3.14	Buchwald-Hartwig amination of heteroleptic iridium(III) complex, <b>3.8</b>	88
Scheme 3.15	Two-step heteroleptic complexation to give <b>3.9</b> :	90
Scheme 3.16	Buchwald-Hartwig amination of heteroleptic iridium(III) complex, <b>3.9</b> , carbazolyl-dendron, <b>2.11</b>	95
Scheme 3.17	Two-step cyclometallation to give red-emitting iridium(III) complex poly(dendrimer) precursor <b>3.10</b>	102
Scheme 3.18	Suzuki coupling and Steglich esterification to give the monomer <b>3.11</b>	104
Scheme 3.19	Grubbs 3 <sup>rd</sup> generation catalysed ring opening olefin-metathesis polymerization of <b>3.11</b> to give <b>PDcR</b>	105
Scheme 6.1	Synthetic progress towards proposed poly(dendrimer)s with branched tether moieties	209

## List of Tables

Table	1.1	Typical efficiencies and lifetimes of various lighting technologies	3
Table	2.1	Optimization of the synthesis of <b>2.3</b> . Synthetic conditions as per Scheme 2.2	32
Table	2.2	Direct synthesis of <b>2.4</b>	33
Table	2.3	. Summary of green-emitting iridium(III) poly(dendrimer) photoluminescent properties	43
Table	2.4	Comparison of radiative and non-radiative decay lifetimes	44
Table	2.5	Device results <b>PDc</b> at 100 cd/m <sup>2</sup>	46
Table	2.6	Comparison of <b>L2</b> <sup>142</sup> and <b>PDc</b> average device performance at 100 cd/m <sup>2</sup> of the same device architecture	50
Table	3.1	Comparison of reaction conditions for the Friedländer quinoline synthesis of <b>3.4</b>	56
Table	3.2	Crystallography data summary table; Ligands	69
Table	3.3	Crystallography data summary table; <b>[Ir(tmq)<sub>3</sub>]</b>	72
Table	3.4	Crystallography data summary table; <b>3.6</b>	74
Table	3.5	Crystallography data summary table; <b>3.7</b>	82
Table	3.6	Crystallography data summary table; Heteroleptic bromide-functionalized iridium(III) complexes	87
Table	3.7	Crystallography data summary table; <b>3.9</b>	93
Table	3.8	Crystallography Data Summary Table- Heteroleptic Dendrimer	97
Table	4.1	Comparison of weight loss in complexes occurring around 400°C	120
Table	4.2	Summary table of photoluminescent quantum yield of red-emitting iridium(III) complexes	130
Table	4.3	Observed photoluminescence lifetime of red-emitting iridium(III) complexes by TCSPC	132
Table	4.4	Redox couplings calculated from cyclic voltammetry.	146



Table	4.5	Energy level estimation from cyclic voltammetry. Values in brackets estimated using irreversible process	147
Table	4.6	Average device characteristics for red-emitting OLEDs. Doping concentration for each material is shown in brackets	148
Table	4.7	Chromaticity of dendrimeric materials containing red-emitting iridium(III) complexes	153

# List of Abbreviations and Symbols

Elements are denoted using standard symbology. Where non-standard symbology is used in chemical structures (i.e. “R”) the group represented by the symbol will be defined in the figure or legend. Equations will have all non-standard symbols defined in the following text. An explanation on abbreviated descriptions of spectroscopic data is contained in the general experimental section 5.

All abbreviations (units and values of constants specified in parentheses) used in this thesis are shown hereafter:

$^1\text{H}$ NMR	Proton nuclei nuclear magnetic resonance
$^{13}\text{C}$ NMR	Carbon-13 nuclei nuclear magnetic resonance
$\epsilon$	Molar extinction coefficient ( $\text{dm}^3 \text{mol}^{-1} \text{cm}^{-1}$ )
$\eta^*$	Luminous Efficacy ( $\text{lm/W}$ )
$\eta_{\text{CB}}$	Charge balance efficiency (%)
$\eta_{\text{ext}}$	External Quantum Efficiency (%)
$\eta_{\text{S/T}}$	Singlet/ triplet charge harvesting efficiency (%)
$\lambda_{\text{ex}}$	Wavelength of excitation (nm)
$\lambda_{\text{max}}$	Wavelength of maximum absorption (nm)
$\mu_{\text{h}}$	Hole mobility ( $\text{cm}^2/(\text{V s})$ )
$\mu_{\text{e}}$	Electron mobility ( $\text{cm}^2/(\text{V s})$ )
$\bar{\nu}$	Wavenumber for infrared absorption peak ( $\text{cm}^{-1}$ )
A	Absorbance (A.U.)
aq	Aqueous
atm	Atmospheric pressure ( $1.01 \times 10^5 \text{ Pa}$ )
ATR	Attenuated total reflectance
b.pt	Boiling point ( $^{\circ}\text{C}$ )
calcd	Calculated value (from molecular formula for elemental microanalysis and mass spectrometry)
Cbz	Carbazolyl moiety
CV	Cyclic voltammetry
conc.	Concentrated
$\bar{D}$	Dispersity defined as $M_w/M_n$
DCTB	<i>trans</i> -2-[3-(4- <i>tert</i> -Butylphenyl)-2-methyl-2-propenylidene]malononitrile

DHB	2,5-dihydroxybenzoic acid
DIT	Dithranol
DSC	Differential scanning calorimetry
EA	Electron affinity (eV)
EJ	Exajoule ( $10^{18}$ Joules)
ESI-MS	Electrospray ionization-mass spectrometry
EQE	External quantum efficiency (%)
Fc/Fc <sup>+</sup>	Ferrocene/ferrocenium couple
Fl	Fluorenyl moiety
FWHM	Full width half maximum
GPC	Gel permeation chromatography
HOMO	Highest occupied molecular orbital (eV)
<i>h</i>	Planck constant ( $6.63 \times 10^{-34}$ J s)
IEA	International Energy Agency
IP	Ionisation potential (eV)
IR	Infrared absorption
<i>J</i>	Coupling constant (Hz)
<i>k<sub>nr</sub></i>	Rate constant: non-radiative component ( $s^{-1}$ )
<i>k<sub>r</sub></i>	Rate constant: radiative component ( $s^{-1}$ )
L	Luminance or brightness ( $cd/m^2$ )
LCD	Liquid-crystal display
LED	Light-emitting diode
LUMO	Lowest unoccupied molecular orbital (eV)
M	Molar concentration ( $mol\ L^{-1}$ )
MALDI-ToF	Matrix-assisted laser desorption/ionization – time of flight
Mp.	Melting point ( $^{\circ}C$ )
<i>M<sub>n</sub></i>	Number-average molecular weight ( $g\ mol^{-1}$ )
<i>M<sub>w</sub></i>	Weight-average molecular weight ( $g\ mol^{-1}$ )
<i>M<sup>n+</sup></i>	Molecular cation where n equals number of charge (n omitted when singly charged)
<i>M+X<sup>+</sup></i>	Ion of molecule with charged adduct where X will be specified as H <sup>+</sup> , Na <sup>+</sup> or
<i>K<sup>+</sup></i>	
M-H	Molecular ion formed by deprotonation
<i>m/z</i>	Mass to charge ratio
OLED	Organic light-emitting diode

PESA	Photoelectron spectroscopy in air
PL	Photoluminescence
PLQY	Photoluminescence quantum yield (%)
$\Phi_{\text{PL}}$	Photoluminescence quantum yield (%)
rt	Room temperature (°C)
s	Total angular momentum
S <sub>0</sub>	Ground state
S <sub>1</sub>	Lowest singlet excited state (eV)
SHE	Standard hydrogen electrode
T <sub>1</sub>	Lowest triplet excited state (eV)
TCSPC	Time-correlated single photon counting
$T_d$	Temperature of 5% mass decomposition during thermal gravimetric analysis
(°C)	
$T_g$	Glass transition temperature (°C)
TGA	Thermal gravimetric analysis
UQ	The University of Queensland
UV-vis	Ultraviolet-visible absorption
VTE	Vacuum thermal evaporation

### 1.1 Motivation

#### 1.1.1 Lighting Technologies: General Lighting and Light-Driven Displays

Humanity has used artificial light sources for millennia beginning with the use of incandescence from combustion to push back the dark of night. Prehistoric humanity are believed to have also used firelight to project shadows allowing the communication of images forming the very first visual displays. Since these early times humans have increased their demand for artificial light sources with a sharp increase in consumption corresponding to the industrial era which brought about longer work days and inventions such as the incandescent bulb.

A particularly important defining moment in the evolution of lighting technologies occurred with the invention of the cathode-ray tube in the early 20<sup>th</sup> century. With this invention light producing devices were being produced for a use other than general lighting. Although intrinsically linked, the two branches of light-emitting devices evolved separately with incandescent and fluorescent sources dominating general lighting and cathode-ray tubes dominating displays for much of the 20<sup>th</sup> century.

General lighting and display technologies have both become fundamental technologies for modern society and are now essentially irreplaceable. Lighting has become indispensable, both occupationally and for leisure, for the majority allowing efficient and safe conditions both inside enclosed spaces and outside of daylight hours.<sup>1</sup> While a fledgling technology compared to the ancient roots of general lighting, devices revolving around light-driven displays have become equally ubiquitous in modern society. With devices requiring displays being increasingly utilized for work, social interactions and leisure activities it is not surprising that the consumer demand for better visual performance and energy efficiency is high. While current lighting and display technologies have proven adequate they are far from ideal due to certain insurmountable limitations. It is believed that organic light-emitting diodes (OLEDs) exhibit the properties required to replace existing technologies such as high efficiencies, low-driving voltage, rapid response times, vivid and tunable colour output, area-emission, wide viewing angle, very low weight and thickness and ability to be dimmed.<sup>2,3</sup> Organic light-emitting diodes may unify the two fields of general lighting and display technologies back into one standard device architecture.

### **1.1.2 Motivation for Improved General Lighting Technologies**

With 20 % of the world's total electrical consumption being consumed for lighting (approximately 7 EJ in 2013), amounting to an annual cost of approximately 1 % of global GDP at US 360 billion, it is unsurprising that there has been a surge in government sponsored programs to replace low-efficiency light sources such as incandescent bulbs.<sup>4</sup> The International Energy Agency (IEA) predicts that shifting to more efficient light sources could reduce household energy consumption by one-third. Most countries have already committed to phasing out incandescent bulbs while promoting light-emitting diodes as the preferred alternative.<sup>5</sup> The energy savings are quite attractive from both an environmental and economic standpoint.

Alongside the global consumption of electricity there is also a considerable consumption of fossil fuels for the purpose of lighting mostly in the form of paraffin- and diesel- fuelled lamps. Most of this consumption is within the developing world where 1.6 billion people live without access to electric lighting, a larger number than when Thomas Edison commercialized the first electric light source in 1880. These burners are exceedingly inefficient compared to even incandescent lamps altogether producing only 1 % of the world's lighting while accounting for 20 % of all CO<sub>2</sub> released for light generation. The economic consequences of fossil fuel lamp usage are also severe with 3 % of the global oil supply being expended.<sup>4</sup>

With the introduction of policies limiting the use of incandescent bulbs the next commercially developed technology has come to dominate the lighting market; fluorescent lamps. Fluorescent lamps, along with their compact form, utilize a low pressure mercury-vapour gas-discharge setup to emit ultraviolet radiation which is absorbed by a phosphor to emit the desired light profile. They are up to five times more efficient and can last up to twenty times longer than incandescent bulbs, however, significant energy is still lost as thermal output and with such widespread adoption questions have been raised regarding the safety of their ultraviolet emission and their mercury content, a very potent and persistent environmental toxin.<sup>6</sup> A comparison of efficiencies and operational lifetimes of the predominant competing lighting technologies can be found in Table 1.1.

Table 1.1: Typical efficiencies and lifetimes of various lighting technologies. Table modified from Thejokalyani *et al.*<sup>6</sup>

Technology	Operational lifetime (h)	Efficiency (lm/W)
Incandescent lamp	750-1500	12-18
Linear fluorescent lamp	20 000	80-100
Compact fluorescent lamp	6000-10 000	60-70
White OLED	10 000	64

The key performance parameters for white organic light-emitting diodes are the colour [indicated by the correlated colour temperature (CCT) or colour-rendering index (CRI)], external quantum efficiency ( $\eta_{\text{ext}}$ , %) and power efficiency ( $\eta^*$ , lm/W) alongside their corresponding luminance ( $L_V$ , cd/m<sup>2</sup>). White OLEDs fabricated by vacuum thermal evaporation have been shown to achieve a power efficiency of 106 lm W<sup>-1</sup> at 1000 cd/m<sup>2</sup> which is greater than the power efficiencies of 60-70 lm/W observed for fluorescent lamps.<sup>7,8</sup> However, these devices could not replace fluorescent lamps at this stage due to insufficient commercial viability. While OLEDs are theoretically a cost efficient lighting technology, it has been noted that currently the costs are high due to the initial expenditure required for fabrication equipment combined with low product yields.<sup>9</sup> One solution to reduce equipment costs while improving output volume is the development of OLEDs fabricated from solution processing techniques.<sup>10</sup>

### 1.1.3 Motivation for Improved Display Technologies

Communicating information in a visual format has always been crucial within society and with the development of computing this has only intensified due to the dominant output component commonly being an electronic dynamic visual display. The adoption of the smart phone as a primary communication appliance by many people has also led to increased demand for better displays. An ideal display would be capable of perfectly reproducing any images for the observer as they would appear to the human eye if viewed in person. This is a difficult task as the human eye has been shown to be capable of differentiating between approximately 10 million different colours<sup>11</sup> and potentially has the ability to detect a single photon.<sup>12</sup>

With the potential for high colour purity, high efficiency and fast response times OLEDs have become, together with liquid-crystal displays (LCD), the dominant technology in commercial displays. The commercial adoption of OLED and LED based displays have

forced technologies such as the cathode ray tube, rear-projection screen and plasma display panels into obsolescence.<sup>13</sup>

The foremost competitor to OLEDs, liquid-crystal displays are a non-emissive display technology that relies upon a separate source for illumination. This external light source applies uniform white light across the entire device. An electroactive liquid crystal layer sandwiched between two perpendicular polarizers give rise to the pixelated display.<sup>14</sup> Light cannot be transmitted through the two perpendicular polarizers unless the light is rotated 90° by the liquid crystal. The rotation of the liquid crystal is controlled by application of an electric field. To produce coloured displays the pixels are attenuated further with colour filters so that only light of the desired colour may transmit.<sup>15</sup> Current LCD technologies are superior to OLEDs in terms of maximum brightness, operation lifetime and fabrication cost. Inversely OLEDs offer advantageous in terms of rapid response times, achieving truly dark pixels, colour and thinner device profiles.<sup>16</sup>

As electronic technological development continues to march onward three distinct areas have become foci in the push for greater performing devices; cost efficiency, power efficiency and novel or versatile properties. Organic light-emitting diodes are already of significant commercial interest due to their promise of improving both financial and energy efficiencies over other competing technologies while also providing new possibilities unavailable to other technologies, such as flexible and transparent displays.<sup>16,17,18</sup> The capability to produce flexible displays demonstrated by OLEDs is in large part due to their intrinsic thin profile, in which less strain is observed during flexion compared to thicker alternatives.<sup>19</sup> OLEDs are also able to be processed using low-temperature fabrication techniques which allow deposition on flexible substrates such as plastics.<sup>20</sup> As OLEDs are very thin and utilize an internal emissive species, it is possible to produce a window-like transparent display giving rise to a host of new applications.<sup>3,21</sup> OLEDs are able to produce such innovative displays as a result of their generally advantageous properties such as high colour vibrancy and contrast ratio and the potential for excellent power efficiency.<sup>22,23</sup>

## **1.2 Organic Light-Emitting Diodes**

### **1.2.1 OLED Architecture and Working Principles**

The general architecture of an organic light-emitting diode is formed by two electrodes with an intermediate layer of organic semiconductor. The organic semiconductor must contain at least one component which shows electroluminescence in order for the device to emit light when stimulated by an electric current. The general architecture of an OLED is shown in Figure 1.1.



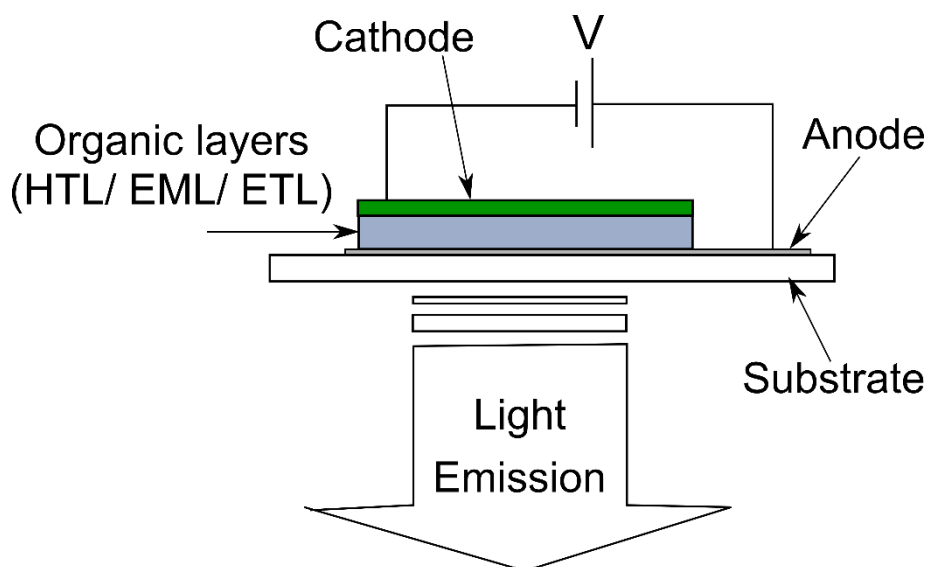


Figure 1.1: Simplified diagram of a bottom-emitting organic light emitting diode. The organic layers typically include at least two layers; commonly the emissive layer (EML) as well as a hole transporting layer (HTL) and/or an electron transporting layer (ETL) are present. Modified from<sup>2</sup>

During operation a bias is applied across the electrodes causing negative (electrons) and positive (electron holes or holes) charges are injected into the organic component. The electric field generated from the electrodes also accelerates the charges towards the opposite electrode.<sup>24</sup> When a pair of opposite charges come within close proximity their Columbic attraction results in recombination to form a neutral exciton.<sup>25</sup> Each exciton will be in either a non-degenerate singlet state or a triply-degenerate triplet state. The populations of the excitons formed as singlet states or triplet states will be 25 % or 75 %, respectively; as defined by spin statistics.<sup>26,27</sup>

The first reported example of a device fitting the basic architecture of an OLED described electroluminescence from 10-20  $\mu\text{m}$  thick crystals of anthracene (0.1 % tetracene impurity) sandwiched between two electrodes.<sup>28</sup> Light emission was observed under application of a bias on the order of hundreds of volts across the crystals. The high voltage required to drive the device was a consequence of the very low conductivity of organic semiconductors which participate in different charge transport mechanisms than their inorganic counterparts.<sup>29</sup> Tang and VanSlyke demonstrated that vast improvements to efficiency could be achieved by the addition of a second organic semiconductor layer and reducing organic layer thicknesses to less than 100 nm. The addition of a second semiconductor layer allowed for greater confinement of charges to a limited emissive region and utilizing thin layers to compensate for the low mobility of the organic components.<sup>30,31</sup>

This requirement for thin layers was originally a limitation as processing such thin layers with minimum defects was challenging, however, as various processing techniques have been optimized their diaphanous nature has become one of the most prized features of OLEDs.<sup>32,33</sup>

In addition to the emissive layer (EML) which contains the emissive chromophore, the other organic semiconductor layers commonly used to control the recombination zone in OLEDs include charge transport layers, electron transport layer (ETL) and hole transport layer (HTL), as well as charge blocking layers, electron blocking layer (EBL) or hole blocking layer (HBL).<sup>34,35,36</sup> The addition of such layers ensure that the charges injected at each electrode are transported into the emissive layer in equal quantities to maximize the recombination to excitons in close proximity to the emissive chromophore. An approximation of this process is shown in Figure 1.2. Often a simple device architecture is preferred and not all described layers are included.<sup>37,38</sup>

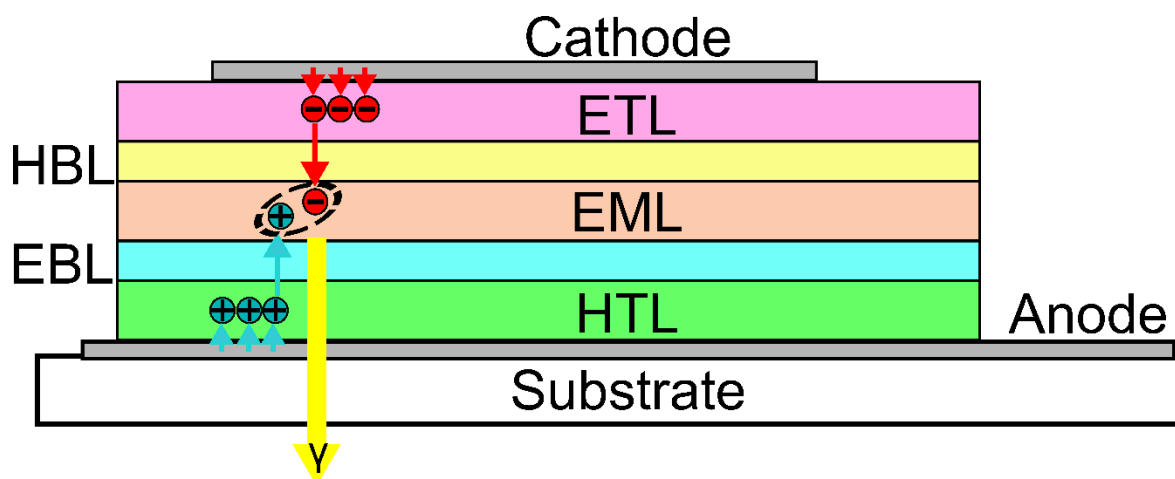


Figure 1.2: Schematic of the general structure of a multilayer OLED. Holes and electrons are injected from the anode and cathode into the hole transporting layer (HTL) and electron transporting layer (ETL), respectively. The charge carriers are free to move into the emissive layer (EML) and are confined within it by the electron blocking layer (EBL) and hole blocking layer (HBL). Recombination can occur within the EML to produce a photon ( $\gamma$ ).

### 1.2.2 Frontier orbitals of organic semiconductors: Importance for OLEDs

The organic semiconductor utilized for each layer is chosen based upon their ability to transport charge carriers in a similar fashion to choosing inorganic semiconductors for an inorganic light-emitting diode.

In describing charges within organic semiconductors, a highly simplified analogy to the inorganic band structure is often employed as organic semiconductors do not have an energy band structure. In this description the lowest unoccupied molecular orbital (LUMO)

of the organic layer replaces the conduction band and the highest occupied molecular orbital (HOMO) takes the place of the valence band.<sup>39</sup>

The electron charge carriers within organic semiconductors are localized over the LUMO of a discrete molecule. The anionic radical that constitutes the organic electron charge carrier is equivalent to the reduced organic species.<sup>40</sup> Conversely, the hole resides within the HOMO of the organic molecule and this cationic radical charge carrier is equivalent to the oxidized organic species.<sup>41,42</sup>

The degree of localization varies between different materials with charges being able to delocalize over multiple atoms within the molecule through extended conjugation. Conjugated polymers are an example of larger delocalization within an organic molecule due to the length of their extended conjugation.<sup>43</sup> Additionally, the charge carriers are stabilized by neighbouring organic molecules through charge-dipole interactions.<sup>44,45</sup>

The energy of the HOMO and LUMO correspond to the ionization potential (IP) and electron affinity (EA) of an organic material. The ionization potential is defined as the energy required to vertically promote a single electron from the HOMO to the vacuum level of a molecule. The electron affinity is defined as the minimum energy an electron must possess to populate the LUMO of a molecule via a vertical transition from the vacuum level.<sup>40,24</sup> The IP of a molecular thin film may be measured by ultraviolet photoelectron spectroscopy (UPS) or photoelectron spectroscopy in air (PESA) while the electron affinity may be probed through inverse photoelectron spectroscopy (IPES).<sup>46,47</sup> Due to limited access to experimental instrumentation the HOMO and LUMO are often estimated from cyclic voltammetry (CV) (and/or UV/Vis absorption/photoluminescence spectroscopy for the optical gap if required). While these techniques do provide energy level estimations they should always be treated carefully as they typically do not describe the material or the transitions as they are encountered within a device. Cyclic voltammetry is commonly collected with the semiconductor in solution while the optical gap determined by spectroscopy does not include the excited state binding energy.<sup>24</sup>

As described in the previous section, opposite charge carriers can recombine assuming they are close enough for Coulombic attraction to dominate. This neutral bound pair, called an exciton, will find the most efficient path to decay to the ground state. Often the most efficient decay pathway is localized on a single molecule and the exciton will diffuse to it. Once localized on a single organic molecule; the hole and electron will occupy the HOMO and an excited orbital (which may be the LUMO or a higher energy orbital), respectively. In OLEDs, hosts and dopants are chosen so that the exciton is energetically more favourable to form on or migrate to the highly emissive dopant. In these cases the

electron of the exciton will decay non-radiatively to the LUMO of the dopant, if it did not inject directly into the LUMO initially, and will proceed to decay to the HOMO; producing a photon and the electron returns to the ground state filling the electron hole.

### 1.2.3 OLED Efficiencies

Once a working device has been fabricated it can be characterized to determine its performance. The most commonly discussed figures of merit for OLEDs are the external quantum efficiency ( $\eta_{\text{ext}}$ , units are %) and power efficiency ( $\eta^*$ , units are lm/W). The external quantum efficiency expresses the ratio of photons leaving the transparent electrode of the device (to the viewer) versus the electron/hole pairs injected from the electrodes into the device. Luminous efficacy describes the luminous flux generated per unit of electrical power.<sup>48,49</sup>

Various measures performance parameters of an OLED vary over different voltage ranges and can also be described versus luminance or brightness ( $L$ , units are  $\text{cd/m}^2$ ). For example the turn-on voltage of an OLED is described as being the applied voltage at which a luminance of  $1 \text{ cd/m}^2$  is measured.

Alongside the efficiency and electrical properties of the device, the spectral output of the device is also characterized to determine its suitability for application. The spectral output of an OLED is typically fitted using colour matching functions to give coordinates that describe the colour of emission relative to the Commission internationale de l'éclairage (CIE) 1931 colour space. For lighting applications where a white OLED is required, the correlated colour temperature (CCT) is also calculated. As the name suggests, the CCT allows the emission colour of a device to be correlated to the colour of emission from an ideal black-body radiation source at various temperatures. The colour rendering index (CRI) of a white OLED is also commonly investigated as it allows determination of how accurately coloured objects appear under its illumination.

Out of these parameters, much emphasis is given to the external quantum efficiency of an OLED as it describes the accumulated losses from all physical processes within a device. As a result, deviations from the expected external quantum efficiency of an OLED provides a clear indication that at least one fundamental process within the device is exhibiting unusual behaviour. It has been well established that the external quantum efficiency of an OLED can be described by equation 1.1.

Equation 1.1.

$$\eta_{\text{ext}} = \eta_{\text{CB}} \cdot \eta_{\text{S/T}} \cdot \Phi_{\text{PL}} \cdot \eta_{\text{out}}$$

Equation 1.1 derives the external quantum efficiency by multiplying the efficiencies of four processes known to result in injected charge pairs not generating harvested photons. The variables are defined as the charge-balance efficiency ( $\eta_{\text{CB}}$ ), the single-triplet harvesting efficiency ( $\eta_{\text{S/T}}$ ), the emissive layer photoluminescent quantum yield ( $\Phi_{\text{PL}}$ ) and the outcoupling efficiency ( $\eta_{\text{out}}$ ).

The charge-balance or charge-capture efficiency describes the efficiency at which injected charges recombine and are captured by the emissive chromophore within the emissive layer.

The singlet/ triplet harvesting efficiency describes the efficiency at which excitons are harvest depending on their multiplicity. If all singlets and triplets are harvested by the emissive chromophore then the singlet/ triplet harvesting efficiency will be unitary.

The photoluminescent quantum yield is the ratio of photons absorbed by the emissive layer versus the photons emitted from the emissive layer. The photoluminescent quantum yield describes the efficiency at which the excited chromophore will radiatively decay.

The outcoupling efficiency of the device is a measure of the population of photons exiting the front of the devices versus the number of photons generated within the device. It is well established within the literature that the outcoupling efficiency of OLEDs is limited to approximately 20 % within the visible spectrum for an isotropic emitter.<sup>50,51</sup> Much of this lost efficiency is due to photons experiencing internal reflection at the glass/air interface resulting in re-adsorption within the organic layers or being waveguided out of the edges of the device. The efficiency resulting from internal reflection at the glass/air interface can be described by equation 1.2; where  $n$  is the refractive index of the glass substrate at the emission wavelength.<sup>52</sup>

Equation 1.2

$$\eta_{\text{out}} = 1/2n^2$$

Over the visible spectrum the refractive index of glass is approximately 1.5 resulting in giving an outcoupling efficiency of 22 %. The remaining losses result from coupling to surface plasmons and free charges at the interface of the metal electrode resulting in photon loss as heat.<sup>53,54,55</sup> As most of these losses are due to the refractive indices at the substrate/air interface, recent advances to improve the outcoupling efficiency have focussed

on developing anisotropic emitters that exhibit preferential alignment perpendicular to the glass-air interface to decrease internal reflection.<sup>56,57</sup> Another successful method to reduce photon loss is to modify the refractive index or topology of the glass-air interface to also give reduced internal reflection.<sup>58,59</sup>

As emissive chromophores play an integral role in the harvesting of charges and subsequent radiative decay, they provide the ideal candidate for structural modification to improve all four parameters described in equation 1.1.

### 1.3 Organic emissive chromophores:

For an organic semiconductor to be applicable as the emissive chromophore within an organic light-emitting diode, the material must exhibit electroluminescence which is often present alongside an associated photoluminescent process. Photoluminescence of an organic semiconductor is observed when an electron of the HOMO is excited into a higher molecular orbital through absorption of an incident photon; followed by spontaneous decay through at least one radiative transition (commonly the LUMO→HOMO transition). During electroluminescence electrical energy in the form of excitons is transferred to an emissive chromophore resulting in an excited species which is then allowed to naturally decay through at least one radiative transition.<sup>60</sup>

#### 1.3.1 Photoluminescence

As electrons are fermions they must obey the Pauli exclusion principle which forbids two electrons of the same spin to occupy the same. The absorption of a photon, which is a boson, results in the excitation of an electron from the singlet ground state to the singlet excited state ( $S_0 \rightarrow S_1$ ). As this is a vertical process the intrinsic spin states of the electrons remain unchanged. The reverse transition, from a singlet excited state to a singlet ground state ( $S_1 \rightarrow S_0$ ), is spin allowed so may occur freely alongside the loss of energy as a photon. This radiative decay is termed fluorescence and materials for which this is the dominant radiative decay mechanism are described as being fluorescent. The majority of photoluminescence exhibited by organic molecules is fluorescence. As it is a spin-allowed transition, fluorescence is often characterized by fast emission processes (on the nanosecond timescale).<sup>61</sup>

The triplet state of a fluorescent emitter is rarely involved in photoluminescence as the absorption transition ( $S_0 \rightarrow S_1$ ) is a vertical and does not allow a change of spin for either electron. Spin inversion of an excited singlet state to give an excited triplet state ( $S_1 \rightarrow T_1$ ) is possible, however, it is kinetically unfavourable and insignificant for fluorescent emitters. If

this transition does occur it is termed intersystem crossing (ISC) and the resulting excited triplet state of the fluorescent chromophore will exhibit exceptionally slow decay ( $T_1 \rightarrow S_0$ ) due to the forbidden nature of the transition.<sup>62</sup> At ambient temperatures this usually results in the triplet excited states decaying through faster non-radiative pathways (*i.e.* heat). The opposite spin inversion ( $T_1 \rightarrow S_1$ ), reverse intersystem crossing (RISC), may also occur but is equally uncommon in the average fluorescent emitter.<sup>63</sup>

One process that allows efficient spin inversion is spin-orbit coupling (SOC). In SOC coupling between the magnetic moment generated by the spin angular momentum of the particle and its orbital angular momentum leads to spin inversion. The spin-orbit coupling is negligible in most organic molecules as they contain only light elements. Osmium, iridium and platinum complexes have been shown to induce very strong spin-orbit coupling leading to very high intersystem crossing rates leading to rapid spin inversion of excited singlets to triplets.<sup>64</sup> Additionally, the heavy metal effect makes the formally forbidden radiative decay of excited triplet states ( $T_1 \rightarrow S_0$ ), termed phosphorescence, significantly more allowed. This is observed in the phosphorescent decay lifetimes (around microseconds) of these materials which are considerably lower than for materials with weak SOC (millisecond or greater).<sup>65</sup>

In very efficient phosphorescent emitters, fluorescence is rarely seen as intersystem crossing to one of the lower energy triplet states is favourable.<sup>66</sup>

### 1.3.2 Electroluminescence

The process of electroluminescence, where the frontier orbitals are occupied by the exciton which then decays to the ground state through emission of a photon, largely mirrors the processes involved in photoluminescence. The most obvious difference between electroluminescence and photoluminescence stems from the fermionic nature of electrons (and therefore electron holes). While absorption of a photon always initially promotes an electron from the singlet ground state to the singlet excited states ( $S_0 \rightarrow S_1, S_2 \dots S_n$ ); the charge carriers within a device may be of either spin and recombination can produce excitons with one of the four possible spin states according to spin-statistics; namely, one singlet state and three triplet states.<sup>67</sup>

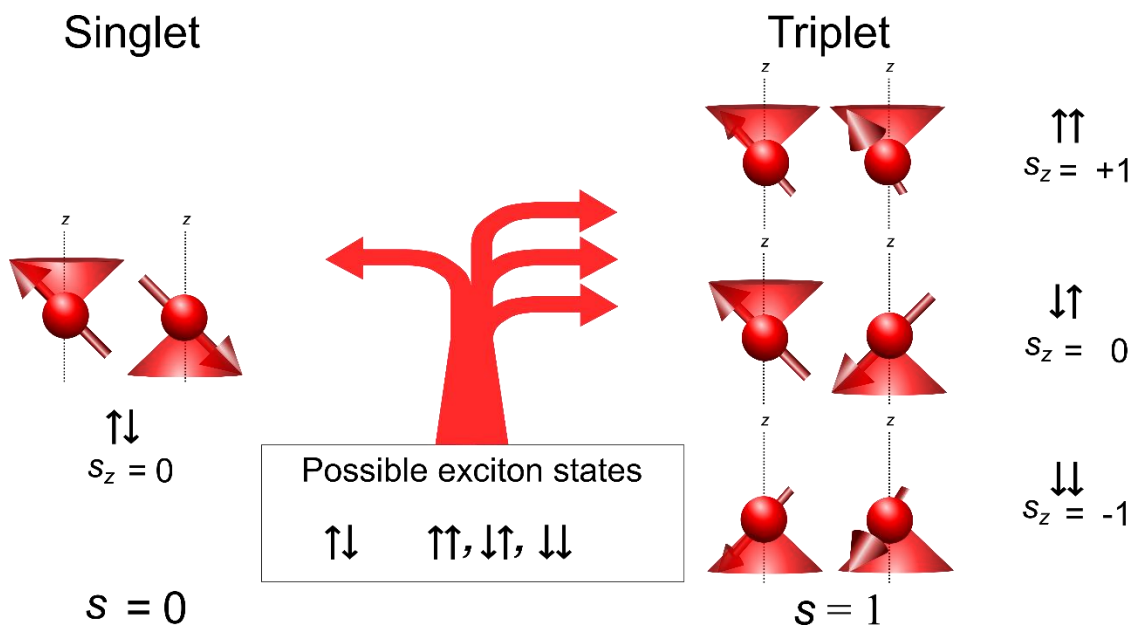


Figure 1.3: Simple visual representation of the spin statistics of recombination based on the vector model of the atom. Only one of the four electron pairs result in a spin angular momentum of zero and being a singlet state. The remaining three have a total angular momentum of one, even though in one case the z-axis spin projection quantum number ( $s_z$ ) is zero.

As discussed previously, essentially all excited triplet states ( $T_1$ ) on fluorescent emitters will decay back to ground state via non-radiative pathways (*i.e.* heat), leading to a loss of 75 % of the generated excitons in the device and a maximum exciton harvesting efficiency ( $\eta_{S/T}$ ) of only 25 %. On the other hand, phosphorescent molecules are capable of harvesting both singlets and triplets equally giving them a maximum exciton harvesting efficiency of 100% due to aforementioned efficient intersystem crossing.<sup>26,27</sup> In relation to the previously described external quantum efficiency equation, equation 1.1, the singlet/triplet harvesting ratio ( $\eta_{S/T}$ ) for fluorescent molecules is only 0.25 resulting in 75 % lost efficiency; while for phosphorescent molecules it is unitary and does not result in any loss of efficiency. A Jablonski diagram illustrating photoluminescence by an electron through fluorescence and phosphorescence are shown in Figure 1.4. Electroluminescence often proceeds through the same pathways with the following differences; the excitation is through either Dexter or Förster energy transfer if charge carriers or excitons instead of photon absorption, and the triplet excited state may be formed directly as dictated by spin statistics.



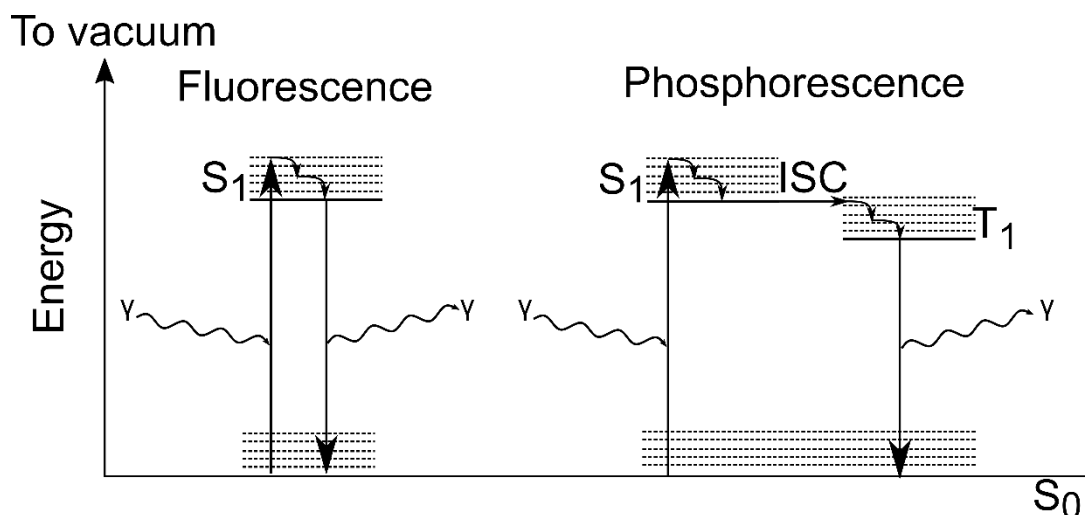


Figure 1.4 Visualization of photoluminescence using a simplified Jablonski diagram

In addition to the extensively investigated phosphorescent materials, two other classes of materials have been shown capable of harvesting both singlets and triplets with equal efficiency. First is thermally-activated delayed-fluorescence (TADF) can occur in fluorescent organic molecules with strong donor-acceptor character. In these material it is possible for environmental vibrational (thermal) energy to overcome the required activation energy for spin-orbit coupling of triplet states within the molecule resulting in efficient upconversion to the singlet excited state ( $T_1 \rightarrow S_1$ ). This spin inversion, commonly referred to as reverse intersystem crossing (RISC).<sup>68,69,70</sup>

Additionally, a series of open-shell organic molecules containing a neutral radical have been shown to exhibit both photoluminescence and electroluminescence. The excitation and emission transitions of these materials only involve an electron moving between doublet states and therefore are not formally forbidden due to their spin.<sup>71</sup> Figure 1.5 illustrates the electron configurations possible in the excited state of closed-shell molecules (singlet and triplet) compared to an open-shell molecule (doublet). The figure also includes an example of an open-shell molecule displaying doublet emission.

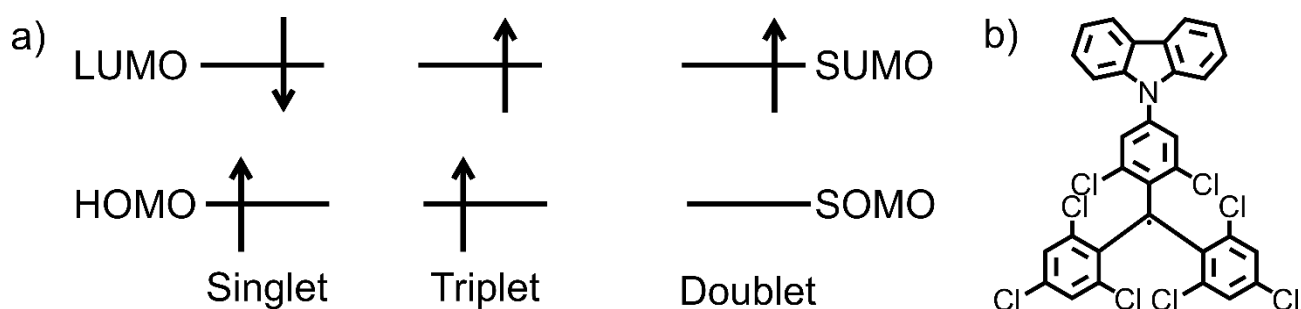


Figure 1.5 Doublet Emission; a) diagram showing the spin states of singlet and triplet excited states for closed-shell molecules and the doublet excited state for an open shell molecule.

The molecular orbitals participating in doublet transitions are the singly-occupied molecular orbital (SOMO) and the singly-unoccupied molecular orbital (SUMO). b) The structure of the most efficient doublet emitter within the series reported by Li *et al.*<sup>71</sup>

### 1.3.3 Phosphorescent iridium(III) complexes

Out of all classes of electroluminescent emitters, phosphorescent iridium(III) complexes have attracted the greatest interest. This is due to a number of advantageous properties shared by many members of the class including; high photo-, chemical and thermal stability, potential for unitary phosphorescent quantum yields ( $\Phi_{\text{PL}}$ ), relatively short phosphorescent lifetimes ( $\tau_{\text{R}}$ ), colour tuning from deep-blue to near infrared region of the electromagnetic spectrum through ligand structure modification and a large cross-section for exciton formation.<sup>66,72,73</sup>

In addition to the already discussed strong spin-orbital coupling exhibited within iridium(III) complexes, the efficient photoluminescence displayed by these complexes is also due to their high ligand-field splitting energy. The d-orbitals of iridium(III) exhibit a high ligand-field splitting energy which is increased by the commonly used high field cyclometallating ligands.<sup>74</sup> This results in cyclometallated iridium(III) complexes having very large energy gap between the d-d orbitals ( $T_{2g}-e_g$ ) inhibiting the non-radiative Laporte-forbidden d-d transitions.<sup>75,76</sup> This large energy gap between the d-d orbitals of cyclometallated iridium(III) complexes decreases the rate of non-radiative metal-centred d-d transitions and also allows efficient near-UV-emitting iridium(III) complexes without the high triplet energy of the excited state decaying via these non-radiative metal-centred d-d transitions.<sup>77,78</sup>

Although other ligand combinations have been shown to be effective<sup>79,80</sup>, *tris*-bidentate iridium(III) complexes are by far the most prevalent. Complexes conforming to the *tris*-bidentate architecture contain one iridium(III) centre with three coordinating bidentate ligands. Typically the iridium(III) centre is bound through the lone pairs of a formally anionic carbon and formally neutral nitrogen. Such ligands are often abbreviated as C^N type ligands. Much of the chemical and thermal stability of iridium(III) complexes originates from the strength of these coordination bonds which are comparable to the strength of most covalent bonds.<sup>66</sup> The saturated coordination sphere of iridium(III) complexes typically exhibit low reactivity. This is a contributing factor to the stability of the cyclometallated iridium(III) complexes, however, it also necessitates the harsh reaction conditions required to induce ligand disassociation of the starting material; commonly chloride ligands.<sup>81</sup> Iridium(III) complexes are quite exceptional organometallic materials in that they exhibit very

high thermal stabilities, are resistant to a wide range of organic reaction conditions and behave similarly to organic materials in terms of purification.

Bidentate ligands bond through adjacent (or *cis*) orbitals of the octahedral iridium(III) complex. The result is a 5- or 6-membered metallocycle. Such ligands are commonly referred to as cyclometallating ligands and the reaction to form such a complex is described as cyclometallation.

When all ligands are identical the complex is described as being homoleptic. The model iridium(III) complex, *fac*-tris-[2-(2-pyridinyl-κN)phenyl-κC]iridium(III) or *fac*-[Ir(ppy)<sub>3</sub>], is an example of a homoleptic iridium(III) complex comprising of C<sup>N</sup> cyclometallating ligands. When all the ligands are not identical the resulting complex is described as being heteroleptic.<sup>82</sup> When a ligand within a heteroleptic complex is known to not be directly involved in the radiative transition of the excited complex it is often labelled as the supporting or ancillary ligand.<sup>83</sup> Common ancillary ligands for phosphorescent iridium(III) complexes are cyclometallating acetylacetonate (O<sup>^</sup>O) or picolinate (N<sup>^</sup>O). Most heteroleptic iridium(III) complexes contain only a single ancillary ligand, however, this is not a fundamental restriction. The archetypical phosphorescent heteroleptic iridium(III) complex is *trans*-*N,N'*-bis[2-(2-pyridinyl-κN)phenyl-κC](acetylacetonato)iridium(III); [Ir(ppy)<sub>2</sub>(acac)]. Figure 1.6 contains the structures of homoleptic [Ir(ppy)<sub>3</sub>] and heteroleptic [Ir(ppy)<sub>2</sub>(acac)].

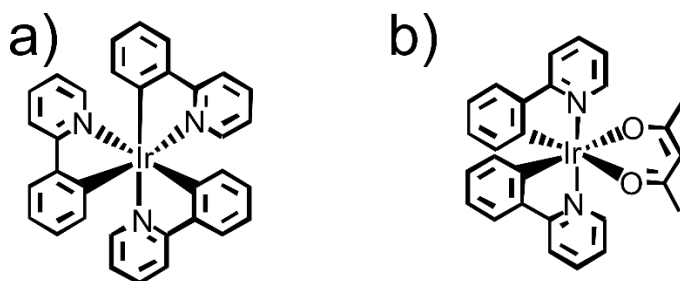


Figure 1.6 Examples of homoleptic and heteroleptic phosphorescent iridium(III) complexes; a) [Ir(ppy)<sub>3</sub>] and b) [Ir(ppy)<sub>2</sub>(acac)], respectively.

From Kasha's law it is known that for a given molecule, the only electronic transition from which appreciable emission can be observed will be the smallest electronic transition in energy for a given multiplicity.<sup>84</sup> As previously described, emission from singlet excited states of efficient phosphorescent materials is negligible due to efficient intersystem crossing to the triplet excited state. Therefore in these molecules only the lowest energy triplet excited state, having threefold multiplicity, will give rise to appreciable emission. The radiative transition from the lowest triplet excited state to the ground state ( $T_1 \rightarrow S_0$ ) typically involves

only the metal-ligand system with the smallest optical gap. While the ligand-metal system or systems exhibiting a larger optical gap will give negligible emission, they are not innocent as they may be involved in non-radiative mechanisms and also contribute strongly to the environment experienced by the emissive ligand-metal system.<sup>85,86</sup>

Phosphorescent iridium(III) complexes do exhibit properties that increase the difficulty of making efficient organic light-emitting diodes. Simple iridium(III) complexes like [Ir(ppq)<sub>3</sub>] often exhibit limited solubility in organic solvents excluding the use of all solution-processing techniques. This is particularly detrimental to the fabrication of large area devices for which vacuum thermal evaporation becomes prohibitively expensive.<sup>87</sup> Iridium(III) complexes must also be well distributed throughout a host material during deposition as close proximity allows inter-chromophore triplet-triplet annihilation which results in non-radiative decay of two excited species.<sup>88,89</sup>

Strategies have been developed to aid in the solubility and decrease the inter-chromophore interactions of iridium(III) complexes including incorporation into polymers, dendrimers and poly(dendrimer)s.

#### 1.3.4 Light-emitting polymers

One strategy towards the development of solution processable iridium(III) complexes has been their incorporation into polymer architectures.<sup>90</sup> The incorporation of phosphorescent moieties into polymer systems was motivated by developments in solution processed polymer light-emitting diodes utilizing fluorescent conjugated polymers.<sup>33,91,92</sup> A non-synthetic approach was also demonstrated by utilizing fluorescent conjugated polymers and phosphorescent metal complexes as a host and dopant system, respectively.<sup>93</sup> Lower than expected efficiencies were observed for these blend systems with significant non-radiative decay via interchromophore interactions occurring due to phase separation of the host and dopant.<sup>94</sup>

One of the earliest approaches to developing phosphorescent polymers was to incorporate phosphorescent moieties into the fluorescent conjugated polymer molecules used in polymer light-emitting diodes such as poly(*p*-phenylene vinylene) (PPV), poly(fluorenes), poly(*p*-phenylenes), poly(*p*-phenylene ethynylenes) and poly(alkylthiophenes).<sup>33,95</sup> The general structures for these conjugated polymer systems without incorporation of phosphorescent moieties is shown in Figure 1.7.

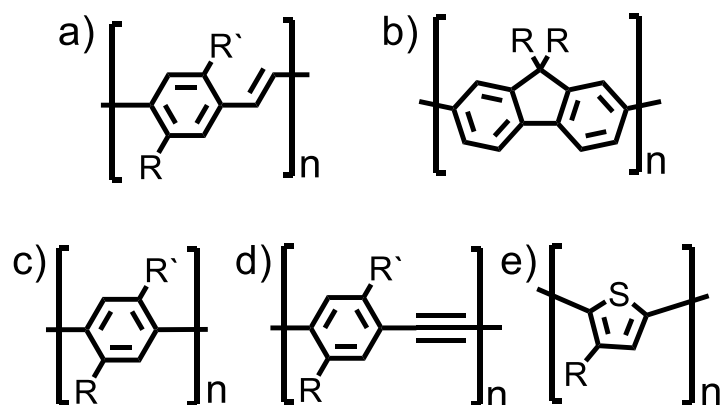


Figure 1.7: General structures of conjugated polymer systems; a) PPV, b) poly(fluorene), c) poly(*p*-phenylene), d) poly(*p*-phenylene ethynylene) and e) poly(alkylthiophene).

This led to the development of polymeric materials that incorporated phosphorescent chromophores, such as iridium(III) or platinum(II) complexes, to allow harvesting of triplet excitons.<sup>96,93</sup> Many examples of polymers functionalized with phosphorescent complexes have been reported in the literature.<sup>93,97,98,99</sup>

Phosphorescent polymers can be divided into multiple types by shared structural attributes. In respect to the position of the phosphorescent complex to the polymer backbone three types of polymer can be observed; main-chain type in which the polymer backbone passes through at least one of the cyclometallating ligands of the complex, side-chain type polymers in which the complexes are attached to the polymer backbone as pendant groups, and chelating-type polymers in which the polymer backbone passes through the metal centres of the complex through at least two mono-functionalized cyclometallating ligands. Many examples of all three types are random copolymers with fewer phosphorescent complex containing monomeric units to decrease the incidence of triplet-triplet annihilation. The general structure along with the structure of an example molecule for main-chain type, side-chain type and chelating type phosphorescent polymers are shown in Figure 1.8.

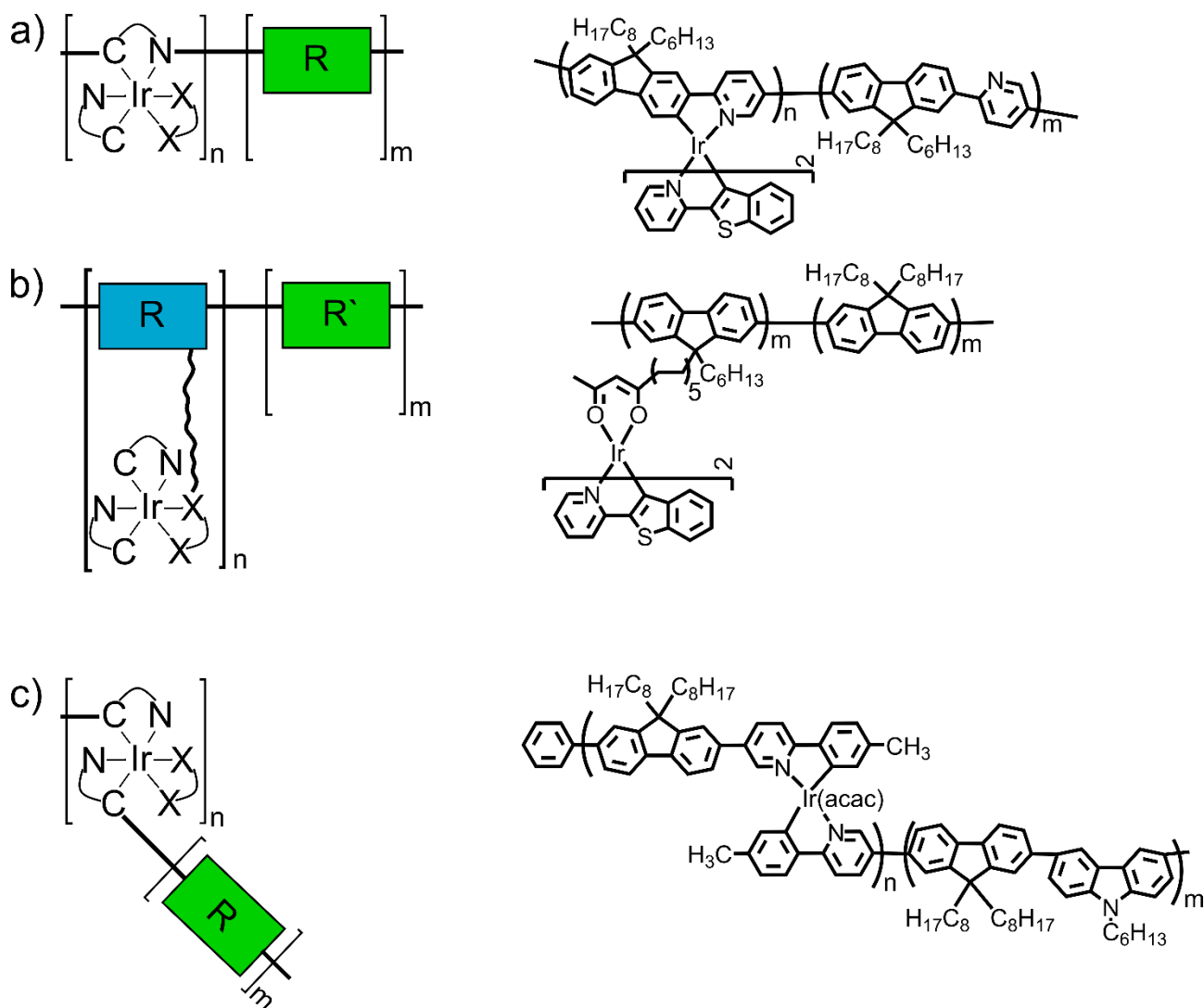


Figure 1.8. Generic structures (left) and literature example (right) of the three types of polymers incorporating phosphorescent complexes; a) main-chain polymer type<sup>100</sup>, b) side-chain polymer type<sup>101</sup>, and chelating polymer type<sup>99</sup>. R and R` are typically as aromatic moieties such as fluorene or carbazole.

While these phosphorescent conjugated polymers demonstrated improved solution processability the efficiencies of subsequent devices were found to be low.<sup>102,103</sup> The cause was found to be efficient Dexter energy transfer from the excited phosphorescent metal complexes to the low energy triplet state of the conjugated polymer backbone; leading to non-radiative decay of the exciton.<sup>89,104,105,106</sup>

To combat this two approaches have been utilized; limiting the conjugation or using a non-conjugated backbone or attaching the phosphorescent moiety as a pendant with a longer spacer to reduce the short-range Dexter energy back transfer.<sup>104,107</sup>

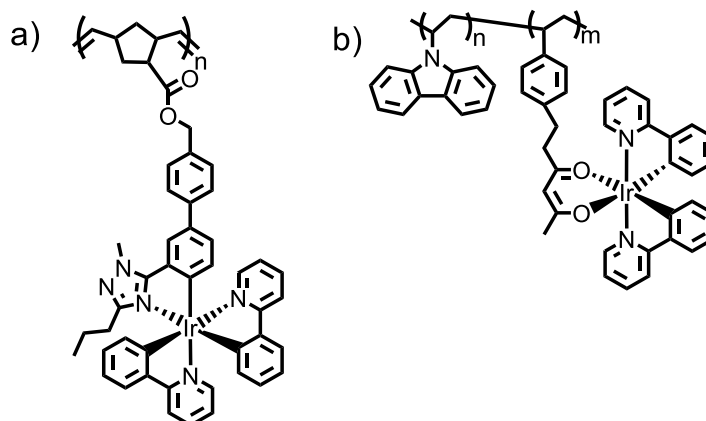


Figure 1.9: Examples of two non-conjugated iridium(III) complex containing polymers: a)<sup>108</sup> and b)<sup>109</sup>

### 1.3.5 Dendrimers containing phosphorescent metal complexes

While light-emitting polymers have been found to exhibit very advantageous properties in terms of solution processability and emissive layer film quality<sup>110</sup>; difficulties were observed in terms of phase separation and triplet energy back transfer. Another approach which aims to emulate some of the advantageous properties of polymer systems while avoiding their most common loss mechanisms, is to utilize macromolecules with dendritic architectures. These materials, termed dendrimer(s), utilize a branched architecture which can be repeated to generate higher generations. This stepwise synthetic approach allows the dendritic moieties, termed dendrons, to reach large molecular weights in few synthetic steps.<sup>111</sup> Because the synthetic pathway to increase the generation of the dendron is chosen to be sequential, the product of each step is always functional allowing for simple modification or attachment to an active moiety.<sup>87</sup>

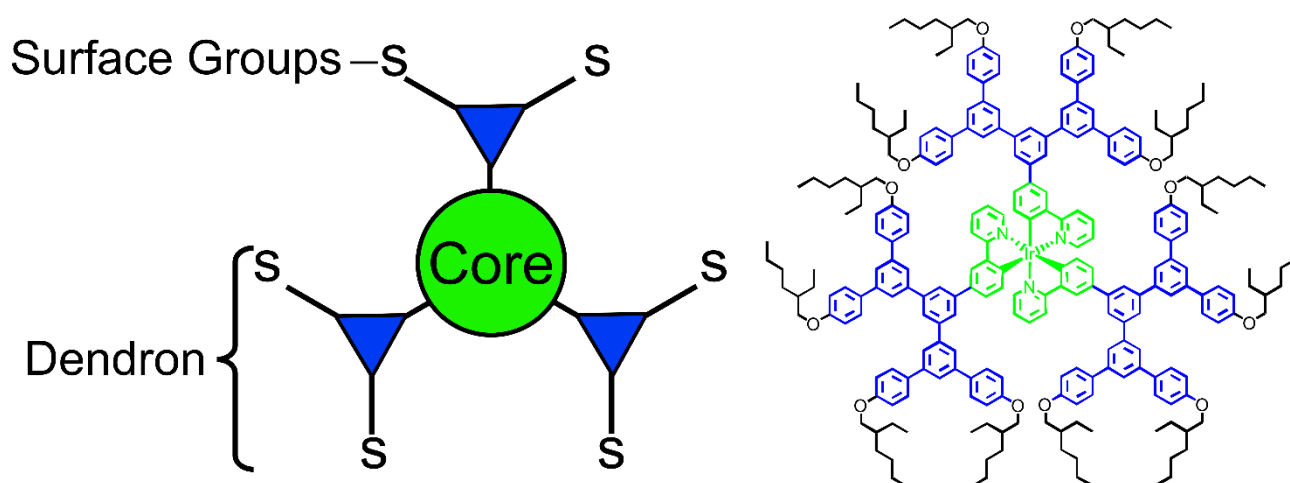


Figure 1.10: The general structure and example of a second generation dendrimer.<sup>112</sup>

Dendrimers are typically bulky and have a high level of dimensionality which limits tight packing and increases solubility which may be enhanced by being functionalized with alkyl surface groups.<sup>113</sup>

As the bulky dendrons create a physical barrier between the emissive cores of neighbouring light-emitting dendrimers, they can be utilized to tune minimize (or ultimately eliminate) any interchromophore interactions. This is of particular import for phosphorescent dendrimers as it allows inhibition of deleterious triplet-triplet annihilation by means of physical separation.<sup>87,114</sup> Phenylene-based dendrons have proven very successful at decreasing the interchromophore interactions between phosphorescent iridium(III) complex containing dendrimers.<sup>115</sup> Figure 1.11 contains the structure of two reported phenylene-based dendrimers containing phosphorescent iridium(III) complexes.



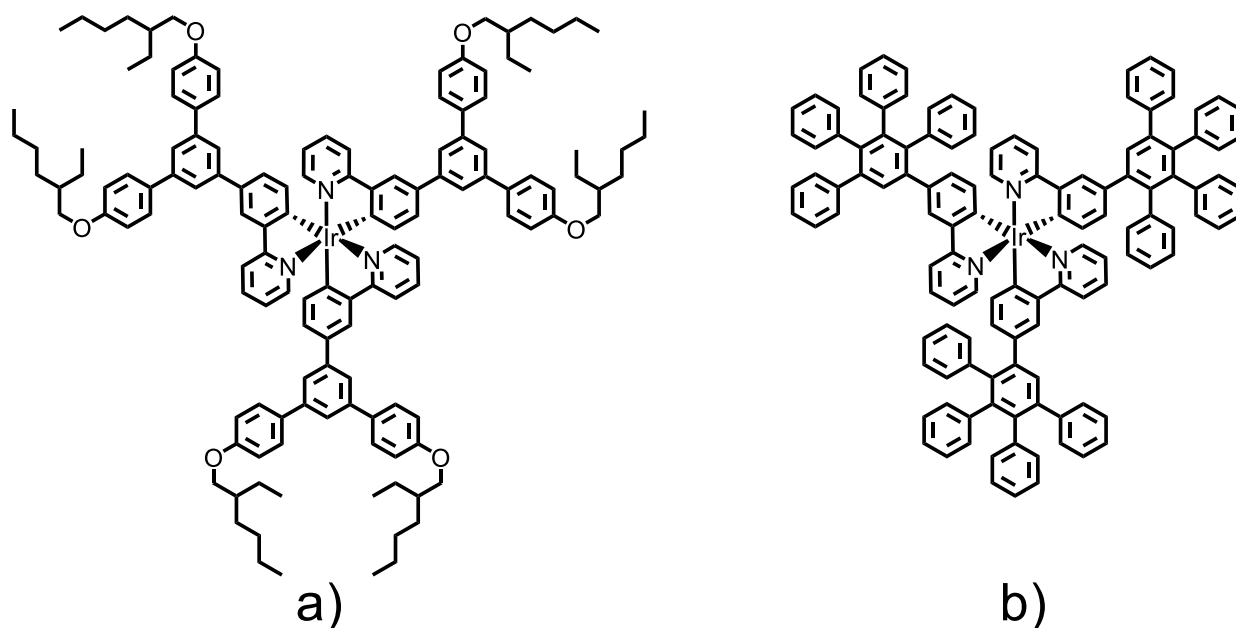


Figure 1.11: Structures of example phenylene-based dendrimers containing iridium(III) complexes; a)<sup>112</sup> and b)<sup>116</sup>

It has been well established that increasing the generation and number of dendrons attached to the phosphorescent core decreases the non-radiative decay via interchromophore interactions indicated by a steady increase in neat film photoluminescence quantum yield ( $\Phi_{\text{PL}}$ ) in respect to dendron generation.<sup>116,117</sup> Additionally, increasing the number of dendrons about the phosphorescent core exhibits the same reduction of non-radiative decay through greater physical separation of the phosphorescent cores.<sup>113</sup> However, the improvements in phosphorescent quantum yield with increasing dendron generation did not result in the same trend for OLED efficiencies. Instead, the device efficiencies are observed to improve initially with increasing dendron generation before an optimal dendron generation is reached and efficiencies begin to deteriorate for higher generations. It has been posited that this effect, is due to the mobility many dendrons being relatively poor which inhibits charge injection into the emissive core.<sup>116,118,119,120</sup> Methods commonly employed to reduce the insulating effect of the dendrons is to limit molecular design to lower generations and to incorporate moieties known to participate in efficient charge transport such as carbazole or triphenylamine.<sup>119,121,122,123</sup> Figure 1.12 shows two reported examples of carbazole or triarylamine-based dendrimers containing phosphorescent iridium(III) complexes.

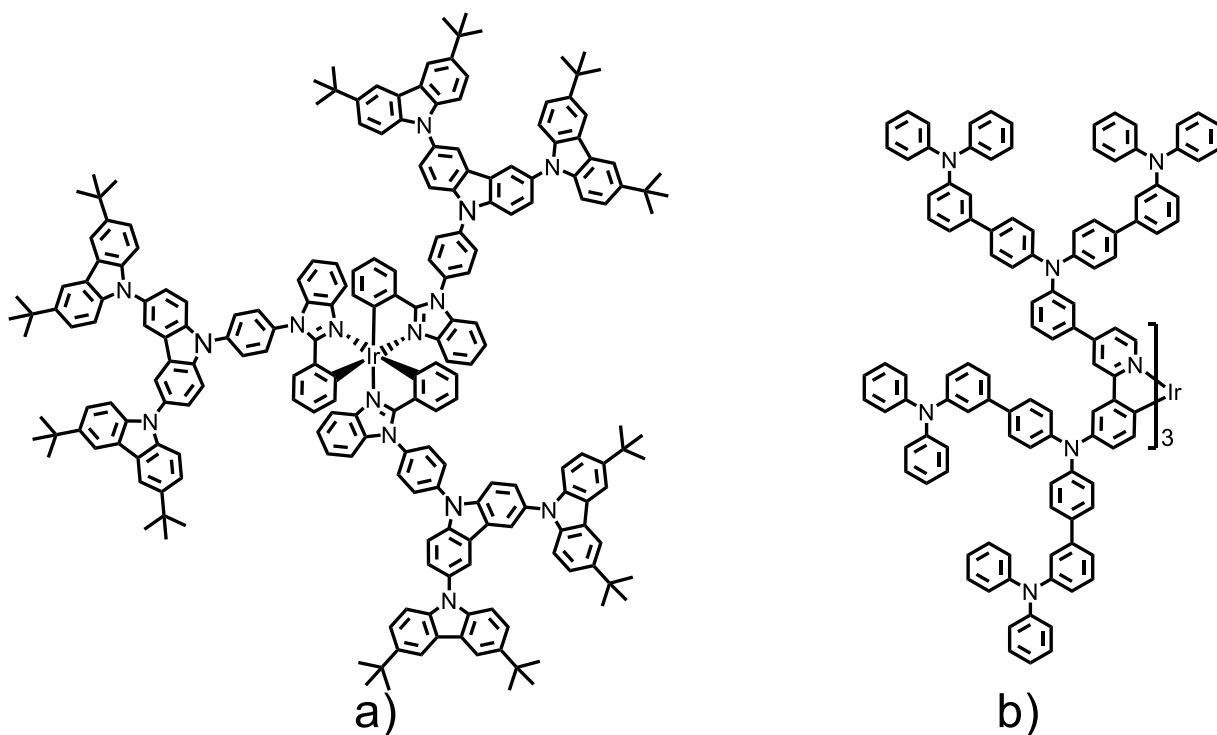


Figure 1.12: Structures of example carbazole and triarylamine-based dendrimers containing phosphorescent iridium(III) complexes; a)<sup>124</sup> and b)<sup>125</sup>

The hole mobilities of dendrimers containing iridium(III) complexes utilizing phenylene-based or carbazole-based dendrons were investigated to determine if incorporation of charge transporting moieties was advantageous. The first, second and third generation of each dendrimer architecture was investigated to gain a greater understanding of how the dendrons affect charge transport. It was found that the hole mobility of the first generation carbazole-based dendrimer under an applied electric field was approximately an order of higher than the phenylene-based analogue.<sup>119,120</sup> Additionally, the carbazole-based dendrimers exhibit improved hole mobilities with increasing dendron generation while the hole mobility in the phenylene-based dendrimers decreased with generation. This was particularly significant as while both types of dendrimer showed improved photoluminescent quantum yield with increasing dendron generation; only the carbazole-based dendrimers exhibited concurrent hole mobility improvement. These results enforced the motivation behind developing dendrimers with electroactive moieties to give materials with improved solution processability, charge mobility and luminescent properties.

### 1.3.6 Poly(dendrimer)s containing phosphorescent iridium(III) complexes

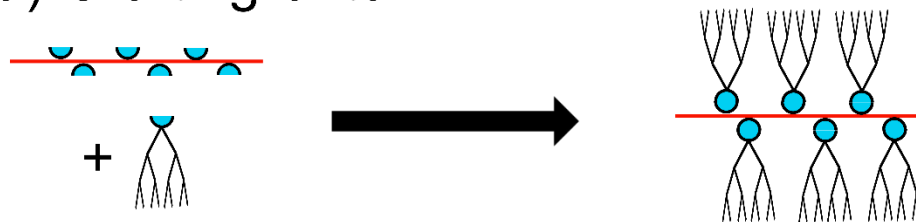
As discussed in the previous section, phosphorescent dendrimers have been extensively investigated as emitters for solution processed organic light emitting diodes.

With a large number of advantageous properties these materials appear very promising for large-area devices fabricated through most solution processing techniques. However, inkjet printing has tighter restrictions regarding the properties of printable ink solutions.<sup>126</sup> For example, the viscosity of the dendrimer solutions that have proven effective for spin-coated devices are similar to the neat solvent, and are incompatible with the inkjet printing technique.<sup>108,127</sup> One of the most successful methods for tailoring inks is to utilize polymeric materials which exert a greater effect on solution viscosity than smaller molecules.<sup>127</sup> This led to the development of phosphorescent iridium(III) complex containing poly(dendrimer)s which combined the solution properties of polymeric materials with those of dendrimers having the additional benefit of chromophore separation due to the bulky sterics of the dendrons.<sup>108</sup>

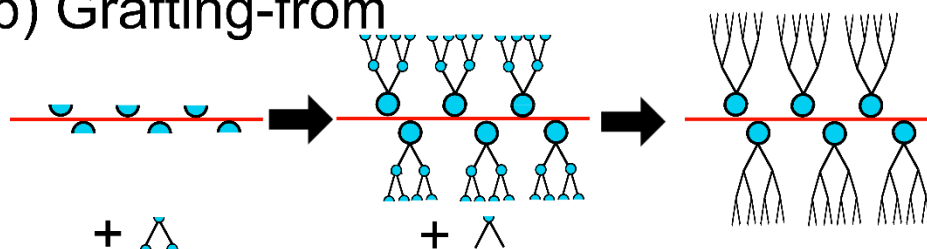
Dendronized polymers are a form of comb or brush polymer in which the pendant groups, or “teeth”, are in the form of the branched dendrons described in the previous section.<sup>128</sup> Dendronized polymers are often treated as a separate class of materials as they exhibit properties incongruous with brush polymers stemming from the very different sterics of their pendant groups. Dendronized polymers have been investigated in fields where their structural properties are essential to their application including biomedical<sup>129</sup>, materials for non-linear optics<sup>130</sup>, energy storage<sup>131</sup>, drug delivery<sup>132</sup> and as fluorescent emitters for OLEDs<sup>133</sup>.

Three methodologies have been employed to synthesize dendronized polymers and brush polymers in general; grafting-onto<sup>134</sup>, grafting-from<sup>135</sup> and grafting-through<sup>136</sup>. A schematic representation of these approaches is displayed in Figure 1.13.

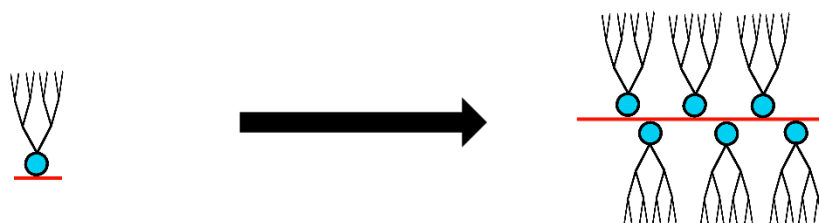
### a) Grafting-onto



### b) Grafting-from




### c) Grafting-through or macromonomer



— Polymer backbone

◐ Coupling-reactive site

 Dendron

 Dendron building block

Figure 1.13: General synthetic pathway for a) grafting-onto, b) grafting-from and c) grafting-through (macromonomer) methodologies to produce a dendronized polymer.

Both grafting-onto and grafting-from methods are post-polymerization functionalization techniques. For grafting-onto synthesis, the dendrons are coupled through to side-groups of the polymer. Grafting-from is similar to grafting-onto, however, the dendrons are not coupled as a single unit but are built up from the polymer backbone. In the grafting-through method, or macromonomer method; a dendronized monomer is synthesized and is polymerized to form the dendronized polymer. It is this polymerization of a macromonomer that gives rise to a poly(dendrimer) which is a polymer of a dendrimer.<sup>108</sup> Since the grafting-onto and grafting-from methods rely on post-polymerization

functionalization; obtaining a defect-free polymer, one in which every active site on every polymer chain has reacted successfully, is very challenging.<sup>137</sup> On the contrary, the grafting-through method can produce a defect-free homopolymer if polymerization is carried out upon a neat dendronized monomer.<sup>138,139</sup>

A series of poly(dendrimer)s incorporating green-phosphorescent iridium(III) complexes for organic light-emitting diodes have been reported by Burn *et al.*<sup>108,113,140,141,142</sup> It was shown that by utilizing a polymeric structure the viscosity of the solutions during processing could be increased substantially compared to polymers while inter-chain. For example; the poly(dendrimer) "d" in Figure 1.14 was found to produce a 10 mg/mL 1,2-dichloromethane solution with a viscosity of 1.30 cSt compared to the equivalent solution of monomer precursor or neat solvent displaying a viscosity of 1.14 cSt and 1.06 cSt, respectively. Increasing the poly(dendrimer) concentration to 25 mg/mL increased the viscosity further to 1.41 cSt.<sup>143</sup> All materials shown in Figure 1.14 were shown to enhance the viscosity of processing solutions.

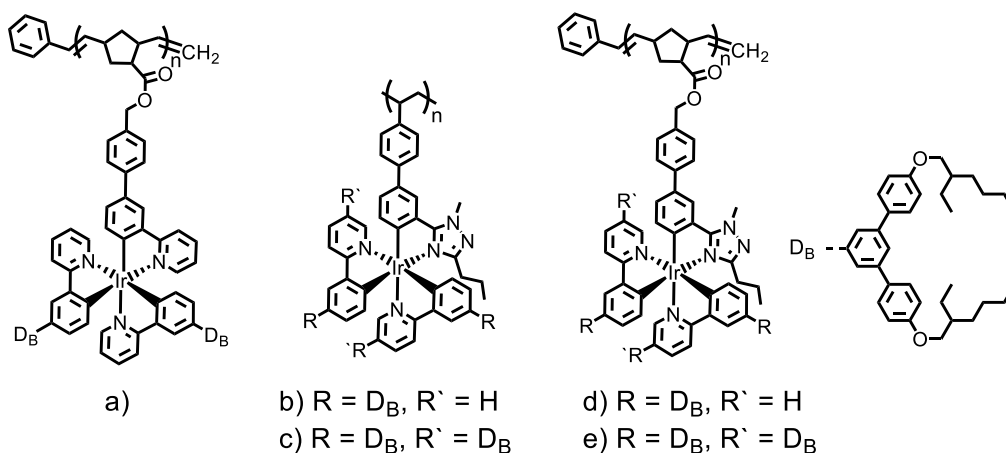


Figure 1.14: A series of phosphorescent iridium(III) complex containing poly(dendrimer)s reported by Burn *et al.*<sup>127,140,143</sup>

The poly(dendrimer)s were also shown to retain decent phosphorescent quantum yields when moving from solution to neat film. Using poly(dendrimer) d) from Figure 1.14 as an example; the photoluminescent quantum yield of the material dropped from 65 % to 44 % when moving from solution to neat film. In comparison, photoluminescent quantum yield of the analogous homopolymer without dendrons dropped from 48 % to 2 % when transitioning from solution to neat film. All investigated poly(dendrimer)s in Figure 1.14 displayed these advantageous photophysical properties suggesting that the intra-chain interchromophore interactions were well controlled by the dendrons functionalizing each

iridium(III) complex. The series demonstrated that phosphorescent iridium(III) complex containing poly(dendrimer)s were a powerful architecture for developing emitters for efficient but simple solution processed OLEDs with external quantum efficiencies reaching 12 % for those utilizing phenylene-based dendrons.

The recent development of a phosphorescent iridium(III) complex containing poly(dendrimer) featuring carbazoyl-dendrons, **L2** (Figure 1.15), was shown to produce very high efficiency devices. Despite only having a photoluminescence quantum yield of 72 %, emissive layers containing 20 % **L2** in CBP were observed to have an average external quantum efficiency of 16 % at 100 cd/m<sup>2</sup> with hero devices achieving maximum external quantum efficiencies of up to 31 % at 30 cd/m<sup>2</sup>.<sup>142</sup>

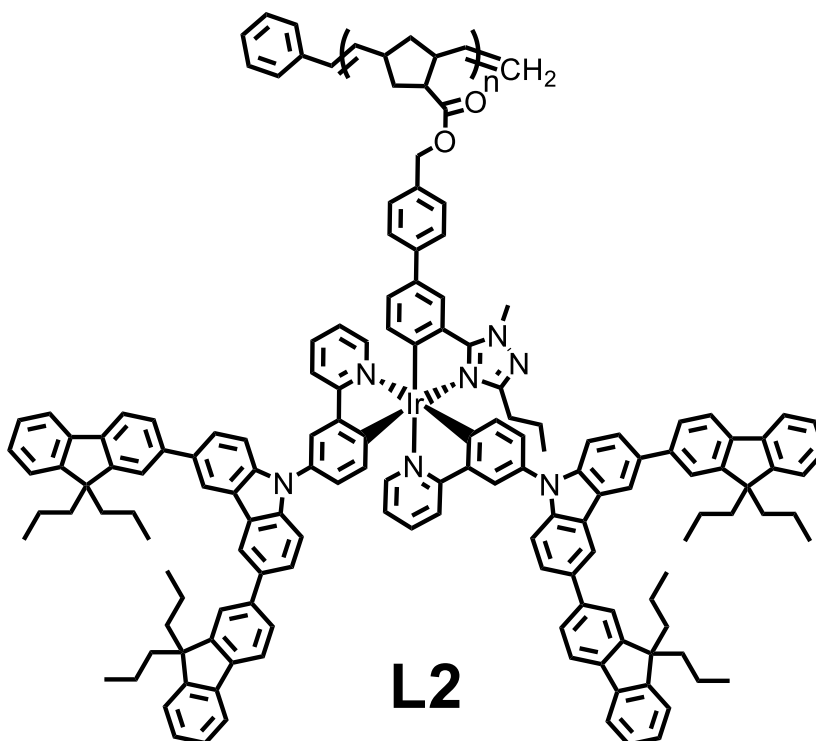


Figure 1.15: The structure of carbazole-based poly(dendrimer), **L2**.<sup>142</sup>

As described in a previous section, the external quantum efficiency of an OLED is determined by the four variables shown in equation 1.1, The outcoupling efficiency ( $\eta_{\text{out}}$ ) of bottom emitting OLEDs on a glass/ITO substrate is known to be approximately 20% for an isotropic emitter. In a perfectly balanced phosphorescent OLED the charge-capture efficiency ( $\gamma$ ) and singlet/ triplet harvesting ( $\eta_{\text{S/T}}$ ) efficiency are unitary. As a result the OLEDs utilizing 20% **L2** in CBP as an emissive layer should be limited to just 14%. This was of great interest as it suggested that the outcoupling efficiency, the parameter responsible for the largest efficiency loss, was higher than expected for these devices.

Two scenarios were proposed to explain the enhanced outcoupling efficiency; the devices exhibited a strong optical cavity effect or the emissive dipoles of the polymers were at least partially self-aligning during device fabrication. The presence of a strong optical cavity effect for these devices was eliminated by measuring their angle dependant emission which was found to be consistent with a Lambertian emitter. This strongly suggested that the high EQEs were a result of advantageous preferential alignment of the polymer chains during spin-coating. This was particularly interesting as it has been recently suggested that dipole alignment during spin-coating is not possible for phosphorescent iridium(III) complexes.<sup>144</sup>

Emissive dipole alignment leading to enhanced outcoupling efficiency has been demonstrated for a number of thermally evaporated phosphorescent iridium(III) complexes and solution processed fluorescent conjugated polymers.<sup>57,145,146,147,148</sup> The observation of emissive dipole alignment occurring within a phosphorescent poly(dendrimer) during solution processing is an exciting development and provides a strong motivation for future investigation of phosphorescent iridium(III) complex within the poly(dendrimer)s framework.

# Synthesis and Properties of Green-Emitting Iridium(III) Poly(dendrimer)s

---

*This chapter describes the design rational and synthesis of poly(dendrimer)s, **PD<sub>B</sub>** and **PD<sub>C</sub>**, based upon the well-studied green-emitting complex [Ir(PPy)<sub>3</sub>]. The synthesis, optical and electrochemical properties of the green-emitting materials are described while providing discussion on how these values are pertinent from the perspective of OLED technology.*

## 2.1 Design rational

The initial aim of the design, synthesis and characterization of the materials contained within this section was to investigate whether the polymerization of phosphorescent iridium(III) complex-based pendant dendronized monomers could be optimized by structural modification to give improved control over the physical and photophysical properties of light-emitting materials. In particular the project aimed to provide understanding on whether the polymerization of the bulky dendronized monomers could be improved through a simple lengthening of the core-backbone tether moiety.

Both materials were designed to be comparable to previous work with the modification limited to a single moiety. Any observed variations in the materials properties could then be confidently attributed to the single minor structural alteration as opposed to more complex interactions that multiple structural changes could induce. The two new poly(dendrimer)s were designed to include modifications to the biphenyl-dendronized literature poly(dendrimer) 1 (**L1**)<sup>108</sup> and the carbazoly-dendronized literature poly(dendrimer) (**L2**) (Figure 2.1).<sup>142</sup>



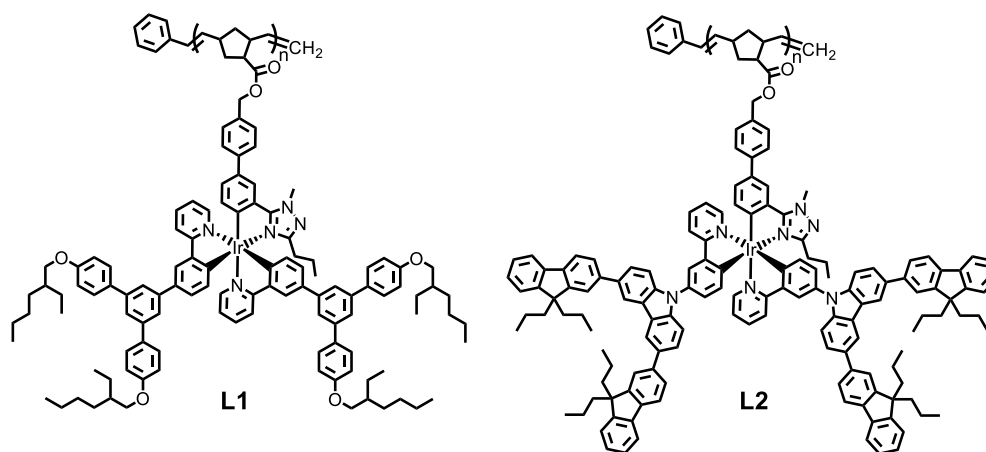


Figure 2.1: Structures of the biphenyl-dendronized literature poly(dendrimer) **1** (**L1**) and the carbazoly-dendronized literature poly(dendrimer) (**L2**) which formed the basis for the design of the targets.

It has been shown that ring-opening metathesis polymerization (ROMP) has the capability to produce high molecular weight, low-dispersity polymers from bulky, sterically-hindered monomers; however, there is a point at which steric bulk inhibits polymer propagation processes.<sup>138,137</sup> This is commonly studied through living polymerization of a series of dendronized monomers. For the lowest generations of dendronized monomer the respective poly(dendrimer)s are expected to show the low dispersity and degree of polymerization comparable to the monomer/catalyst ratio characteristic of a true living polymerization. Steric bulk quickly becomes apparent within the series with higher monomer dendron generation leading to increasing polymer dispersity until a generation is reached where propagation of the polymerization ceases to occur.

It was believed that the ring-opening metathesis polymerization of the two previously reported poly(dendrimer)s, **L1** and **L2**, was being sterically inhibited by the bulky dendronized pendant groups. This led to a limiting of polymer chain length and a lack of reproducibility. Although both poly(dendrimer)s only contain first generation dendrimers, each octahedral iridium(III) complex bears two dendron-adorned ligands producing significant steric bulk.

Two poly(dendrimer)s, **1** and **2**, were designed to determine if increasing the length of the tether could alleviate the deleterious effects of steric hindrance on the polymerization. This was done through a single modification to the previously reported poly(dendrimer)s, **L1** and **L2**, where an additional phenyl ring was inserted into the tether (Figure 2.2).

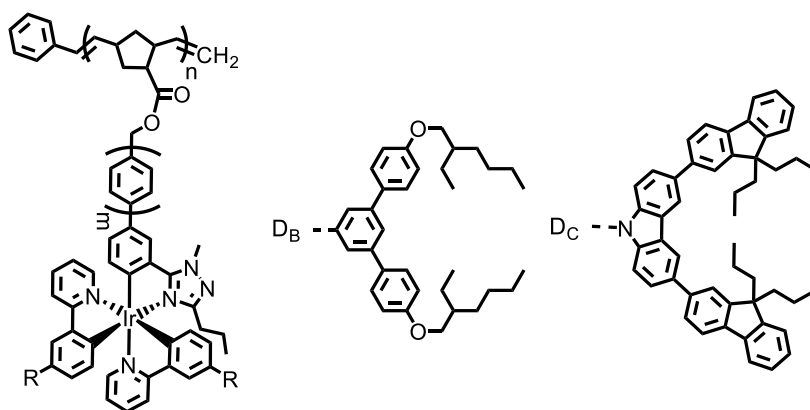


Figure 2.2: Structures of previously reported poly(dendrimer)s **L1**<sup>108</sup> (R= D<sub>B</sub>, m = 1) and **L2**<sup>142</sup> (R= D<sub>C</sub>, m = 1) with the lengthened tether poly(dendrimer)s **PD<sub>B</sub>** (R= D<sub>B</sub>, m = 2) and **PD<sub>C</sub>** (R= D<sub>C</sub>, m = 2).

Insertion of another phenyl moiety into the tether was chosen due to the presence of literature evidence suggesting that maintaining rigidity using aryl tethers aids in ring-opening olefin-metathesis polymerization of bulky monomers while alkyl tethers appear to be ineffective.<sup>137</sup> Additionally there was literature evidence suggesting that increasing flexibility in a phosphorescent poly(dendrimer) system was detrimental to the material's photoluminescent properties.<sup>127</sup>

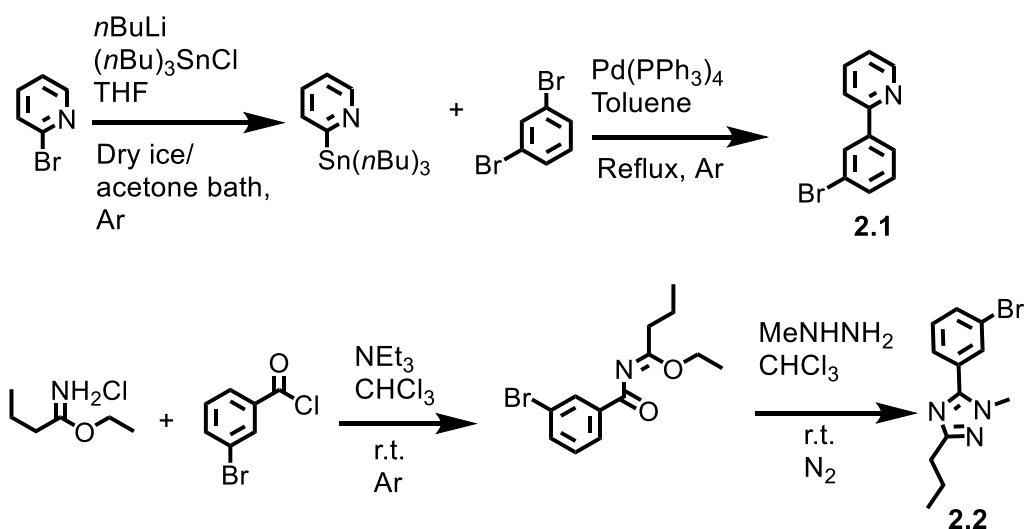
## 2.2 Synthesis

The chosen synthetic route paralleled the previously reported synthetic pathways closely, only deviating with the incorporation of the lengthened tether.

### 2.2.1 Brominated Ligands

To allow coupling to the first generation dendron, the synthesis of a brominated derivative of the emissive ligand and ancillary ligand was required (Scheme 2.1). 2-(3-Bromophenyl)pyridine (**2.1**) was synthesized in two-steps by lithiation and transmetallation of 2-bromopyridine to give 2-(tri-*n*-butylstannyl)pyridine followed by a Stille coupling to 1,2-dibromobenzene with an overall yield of 63 %.

The ancillary ligand (**2.2**) was prepared by *N*-acylation of ethyl butyrimidate hydrochloride using 3-bromobenzoyl chloride under basic conditions followed by a cyclization with methylhydrazine with a two-step yield of 71 %.



Scheme 2.1: Synthetic scheme of brominated ligands

### 2.2.2 Tether

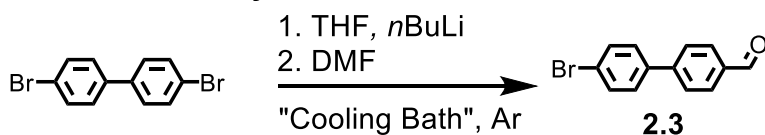
The tether moiety was required to contain the same functionality as was used to produce **L1** and **L2** but with an additional phenyl ring. As a result 4-(4-[pinacolatoboronanyl]phenyl)benzyl alcohol (**2.5**) was designed to replace the literature 4-formylphenylboronic acid or 4-(hydroxymethyl)phenylboronic acid (Scheme 2.2).

Prior to finding the literature reaction ultimately used in the synthesis of 4-(4-bromophenyl)benzaldehyde (**2.3**) other alternatives were attempted. This included lithiation of 4,4'-dibromobiphenyl followed by formylation, cooled with dry ice/ acetone or liquid nitrogen/ diethyl ether, as well as Suzuki couplings of 4-formylphenylboronic acid and 4-(hydroxymethyl)phenylboronic acid with 1-bromo-4-iodobenzene to synthesize **2.3** and the subsequent alcohol (**2.4**) respectively.

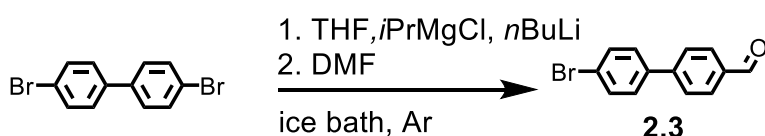
Both pathways were found to be unsatisfactory. Lithiation of 4,4'-dibromobiphenyl, cooled in a dry ice/ acetone (-78°C) or liquid nitrogen/ diethyl ether (maintained at approximately -100°C), followed by formylation gave rise to what appeared to be the dialdehyde as well as dehalogenated materials by <sup>1</sup>H NMR. The formation of side products led to significantly decreased yield and difficulties in purification. Attempts at synthesis of **2.3** via Suzuki couplings consistently fell short of expectations due to the reaction, as monitored by thin layer chromatography (TLC), appearing to cease before full conversion to the product. The major concern for the Suzuki couplings attempted was that they appeared to lack robustness. Although a yield of up to 73 % of **2.3** was obtained via Suzuki coupling other attempts following the same procedure resulted in much lower yields or at times no product at all. The highest yields obtained for **2.3** (Scheme 2.2) are compared in Table 2.1. As noted in the table, many of the conditions proved to not be robust with repeated

experiments failing or producing much lower yields. As it plays a role in the time required per reaction, the difficulty of the purification is also included.

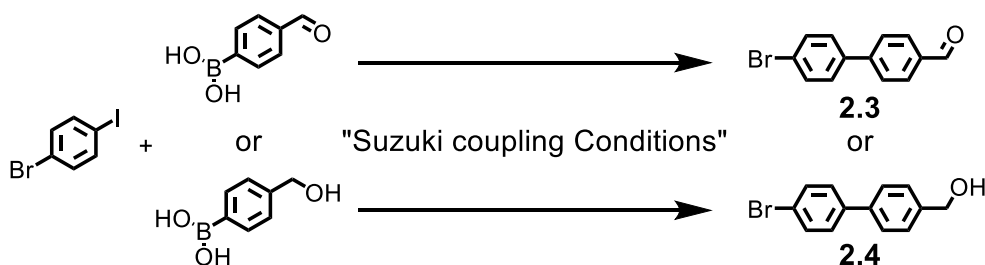
**Metallation/ formylation:**



Cooling Bath: Lithiation a) CO<sub>2</sub>(s)/ acetone (~ -78°C) or Lithiation b) N<sub>2</sub>(l)/ Et<sub>2</sub>O (~ -100°C)



**Suzuki Coupling:**



Suzuki coupling conditions:

- Pd(PPh<sub>3</sub>)<sub>4</sub>, 2 M Na<sub>2</sub>CO<sub>3</sub> (aq), toluene, EtOH, reflux, Ar
- Pd(PPh<sub>3</sub>)<sub>4</sub>, anhydrous THF, CsF, reflux, Ar
- Pd(OAc)<sub>2</sub>, P(*o*-tolyl)<sub>3</sub>, 2 M Na<sub>2</sub>CO<sub>3</sub> (aq), toluene, EtOH, reflux, Ar
- Pd(PPh<sub>3</sub>)<sub>4</sub>, THF, NaOH (aq), reflux, Ar

Scheme 2.2: Synthetic methods of **2.3** and **2.4** attempted

Table 2.1: Optimization of the synthesis of **2.3**. Synthetic conditions as per Scheme 2.2

Conditions	Best yield (%)	Purification	Notes
Lithiation a)	Trace	n/a	n/a
Lithiation b)	Trace	n/a	n/a
Suzuki a)	44	Difficult	Not-robust
Suzuki b)	73	Difficult	Not-robust
Suzuki c)	71	Difficult	Not-robust
<i>n</i> BuLi/ <i>i</i> PrMgCl	73	Simple	Robust

Bypassing the synthesis of **2.3** was also attempted by forming **2.4** directly using Suzuki coupling. The direct formation of the alcohol proved even less optimal with the

highest yield of **2.4** obtained being 28% whilst exhibiting the same lack in robustness where some batches would fail to form product or give lower yields. The highest yields obtained for **2.4** under attempted conditions (Scheme 2.2) are compared in Table 2.2. As in the previous table the purification difficulty and robustness of the reaction is indicated.

Table 2.2: Direct synthesis of **2.4**

Conditions	Best yield (%)	Purification	Notes
Suzuki a)	19	Difficult	Not-Robust
Suzuki b)	Failed	n/a	n/a
Suzuki d)	28	Difficult	Not-Robust

It is believed that the difficulties experienced in the Suzuki couplings are likely due to the catalyst becoming poisoned before the reaction completes. Addition of further aliquots of catalyst failed to promote further reaction supporting the hypothesis that an effective poison is present in the reaction mixture when the reaction is observed to cease. As the agent that poisons the catalyst appears to form at different points in the reaction, sometimes allowing significant product formation and other times none, while being potent enough to stop additional aliquots of catalyst from performing it is likely a byproduct formed during the reaction rather than an impurity in the starting materials.

A search of the literature appears that the difficulties I encountered are consistent with the results of others. Reported yields of **2.3** vary considerably for the metalation/formylation (40 %<sup>149</sup> to 95 %<sup>150</sup>) and Suzuki coupling (53 %<sup>151</sup> and 95 %<sup>152</sup>).

The set of conditions found to be optimal for the synthesis of **2.3** was a metalation-formylation reported by Gallou *et al.*<sup>153</sup> The reaction was found to be robust and to form **2.3** without any observable byproducts. This clean reaction proved exceptionally easy to purify as the product was simple to separate from the starting material.

The conditions involved metalation of 4,4'-dibromobiphenyl in anhydrous tetrahydrofuran using a combination of iso-propylmagnesium chloride (tetrahydrofuran solution) and *n*-butyllithium (alkane solution) followed by quenching with *N,N*-dimethylformamide then hydrolysis of the hemiaminal to afford the formylated product, 4-(4-bromophenyl)benzaldehyde (**2.3**), in 73 % yield. The reaction was performed under argon and cooled by an ice bath.

The reaction is as the use of two organometallic reagents appears to provide the selective metalation lacking in the previously attempted lithiations at a much higher temperature. The presence of the dialdehyde was absent by thin layer chromatography and

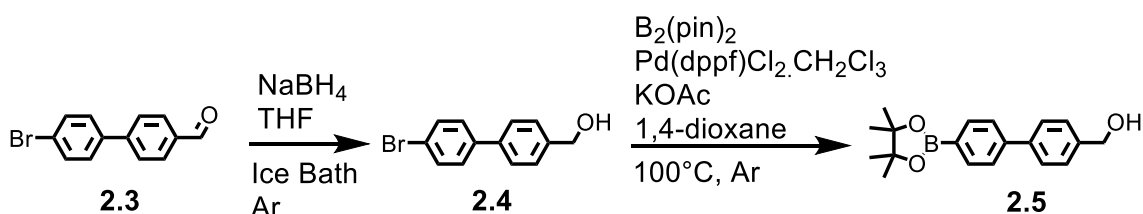
$^1\text{H}$  NMR of the crude material supporting the high degree of selectivity obtained under these conditions.

The proposed mechanism given by Gallou *et al* is that treatment of a solution containing an aryl bromide with the organomagnesium reagent and subsequent treatment with the organolithium reagent results in the more stable and selective  $\text{Ar}_3\text{MgLi}$  intermediate complex. The formylation then proceeds as expected via nucleophilic addition of the formally anionic aryllithium onto the carbonyl of *N,N'*-dimethylformamide giving the intermediate deprotonated hemiaminal. Protonation during the aqueous workup results in elimination of dimethylamine to afford the aldehyde.

The advantages of utilizing the prescribed method were twofold; a yield of (73 %) was sufficient that repeated synthesis was not required and the only materials observed in the crude were the desired product and the starting material leading to rapid, simple purification with recovery of the starting material.

Reduction of **2.3** with sodium borohydride gave 4-(4-bromophenyl)benzyl alcohol (**2.4**) in 28 % yield. The observed yield is very low for a simple reduction of an aldehyde to an alcohol. The presence of multiple unknown impurities were consistently observed in this reduction by both thin layer chromatography and  $^1\text{H}$  NMR. These impurities were a very minor constituent of the crude, however, and the losses in yield appeared during purification by column chromatography over silica. Each subsequent purification by column chromatography would afford less material. This was observed even when the chromatography was unsuccessful and the concentration of impurities remained relatively unchanged. It is likely that a greater yield could be obtained by avoiding column chromatography over silica, however, the yields were sufficient to allow the synthesis of the subsequent products and optimization was not performed.

To allow Suzuki coupling of the tether to the iridium(III) complex the aryl bromide, **2.4**, was subjected to Miyaura borylation giving 4-(4-[pinacolatoboronanyl]phenyl)benzyl alcohol (**2.5**) in approximately 22 % yield (Scheme 2.3). Unfortunately **2.5** could not be obtained in a pure form as the boronic ester moiety was found to partially hydrolyse upon exposure to any moisture. It was found that hydrolysis had no noticeable effect upon the subsequent Suzuki couplings and so later syntheses involved its use without further purification beyond the removal of excess bis(pinacolato)diboron through sublimation under vacuum.

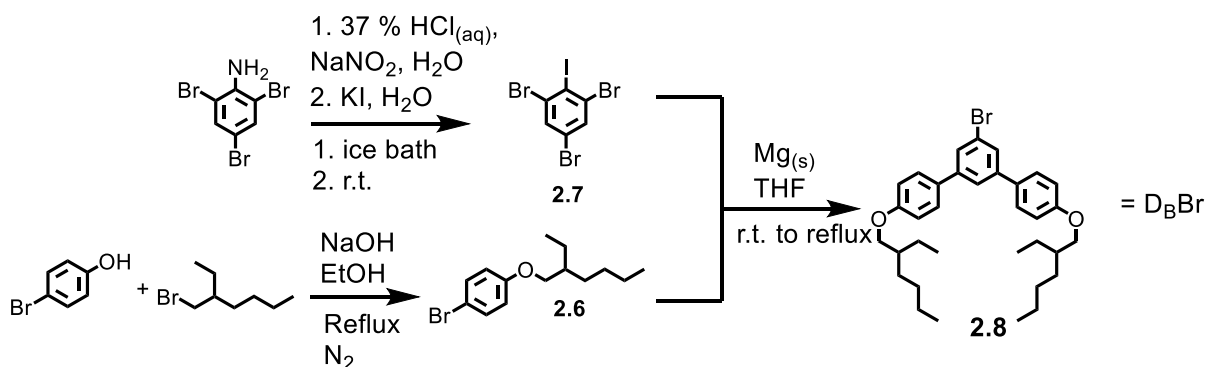


Scheme 2.3: Synthetic scheme of lengthened tether.

### 2.2.3 Dendrons

The first generation, biphenyl dendron ( $D_B$  moiety) was prepared using a convergent synthesis. Synthesis of the surface groups was accomplished via the Williamson ether synthesis of 4-bromophenyl and 2-ethylhexyl bromide to give 1-bromo-4-([2-ethylhexyl]oxy)benzene (**2.6**, 76 % yield). The central aryl moiety was synthesized from 2,4,6-tribromoaniline by a modified Sandmeyer reaction to give 1,3,5-tribromo-2-iodobenzene (**2.7**) in 51 % yield.

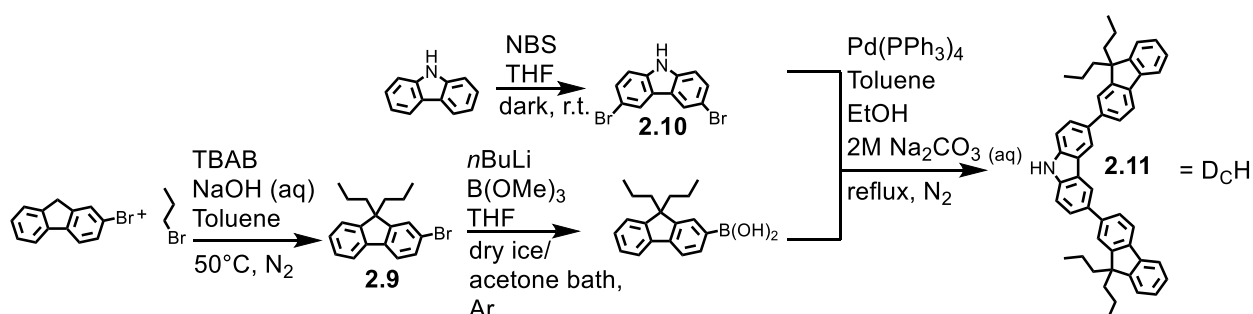
The formation of the desired biphenyl-dendron bromide (**2.8**) was carried out by modification of a the *m*-terphenyl synthesis reported by Du *et al* (Scheme 2.4).<sup>154</sup> The reaction mechanism begins with formation of the Grignard reagent of **2.6** in excess allowing a metal-halogen exchange with the aryl iodide of **2.7**. Elimination of magnesium halide affords the reactive benzyne intermediate *in situ*. Nucleophilic addition of metallated **2.6** onto the benzyne intermediate occurs followed by a second elimination of magnesium bromide and a final nucleophilic addition to give the *m*-terphenyl anion. Protonation gave **2.8** in 20 % yield.



Scheme 2.4: Synthesis scheme of first generation biphenyl-dendron.

The synthesis of the first generation, carbazoyl-dendron was also convergent. Bromination of carbazole with *N*-bromosuccinimide gave 3,6-dibromo-9*H*-carbazole (**2.10**, 97 %) and base catalysed alkylation of 2-bromo-9*H*-fluorene with *n*-propyl bromide gave 2-bromo-9,9-dipropyl-9*H*-fluorene (**2.9**, 80 %). The boronic acid of **2.9** was produced by lithiation/ borylation and was subsequently coupled without further purification to **2.9** under

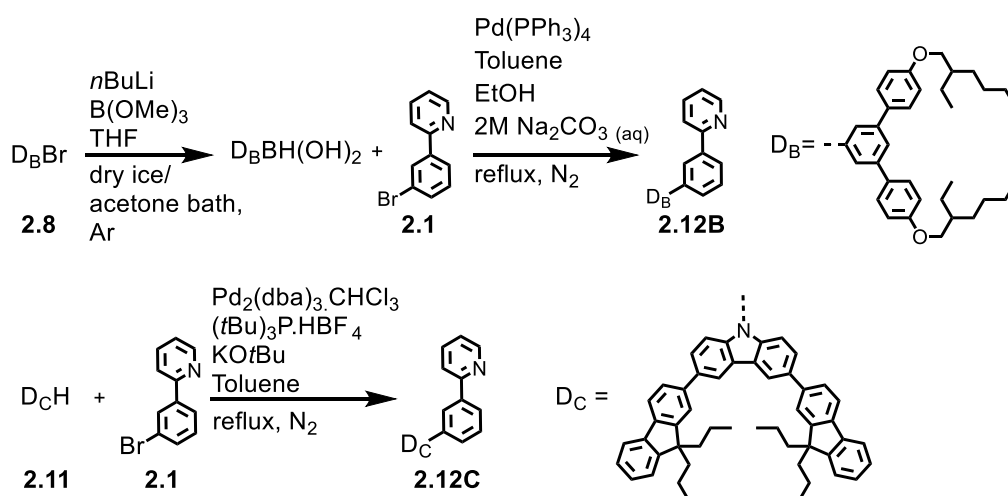
aqueous Suzuki coupling conditions giving the carbazolyl-dendron (**2.11**) with a two-step yield of 35 %.



Scheme 2.5: Synthesis scheme of first generation carbazolyl-dendron.

## 2.2.4 Dendronized Ligands

The dendronized ligands were both prepared via palladium(0) coupling onto **2.1**. The brominated biphenyl-dendron **2.8** was first converted to the boronic acid by lithiation and borylation. This was then reacted with **2.1** under Suzuki coupling conditions to give the first generation, biphenyl, dendronized ligand (**2.12B**, 68 %). The carbazolyl-dendron was similarly coupled to **2.1** under Buchwald-Hartwig amination conditions giving the alternate the first generation, carbazolyl, dendronized ligand (**2.12C**, 86 %).



Scheme 2.6: Synthetic scheme of dendronized ligands

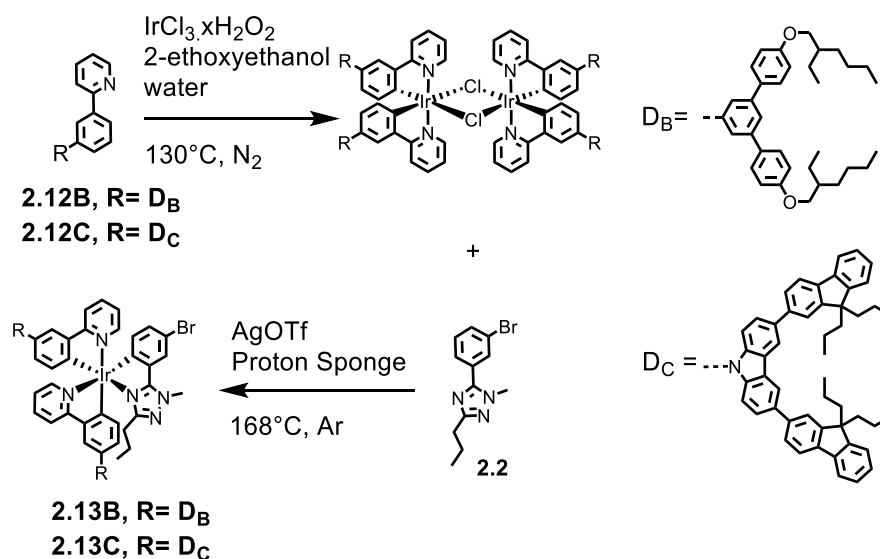
## 2.2.5 Complexation and monomer synthesis

With the formation of both dendronized ligands the synthetic pathway becomes analogous with only the dendrons being dissimilar. The desired iridium(III) complex is formed via the commonly encountered modification to the Nonoyama route. A mixture of dendronized ligand ( $D_B$ : **2.12B** or  $D_C$ : **2.12C**) in azeotropic 2-ethoxyethanol/ water was



heated in a bath at 130°C in the presence of iridium(III) chloride hydrate to give the canary yellow  $\mu$ -chloro dimer.

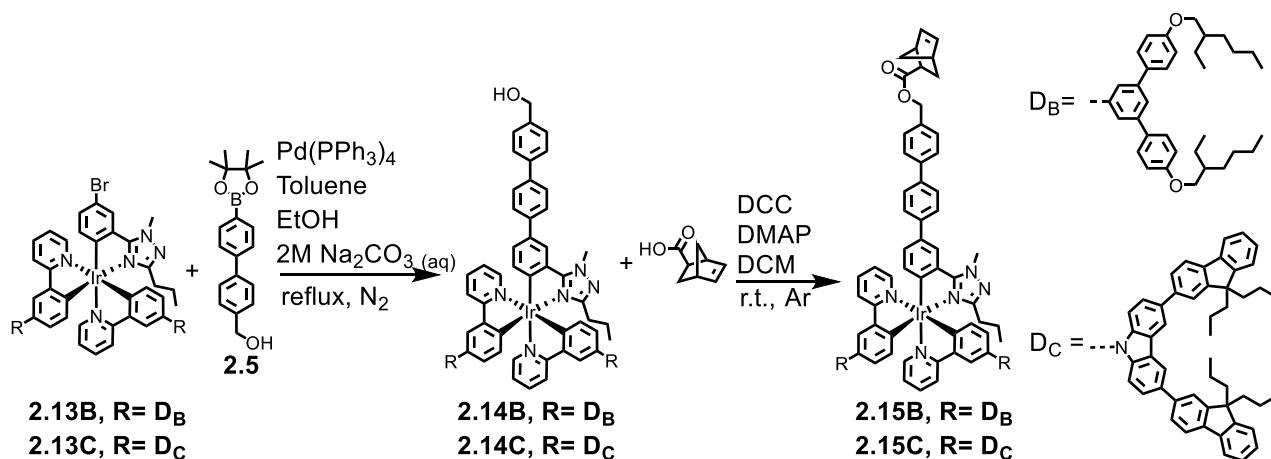
After aqueous workup and removal of all solvent final *ortho*-metallation was accomplished by suspension of the dimer, silver(I) triflate and 'proton sponge' (*N,N,N',N'*-Tetramethyl-1,8-naphthalenediamine) in excess ancillary ligand **2.2**. The mixture was heated in an oil bath set at 168°C with stirring in an attempt to homogenize the melt. It has been shown that the thermodynamic product, the *facial* isomer, forms exclusively (to the limits of detection) when the chelation is performed at this temperature.<sup>140</sup> There is a compromise, however, as formation of the *facial* isomer from the  $\mu$ -chloro dimer requires rearrangement of the dendronized ligands which results in lower yields for heteroleptic complexes as other *facial* iridium(III) complexes are formed with different ratios of dendronized ligand to ancillary ligand. In both cases the desired complex was isolated ligand over the two-steps (D<sub>B</sub>: **2.13B**, 14 % yield or D<sub>C</sub>: **2.13C**, 23 % yield). For both **2.13B** and **2.13C**; the proton signals originating from the dendronized ligands of were observed to be equivalent by <sup>1</sup>H NMR spectroscopy which strongly indicates exclusive formation of the *facial* isomer.



Scheme 2.7: Synthetic scheme of cyclometallated complex

A Suzuki coupling was performed to attach the tether (**2.5**) to the ancillary ligand of the iridium(III) complex (D<sub>B</sub>: **2.13B** or D<sub>C</sub>: **2.13C**). When the biphenyl-dendron containing complex (**2.13B**) was used, the resultant alcohol (**2.14B**) was able to be isolated as a pure material in 69 % yield. This material was then subjected to a Steglich esterification with *exo*-5-norbornenecarboxylic acid to give the monomer (**2.15B**) in 38 % yield. The carbazolyl-dendron alcohol analogue, **2.14C**, contained a trace impurity that could not be identified or

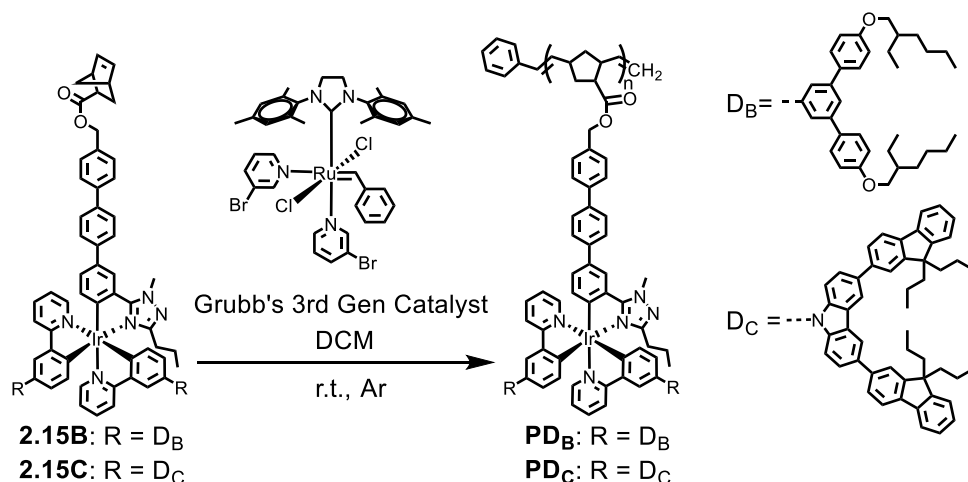
removed. As such it was carried through the same Steglich esterification step to give the monomer (**2.15C**), which could be obtained in a pure state with a two-step yield of 51 %. From analysis of the crude  $^1\text{H}$  NMR and thin layer chromatography the reaction yields for the alcohol (**2.13B**) and the monomers (**2.15B** and **2.15C**) were likely close to quantitative, however, significant losses of mass were observed during purification by column chromatography over silica which was required to remove trace impurities. If these losses could be avoided the yields would likely have been considerably higher.



Scheme 2.8: Synthetic scheme of monomer

## 2.2.6 Polymerization

Synthesis of the first poly(dendrimer) ( $\text{PD}_\text{B}$ ) by ring-opening olefin-metathesis polymerization (ROMP) of **2.15B** was attempted using the conditions as reported by Wen-Yong Lai *et al.*<sup>108</sup> Commercial Grubbs 3<sup>rd</sup> Generation catalyst in tetrahydrofuran was added to the monomer solution in tetrahydrofuran and the reaction progress was monitored by thin layer chromatography (monomer: catalyst, 100:1).



Scheme 2.9: Polymerization synthetic scheme

Unexpectedly the reaction proved very sluggish and was left to stir for four days in hopes that it would continue. The reaction was quenched with ethyl vinyl ether; although it is likely that the polymerization had already terminated before this time. Due to the large proportion of unreacted monomer, determined by TLC and gel permeation chromatography (GPC), remaining in the mixture the literature method of purification of precipitation into methanol proved ineffective at achieving separation. The polymer was eventually isolated by size exclusion chromatography utilizing BioRad Laboratories Bio-Beads S-X1 Support #1522151 with tetrahydrofuran as the mobile phase (36 %, GPC:  $M_n = 41,557$  Da,  $\bar{D} = 2.33$ ). The expected molecular weight of a polymer can be estimated as the product of the monomer: catalyst ratio (in this case 100) and the molecular weight of the monomer measured by GPC (**2.15B**  $M_n = 2162$  Da). Although the molecular weights determined by GPC often vary from the true molecular weights (inherently due to the mechanism of separation and the size-shape interaction) the predicted molecular weight of approximately 200 kDa were far from the measured  $M_n$  of 42 kDa. This, in combination with the low yield and high dispersity index (living polymerization  $\bar{D} \leq 1.2$ ), indicated that the polymerization was not progressing as the desired living polymerization.

Examination of the literature indicated that tetrahydrofuran, although an adequate solvent for ROMP, was not the optimal solvent due to the coordination of the solvent oxygen decreasing catalyst reactivity. The commercial catalyst was also found by  $^1\text{H}$  NMR to have degraded on storage indicated by a strong benzaldehyde signal and diminished ylidene proton signal. All future polymerizations were conducted using in-house Grubbs 3<sup>rd</sup> generation catalyst prepared from the more stable Grubbs 2<sup>nd</sup> generation catalyst.

A final polymerization of **2.15B** was conducted utilizing dichloromethane as the solvent. The reaction proceeded much better than the previous attempt with **PD<sub>B</sub>** being isolated in 72 % yield (GPC:  $M_n = 64,837$  Da,  $\bar{D} = 2.09$ ). Although a considerable improvement over the previous polymerizations, the broad dispersity index indicated that the desired living polymerization remained elusive.

The monomer **2.15C** in dichloromethane was subjected to ring-opening olefin-metathesis polymerization upon addition of Grubbs' 3<sup>rd</sup> Generation catalyst (dichloromethane solution 100:1, monomer:catalyst) to afford the second poly(dendrimer) (**PD<sub>C</sub>**) in 39 % yield (GPC:  $M_n = 77,165$  Da,  $\bar{D} = 3.86$ ). As in the case of **PD<sub>B</sub>**, it can be concluded that the polymerization to form **PD<sub>C</sub>** did not proceed in the fashion of a living polymerization.

Conducting polymerizations for optimization would have been ideal, however, difficulties in isolating enough of the pure monomers hindered further experiments. The

quantities of **PD<sub>B</sub>** and **PD<sub>C</sub>** were sufficient for preliminary analysis. During these polymerizations there was no indications of having greater control by employing a longer tether as the polymerizations to form **PD<sub>B</sub>** and **PD<sub>C</sub>** appeared to give dispersity indices further away from the ideal of a living polymer than the short-tether literature poly(dendrimer)s, **L1** and **L2**.

## 2.3 Properties of green-emitting poly(dendrimer)s

### 2.3.1 Photophysical

This section describes the photophysical properties of poly(dendrimer)s, **PD<sub>B</sub>** and **PD<sub>C</sub>**. All photophysical measurements were performed by Fatemeh Maasoumi. UV-vis absorption and photoluminescence spectra of **PD<sub>B</sub>** and **PD<sub>C</sub>** in solution, neat film and 20 wt% blended with CBP host were measured (Figure 2.2).

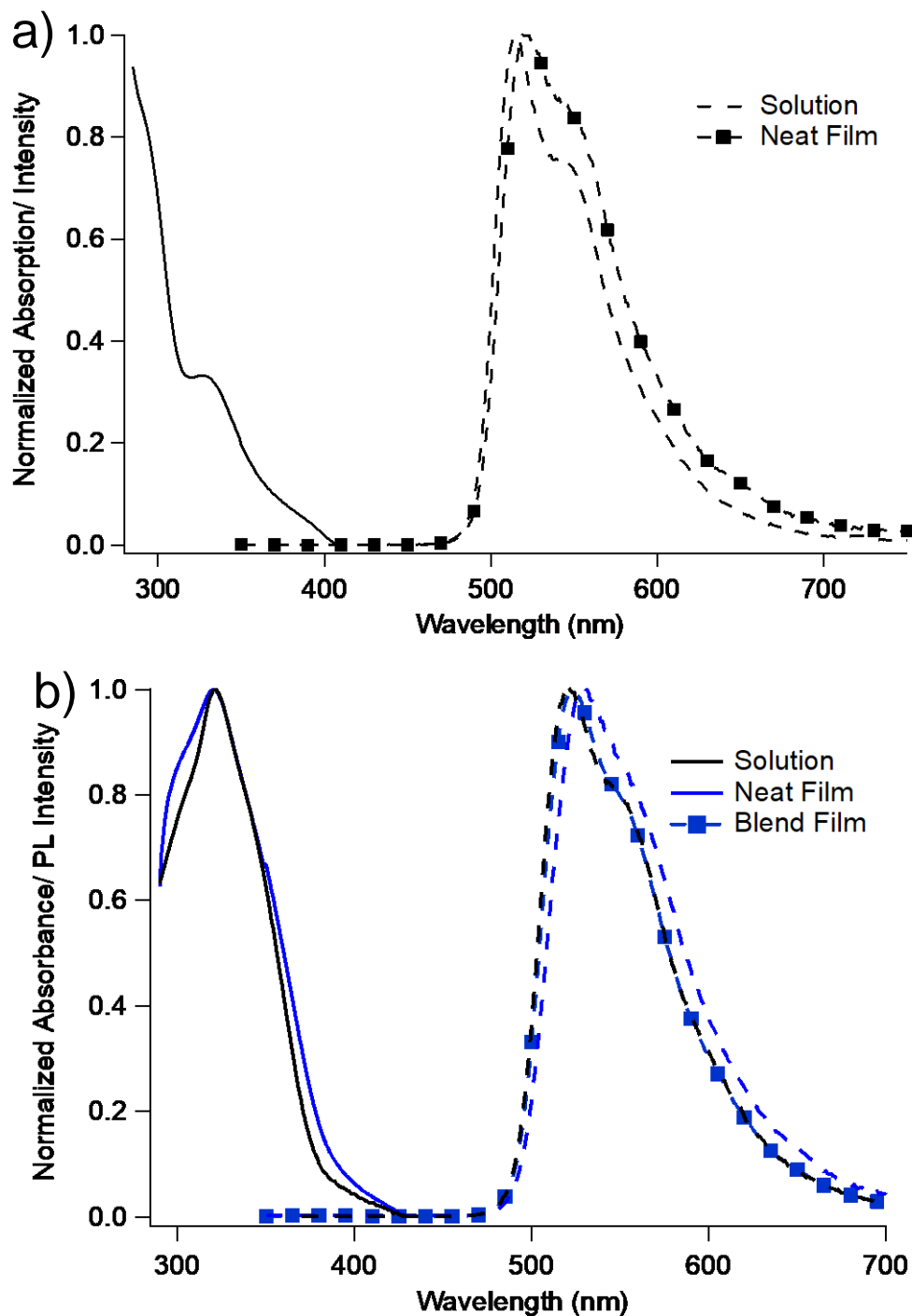


Figure 2.3: Normalized Absorption and Emission Spectra of **PD<sub>B</sub>** (a) in solution (toluene) and neat film; and **PD<sub>C</sub>** (b) in solution (toluene), as a neat and blended film (20 wt% in CBP)

The primary transitions giving rise to the observed solution absorption spectra of both **PD<sub>B</sub>** and **PD<sub>C</sub>**, shown in Figure 2.2, can be grouped into either metal-to-ligand charge transfer (MLCT) transitions or  $\pi$ - $\pi^*$  transitions arising from the aromaticity of the dendrons and ligands. For **PD<sub>B</sub>** and **PD<sub>C</sub>**, transitions observed at wavelengths longer than 350 nm and 380 nm respectively are attributed to MLCT transitions. The MLCT transitions are characteristically much weaker than the  $\pi$ - $\pi^*$  transitions observed at the shorter wavelengths. The maxima at 326 nm (**PD<sub>B</sub>**) and 321 nm (**PD<sub>C</sub>**) are attributed to the chromophores with the largest conjugation length, biphenyl and fluorenyl respectively, within the dendrons.

The solution photoluminescence spectra of **PD<sub>B</sub>** and **PD<sub>C</sub>** display emission maxima at 515 nm and 521 nm, respectively. Both polymers exhibit a second maxima attributed to the next vibronic transition of the triplet emission. Upon transitioning from solution to neat-film the emission maxima of **PD<sub>B</sub>** remains unchanged at 515 nm while a slight red-shift is observed for **PD<sub>C</sub>** to 531 nm. This behaviour is consistent with the literature poly(dendrimer)s where the biphenyl-dendronized (**L1**) is shown to have an emission maxima of 517 nm in both solution and neat-film while carbazolyl-dendron variant (**L2**) exhibits a 10 nm red-shift from 520 nm to 530 nm going from solution to neat film, respectively.

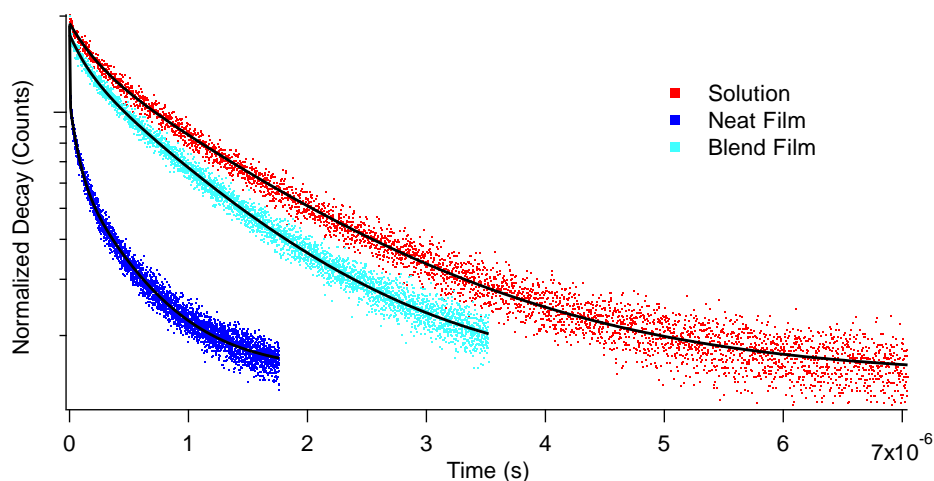


Figure 2.4: Normalized TCSPC Decay Profiles of **PD<sub>C</sub>** in solution (toluene), as a neat film and blended film (20 wt% in CBP)

Table 2.3. Summary of green-emitting iridium(III) poly(dendrimer) photoluminescent properties.

	Solution			Neat Film			Blend Film		
	$\lambda_{\max}^{\text{Em}}$ (nm)	$\Phi_{\text{PL}}$ (%)	$\tau_{\text{obs}}$ ( $\mu\text{s}$ )	$\lambda_{\max}^{\text{Em}}$ (nm)	$\Phi_{\text{PL}}$ (%)	$\tau_{\text{obs}}$ ( $\mu\text{s}$ )	$\lambda_{\max}^{\text{Em}}$ (nm)	$\Phi_{\text{PL}}$ (%)	$\tau_{\text{obs}}$ ( $\mu\text{s}$ )
<b>L1</b>	517	65	1.4	517	44	0.73			
<b>L2</b>	520	72	1.5	530	35	0.49*	524	74	1.3*
<b>PD<sub>B</sub></b>	515	55	0.99*	515	15				
<b>PD<sub>C</sub></b>	521	56	1.2*	531	21	0.32*	524	55	1.0*

<sup>a</sup>Photoluminescent (PL) spectra, lifetime, and quantum yields were recorded in toluene at an optically dilute (Abs = ~0.10 A.U. at PL excitation wavelength) concentrations. <sup>b</sup>Solution quantum yield measurements were recorded against quinine sulphate in 0.5 M sulfuric acid as external standard ( $\Phi_{\text{PL}} = 55\%$ ,  $\lambda_{\text{exc}} = 350\text{ nm}$ ). <sup>c</sup>Calculated from by TCSPC with 372 nm diode. \*Weighted average of observed lifetimes.<sup>108,142</sup> Shaded values were not reported or not measured.

To further characterize the photophysical properties of the poly(dendrimer)s photoluminescent (PL) quantum yields ( $\Phi_{\text{PL}}$ ) and the PL lifetimes ( $\tau$ ) were measured. The results are detailed in Table 2.1. Both poly(dendrimer)s that contained the extended biphenyl tether had lower photoluminescent quantum yields in solution and as neat films compared to the shorter tether literature equivalents. The drop in quantum yield is particularly large in the neat films (>50 %) compared to in solution (around 20 %).

The measured PL lifetimes of **PD<sub>B</sub>** and **PD<sub>C</sub>** in solution had to be fitted using a two exponential components which was not consistent with the single exponential decays observed for **L1** and **L2** in solution. This indicates that a second decay pathway is present in the photoluminescence of **PD<sub>B</sub>** and **PD<sub>C</sub>** in solution. As the experiments were performed on optically dilute solutions, any interactions are expected to be limited to between neighbouring pendants of the same polymer chain (intrachain, interchromophore). Both **PD<sub>B</sub>** and **PD<sub>C</sub>** also showed greater decreases in PL lifetime in neat films when compared to **L1** and **L2** which is likely resulting from increased incidence of deleterious interchain, interchromophore interactions. It is then reasoned that the increase to the tether length led to increasing interchromophore interactions between both neighbouring pendants within the same chain (intrachain) and those of other chains packing nearby (interchain).

In an attempt to determine why the increased tether length resulted in increased interchromophore interactions the radiative ( $k_{\text{R}}$ ) and non-radiative ( $k_{\text{NR}}$ ) decay rates can be

calculated (equations 2.1.a and 2.1.b) and compared (Table 2.4). While not ideal, the calculations had to be simplified by using the weighted average PL lifetimes whenever multi-exponential decays were observed.

Equation 2.1:

$$\text{a) } \Phi_{\text{PL}} = k_{\text{R}} / (k_{\text{R}} + k_{\text{NR}})$$

$$\text{b) } 1/\tau_{\text{obs}} = k_{\text{R}} + k_{\text{NR}}$$

Table 2.4. Comparison of radiative and non-radiative decay lifetimes

	Solution		Neat Film		Blend Film	
	$k_{\text{R}} (\text{s}^{-1})$	$k_{\text{NR}} (\text{s}^{-1})$	$k_{\text{R}} (\text{s}^{-1})$	$k_{\text{NR}} (\text{s}^{-1})$	$k_{\text{R}} (\text{s}^{-1})$	$k_{\text{NR}} (\text{s}^{-1})$
<b>L1</b>	$4.6 \times 10^5$	$2.5 \times 10^5$	$6.0 \times 10^5$	$7.7 \times 10^5$		
<b>L2</b>	$4.8 \times 10^5$	$1.9 \times 10^5$	$7.1 \times 10^5$	$1.3 \times 10^6$	$5.7 \times 10^5$	$2.0 \times 10^5$
<b>PD<sub>B</sub></b>	$5.6 \times 10^5$	$4.5 \times 10^5$				
<b>PD<sub>C</sub></b>	$4.7 \times 10^5$	$3.7 \times 10^5$	$6.6 \times 10^5$	$2.5 \times 10^6$	$5.5 \times 10^5$	$4.5 \times 10^5$

Shaded values were not reported (**L1**) or not measured (**PD<sub>B</sub>**).

The radiative decay rates ( $k_{\text{R}}$ ) of the poly(dendrimer)s in solution were very similar all falling between  $4.6 \times 10^5 \text{ s}^{-1}$  and  $5.6 \times 10^5 \text{ s}^{-1}$ . This indicates that the emissive chromophores are essentially identical in all four poly(dendrimer)s. It can be concluded that any differences observed when the long tether is present do not originate from changes in the emissive species but are from environmental interactions; for example increased interchromophore triplet-triplet annihilation rates. This is supported by the absence of differences in the photoluminescence spectra between tether lengths.

The non-radiative decay rates ( $k_{\text{NR}}$ ) of **PD<sub>B</sub>** and **PD<sub>C</sub>** in solution were observed to be approximately twice that of the literature materials. Due to the errors associated with the fitting parameters the absolute differences are likely insignificant, however, the additional solution PL decay component observed for **PD<sub>B</sub>** and **PD<sub>C</sub>** would support the long tether poly(dendrimer)s having greater non-radiative decay rates than **L1** and **L2**.

The radiative and non-radiative decay rates of **PD<sub>C</sub>** in the neat film were observed to be on the same order of magnitude as the corresponding literature material, however, the decay of **PD<sub>C</sub>** could only be accurately fitted to a model containing three decay components while **L2** only exhibited two. This cast considerable doubt on whether the similarities were significant.



While the lifetimes and rates obtained from the fitted data may be ambiguous, the presence of an additional decay component in the time-resolved PL measurement of **PD<sub>c</sub>** as a neat film was a significant feature. As an additional PL decay component was also observed for **PD<sub>c</sub>** in solution when compared to **L2**, it was proposed that the additional PL decay component in the neat film shares the same pathway. From this it is likely the three decay pathways which contribute to the time-resolved PL measurement of **PD<sub>c</sub>** as a neat film were; the radiative pathway, the non-radiative interchain pathway and the non-radiative intrachain pathway.

The radiative and non-radiative decay lifetimes of the carbazoyl-dendron containing **PD<sub>c</sub>** and **L2** blended in CBP mirrored the values observed in solution. It can be concluded that the host was effective at separating the polymer chains preventing the increased interchromophore interactions observed for the neat films.

Ultimately the reduced photoluminescent quantum yields combined with the additional decay component observed in the solution, which appears to carry through to the neat film, indicated that increasing the tether length through addition of a phenyl moiety causes deleterious intrachain, interchromophore interactions that appear absent in materials featuring the shorter tether. The emission spectra of **PD<sub>B</sub>** and **PD<sub>c</sub>** are almost identical to their parent poly(dendrimer)s and the calculated radiative decay rates ( $k_R$ ) of all four materials are very similar suggesting that the emissive pathway is unaltered by the additional phenyl moiety. This provides further evidence that the structural modification to lengthen the tether had introduced a non-radiative intrachain decay pathway which resulted in increased non-radiative decay rates.

Photoelectron spectroscopy in air (PESA) measurements were performed by Dr Dani Stoltzfus to obtain the ionization potential (IP) of poly(dendrimers), **PD<sub>B</sub>** and **PD<sub>c</sub>**, in neat films. From these measurements the IP of **PD<sub>B</sub>** and **PD<sub>c</sub>** were estimated to be 5.3 and 5.4 eV, respectively.

### 2.3.2 Device performance

Organic light-emitting diodes were fabricated to characterize the performance of **PD<sub>c</sub>** as an emissive material. Devices utilizing **PD<sub>B</sub>** were unable to be fabricated due to synthetic difficulties making the material unavailable during the timeframe available for device fabrication.

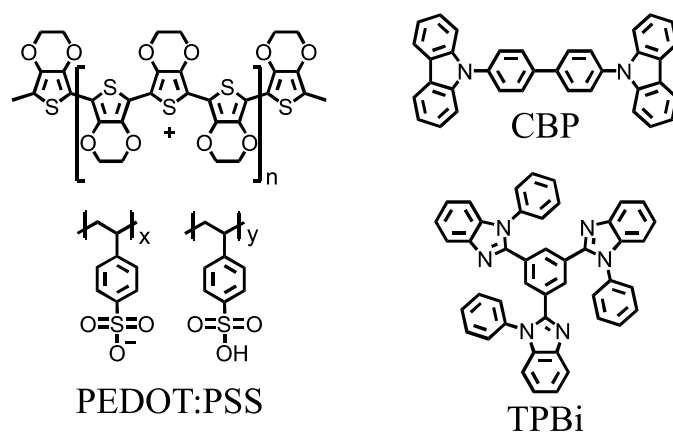


Fig 2.5. Structure of commercial materials used in devices: poly(3,4-ethylenedioxythiophene)-poly(styrenesulfonate) (PEDOT:PSS), 4,4'-bis(N-carbazolyl)-1,1'-biphenyl (CBP) and 1,3,5,-tris(2-N-phenylbenzimidazolyl)benzene (TPBi).

The devices utilized a device architecture that allowed direct comparison to the two literature poly(dendrimer)s: indium tin oxide/ PEDOT:PSS (40 nm)/ *emissive layer*/dendrimer/1,3,5,-tris(2-N-phenylbenzimidazolyl)benzene (35 nm)/ lithium fluoride (1 nm)/ aluminium (100 nm). The *emissive layer* consisted of either 50 nm of neat **PDc** (neat devices) or 50-55 nm of a 20 wt% blend of **PDc** in 4,4'-bis(N-carbazolyl)-1,1'-biphenyl (CBP) host (blend devices) deposited from solution by spin-coating. Table 2.5 contains a summary of the device performance characteristics at a luminance of 100 cd/m<sup>2</sup>. Included within this table is the average and hero devices for both neat and blend devices.

Table 2.5: Device results **PDc** at 100 cd/m<sup>2</sup>

	$\eta_{\text{ext}}$ (%)	$\eta^*$ lm/W	Turn-on Voltage* (V)	$\eta_{\text{ext}}$ (theory) (%)
Neat Average	6 ± 1	9 ± 2	5.9 ± 0.1	4
Neat Hero	7	12	5.9	4
Blend Average	10 ± 1	18 ± 2	6.0 ± 0.1	11
Blend Hero	19	38	6.2	11

\*Defined as a brightness of 5 cd/m<sup>2</sup>. The average neat film performance values was obtained from 6 pixels on one substrate, with the blend data quoted from 7 pixels on 2 substrates. Outliers, including the blend hero device, were excluded from the calculated averages.

Devices utilizing an emissive layer of neat **PDc** exhibited mediocre performance with high turn-on voltages of 5.9 ± 0.1 V, where the turn-on voltage is defined as being the first measured voltage achieving a luminance of 5 cd/m<sup>2</sup>. The devices obtained an external

quantum efficiency ( $\eta_{\text{ext}}$ ) of  $6 \pm 1 \%$  at the application relevant luminance of  $100 \text{ cd/m}^2$  and achieved maximum brightness of approximately  $10,000 \text{ cd/m}^2$  at around  $9 \text{ V}$  (Figure 2.4).

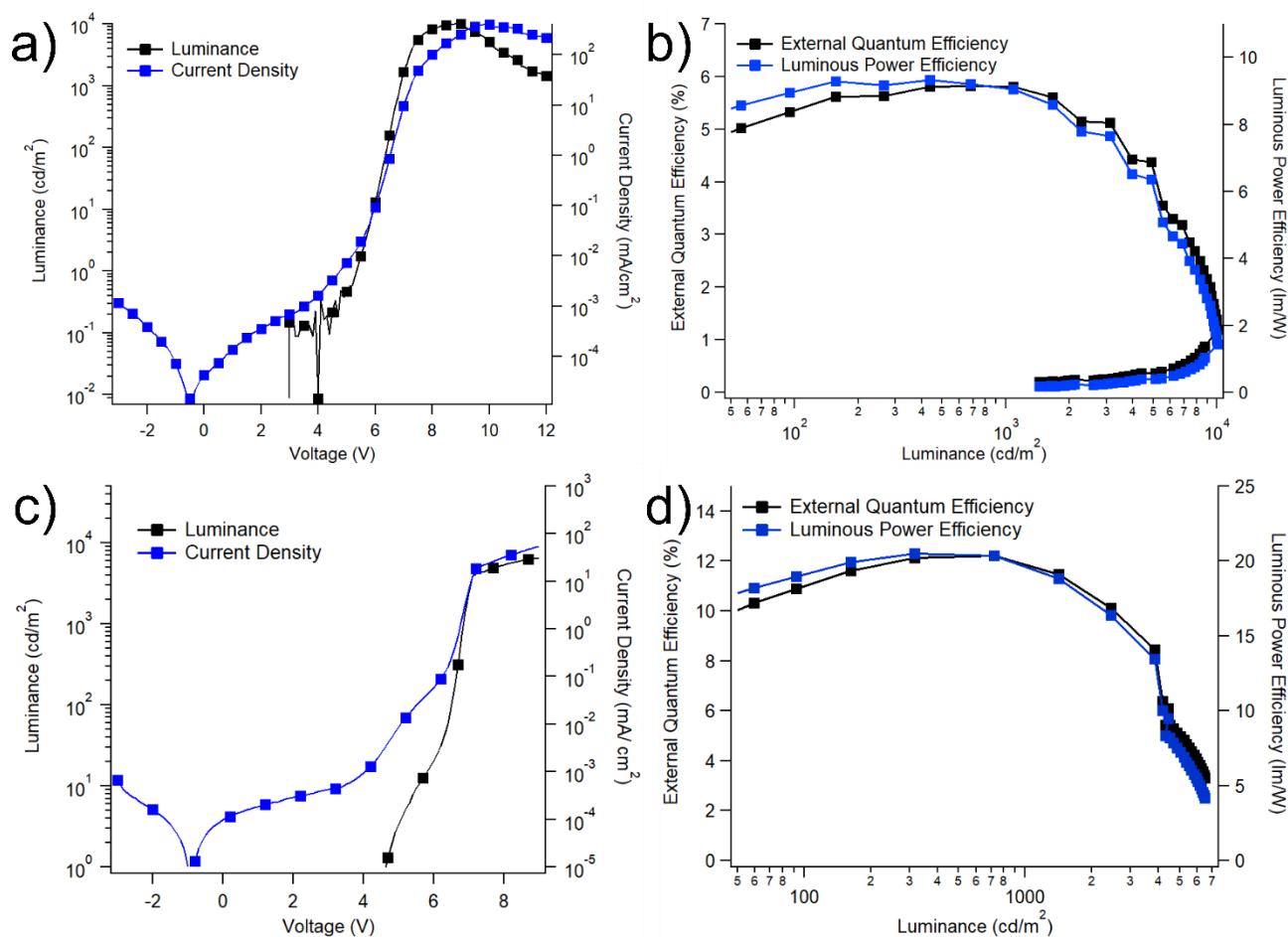


Figure 2.6: Characteristics of devices utilizing **PDC**: a) J-V-L curve of neat devices, b)  $\eta_{\text{ext}}$  and power efficiency ( $\eta^*$ ) as a function of luminance of neat devices, c) J-V-L curve of blend devices, d)  $\eta_{\text{ext}}$  and power efficiency ( $\eta^*$ ) as a function of luminance of blend devices

The blend devices utilizing a film of 20 % **PDC** blended with CBP as host exhibited the same turn-on voltage as the neat films, within error, of  $6.0 \pm 0.1 \text{ V}$ . As anticipated by the  $\Phi_{\text{PL}}$ , the  $\eta_{\text{ext}}$  of the blend devices was greatly improved reaching  $10 \pm 1 \%$  at  $100 \text{ cd/m}^2$ . The brightness of the blend devices was not observed to reach a maxima. Instead a sharp gradient change was observed above  $7 \text{ V}$  at a brightness of just over  $4,000 \text{ cd/m}^2$ . At this point the brightness gradient becomes noticeable more shallow until the measurement ceased at  $9 \text{ V}$  with a brightness of approximately  $6,500 \text{ cd/m}^2$ , considerably lower than the neat film devices. The measurements were stopped at  $9 \text{ V}$  as the blends were shown to burnout and give unreliable results beyond this point.

The electroluminescence spectra of the devices were consistent with the photoluminescence spectra of the films suggesting the emissive chromophore is identical (Figure 2.5). The spectral profile showed no indication of strong optical cavity effects. The devices produced emission within the green region with the neat devices exhibiting a more red-shifted emission. The CIE coordinates of the neat and blend devices were (0.38, 0.59) and (0.34, 0.61), respectively.

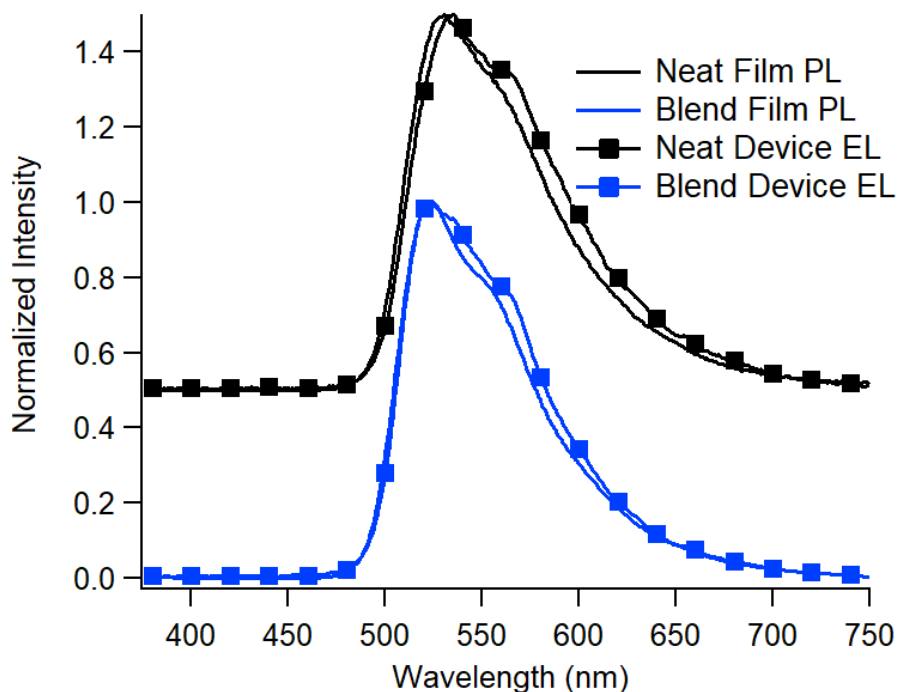


Figure 2.7: Comparison between the photoluminescence and electroluminescence of **PDc** films and devices. Neat results are offset along the y-axis for clarity.

Whilst the average device results appear to be superficially unremarkable, the values obtained are incredibly close to the theoretical external quantum efficiencies expected for devices utilizing **PDc** as an emissive species. The hero device, which was removed from the data set prior to calculating the average results to avoid bias, achieves an external quantum efficiency of 19 % at 100 cd/m<sup>2</sup> which is well beyond the theoretical achievable value. The parameters which contribute to the external quantum efficiency of an OLED are well defined within the literature by equation 2.2.

Equation 2.2.

$$\eta_{\text{ext}} = \gamma \cdot \eta_{\text{S/T}} \cdot \Phi_{\text{PL}} \cdot \eta_{\text{out}}$$

For any OLED, the external quantum efficiency ( $\eta_{\text{ext}}$ ) will equal the product of the charge balance within the device ( $\gamma$ ), the singlet/triplet harvesting efficiency ( $\eta_{\text{S/T}}$ ), the

photoluminescence quantum yield of the emissive layer  $\Phi_{PL}$ , and the efficiency at which the produced photons can escape from the transparent layer of the device which is referred to as the out-coupling efficiency ( $\eta_{out}$ ). If the out-coupling efficiency is not taken into account then the product is the internal quantum efficiency which describes the efficiency of photon generation.

In a perfectly optimized device the charges must be balanced within the emissive layer ( $\gamma = 1$ ). When a phosphorescent emitter is used, which is the case for **PDc**, both singlet and triplet excitons will be harvested ( $\eta_{S/T} = 1$ ). As such the maximum achievable external quantum efficiency of an optimized device employing a phosphorescent emitter within the emissive layer will be the product of the phosphorescent quantum yield of the emissive layer and the out-coupling efficiency ( $\eta_{ext} = \Phi_{PL} \cdot \eta_{out}$ ).

The out-coupling efficiency for bottom-emitting devices utilizing an indium-tin-oxide on glass anode has been established as approximately 20 % for isotropic emission within the green region. This is due to the refractive indices of the materials within the device and the atmosphere.

Therefore, the theoretical maximum  $\eta_{ext}$  for the neat and blend devices utilizing **PDc** as the emissive material can be calculated to be 4 % and 11 %, respectively. The obtained average efficiencies for the blend devices are within the region of the theoretical maximum with  $\eta_{ext} = 10 \pm 1$  % at 100 cd/m<sup>2</sup>. The situation changes when examining both the hero blend device, which achieved  $\eta_{ext}$  of 19 % at 100 cd/m<sup>2</sup>, and the neat devices, which averaged  $6 \pm 1$  % at 100 cd/m<sup>2</sup>, both significantly surpassing the maximum theoretical values based upon the  $\Phi_{PL}$  of the layers.

To obtain external quantum efficiencies greater than those predicted by equation 2.2, at least one other effect must be in play to alter one of the variables. The primary causes of this discrepancy identified within the literature for phosphorescent emitters are either enhancement through strong optical cavity effects or deviation from the assumed isotropic emission. The emission of **L2** utilizing the same device architecture was examined and found to be Lambertian within experimental error.<sup>142</sup> From this it can be concluded that the devices containing **PDc** are extremely unlikely to be experiencing enhancement from optical cavity effects leaving alignment resulting in anisotropic emission as the only alternative.

Chromophore alignment resulting in anisotropic emission is well established within the literature for evaporation processed devices and has generally been attributed to dipole alignment. While alignment of solution-processed fluorescent emitters has been observed, the same alignment of phosphorescent emitters during solution-processing was thought to

be impossible as the interfacial interactions driving dipole alignment are absent in this regime.<sup>144</sup>

Due to the heteroleptic nature of **PDc** it is known that each chromophore must exhibit anisotropic emission, however, it has been assumed that during solution-processing there would be insufficient interactions to drive any preferential orientation during deposition giving random orientation and isotropic emission. These results suggest that the orientation of **PDc** deviates considerably from being perfectly random; giving rise to chromophore alignment resulting in anisotropic emission and enhanced out-coupling efficiency. This alignment appears to be partially disrupted by the host in the blend devices where the average external quantum efficiency does not surpass the theoretically achievable maximum.

### 2.3.3 Device performance: Comparison of L2 and PDc

After fully investigating the performance of organic light-emitting diode utilizing **PDc** a comparison can be made to the reported short tether analogue **L2**. The comparison of the average device results using both poly(dendrimer)s as either a neat or blend emissive layer alongside their photoluminescent quantum yields.

Table 2.6: Comparison of **L2**<sup>142</sup> and **PDc** average device performance at 100 cd/m<sup>2</sup> of the same device architecture

	$\eta_{\text{ext}}$ (%)	$\eta^*$ (lm/W)	Turn-on Voltage (V)	$\Phi_{\text{PL}}$ (%)
<b>L2</b> Neat	7 ± 1	13 ± 1	5.1 ± 0.1	65
<b>PDc</b> Neat	6 ± 1	9 ± 2	5.4 ± 0.2	21
<b>L2</b> Blend	12 ± 2	26 ± 4	4.9 ± 0.3	83
<b>PDc</b> Blend	10 ± 1	19 ± 2	5.8 ± 0.3	55

The lower turn-on voltages for **L2** in the neat devices was not shared by **PDc** in which no significant variation between neat and blend device turn-on voltages was observed. Despite large differences in photoluminescence quantum yield both materials achieved comparable external quantum efficiencies. Interestingly the blend devices utilizing **L2** also produced a hero device which achieved an external quantum efficiency of 29 % at 18 cd/m<sup>2</sup>. It was shown that blend devices using **L2**, in which the TPBi layer was exchanged for 1,3,5-Tri(m-pyridin-3-ylphenyl)benzene (TmPyPB), achieved external quantum efficiencies of 16 ± 3 % at above 50 cd/m<sup>2</sup> with a hero device reaching 31 % at 30 cd/m<sup>2</sup>.

This provides a strong indication that the poly(dendrimer)s containing carbazoyl-dendrimer pendant groups preferentially align in an advantageous manner during spin-coating. The lengthening of the bridge did not result in large changes to device performance despite the measured film photoluminescence quantum yields of **PDc** and **L2** being quite different.

### 2.3 Summary

The poly(dendrimer)s, **PD<sub>B</sub>** and **PD<sub>c</sub>**, were designed, synthesized and characterized to investigate the effect of increasing tether length on material performance in organic light-emitting diodes. Although initially intended to improve control during ring-opening olefin-metathesis polymerization there was no observed improvement between the longer tether materials and the previously reported analogues.

The spectroscopic properties of **PD<sub>B</sub>** and **PD<sub>c</sub>**, characterized and compared to **L1** and **L2**. Both **PD<sub>B</sub>** ( $\Phi_{\text{PL}} = 55\%$ ) and **PD<sub>c</sub>** ( $\Phi_{\text{PL}} = 56\%$ ) exhibited reduced solution photoluminescence quantum yields compared to **L1** ( $\Phi_{\text{PL}} = 65\%$ ) and **L2** ( $\Phi_{\text{PL}} = 72\%$ ). This difference became more prominent in the neat films where the phosphorescent quantum yields of **PD<sub>B</sub>** and **PD<sub>c</sub>** dropped to 15% and 21% respectively compared to 44% and 35% for **L1** and **L2**, respectively. From analysis of the radiative and non-radiative decay rates of the poly(dendrimer)s in solution and films the cause of the decreased photoluminescence quantum yield was ascertained to be the result of a non-radiative intrachain, interchromophore interaction introduced through lengthening the tether moiety.

Devices were fabricated using **PD<sub>c</sub>** as the emissive species and device performance. The green-emitting neat and blend devices achieved an average external quantum efficiencies at 100 cd/m<sup>2</sup> of  $6 \pm 1\%$  ( $9 \pm 2$  lm/W) and  $10 \pm 1\%$  ( $19 \pm 2$  lm/W) at 100 cd/m<sup>2</sup>. Additionally a hero blend device achieved 19% (38 lm/W) at the same brightness.

The efficiencies observed for the neat devices and hero blend device surpassed the theoretical maximum achievable for **PD<sub>c</sub>** with its measured  $\Phi_{\text{PL}}$ . This was consistent with the reported behaviour of **L2** which also surpassed the theoretical maximum external quantum efficiencies. It was theorized that the poly(dendrimer)s containing carbazoyl-dendrimer pendant groups exhibit preferential alignment during spin-coating which gives rise to the enhanced efficiency through anisotropic emission. While increasing the length of the tether was found to decrease the photoluminescence quantum yield of **PD<sub>c</sub>** compared to **L2**; in devices the external quantum efficiencies were comparable. Despite this the devices using **PD<sub>c</sub>** did not reach the luminous power efficiencies shown for **L2**.

# Synthesis of Red-Emitting Dendrimers and Poly(dendrimer) Containing Iridium(III) Complexes

---

*This chapter describes the design rationale and synthetic progress towards two red-emitting poly(dendrimer)s, IT1 and IT2, including synthetic difficulties that resulted in re-evaluation of the target materials. The chapter progresses to describes the design rational and synthesis of four dendrimers (Hom1, Hom2, Het1, Het2) and a poly(dendrimer) (PDcR) all containing an analogous red-emitting iridium(III) core functionalized with first generation carbazolyl-dendrons. A final small molecule analogue ([Ir(tmq)<sub>3</sub>]) was also synthesized and is included alongside the other materials. The thermal, optical and electrochemical properties of the red emitting materials are described while providing discussion on how these values are pertinent from the perspective of OLED technology.*

## 3.1 Initial Targets

### 3.1.1 Design rational

The aim behind the design, synthesis and characterization of the materials contained within this section was to investigate whether the improvements in optical properties and device results observed for poly(dendrimer)s containing carbazolyl-dendronized 2-phenylpyridine (ppy) ligated iridium(III) complexes can also be observed for an analogous red emitting iridium(III) material.

In order to provide a comparison with previous work and reduce potential compounding variables the initial targets were designed to be as similar to previous work as possible. Therefore the molecular design employed the same modular approach used for the previously reported carbazolyl-dendronized poly(dendrimer)s. While the backbone, dendron and ancillary ligand of the new targets were to be identical to the reported green-emissive poly(dendrimer)s, the iridium(III) complexes were modified to emit within the red region of the visible spectrum by replacement of the green-emitting 2-phenylpyridine ligands. Keeping the structural alterations to a minimum was deemed necessary as relatively small unnecessary changes are unlikely to be innocent.<sup>82,85,155</sup>

With the majority of the structure decided, all that remained was to choose a replacement ligand with a reported ability to produce efficient emission within the red region of the visible spectrum while also being open to the required structural modification to functionalize with the dendron. From examination of the literature a prime candidate was



found (Figure 3.1), which had good colour purity with CIE 1931 co-ordinates of (0.67, 0.33) compared to the standard Red Green Blue (sRGB) colour space ideal red of (0.64, 0.33) and a  $\Phi_{\text{PL}}$  of 55 %.<sup>156</sup> The emissive ligands of the heteroleptic iridium(III) complex employ 4-methyl-2-(thiophen-2-yl)quinoline (tmq) as the ligand, which forms the emissive chromophore. The ease with which the ligand could be functionalized at the 5-thienyl position made it even more attractive.

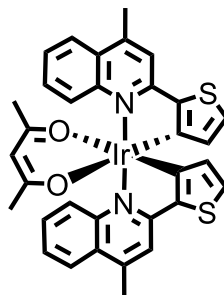


Figure 3.1: Structure of a red-emitting iridium(III) complex used to fabricate high efficiency organic light-emitting diodes reported by Cheng *et al.*<sup>156</sup>

The addition of a second dendron onto this substrate would have been more challenging. Exchanging the methyl-group for a functionalized *p*-phenyl-moiety allowed a simpler path to the doubly dendronized ligand with relatively little electronic alteration to the emissive chromophore. During the project another article was published that examined a homoleptic complex based on the 4-phenyl-2-(thiophen-2-yl)quinoline (tpq) ligand reporting that it was also a respectable red-emitting material producing organic light-emitting diodes CIE coordinates of (0.64, 0.34) and external quantum efficiencies up to 21 %.<sup>157</sup>

With the ligand system decided the other moieties could be attached to produce the singly dendronized **IT1** and the doubly dendronized **IT2** (Figure 3.2).

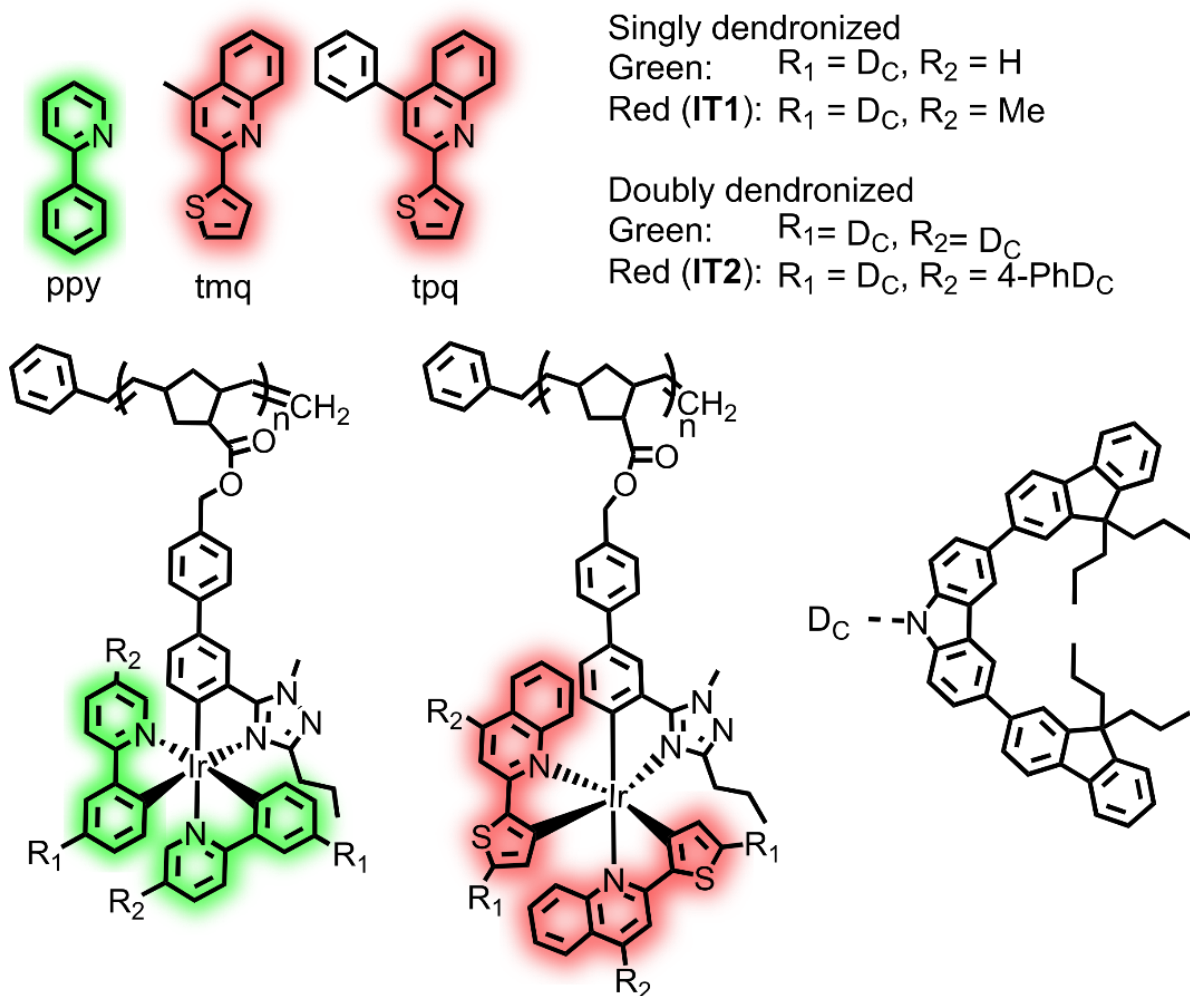


Figure 3.2: Structural relationship of previously reported green-emitting carbazolyldendronized poly(dendrimer)s and the analogous IT1 and IT2.

### 3.1.2 Synthesis

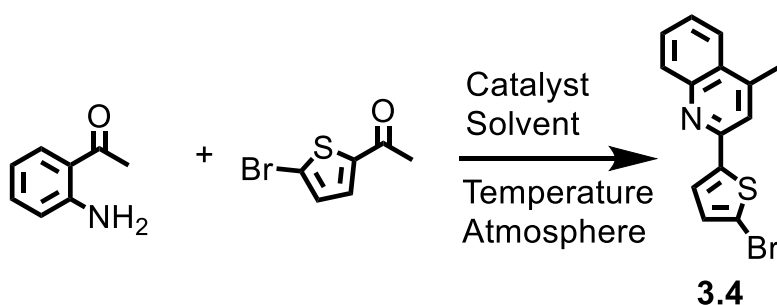
The methodology chosen for synthesis followed previous chapters in that, whenever possible, convergent routes were taken over linear synthesis. Throughout this chapter, when the products are referred to as being isolated in “trace” amounts this refers to a measured mass under 1 % of the possible yield. Many times the mass was too low to be accurately measured due to the errors associated with the much heavier standard laboratory glassware suggesting that the mass was on the order of 1 mg which in all cases would be well below 1 % of the possible yield. All cases referred to as being obtained in “trace” amounts were also unlikely to be completely dry and pure so the yields were likely even lower than those measured. In most cases the trace products obtained were only sufficient to obtain a weak  $^1H$  NMR and a mass spectrum. In all cases the mass spectra provided a strong indication that the desired product was formed. The  $^1H$  NMR were less conclusive as only the particularly intense signals were resolved, however, the integration and chemical shifts of these signals would be consistent with the desired products indicated by mass spectrometry.

Buchwald-Hartwig amination was chosen to couple **2.11**, synthesis detailed in chapter 2, to the aromatic ligands as it had proven in previous work to be the most robust coupling reaction for this particular carbazoyl-moiety. To achieve this coupling the brominated ligands, 2-(5-bromothiophen-2-yl)-4-methylquinoline (**3.4**) and 4-(4-bromophenyl)-2-(5-bromothiophen-2-yl)quinoline, were to be synthesized by Friedländer quinoline synthesis from 2-acetyl-5-bromothiophene and either 2'-aminoacetophenone or (2-aminophenyl)(4-bromophenyl)methanone, respectively (Scheme 3.1).

### 3.1.2.1 Friedländer quinoline synthesis of brominated ligands

Multiple conditions were used for the Friedländer quinoline synthesis of **3.4**. The reaction mechanism is acid catalysed and proceeds through two dehydration steps. Therefore all steps include an acid catalyst and a dehydrating reagent or condition to push the equilibrium towards product formation.

The first conditions used to produce **3.4** were those reported for the synthesis of the hydrochloride salt of the structurally related 4-methyl-2-(thiophen-2-yl)quinoline (**3.3**). The conditions involved heating a mixture of trimethylsilyl chloride, 2-acetyl-5-bromothiophene and 2'-aminoacetophenone in anhydrous *N,N*-dimethylformamide at 95°C (Scheme 3.1).<sup>158</sup> This was performed within a pressurized vessel due to the boiling point of trimethylsilyl chloride being only 57°C and the vessel was purged with nitrogen prior to adding the reactants. In this case trimethylsilyl chloride acts as both a Lewis acid and a dehydrating agent while *N,N*-dimethylformamide is the solvent. The reported methodology isolated the hydrochloride salt through precipitation and recrystallization. This did not work when 2-acetylthiophene was replaced with 2-acetyl-5-bromothiophene to give **3.4**, as a by-product hindered precipitation. The workup was modified to transform the product to the free base through treatment with alkaline aqueous solution followed by standard column chromatography over silica. The yield of **3.4** was found to be reasonable at 65 % (Table 3.1).



Scheme 3.1: Generic synthetic pathway attempted to give **3.4** with details of each attempted reaction condition are in Table 3.1.

Table 3.1: Comparison of reaction conditions for the Friedländer quinoline synthesis of **3.4**

Conditions	Catalyst	Solvent	Temperature	Atmosphere	Yield (%)
1	Me <sub>3</sub> SiCl	DMF	95°C	nitrogen	65
2	conc. H <sub>2</sub> SO <sub>4</sub>	acetic acid	reflux	nitrogen	0 <sup>†</sup>
3	PTSA.H <sub>2</sub> O	melt	100°C	air	n/a <sup>‡</sup>
4	PTSA.H <sub>2</sub> O	toluene	reflux	nitrogen	94*

<sup>†</sup>No traces of product were observed so the yield is reported nominally as 0. <sup>‡</sup>Product observed by thin layer chromatography (TLC), however, isolation of pure material to determine yield was not possible due to by-products. \*Conducted using Dean-Stark apparatus.

Although the first conditions proved effective multiple times, the inherent safety issues of using a pressurized vessel led to the search for an alternative synthetic route. The second conditions utilized a more generic acidic-dehydrating environment of catalytic concentrated sulfuric acid (97 %) in acetic acid as the solvent with heating at reflux under an inert atmosphere. Under these conditions thin layer chromatography showed an absence of any product. At the same time the starting 2'-aminoacetophenone was completely consumed while the band co-eluting with 2-acetyl-5-bromothiophene was still extremely intense on the TLC plate. The presence of many additional bands in the thin layer chromatography indicated that only undesirable products were being produced under these conditions. A repeated synthesis under these conditions was conducted which confirmed these results.

Another article suggested promising yields for Friedländer quinoline syntheses could be obtained through heating a mixture of the starting materials and *p*-toluenesulphonic acid (PTSA) in the melt at 100°C open to the atmosphere.<sup>159</sup> In this case the molten *p*-toluenesulphonic acid acts as both the catalyst and the solvent. The authors speculated that the high yields were obtained due to water being allowed to escape out of the open system shifting equilibrium towards the products. The third reaction conditions involved heating the starting materials in Scheme 3.1 with *p*-toluenesulphonic acid monohydrate (PTSA.H<sub>2</sub>O) at 100°C in air. As previously, this was performed in duplicate. Both attempts were followed by thin layer chromatography, which indicated the presence of product. However, the formation of multiple by-products was observed. It was theorized that these were the result of aerobic oxidation of either the starting materials, products or intermediates. The isolation of the product proved exceptionally challenging and an accurate yield could not be obtained.

As the third conditions had shown promise with the exception of by-product formation, they were modified so the reaction could be performed under an inert atmosphere while still

removing water from the system to shift the equilibrium towards product formation. The fourth reaction conditions were performed using a mixture of 2-acetyl-5-bromothiophene and 2'-aminoacetophenone with *p*-toluenesulphonic acid monohydrate as the catalyst in toluene heated at reflux under a nitrogen atmosphere. A Dean-Stark apparatus was employed to remove water from the system via the toluene-water azeotrope. As shown in Table 3.1, these conditions proved the most effective with **3.4** being isolated in 92 % yield.

Prior to departing from the initial Friedländer quinoline synthesis conditions the synthesis of the ligand with two aryl bromide functionalities was synthesized. A mixture of 2-acetyl-5-bromothiophene and (2-nitrophenyl)(4-bromophenyl)methanone (**3.1**) in *N,N*-dimethylformamide with trimethylsilyl chloride was heated at 95°C in a pressurized vessel to give the ligand, 4-(4-bromophenyl)-2-(5-bromothiophen-2-yl)quinoline, in 38 % yield.

While <sup>1</sup>H NMR and mass spectrometry indicated that the isolated material was the product; full characterization of this material was not performed as difficulties, discussed in the following section, resulted in the re-evaluation of the target materials and synthetic routes which did not include 4-(4-bromophenyl)-2-(5-bromothiophen-2-yl)quinoline.

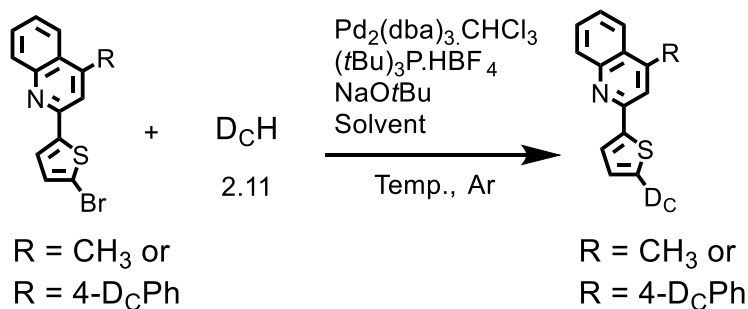
The synthetic details of the precursors commercially unavailable, (2-nitrophenyl)(4-bromophenyl)methanone (**3.1**) and (2-aminophenyl)(4-bromophenyl)methanone (**3.2**), are described in section 3.2.2.1 alongside the syntheses in which they were successfully employed.

### 3.1.2.2 Buchwald-Hartwig amination and cyclometallation

The Buchwald-Hartwig aminations were conducted on both the single and doubly brominated ligand under previously used conditions (Scheme 3.2). This involved heating the ligands in refluxing the aryl bromide and carbazoyl-dendron in either toluene or xylene utilizing tris(dibenzylideneacetone)dipalladium(0)-chloroform adduct/ tri-*tert*-butylphosphonium tetrafluoroborate as the catalyst in the presence of sodium *tert*-butoxide as base.

The amination of the singly brominated ligand by the carbazoyl-dendron proceeded in refluxing toluene in 65 % yield, however, the doubly dendronized ligand was not formed under these conditions with much of the starting material remaining. Common wisdom suggested that attempting the reaction at higher temperature would assist the reaction in coupling to two sites. The temperature of the reaction was increased by performing the Buchwald-Hartwig amination of the doubly brominated ligand in refluxing xylene. The result matched the reaction performed in toluene with no observed product formation and the starting materials remained. To confirm these results the amination was performed again in

refluxing xylene with both the singly brominated ligand (**3.4**) and the doubly brominated ligand. In both cases the reaction did not proceed with only starting materials observed. Since the amination of **3.4** proceeded in refluxing toluene, it was determined that higher temperatures must result in the catalyst becoming poisoned by a by-product or competing mechanism.

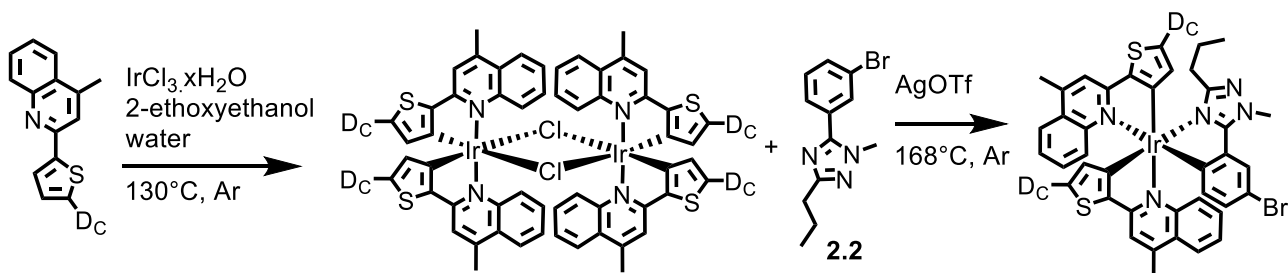


Scheme 3.2: Buchwald-Hartwig amination to give singly and doubly dendronized ligand.

Concurrently the cyclometallation of iridium(III) chloride hydrate by the singly dendronized ligand was conducted in aqueous 2-ethoxyethanol at 130 °C. This appeared to work well to give the deep red  $\mu$ -chloro-bridged iridium(III) dimer in approximately quantitative yield. The subsequent cyclometallation of the  $\mu$ -chloro-bridged iridium(III) dimer by **2.2** was performed heating in an oil bath at 168 °C with silver(I) triflate as a chloride scavenger (Scheme 3.3).

An extremely faint band was observed by thin layer chromatography which exhibited reasonable polarity and phosphorescent red-emission. The band was isolated but only trace material was obtained and it was too little to obtain an accurate weight (< 1 mg). The traces were just sufficient for analysis by mass spectroscopy and to obtain a very weak <sup>1</sup>H NMR. The most intense pattern observed in the mass spectrum matched the expected pattern for the desired product. Signals believed to originate from both ligands were observed in the <sup>1</sup>H NMR and, although weak, the integration matched with the expected.

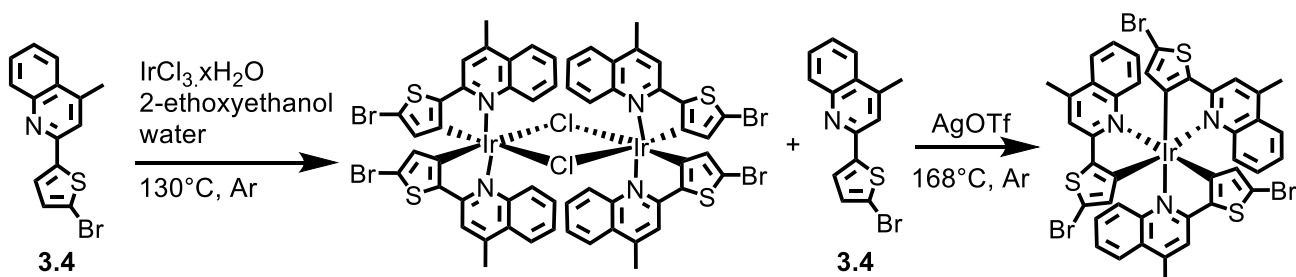
The remaining mass consisted of recovered **2.2** and intensely coloured (brown to black) solids that were only sparingly soluble in organic solvents and insoluble in water. No dendronized ligand was recovered and it was believed have formed part of the sparingly soluble by-product. The <sup>1</sup>H NMR spectrum of this material contained weak and very broad signals within the aromatic and aliphatic regions. This suggested the primary products were of large molecular weight; either organic polymers formed during partial decomposition or ligated inorganic clusters. The reaction was repeated yielding the same results.



Scheme 3.3: Cyclometallation of dendronized ligand.

It was hypothesized that the undesired material, which appeared to compose most of the mass of the products, may have been the result of the ligand having inadequate chemical or thermal stability for the reaction. Looking for an alternate route to the desired materials it was decided to examine whether the singly brominated precursor, **3.4**, could form the homoleptic cyclometallated iridium(III) complex.

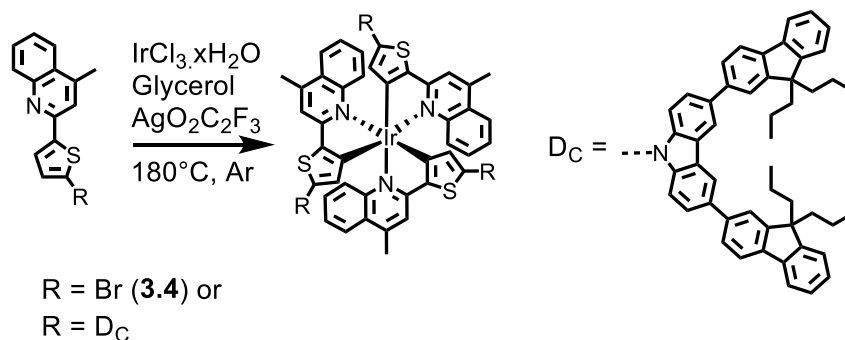
The cyclometallation of iridium(III) chloride hydrate by **3.4** was conducted in aqueous 2-ethoxyethanol at 130 °C. Similar to the singly dendronized ligand the deep red  $\mu$ -chloro-bridged iridium(III) dimer was isolated in quantitative yield. The subsequent cyclometallation of the  $\mu$ -chloro-bridged iridium(III) dimer by additional **3.4** was performed heating the melt in an oil bath at 168 °C with silver(I) triflate as a chloride scavenger (Scheme 3.4).



Scheme 3.4: Cyclometallation of **3.4**.

The primary product was again found to be a sparingly soluble, black/brown solid. The red-emitting band was isolated and found to be only 0.8 % yield of the homoleptic iridium(III) complex. The excess ligand was not able to be recovered suggesting that the reactivity of both ligands prefers the formation of the undesirable polymer-like material.

To investigate whether different cyclometallation reaction conditions may offer improved results, a one-pot synthesis was attempted using both the singly dendronized ligand and **3.4**. This involved heating a mixture of the ligand and iridium(III) chloride hydrate in glycerol in the presence of silver(I) trifluoroacetate as a chloride scavenger in an oil bath at 180°C (Scheme 3.5).



Scheme 3.5: One-pot cyclometallation of iridium(III) by **3.4** or the singly dendronized ligand.

Both ligands were consumed to form what appeared to be the same undesired polymeric material.

### 3.1.3 Summary

The inability to isolate the cyclometallated iridium(III) complexes in useful yields led to the initial syntheses being postponed indefinitely. It is believed that the initial targets could be synthesized, however, it had become clear that they could not be formed via the same route used for the green-emitting poly(dendrimer)s.

The target molecules were re-evaluated in hopes of providing greater understanding of carbazoly-dendronized red-emissive iridium(III) complexes featuring the “quinoline-thiophene” ligand moiety.

## 3.2 Re-evaluated Targets

### 3.2.1 Design rationale

#### 3.2.1.1 Design rationale of dendrimers containing homoleptic iridium(III) complexes

Due to the synthetic obstacles encountered in the attempted synthesis of two red-emitting poly(dendrimer)s; it was decided that the synthesis of a series of analogous dendrimers, if possible, could expand our understanding for future poly(dendrimer) systems while being interesting materials themselves.

As amination of the doubly-dendronized ligand proved problematic, all re-evaluated targets were furnished with only a single dendron per ligand. Utilizing the available ligand precursors from the initial targets; two homoleptic iridium(III) complexes were designed with the ligands functionalized by a single carbazoly-dendron at either of two different positions (Figure 3.3)



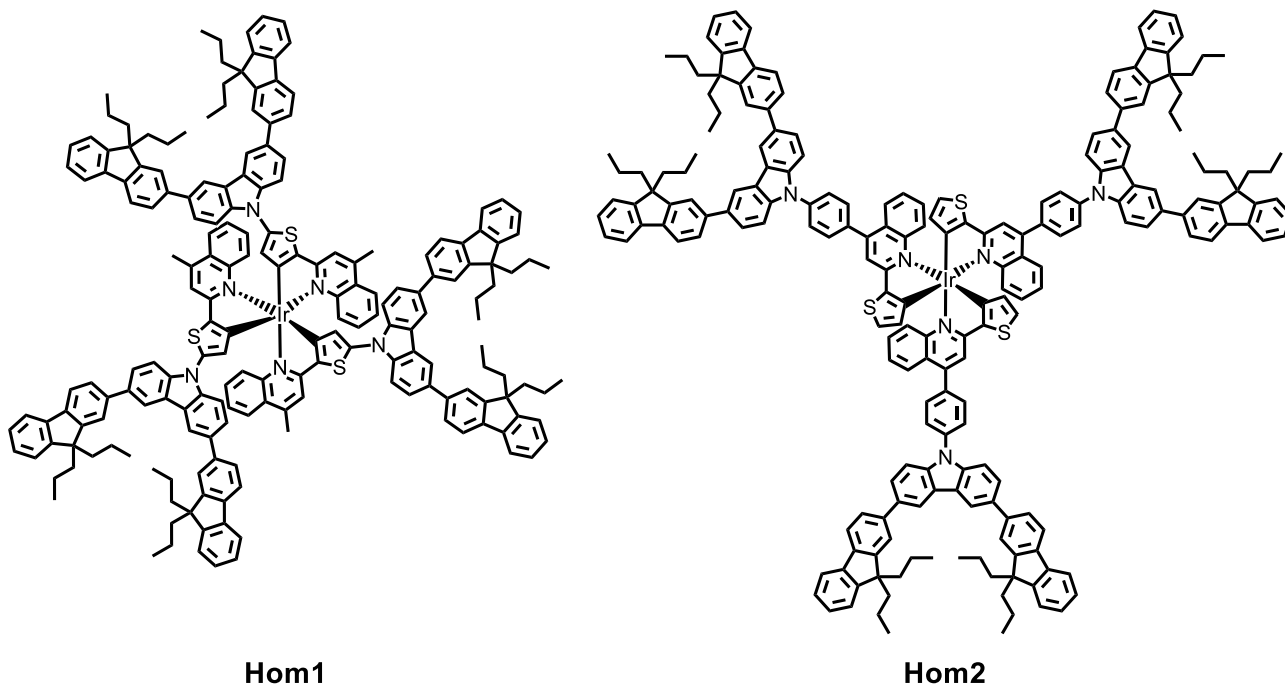


Figure 3.3: Red-emitting, homoleptic iridium(III) carbazoyl-dendrimers; **Hom1** and **Hom2**.

The homoleptic iridium(III) complex at the centre of **Hom1** and **Hom2** are structurally very similar. This allows any disparity observed in the properties of the materials can be attributed to the presence of carbazoyl-dendrons.

It can be hypothesized that the most significant effects will be caused by either sterics or due to electronics. It is believed that **Hom1** will be considerably smaller, and its dendrons will experience considerably more frustration in solution, than **Hom2** due to the dendrons' distance from and angle respective to the iridium(III) centre. In respect to electronics, the electron donating carbazoyl-dendrons of **Hom1** are attached directly to the thiophene which is believed to host at least some of the orbitals which contribute to the emissive metal-ligand charge-transfer state. In contrast, the dendrons of **Hom2** are connected through a phenyl-moiety, which is not expected to be in conjugation with the emissive moiety and is not expected to have a strong electronic effect. Any divergent properties originating from the methyl- or phenyl- moieties can be gleaned by comparison with **[Ir(tm<sub>q</sub>)<sub>3</sub>]** and the previously reported **[Ir(tp<sub>q</sub>)<sub>3</sub>]**.

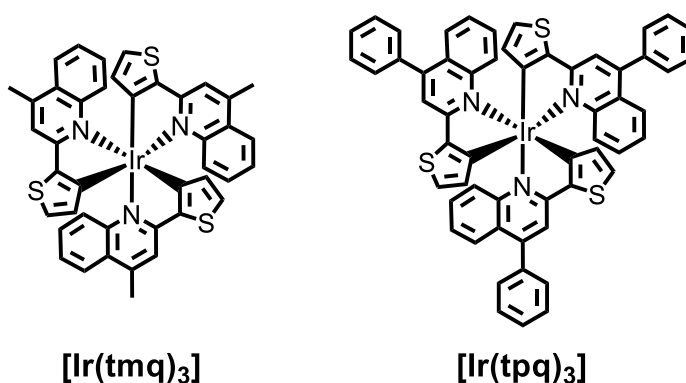


Figure 3.4: The small molecule iridium(III) complexes comprising the analogous emissive centre to **Hom1** and **Hom2**; **[Ir(tmq)<sub>3</sub>]** and **[Ir(tpq)<sub>3</sub>]**, respectively. **[Ir(tmq)<sub>3</sub>]** is synthesized in this work while **[Ir(tpq)<sub>3</sub>]** has been previously reported.<sup>157</sup>

With the targets designed and a belief that they may contribute significantly to the current literature, the optimal synthetic pathway had to be determined. In section 3.1.2 it was noted that the brominated ligand, **3.4**, was too unstable under the reaction conditions required to produce the cyclometallated, *fac*- iridium(III) complex in useful quantities. Therefore the analogous complex without bromide functionality, **[Ir(tmq)<sub>3</sub>]** (Figure 3.4), from 4-methyl-2-(thiophen-2-yl)quinoline (**3.3**) had to be synthesized prior to bromination. Additionally **[Ir(tmq)<sub>3</sub>]** could potentially be examined as an emitter within a vacuum thermal evaporation fabricated OLED to compare to the solution processed devices containing the dendrimeric emitters.

The synthetic pathway to produce **Hom2** had to deviate from that used for **Hom1** as bromination could not be performed after complexation. This was because the desired position, the 4-position on the phenyl ring, was not sufficiently reactive for selective functionalization from **[Ir(tpq)<sub>3</sub>]**. Conveniently, the brominated ligand for **Hom2**, 4-(4-bromophenyl)-2-(thiophen-2-yl)quinoline (**3.5**), was found to have sufficient thermal stability for complexation with iridium(III) to give the desired brominated complex without the need for subsequent bromination.

### 3.2.1.1 Design rationale of dendrimers containing heteroleptic iridium(III) complexes

In addition to the homoleptic iridium(III) complexes, two analogous heteroleptic iridium(III) complex containing the same ligands were designed with acetoacetate as the ancillary ligand (Figure 3.6). Small molecule heteroleptic iridium(III) complexes utilizing these ligands have already been reported as efficient red-emitters for organic light emitting diodes.<sup>156,160</sup> Therefore the aim of the heteroleptic dendrimers within the series was to

investigate whether functionalization with dendrons could produce analogues for efficient solution-processed OLEDs.

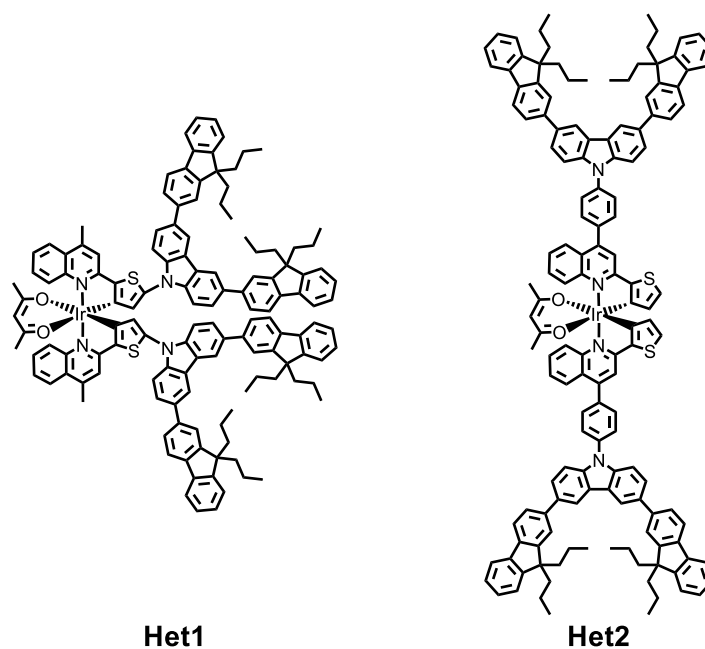


Figure 3.5: Red-emitting, heteroleptic iridium(III) carbazoyl-dendrimers; **Het1** and **Het2**.

As in the case of the homoleptic iridium(III) complex; 4-(4-bromophenyl)-2-(thiophen-2-yl)quinoline (**3.5**) was chosen as the ligand for cyclometallation to eventually give **Het2**.

To synthesize **Het1** the brominated 2-(5-bromothiophen-2-yl)-4-methylquinoline (**3.4**) was used instead of 2-thiophenyl-4-methylquinoline (**3.3**). This route was chosen due to metal acetylacetonato complexes having known reactivity towards electrophiles, including *N*-bromosuccinimide and other brominating agents which would result in substitution at the enolate position. Although selective bromination of the thiophenes may have been possible it was decided wise to avoid potential unselective pathways wherever alternatives were available. As **3.4** was demonstrated to form the desired  $\mu$ -dichloro-bridged dimer in section 3.1.2, this was deemed the optimal pathway to obtain the desired acetylacetonate complex. This was possible, in contrast to the unsuccessful attempts to form the intermediate of **IT1**, because the reaction conditions for the chelation of acetylacetonate are considerably milder than those required to form the fully cyclometallated, *facial* iridium(III) complex.

Following this synthetic pathway four iridium(III) complex containing dendrimers could be synthesized. The four dendrimers were expected to exhibit the greatest similarities depending on the iridium(III) complex at their core; either homoleptic or heteroleptic. Each dendrimer, homoleptic or heteroleptic, would also share its dendronized ligand with a partner

dendrimer, heteroleptic or homoleptic, respectively (Figure 3.6). This would allow evaluation of any observed variances in photophysical and electroluminescent properties between the dendrimeric partners. From this the effects of dendron may be postulated; whether it originate from electronic, steric or morphological effects.

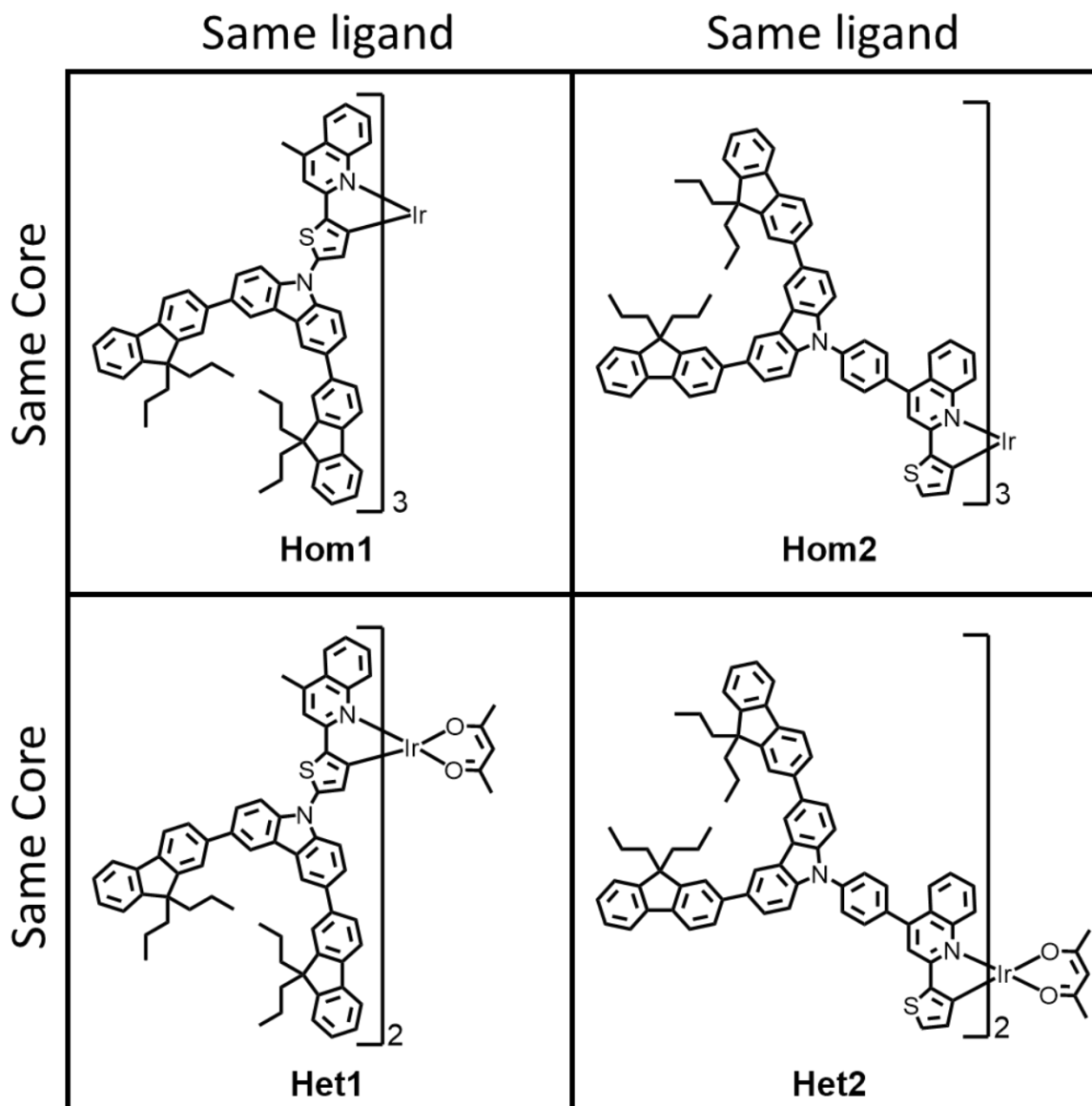


Figure 3.6: Structural comparison of target red-emitting dendrimers. The materials in the same row contain the same emissive iridium(III) complex, either homoleptic or heteroleptic, while those sharing a column contain the same dendronized ligand.

### 3.2.2 Possible isomers of re-evaluated targets

It has been well documented that the isomer of a cyclometallated iridium(III) complex has a profound effect on the photophysical properties of the material and ultimately its capacity to fabricate efficient organic light-emitting diodes.<sup>161,162,163</sup> Through evaluation by

$^1\text{H}$  NMR various isomers were observed in the synthesis of the re-evaluated targets. Therefore this section will define the structural relationship in respect to the nomenclature.

Octahedral complexes, which is the preferred geometry for iridium(III) systems for the majority of ligands, are known to form as two geometric isomers when they are of the generic formula  $[\text{ML}_3^a\text{L}_3^b]$ . These are the *facial* (*fac*-) isomer where the identical ligands can be observed on the same face of the octahedron and the *meridional* (*mer*-) isomer in which the identical ligands are in a plane which passes through the metal centre. For homoleptic iridium(III) complexes with bidentate ligands the identical ligand is from the perspective of the coordinating bond. Therefore, in a *facial* homoleptic iridium(III) complex with  $\text{C}^-\text{N}^-$  bidentate ligands, each of the formally anionic carbons are on a face while each of the nitrogens are on the opposing face of the octahedron. This may also be described as being *fac*- $[\text{Ir}(\text{C}^-\text{N}^-)_3]$  where  $\text{L}_3^a$  is from the perspective of the carbanion and  $\text{L}_3^b$  is the same ligand from the perspective of the nitrogen (Figure 3.7).

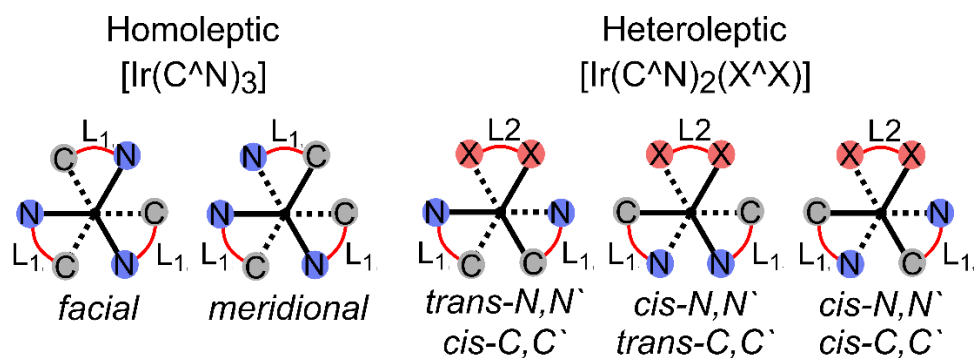


Figure 3.7: Possible isomers of the homoleptic and heteroleptic iridium(III) complex containing dendrimers

In the case of complexes of the generic formula  $[\text{ML}_4^a\text{L}_2^b]$  the *trans*- $\text{L}^b, \text{L}^b$  isomer has both identical  $\text{L}^b$  ligands axial to one another and the *cis*- $\text{L}^b, \text{L}^b$  isomer is where the  $\text{L}^b$  ligands are adjacent. Although technically of the generic formula  $[\text{ML}_2^a\text{L}_2^b\text{L}_2^c]$ , the heteroleptic complexes (fitting the formula:  $[\text{Ir}(\text{C}^-\text{N}^-)_2(\text{acac})]$ ) can also be described in the stereoisomer terminology of *trans* or *cis*. This is a result of any bidentate ligand only being capable of chelation *cis*- to itself which limits the number of possible arrangements. As a result, the possible isomers of the heteroleptic-acetylacetonate iridium(III) complexes are *trans*- $\text{N}, \text{N}^-$ , *cis*- $\text{C}, \text{C}^-$ ; *cis*- $\text{N}, \text{N}^-$ , *trans*- $\text{C}, \text{C}^-$  and *cis*- $\text{N}, \text{N}^-$ , *cis*- $\text{C}, \text{C}^-$ . For iridium(III) complexes it is common to refer to them as the *trans*- $\text{N}, \text{N}^-$  isomer and the *cis*- $\text{N}, \text{N}^-$  isomers. This is largely because the symmetrical *trans*- $\text{N}, \text{N}^-$  isomer forms preferentially under the standard conditions, likely being the thermodynamically favoured product, and is thus more commonly encountered within the literature.<sup>163</sup>

There is also the potential for regioisomers (also referred to as structural isomers or constitutional isomers) to form within the proposed synthetic scheme. If functionalization were to occur at an undesirable position a regioisomer would be formed. This will be shown to be the case during the synthesis of **Het1**.

The iridium(III) complexes within this thesis also exhibit chirality resulting from the arrangement of their bidentate ligands around the metal centre with each material consisting of a pair of enantiomers ( $\Lambda$  or  $\Delta$ ). It is known that these enantiomers exhibit circularly polarized emission if separated, however, formation under standard conditions results in a racemic mixture with separation only possible through high performance chiral chromatography techniques.<sup>164,165</sup> As a result the bulk racemic mixture appears identical to a non-chiral material. Additionally the environment experienced by the enantiomers are identical resulting in them being indistinguishable by techniques such as <sup>1</sup>H NMR and as such could not be the cause of the inequivalent ligand signals. While it is important to note that all iridium(III) complexes described in this chapter are known to be enantiomers. No effort was made to separate the enantiomers and it will be appreciated that in the discussion a racemic mixture is assumed.

### 3.2.3 Synthesis

The synthetic pathways for the dendrimers follow similar synthetic pathways, however, each was found to have unique challenges associated with it. This section will include the synthesis of the ligands utilized for the cyclometallation of iridium(III) followed by the detailed description of the synthesis and structural characterization of each dendrimer within its own sub-section.

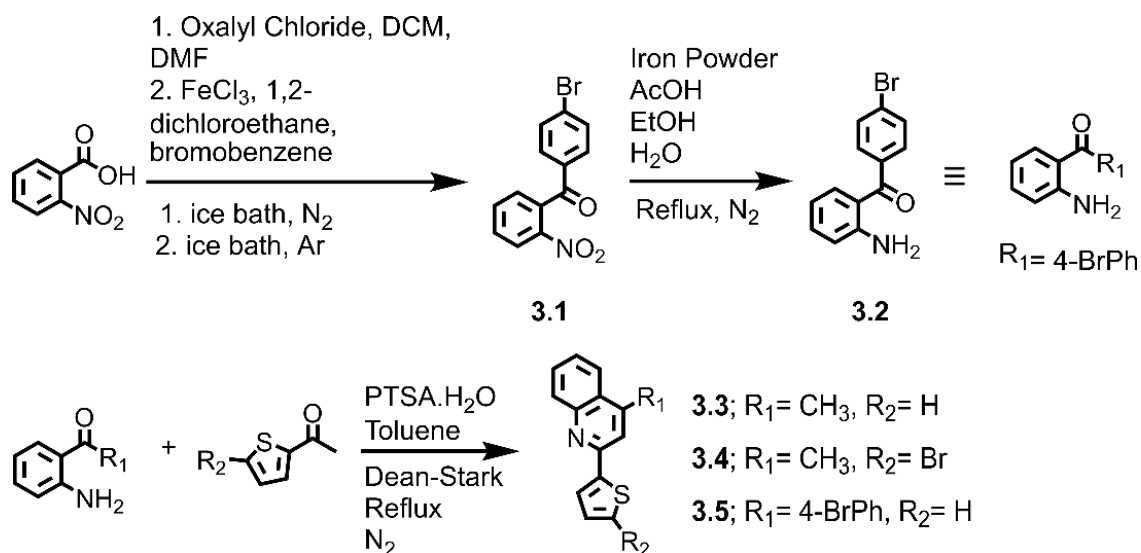
This section contains numerous structure elucidations from single-crystal X-ray diffraction analysis which involved significant contribution by others. The diffraction patterns of the crystals were collected by members of the research group of A. Prof. Jack Clegg, in particular Dr Aidan J. Brock and Mr Jacob Whittaker. Structure refinement was conducted by myself but with assistance from A. Prof. Jack Clegg, Dr Aidan J. Brock and Mr Jacob Whittaker. The crystallography of **Het2** was an exception as my experience was insufficient to complete it and as such it was refined by Mr Jacob Whittaker. The images of the structures were compiled by Mr Jacob Whittaker.

Full experimental details of the single crystal X-ray diffraction are included in Chapter 6, General Experimental.

### 3.2.3.1 Synthesis of Ligands

The planned route for the synthesis of the ligands began, as described in section 3.1.2, with Friedländer quinoline synthesis. The starting materials 2'-aminoacetophenone, 2'-acetylthiophene and 5'-bromo-2'-acetylthiophene were commercially available while (2-aminophenyl)(4-bromophenyl)methanone (**3.2**) had to be synthesized.

Literature procedures were followed to first isolate the acyl chloride of 2-nitrobenzoic acid via reaction with the iminium chloride intermediate from oxalyl chloride and catalytic *N,N*-dimethylformamide. The isolated 2-nitrobenzoyl chloride was reacted, without purification, with bromobenzene in an iron(III) chloride catalysed Friedel-Crafts acylation giving 4-bromophenyl(2-nitrophenyl)methanone (**3.1**) in a two-step yield of 26 %. Reduction of **3.1** by iron powder in refluxing aqueous ethanol/ acetic acid gave (2-aminophenyl)(4-bromophenyl)methanone (**3.2**) in 91 % (Scheme 3.6).



Scheme 3.6: Synthesis of ligands for red-emitting iridium(III) complexes.

The Friedländer quinoline syntheses were performed under the modified literature conditions developed in section 3.1.2.1. The method was modified to be performed under an inert atmosphere utilizing the toluene-water azeotrope to remove water via a Dean-Stark apparatus and the yields were improved significantly. Under these conditions the reaction of 2'-aminoacetophenone with either 2-acetylthiophene or 2-acetyl-5-bromothiophene gave 4-methyl-2-(thiophen-2-yl)quinoline (**3.3**) or 2-(5-bromothiophen-2-yl)-4-methylquinoline (**3.4**) in 68 or 94 % yield, respectively. Similarly, 4-(4-bromophenyl)-2-(thiophen-2-yl)quinoline (**3.5**) was obtained through the reaction of **3.2** with 2-acetylthiophene under these conditions in 73 % yield.

Structure elucidation of the ligands; **3.3**, **3.4** and **3.5**; was conducted by analysis of solvent grown crystals by single-crystal X-ray diffraction. The resulting structures increased the already very high confidence in the structural assignments by complementary characterization.

Waxy crystals were observed to be the preferred form for all three ligands, **3.3**, **3.4** and **3.5**. Previous reported syntheses of **3.3** reported it as an oil, however, it was observed within this project to slowly solidify; and to grow crystals from solution at ambient temperatures (Mpt 69°C).

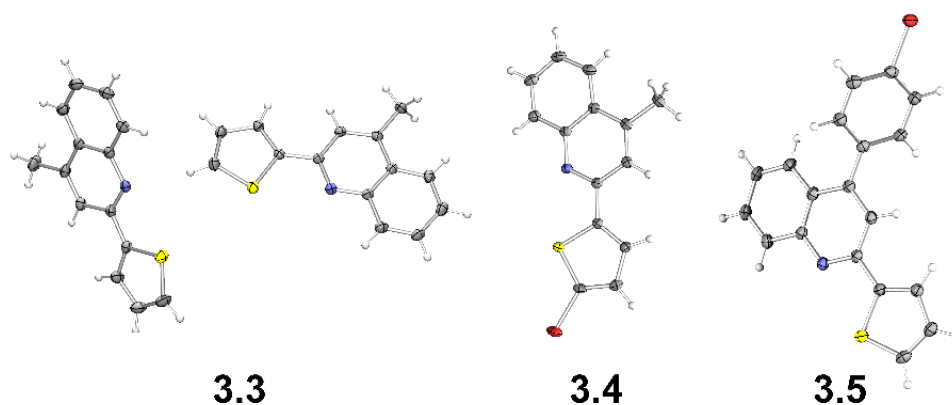


Figure 3.8: Structure of the ligands, **3.3**, **3.4** and **3.5**, within their asymmetric unit cell as determined by single-crystal X-ray diffraction experiments.



Table 3.2: Crystallography data summary table; Ligands

Material	<b>3.3</b>	<b>3.4</b>	<b>3.5</b>
Empirical Formula	C <sub>14</sub> H <sub>11</sub> NS	C <sub>14</sub> H <sub>10</sub> BrNS	C <sub>19</sub> H <sub>12</sub> BrNS
Formula Weight	225.30	304.20	366.27
Temperature/K	100(2)	100(2)	100(2)
Crystal System	monoclinic	monoclinic	monoclinic
Space Group	<i>P2<sub>1</sub>/c</i>	<i>P2<sub>1</sub>/n</i>	<i>P2<sub>1</sub>/c</i>
a/ Å	14.219(3)	10.299(2)	11.003(2)
b/ Å	10.785(2)	9.6510(19)	14.038(3)
c/ Å	15.608(3)	13.208(3)	10.974(2)
α/ °	90	90	90
β/ °	106.87(3)	111.12(3)	115.86
γ/ °	90	90	90
Volume/ Å <sup>3</sup>	2290.5(9)	1224.7(5)	1525.3(6)
Z	8	4	4
ρ <sub>calc</sub> g/cm <sup>3</sup>	1.307	1.650	1.595
μ/ mm <sup>-1</sup>	0.251	3.501	2.826
F(000)	944.0	608.0	736.0
Crystal Size/ mm <sup>3</sup>	0.3 × 0.2 × 0.15	0.35 × 0.25 × 0.1	0.03 × 0.02 × 0.01
Radiation	synchrotron (λ = 0.7108)	synchrotron (λ = 0.7108)	synchrotron (λ = 0.7108)
2θ range for data collection/ °	2.994 to 56.57	5.362 to 56.564	4.114 to 55.788
Index ranges	-18 ≤ h ≤ 18, -14 ≤ k ≤ 14, -20 ≤ l ≤ 20	-13 ≤ h ≤ 13, -12 ≤ k ≤ 12, -17 ≤ l ≤ 17	-14 ≤ h ≤ 14, - 18 ≤ k ≤ 18, - 14 ≤ l ≤ 14
Reflections collected	34470	19412	24678
Independent reflections	5414 [R <sub>int</sub> = 0.0428, R <sub>sigma</sub> = 0.0267]	2964 [R <sub>int</sub> = 0.0447, R <sub>sigma</sub> = 0.0210]	3618 [R <sub>int</sub> = 0.0379, R <sub>sigma</sub> = 0.0185]
Data/restraints/parameters	5414/0/292	2964/0/156	3618/0/199
Goodness-of-fit on F <sup>2</sup>	1.057	1.095	1.069
Final R indexes [I > 2σ(I)]	R <sub>1</sub> = 0.0375, wR <sub>2</sub> = 0.0967	R <sub>1</sub> = 0.0306, wR <sub>2</sub> = 0.0756	R <sub>1</sub> = 0.0311, wR <sub>2</sub> = 0.0746
Final R indexes [all data]	R <sub>1</sub> = 0.0382, wR <sub>2</sub> = 0.0973	R <sub>1</sub> = 0.0316, wR <sub>2</sub> = 0.0761	R <sub>1</sub> = 0.0361, wR <sub>2</sub> = 0.0772
Largest diff. peak/hole / e Å <sup>-3</sup>	0.34/-0.23	0.92/-0.79	0.53/-0.81

The ligands, **3.3**, **3.4** and **3.5**, were found to form crystals excluding any other molecules. The quinoline and thiophene rings occupy the same plane indicating extended conjugation through this system. This is expected as they form what can be described as a donor-acceptor system with the electron-donating thiophene feeding electron density toward

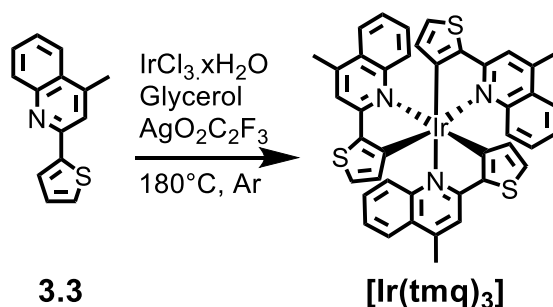
the electron-withdrawing quinoline moiety. Because of this the phenyl ring of **3.5** does not exhibit significant conjugation to the other two rings and is observed to occupy its own plane with an offset of 55.1° from the former.

As the crystals were grown at room temperature the observed conformation in the crystal should reflect the preferred orientation in the solution phase. All three ligands appear to prefer the *syn*- conformational isomer. The *syn*- isomer is assigned as the conformational isomer in which the hetero-atoms with lone pairs are on the same side of the bond. In order to form the iridium(III) complexes rotation about the quinoline-thiophene bond to the *anti*- isomer is required. This should not be considered a significant obstacle as the high temperatures used in the complexation reactions would endow more than sufficient energy to power the necessary rotation.

Ultimately the structures of the three ligands, **3.3**, **3.4** and **3.5**, were confirmed through the complementary technique of single-crystal X-ray diffraction. All three crystal structures were found to contain only the molecules of interest.

### 3.2.3.2 Synthesis of Hom1; Complexation

The synthesis of the homoleptic iridium(III) complexes was conducted following the relatively unorthodox albeit very successful one-pot, one-step complexation detailed by Jin *et al.*<sup>157</sup> Heating a solution of iridium(III) chloride hydrate and **3.3** in glycerol at 180°C, in the presence of silver(I) trifluoroacetate as a chloride scavenger, gave the *fac*-homoleptic iridium(III) complexes **[Ir(tmq)<sub>3</sub>]** a respectable yield of 25 %.



Scheme 3.7: One-pot synthesis of **[Ir(tmq)<sub>3</sub>]**

Diffraction quality crystals of **[Ir(tmq)<sub>3</sub>]** were obtained by growth from solution as well as growth within the gaseous phase during purification by sublimation. While the solution grown crystals were sufficient for structure elucidation of the complex, the growth of crystals from gas phase deposition during vacuum sublimation is under very similar conditions to vacuum thermal evaporation deposition.

This is very significant as, although the primary focus of this project is the synthesis of solution processable dendrimers, **[Ir(tmq)<sub>3</sub>]** could prove to be a successful emissive dopant but only for evaporated devices due to its sparing solubility. The observed packing may provide insight to future investigations on how **[Ir(tmq)<sub>3</sub>]** behaves in the gaseous phase. For example, crystal structures obtained of materials grown from the vapour phase provides a strong starting point for any computer modelling of evaporation processes.

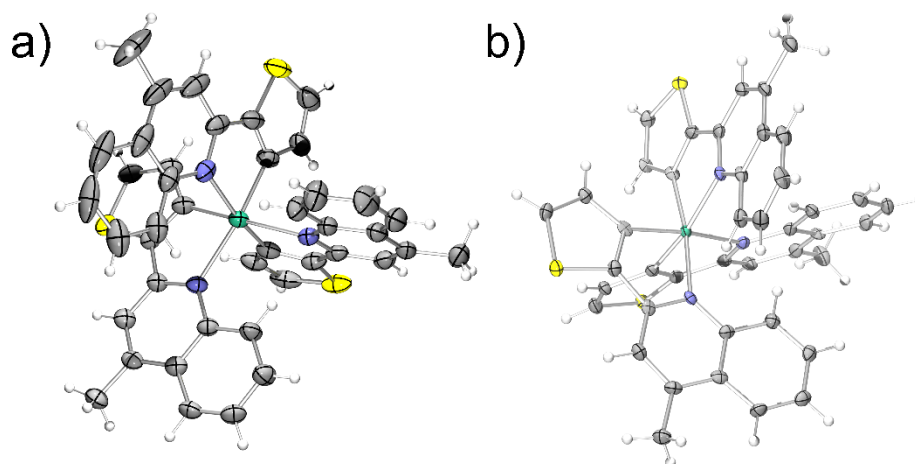


Figure 3.9: Structure of **[Ir(tmq)<sub>3</sub>]** as determined by single-crystal X-ray diffraction experiments performed on a crystal grown from either a) solution by layer diffusion or b) during sublimation. The structure in a) is solvated by a disordered dichloromethane molecule hidden for clarity.

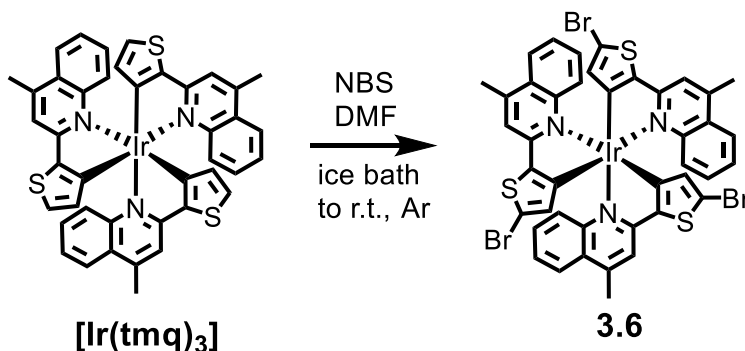
Table 3.3: Crystallography data summary table; **[Ir(tmq)<sub>3</sub>]**

<b>[Ir(tmq)<sub>3</sub>]</b> grown from:	<b>Solution</b>	<b>Sublimation</b>
Empirical Formula	C <sub>43</sub> H <sub>30</sub> Cl <sub>2</sub> IrN <sub>3</sub> S <sub>3</sub>	C <sub>42</sub> H <sub>30</sub> IrN <sub>3</sub> S <sub>3</sub>
Formula Weight	953.98	865.07
Temperature/K	100(2)	100(2)
Crystal System	triclinic	triclinic
Space Group	<i>P</i> -1	<i>P</i> -1
<i>a</i> / Å	11.047(2)	10.654(2)
<i>b</i> / Å	15.964(3)	11.667(2)
<i>c</i> / Å	21.775(4)	14.179(3)
$\alpha$ / °	83.03(3)	91.75(3)
$\beta$ / °	81.84(3)	103.13(3)
$\gamma$ / °	77.02(3)	103.60(3)
Volume/ Å <sup>3</sup>	3688.2(14)	1661.7(6)
Z	4	2
$\rho_{\text{calc}}$ g/cm <sup>3</sup>	1.718	1.729
$\mu$ / mm <sup>-1</sup>	3.975	4.243
F(000)	1844.0	856.0
Crystal Size/ mm <sup>3</sup>	0.2 × 0.08 × 0.03	0.1 × 0.05 × 0.04
Radiation	synchrotron ( $\lambda$ = 0.7108)	synchrotron ( $\lambda$ = 0.7108)
2 $\theta$ range for data collection/ °	1.898 to 52.75	2.962 to 49.43
Index ranges	-13 ≤ <i>h</i> ≤ 13, -19 ≤ <i>k</i> ≤ 19, -27 ≤ <i>l</i> ≤ 27	-12 ≤ <i>h</i> ≤ 12, -13 ≤ <i>k</i> ≤ 13, -16 ≤ <i>l</i> ≤ 16
Reflections collected	51255	17557
Independent reflections	13663 [ <i>R</i> <sub>int</sub> = 0.0339, <i>R</i> <sub>sigma</sub> = 0.0320]	5123 [ <i>R</i> <sub>int</sub> = 0.0263, <i>R</i> <sub>sigma</sub> = 0.0257]
Data/restraints/parameters	13663/0/1000	5123/0/446
Goodness-of-fit on F <sup>2</sup>	1.056	1.135
Final R indexes [ <i>I</i> > 2 $\sigma$ ( <i>I</i> )]	<i>R</i> <sub>1</sub> = 0.0365, <i>wR</i> <sub>2</sub> = 0.0885	<i>R</i> <sub>1</sub> = 0.0273, <i>wR</i> <sub>2</sub> = 0.0810
Final R indexes [all data]	<i>R</i> <sub>1</sub> = 0.0409, <i>wR</i> <sub>2</sub> = 0.0915	<i>R</i> <sub>1</sub> = 0.0280, <i>wR</i> <sub>2</sub> = 0.0817
Largest diff. peak/hole / e Å <sup>-3</sup>	1.83/-1.83	0.89/-1.83

Through obtaining the crystal structure of **[Ir(tmq)<sub>3</sub>]** it became possible to unambiguously assign the structure as the *facial* isomer. Crystallography cannot exclude the presence of other isomers as the analysed crystals may not be representative of the bulk. When combined with the complementary <sup>1</sup>H NMR, however, the absence of signals originating from other molecules shows that the bulk **[Ir(tmq)<sub>3</sub>]** contains no other geometric isomers.

### 3.2.3.3 Synthesis of Hom1; Bromination

A solution of **[Ir(tmq)<sub>3</sub>]** in anhydrous *N,N*-dimethylformamide was cooled in an ice bath and treated with *N,N*-bromosuccinimide with the exclusion of light. While <sup>1</sup>H NMR analysis of the crude indicated full conversion to the desired product brominated at the three 5-thiophenyl sites, **3.6**; the yield obtained after purification was 39 %.



Scheme 3.8: Bromination of **[Ir(tmq)<sub>3</sub>]** to give **3.6**

The limited solubility of **3.6** likely led to the lower than expected yield. During liquid chromatography over silica a portion of red-coloured, red-emissive material was always observed to adsorb strongly to the stationary phase. This adsorbed material was very resilient to desorption into solvent. Further optimization by excluding chromatography may improve product yield further.

From initial <sup>1</sup>H NMR evaluation of **3.6** the bromination appeared to have occurred regioselectively and the presence of species other than the tri-brominated product were not observed by <sup>1</sup>H NMR or mass spectroscopy.

The crystal structure of **3.6** was obtained from a crystal grown from solution techniques by layer diffusion. As suggested by <sup>1</sup>H NMR spectroscopy, the crystal structure confirmed the identity of the primary constituent of **3.6** as the *facial* isomer with a bromide functionality at each of the three 5-thiophenyl positions of the ligands. Discussed in more depth in the following section, <sup>1</sup>H NMR spectroscopy indicates the presence of another isomer and the crystal structure is representative of the dominant isomer only.

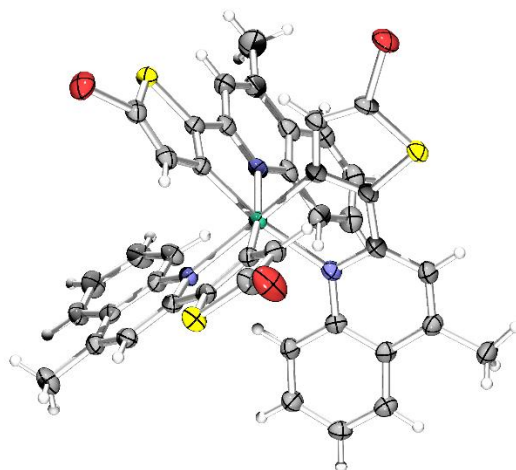


Figure 3.10: Structure of the homoleptic bromide-functionalized iridium(III) complex, **3.6**, determined by single-crystal X-ray diffraction experiments.

Table 3.4: Crystallography data summary table; **3.6**

Material	<b>3.6</b>
Empirical Formula	$C_{43}H_{27}Br_3Cl_{1.83}IrN_3S_3$
Formula Weight	1178.48
Temperature/K	100(2)
Crystal System	triclinic
Space Group	<i>P</i> -1
<i>a</i> / Å	11.288(2)
<i>b</i> / Å	13.007(3)
<i>c</i> / Å	14.445(3)
$\alpha$ / °	99.21(3)
$\beta$ / °	92.61(3)
$\gamma$ / °	97.05(3)
Volume/ Å <sup>3</sup>	2073.1(8)
<i>Z</i>	2
$\rho_{\text{calc}}$ g/cm <sup>3</sup>	1.888
$\mu$ / mm <sup>-1</sup>	6.416
<i>F</i> (000)	1134.0
Crystal Size/ mm <sup>3</sup>	0.12 × 0.04 × 0.005
Radiation	synchrotron ( $\lambda$ = 0.7108)
2 $\theta$ range for data collection/ °	2.862 to 52.746
Index ranges	-13 ≤ <i>h</i> ≤ 14, -16 ≤ <i>k</i> ≤ 16, -18 ≤ <i>l</i> ≤ 18
Reflections collected	30159
Independent reflections	7817 [ <i>R</i> <sub>int</sub> = 0.0329, <i>R</i> <sub>sigma</sub> = 0.0227]
Data/restraints/parameters	7817/0/510
Goodness-of-fit on <i>F</i> <sup>2</sup>	1.037
Final <i>R</i> indexes [ <i>I</i> > 2 $\sigma$ ( <i>I</i> )]	<i>R</i> <sub>1</sub> = 0.0366, <i>wR</i> <sub>2</sub> = 0.0964
Final <i>R</i> indexes [all data]	<i>R</i> <sub>1</sub> = 0.0391, <i>wR</i> <sub>2</sub> = 0.0982
Largest diff. peak/hole / e Å <sup>-3</sup>	1.60/-1.61

### 3.2.3.4 Synthesis of Hom1; Buchwald-Hartwig Amination

To form the desired dendrimer (**Hom1**) the carbazoyl-dendron (**2.11**) was coupled to the brominated complex (**3.6**) under Buchwald-Hartwig amination conditions. The first attempt involved heating **2.11** and **3.6** in refluxing anhydrous toluene in the presence of tris(dibenzylideneacetone)dipalladium(0)-chloroform adduct/ tri-*tert*-butylphosphonium tetrafluoroborate as the catalyst/ ligand system and sodium *tert*-butoxide as the base under an inert atmosphere. Under these conditions only trace quantities of what was expected to be **Hom1** could be isolated. The isolated products appeared to be variously coupled intermediates by <sup>1</sup>H NMR and mass spectroscopy with a mixture of the doubly coupled intermediates being the predominant products.

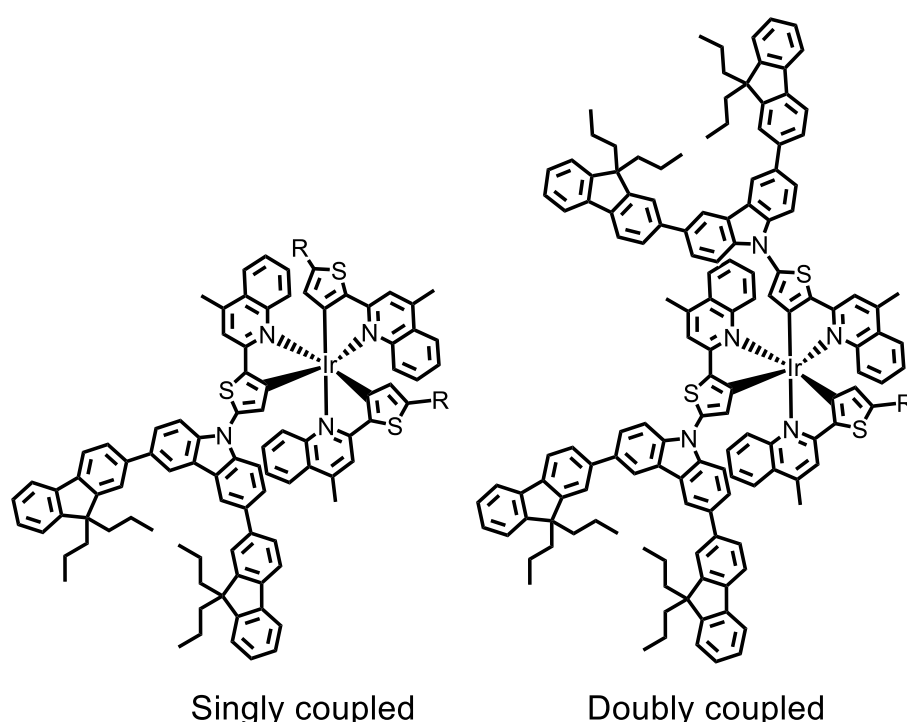


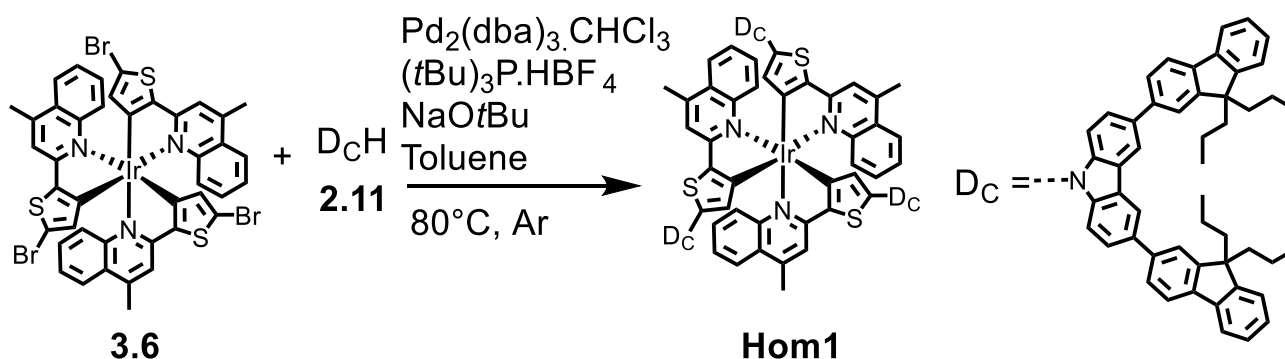
Figure 3.11: Suspected side products formed during Buchwald-Hartwig amination of **3.6**. These are intermediates or deactivated intermediates within the synthesis of **Hom1**.

As the palladium(0) catalysed coupling is stepwise, the isolation of the singly and doubly coupled complexes indicated that the reaction was successfully initiated but the process ceased prior to forming significant product.

Due to the precious nature of **3.6** the literature was examined to see if similar couplings had been reported in hopes of improved yields to reduce loss. The only reported coupling of a carbazole moiety onto a 2-bromothiophene under Buchwald-Hartwig amination conditions utilized the same conditions as above but with heating at 80°C as opposed to

refluxing toluene or xylene used for the first attempt to form **3.6**. At this lower temperature the coupling onto the substrate containing three 2-bromothiophene moieties was reported to give the product in 81 % yield.<sup>166</sup> The authors did not note why the temperature was lowered from the more commonly encountered refluxing solvents.

Following the literature findings; the Buchwald-Hartwig amination of **3.6** by **2.11** was repeated utilizing tris(dibenzylideneacetone)dipalladium(0)-chloroform adduct/ tri-*tert*-butylphosphonium tetrafluoroborate as the catalyst/ ligand system, sodium *tert*-butoxide as the base and anhydrous toluene as the solvent under an inert atmosphere heating in an oil bath at 80°C.



Scheme 3.9: Coupling of carbazoyl-dendron (**2.11**) to the brominated homoleptic iridium(III) core (**3.6**) by Buchwald-Hartwig amination.

These conditions were employed in the final synthesis of **Hom1** where a batch of **3.6** was aminated by **2.11**. The batch of the brominated complex, **3.6**, was synthesized in a quantity that was believed would give sufficient **Hom1** for full characterization.

A common attribute for many of the materials reported in this chapter is an affinity for trapping alkane solvents which have the potential to obscure the quoted yields. The brominated complex, **3.6**, was no exception and the progress of solvent removal from this batch under vacuum ( $\sim 10^{-1}$  mbar) and elevated temperature (40°C) was monitored by <sup>1</sup>H NMR. After two weeks of steadily decreasing solvent signals, new signals were observed in the aromatic region. This batch of **3.6** subjected to the Buchwald-Hartwig amination, despite containing traces of petroleum spirits, to form **Hom1** for fear that it was undergoing some form of degradation.

During the process of isolating **Hom1** formed during this reaction, an impurity was identified by <sup>1</sup>H NMR which could not be separated from the primary product. Repeated attempts of column chromatography over silica and size exclusion chromatography were used to remove the small quantity of impurity, however, the concentration appeared unaffected when analysed by <sup>1</sup>H NMR spectroscopy. Analysis by gel permeation



chromatography showed that the mixture was a single peak with a dispersity of 1.0 (non-disperse) shown in Figure 3.12.

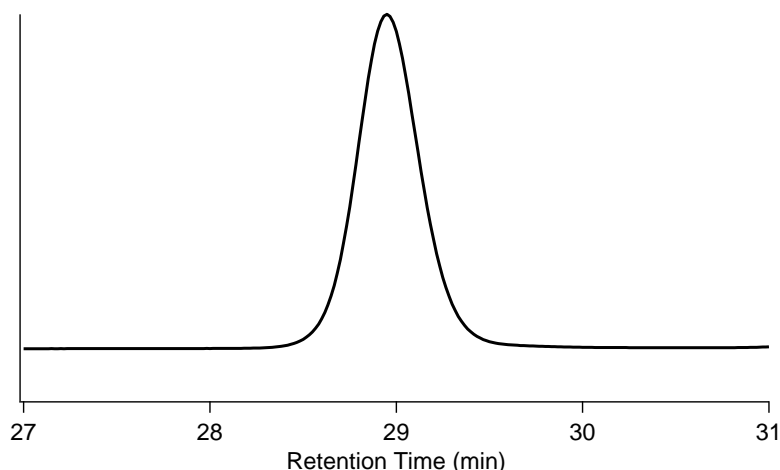


Figure 3.12: Gel permeation chromatogram of **Hom1**. The mixture appears as a single non-disperse peak.

From these results it appeared that the impurity exhibited polarity and a hydrodynamic radius that was indistinguishable from the dominant material within the mixture leading to the inability to separate them through chromatography. These similarities lead to the conclusion that the mixture contained two materials, one dominant, that were isomers.

The formation of an additional isomer during the Buchwald-Hartwig amination could not be rationalized so the previous materials were examined for the presence of the minor isomer. The likely candidates for the identity of the minor isomer were either an alternate geometric isomer (*meridional*) formed during the complexation or a regioisomer formed during the bromination where a single ligand was substituted at a different position. By determining when in the synthetic scheme the isomerism had been introduced, the identity of the isomer could be inferred. One dimensional  $^1\text{H}$  NMR spectroscopy was utilized to identify the presence of the isomer. Full assignment of the minor isomer was impossible due to the significant overlap by the more intense major isomer.

The products of the complexation and the bromination; **[Ir(tmq)<sub>3</sub>]** and **3.6**, respectively; both exhibited poor solubility in all solvents. It was believed that at least one of these intermediates had contained a minor isomer which was not identified due to the weak  $^1\text{H}$  NMR spectra of the dilute but saturated solutions. To improve resolution the  $^1\text{H}$  NMR spectra of both materials were collected using a very high number of scans to obtain a greater signal to noise ratio.

The most prominent proton signal shared by all three complexes is the thiophenyl proton alpha to the Ir-C bond ( $H_\alpha$ ). Due to its proximity to the heavy iridium electron density it experiences a strong shielding effect resulting in it always being the most upfield proton of the aromatic region. Because of this it is an excellent diagnostic signal being well removed from the remaining aromatic signals. The  $H_\alpha$  signals of any minor isomers are also expected to be observed in a similar region as they are also in close proximity to the iridium centre.

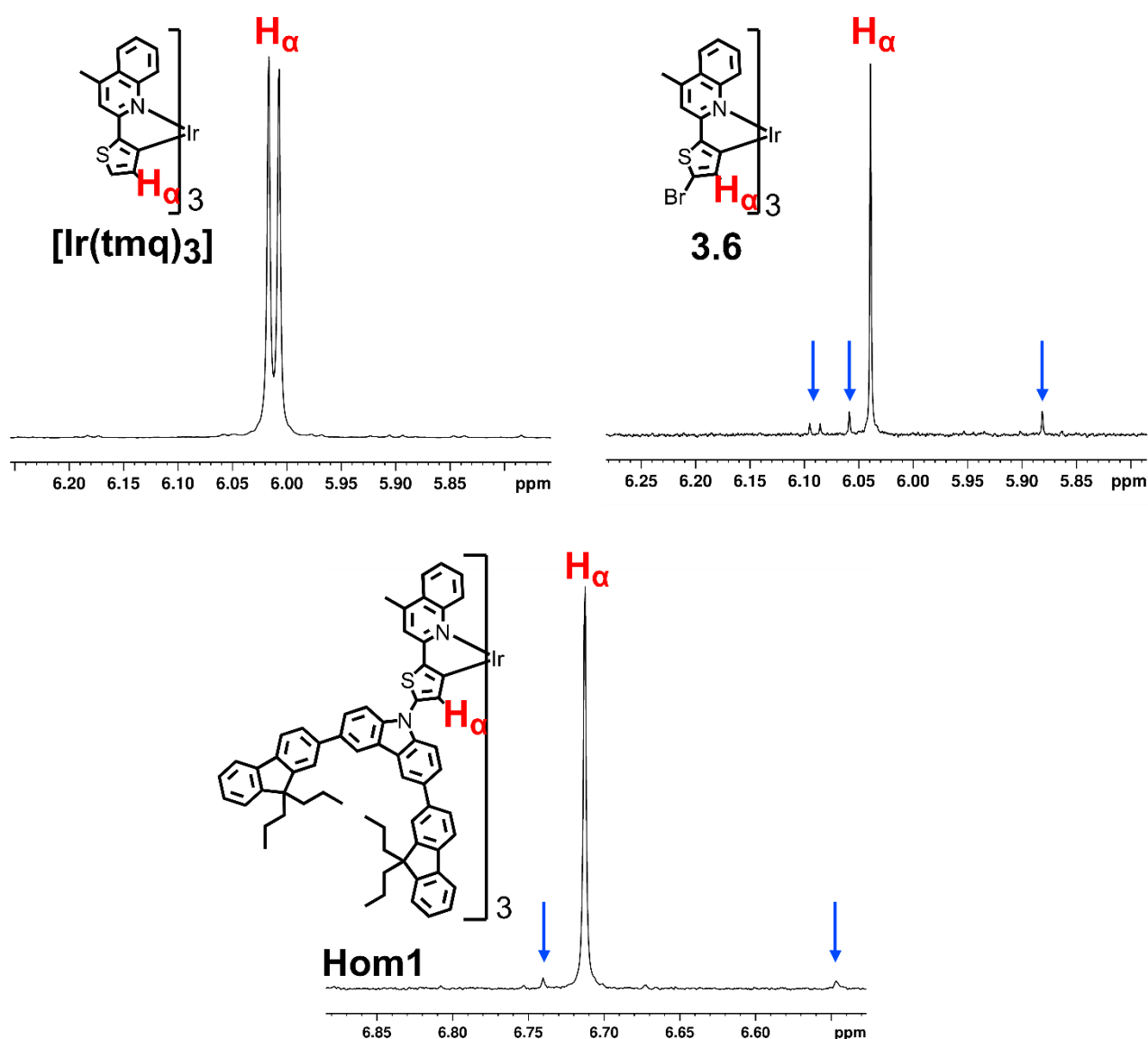


Figure 3.13:  $^1\text{H}$  NMR investigation of isomerism in **Hom1**: The thiophenyl proton alpha to the Ir-C bond ( $H_\alpha$ ) are examined as diagnostic peaks. The signals corresponding to the  $H_\alpha$  of the major isomer are labelled in red. The weak signals corresponding to the minor isomer are indicated by blue arrows.

From the evaluation shown in Figure 3.13 it was concluded that the batch of  $[\text{Ir}(\text{tmq})_3]$  contained only the single *facial* isomer ruling out the possibility that *meridional* isomer could be responsible for the additional signals observed in **Hom1**. As the additional signals appear only upon bromination it is concluded that the new isomer is a regioisomer with one ligand brominated at a different position. The similarity in the peak pattern observed between the dominant product and the regioisomer of both **3.6** and **Hom1** is quite striking and provides support that the impurity is a regioisomer and behaves in the same manner as the dominant isomer. It should be noted that the signals from the second isomer may appear weak due to its asymmetry, however, they equate to 18 % and 8 % of **3.6** and **Hom1** respectively.

Unfortunately it is very difficult to determine the substitution pattern of the second regioisomer due to the complexity of the  $^1\text{H}$  NMR pattern due to asymmetry and the extensive overlapping of the far more intense signals from the dominant isomer. It does appear that two of the three ligands were substituted as in the desired material, at the 5-thiophenyl position while the third ligand was substituted at another position. As the bromination was carried out with the exclusion of light at reduced temperature, the bromination by *N*-bromosuccinimide should have occurred exclusively through electrophilic substitution. As the bromination of quinolines is typically limited to radical mechanisms, the minor regioisomer likely has a single ligand with the dendron attached at the 4-thiophenyl rather than the 5-thiophenyl position. The structure of the unambiguous major isomers and the most probable candidates for the minor isomers of **3.6** and **Hom1** are shown in Figure 3.15

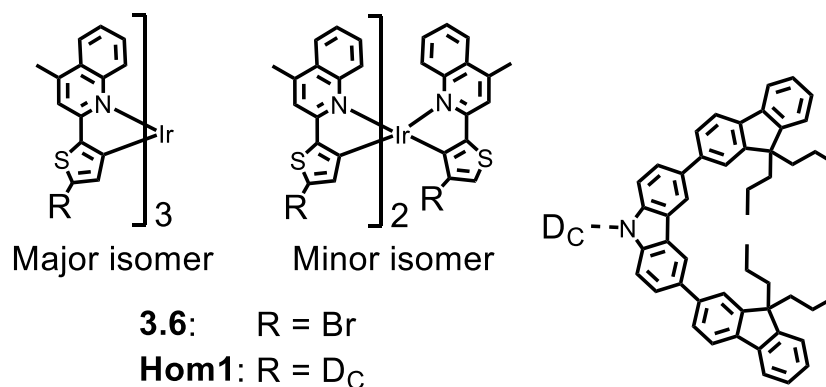


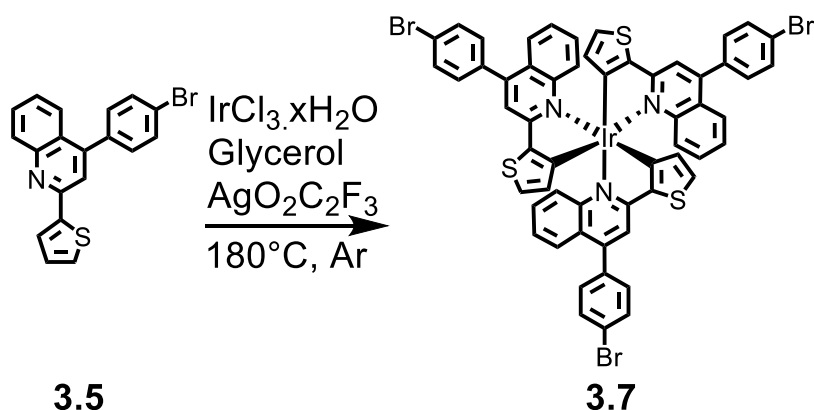
Figure 3.14: Structures of the major and minor isomers of **3.6** and **Hom1**.

Ultimately **Hom1** was isolated in 20 % yield over two steps from  $[\text{Ir}(\text{tmq})_3]$  as a mixture of regioisomers (92 % major isomer by  $^1\text{H}$  NMR) under the cooler conditions shown in Scheme 3.9. There is a very high likelihood that the yield of **Hom1** was much greater than

that isolated due to losses encountered during the multiple unsuccessful attempts to remove the regioisomer.

### 3.2.3.5 Synthesis of Hom2; Complexation

The 4-bromophenyl- functionalized iridium(III) complex, **3.7**, was synthesized using the one-pot cyclometallation previously described. A mixture of the 4-bromophenyl functionalized ligand (**3.5**), iridium(III) chloride hydrate and silver(I) trifluoroacetate in glycerol was heated under an inert atmosphere in an oil bath at 180°C. The deep red crystalline complex, **3.7**, was isolated in 14 % yield.



Scheme 3.10: One-pot synthesis of 4-bromophenyl-functionalized iridium(III) complex, **3.7**

The yield of isolated **3.7** was consistently lower than for the non-halogenated  $[\text{Ir}(\text{tmq})_3]$ . Through  $^1\text{H}$  NMR analysis of the crude and between purification attempts it was deduced that the actual amount of **3.7** formed was significantly greater than the yield isolated. As was the case of  $[\text{Ir}(\text{tmq})_3]$  and its bromination product (**3.6**), the solubility of **3.7** is believed to be a limiting factor in obtaining maximum yields.

The 4-bromophenyl-functionalized iridium(III) complex, **3.7**, exhibited exceptionally poor solubility and very slow dissolution kinetics even when compared to the other materials described in this chapter. Attempts at optimizing the purification indicated that the major losses of **3.7**, indicated by  $^1\text{H}$  NMR and mass differences, occurred during chromatography over silica. It is likely then that **3.7** adsorbs onto the silica and becomes nearly inaccessible to solvent. Attempts at desorbing the material into solvent over days liberated only traces of product. Unfortunately a minor impurity could not be removed by any other method attempted and chromatography over silica was unavoidable.

The crystal structures of **3.7** functionality was obtained from crystals grown from solution by evaporation.

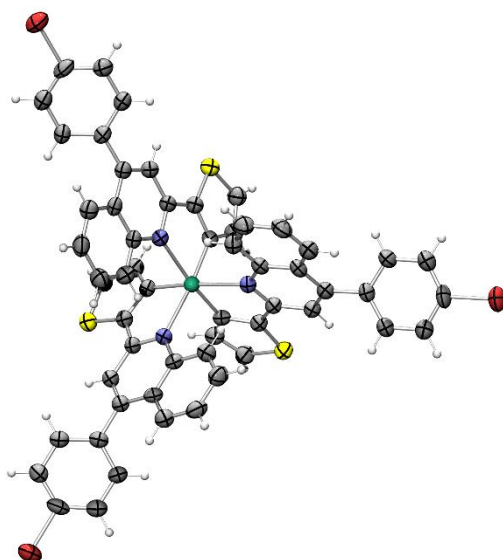


Figure 3.15: Structure of the homoleptic 4-bromophenyl-functionalized iridium(III) complexes, **3.7**, as determined by single-crystal X-ray diffraction experiments.

In complement with  $^1\text{H}$  NMR, the crystal structure enabled unambiguous assignment of **3.7** as being the expected *facial* isomer. As with  $[\text{Ir}(\text{tmq})_3]$ , the absence of other signals in the  $^1\text{H}$  NMR spectrum indicates that the obtained crystals were representative of the bulk and that only the *facial* geometric isomer was present. In contrast to the homoleptic iridium(III) complex with 5-bromothiophenyl moieties (**3.6**); the 4-bromophenyl-functionalized homoleptic iridium(III) complex (**3.7**) did not contain any regioisomers as the bromide functionality was incorporated prior to complexation.

Table 3.5: Crystallography data summary table; **3.7**

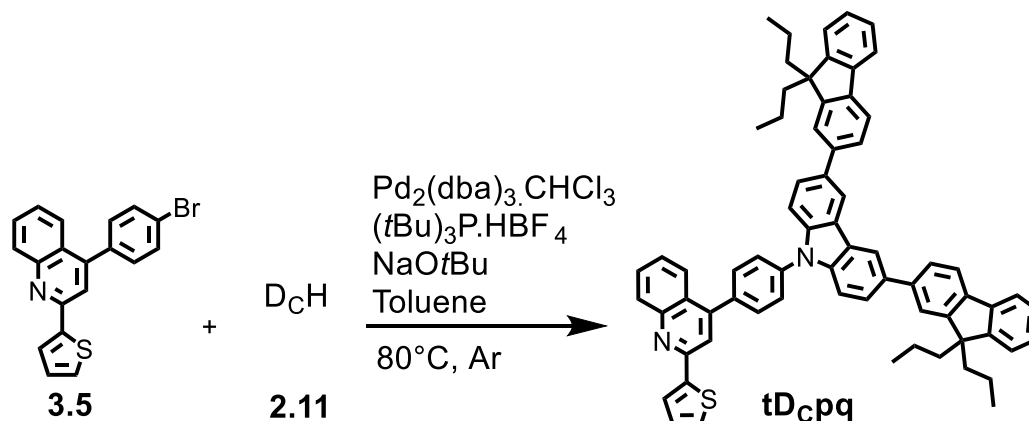
Material	<b>3.7</b>
Empirical Formula	C <sub>57</sub> H <sub>33</sub> Br <sub>3</sub> IrN <sub>3</sub> O <sub>0.17</sub> S <sub>3</sub>
Formula Weight	1290.65
Temperature/K	100(2)
Crystal System	trigonal
Space Group	<i>P</i> -3 <i>c</i> 1
a/ Å	17.712(3)
b/ Å	17.712(3)
c/ Å	17.804(4)
α/ °	90
β/ °	90
γ/ °	120
Volume/ Å <sup>3</sup>	4837.1(17)
Z	4
ρ <sub>calc</sub> g/cm <sup>3</sup>	1.772
μ/ mm <sup>-1</sup>	5.411
F(000)	2509.0
Crystal Size/ mm <sup>3</sup>	0.03 × 0.03 × 0.01
Radiation	synchrotron (λ = 0.7108)
2θ range for data collection/ °	2.656 to 52.744
Index ranges	-21 ≤ h ≤ 22, -22 ≤ k ≤ 22, -22 ≤ l ≤ 22
Reflections collected	67451
Independent reflections	3313 [R <sub>int</sub> = 0.0797, R <sub>sigma</sub> = 0.0213]
Data/restraints/parameters	3313/0/205
Goodness-of-fit on F <sup>2</sup>	1.042
Final R indexes [I > 2σ(I)]	R <sub>1</sub> = 0.0468, wR <sub>2</sub> = 0.1277
Final R indexes [all data]	R <sub>1</sub> = 0.0595, wR <sub>2</sub> = 0.1371
Largest diff. peak/hole / e Å <sup>-3</sup>	1.67/-1.23

### 3.2.3.6 Synthesis of Hom2; Buchwald-Hartwig Amination

To form the desired dendrimer (**Hom2**) the carbazoyl-dendron (**2.11**) was coupled to the 4-bromophenyl-functionalized iridium(III) complex (**3.7**) under Buchwald-Hartwig amination conditions. The first attempt involved heating **2.11** and **3.6** in refluxing anhydrous toluene in the presence of tris(dibenzylideneacetone)dipalladium(0)-chloroform adduct/ tri-*tert*-butylphosphonium tetrafluoroborate as the catalyst/ ligand system and sodium *tert*-butoxide as the base under an inert atmosphere. The desired product, **Hom1**, was isolated in approximately 18 % yield under these conditions at a small scale.

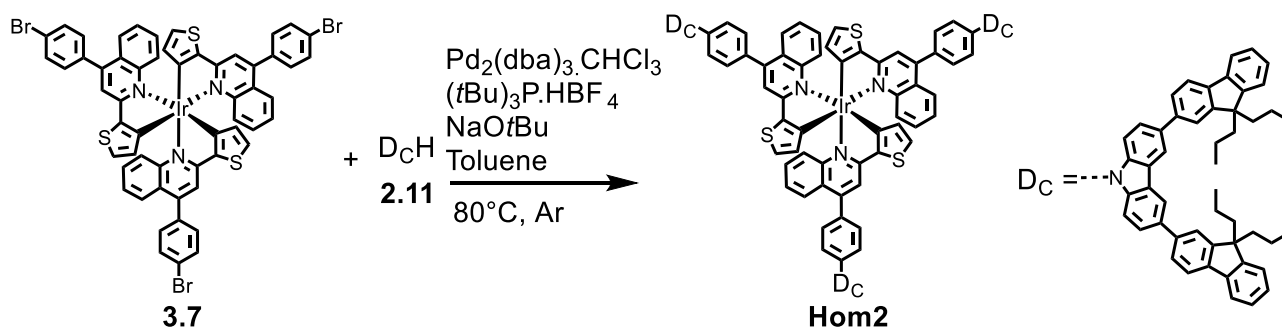
It was hypothesized that the yield of **Hom2** may be improved by heating the amination in an oil bath at 80°C rather than in refluxing toluene as this had worked for **Hom1**. It was not known whether the reactivity at the 4-bromophenyl moiety could be compared to that of the 2-bromothiophenyl. To avoid consumption of the precious **3.7**, a test coupling of **2.11** onto the 4-bromophenyl-functionalized ligand (**3.5**) was performed to investigate whether

the reaction would proceed at 80°C. The test product, **tDcpq**, was obtained in the respectable yield of 62 % which indicated that the cooler conditions may help improve the yield for **Hom2**.



Scheme 3.11: Buchwald-Hartwig amination to examine reactivity of the 4-bromophenyl position at 80°C.

As the Buchwald-Hartwig amination appeared to proceed well on the 4-bromophenyl-functionalized ligand, **3.5**; these conditions were utilized in the synthesis of **Hom2**. The amination by the carbazoyl-dendron (**2.11**) onto the 4-bromophenyl-functionalized iridium(III) complex (**3.7**) in anhydrous toluene in the presence of tris(dibenzylideneacetone)dipalladium(0)-chloroform adduct/ tri-*tert*-butylphosphonium tetrafluoroborate as the catalyst/ ligand system and sodium *tert*-butoxide as the base under an inert atmosphere heated in an oil bath at 80°C proceeded smoothly to give the homoleptic carbazoyl-dendronized iridium(III) complex, **Hom2**, in 48 % yield.

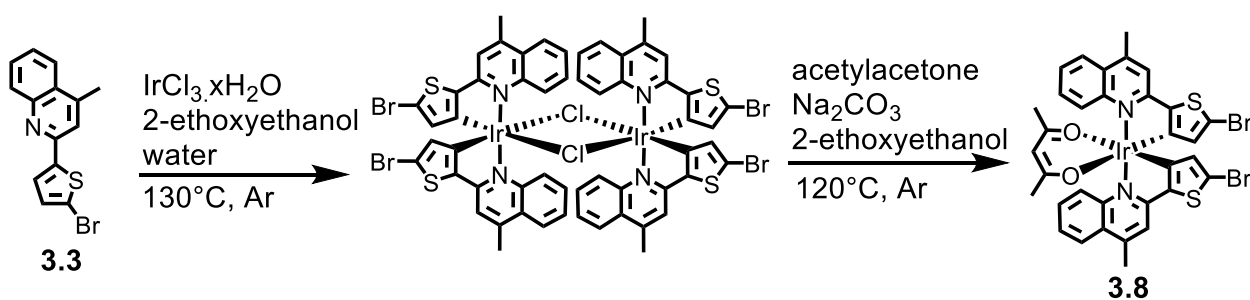


Scheme 3.12: Coupling of carbazoyl-dendron (**2.11**) to the brominated homoleptic iridium(III) core (**3.7**) by Buchwald-Hartwig amination to give the dendronized homoleptic iridium(III) core (**Hom2**).

Because the precursor, **3.7**, could be isolated as a single geometric and regioisomer; it was expected that **Hom2** would also be a single geometric and regioisomer. The  $^1\text{H}$  NMR suggested that this is the case as all observed signals could be attributed to the *facial* isomer as described.

### 3.2.3.7 Synthesis of Het1; Complexation

The  $\mu$ -dichloro-bridged iridium(III) dimer of the 5-bromothiophenyl-functionalized ligand (**3.3**) was synthesized by a modified Nonoyama route. Cyclometallation of iridium(III) chloride hydrate by **3.3** in aqueous 2-ethoxyethanol occurred with heating in an oil bath at  $130^\circ\text{C}$  under an inert atmosphere. After extraction the residues containing the  $\mu$ -dichloro-bridged iridium(III) dimers taken up into 2-ethoxyethanol and chelated by acetylacetonate in the presence of  $\text{Na}_2\text{CO}_3$  as a mild base heating in an oil bath at  $120^\circ\text{C}$  to give 5-bromothiophenyl-functionalized heteroleptic iridium complex, **3.8**, in 43 % yield.



Scheme 3.13: Two-step heteroleptic complexation: The  $\mu$ -dichloro-bridged iridium(III) dimer is formed using the Nonoyama route followed by chelation of the isolated complex by acetylacetonate.

Analysis of the resulting complex by  $^1\text{H}$  NMR indicated that the complex had been isolated as a mixture of the desired *trans-N,N'* isomer as the major product with a minor isomer displaying asymmetry indicative of a *cis-N,N'* isomer.

Attempts at separating the two isomers proved fruitless. This was likely due to a combination of their properties being very similar and the limitations of available purification techniques.



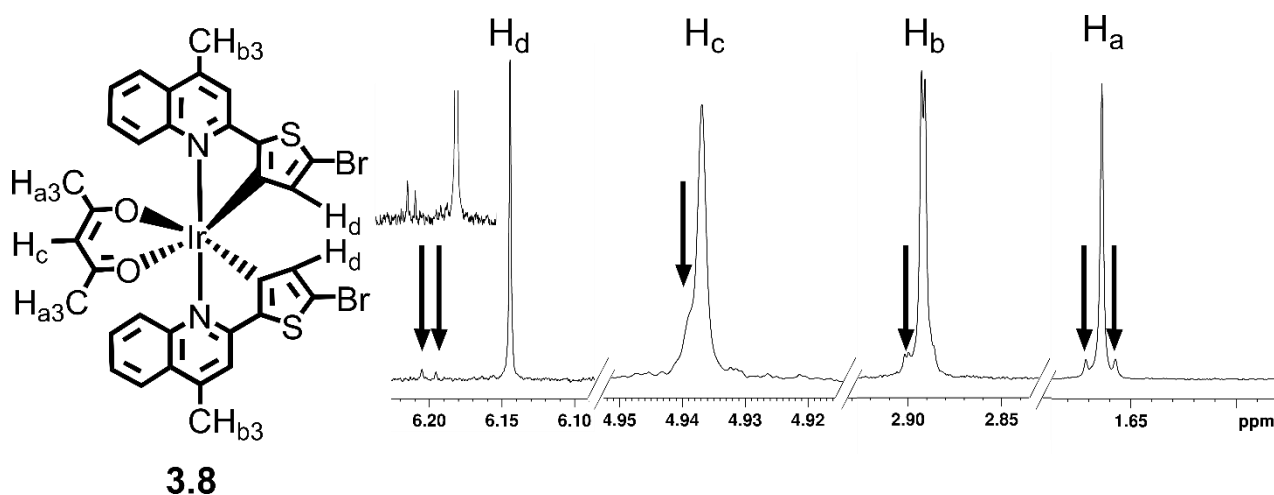


Figure 3.16: Proton NMR signals indicating that **3.8** is a mixture of two heteroleptic iridium(III) complexes. Peak assignments are shown. Signals corresponding to the minor isomer are indicated by arrows.

The proton signals shown in Figure 3.16 correspond to those where the minor isomer is most clearly identifiable. The thiophenyl proton alpha to the C-Ir bond (assigned as H<sub>d</sub> in Figure 3.16) is a particularly potent diagnostic peak as it is sharp, shifted upfield due to shielding from the nearby iridium(III) electron density, and appears to be strongly influenced by the neighbouring ligands.

The conditions used to form **3.8**, often referred to as the Nonoyama method, are the most common conditions used to form the  $\mu$ -dichloro-bridged dimer. The reaction entails heating iridium(III) chloride hydrate in the presence of the HC<sup>^</sup>N ligand in aqueous 2-ethoxyethanol at or near reflux.<sup>167,163</sup> The  $\mu$ -dichloro-bridged dimer is commonly formed as a precursor to the desired product, as was the case for **3.8**. However, when fully characterized in the literature the dimers almost always exhibit mutual *trans-N,N'* isomerism.<sup>168,169,170</sup> It is known that reactions with chelating ligands such as acetylacetonate the resultant complex maintains the *trans-N,N'* conformation of the parent dimer.

Cola *et al* have shown that both *trans-N,N'* and *cis-N,N'* isomers of iridium(III) complexes employing 2,2'-bipyridyl ancillary ligand can be deliberately synthesized by reducing the temperature during the formation of the  $\mu$ -dichloro-bridged dimer.<sup>163</sup> Following chelation with 2,2'-bipyridyl the isomers can be separated by high performance liquid chromatography. Cola *et al* also synthesized the same complexes as the pure *trans-N,N'* isomers from the dimer formed under refluxing conditions.

While the deliberate synthesis of a *cis-N,N'* isomer requires reduced reaction temperatures during  $\mu$ -dichloro-bridged dimer; accidental formation of a *cis-N,N'* has been reported as a result of thermally induced isomerism.<sup>162,161</sup> This is not overly surprising as

high temperatures are commonly used to ensure the formation of *facial* isomers in tris-C^N iridium(III) complexes, which require ligand reorganization from the *trans-N,N'*  $\mu$ -dichloro-bridged dimer.

There is no definitive cause for the observed *cis-N,N'* impurity in **3.8**. However, the two most likely scenarios are thermal isomerism occurred during the acetylacetonone chelation reaction or the steric hindrance of the quinoline moieties results in slightly higher temperature requirements to ensure pure formation of the *trans-N,N'* isomer. As the conditions used have been detailed within the literature multiple times without mention of additional isomers, it was more likely that the latter resulted in the formation of the *cis-N,N'* isomer as it is unique to this ligand system.

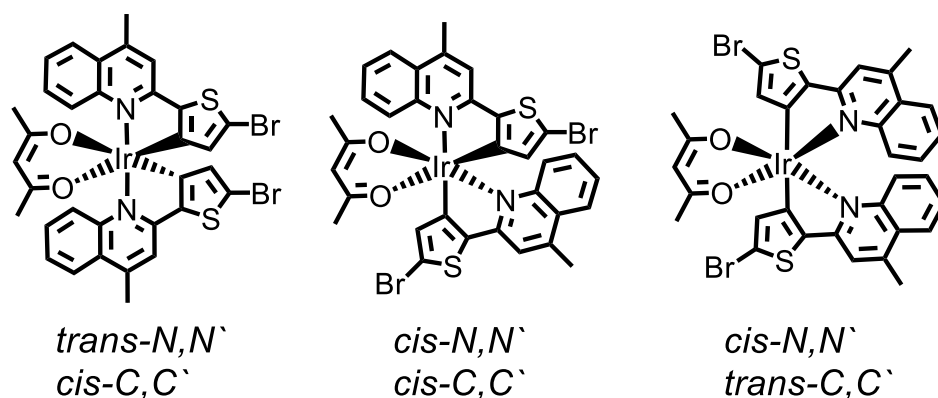


Figure 3.17: Possible geometric isomers of **3.8**.

The minor isomer in the mixture of **3.8** is most likely to be the *cis-N,N'*; *cis-C,C'* isomer. The  $^1\text{H}$  NMR strongly indicates that the aromatic ligands of the minor constituent are inequivalent. This inequivalence is expected for the *cis-N,N'*; *cis-C,C'* isomer but not for the *cis-N,N'*; *trans-C,C'* isomer which has a similar symmetry to the *trans-N,N'* isomer. The most commonly cited rationale for the preferential isomerism observed in cyclometallated iridium(III) complexes is the strong electronic effects of the formally anionic carbon ligands result in the formation of any *trans-C,C'* isomers being very unfavourable. These factors suggest that the *cis-N,N'*; *cis-C,C'* isomer is the minor component of **3.8**.

Diffraction quality crystals of the heteroleptic 5-bromothiophenyl-functionalized iridium(III) complex (**3.8**) were grown from solution and analysed by X-ray diffraction. The subsequent structures determined that the crystals contained a single geometric isomer and were solvated (dichloromethane and methanol).

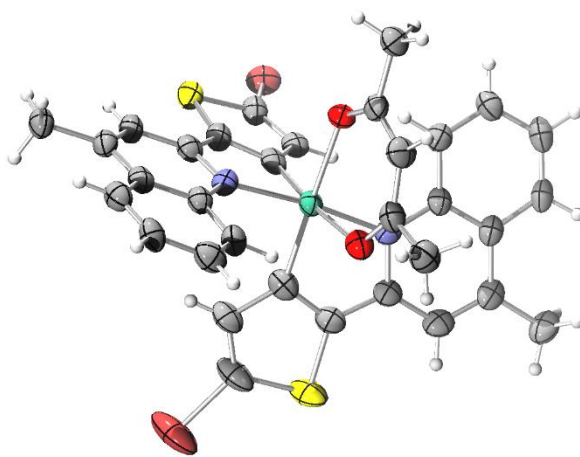


Figure 3.18: Structure of the heteroleptic bromide-functionalized iridium(III) complex, **3.8**.

Table 3.6: Crystallography data summary table; Heteroleptic bromide-functionalized iridium(III) complexes

Material	<b>3.8</b>
Empirical Formula	$C_{34.33}H_{27}Br_2Cl_2IrN_2O_{2.5}S_2$
Formula Weight	994.62
Temperature/K	100(2)
Crystal System	monoclinic
Space Group	<i>C2/c</i>
a/ Å	24.563(5)
b/ Å	17.325(4)
c/ Å	16.604(3)
$\alpha$ / °	90
$\beta$ / °	104.66(3)
$\gamma$ / °	90
Volume/ Å <sup>3</sup>	6836(3)
Z	8
$\rho_{calc}$ g/cm <sup>3</sup>	1.933
$\mu$ / mm <sup>-1</sup>	6.560
F(000)	3840.0
Crystal Size/ mm <sup>3</sup>	0.07 × 0.07 × 0.03
Radiation	synchrotron ( $\lambda = 0.7108$ )
2 $\theta$ range for data collection/ °	2.91 to 52.748
Index ranges	-30 ≤ h ≤ 30, -21 ≤ k ≤ 21, -20 ≤ l ≤ 20
Reflections collected	46807
Independent reflections	6439 [ $R_{int} = 0.0451$ , $R_{sigma} = 0.0259$ ]
Data/restraints/parameters	6439/1/428
Goodness-of-fit on F <sup>2</sup>	1.045
Final R indexes [ $I > 2\sigma(I)$ ]	$R_1 = 0.0516$ , $wR_2 = 0.1367$
Final R indexes [all data]	$R_1 = 0.0576$ , $wR_2 = 0.1419$
Largest diff. peak/hole / e Å <sup>-3</sup>	3.42/-2.56

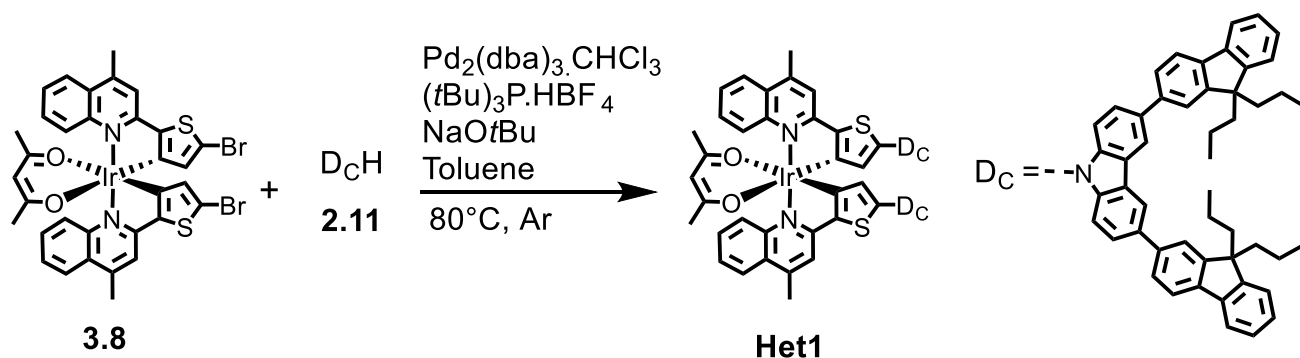
As suggested by the  $^1\text{H}$  NMR, the geometric isomer of **3.8** was found to be *trans-N,N'*. However, it was also known from the  $^1\text{H}$  NMR that this structure cannot be representative of the bulk as there are additional signals present. From the accumulated results there was strong evidence that **3.8** was isolated in 43 % yield as a mixture of the major *trans-N,N'*; *cis-C,C'* isomer (95 %) with the remainder being the *cis-N,N'*; *cis-C,C'* isomer (5 %). The composition was estimated by  $^1\text{H}$  NMR.

It is noteworthy that only a single geometric isomer of **3.8** was observed during single-crystal X-ray experiments as this alludes to a geometric-isomerically pure material being obtained by during crystallization. This suggests that the isomers should be separable by careful recrystallization. Despite this,  $^1\text{H}$  NMR analysis showed relative concentrations of the two geometric isomers did not vary significantly over the course of multiple recrystallizations.

The most plausible scenario to explain these observations is that both isomers have very similar solubilities causing them to crystallize as separately, however, still being inseparable within the bulk. It is likely that the minor isomer was not observed in X-ray diffraction experiments due to experimental bias. It is likely that the lower concentration of the minor isomer resulted in crystals that were regarded as inferior for single-crystal X-ray diffractometry due to either smaller size or possibly inter-growth with crystals of the major isomer.

#### 3.2.3.8 Synthesis of Het1; Buchwald-Hartwig Amination

The Buchwald-Hartwig amination of the heteroleptic iridium(III) complex, **3.8**, was conducted using the same conditions found to be optimal for the synthesis of **Hom1** and **Hom2**. A solution of the 5-bromothiophenyl-functionalized heteroleptic iridium(III) complex, **3.8**, and the carbazoyl-dendron, **2.11**; in the presence of tris(dibenzylideneacetone)dipalladium(0)-chloroform adduct/ tri-*tert*-butylphosphonium tetrafluoroborate as the catalyst/ ligand system and sodium *tert*-butoxide as the base; was heated in an oil bath at 80°C under an inert atmosphere to give **Het1** in 33 % yield.



Scheme 3.14: Buchwald-Hartwig amination of heteroleptic iridium(III) complex, **3.8**, carbazoyl-dendron, **2.11**.

While the brominated precursor, **3.8**, was known to be an inseparable mixture of two geometric isomers; the  $^1\text{H}$  NMR spectrum of the dendronized heteroleptic iridium(III) complex, **Het1**, was found to only show signals corresponding to the *trans-N,N'* geometric isomer. It was found that the minor isomer was efficiently removed from the crude during purification by size exclusion chromatography. While the isomers of the bromide precursor were of a similarly size, substitution with the bulky carbazoyl-dendrons results in the different isomer geometries having very different hydrodynamic radii.

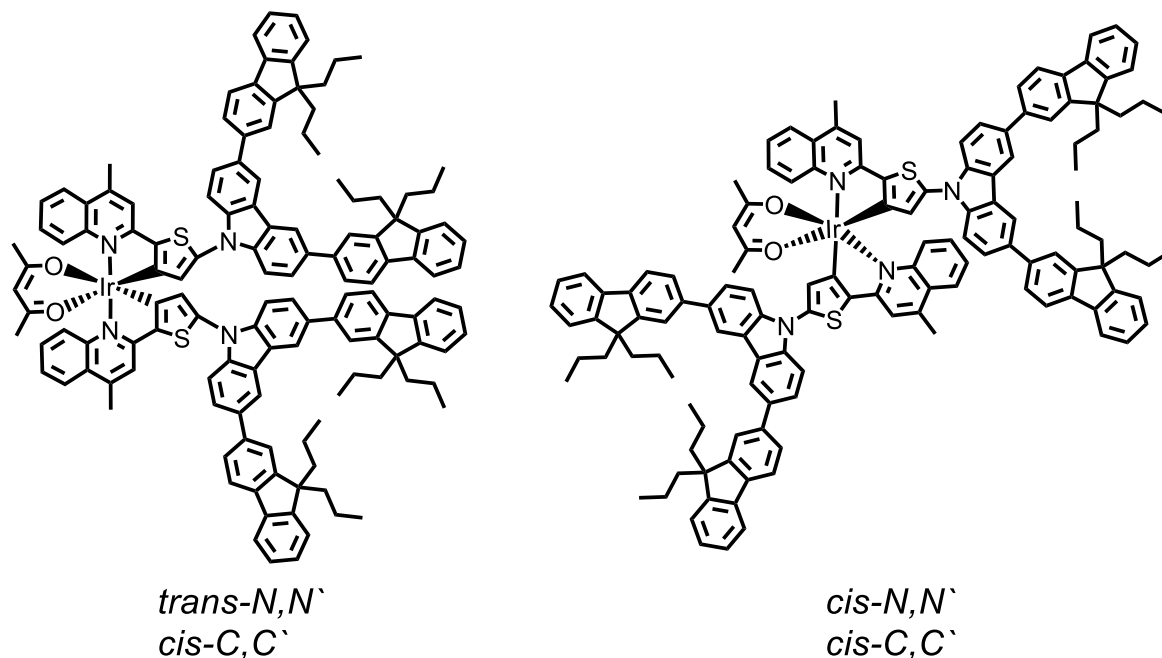


Figure 3.19: Structures of the geometric isomers of **Het1** synthesized from **3.8**. The different geometries result in large differences in hydrodynamic radii.

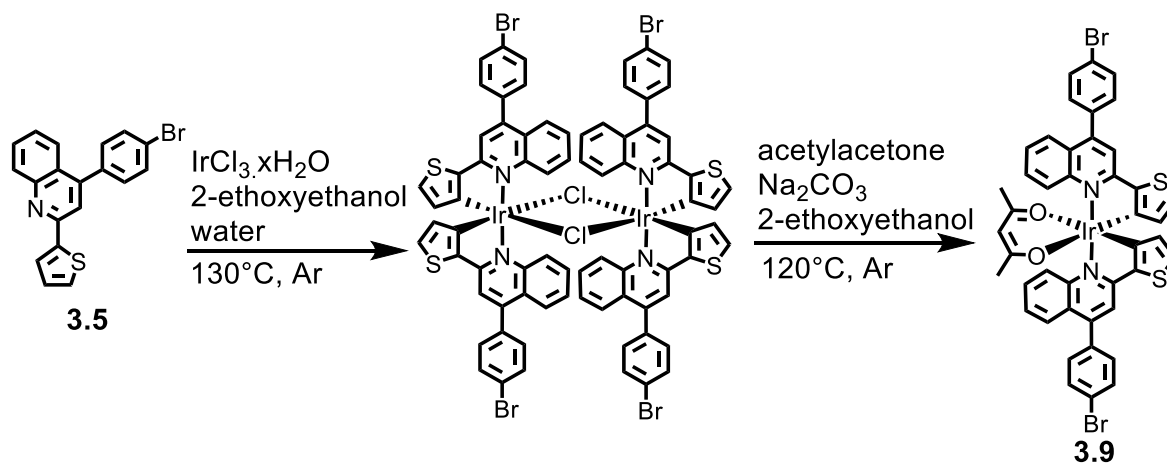
The dendrons of the *trans-N,N'* geometric isomer of **Het1** project from a shared edge of the octahedral complex while the dendrons of the *cis-N,N'*; *cis-C,C'* isomer project from

opposite faces. The major *trans-N,N'* isomer therefore appears more compact than the minor isomer component. This variation in dendrimer geometry allows separation of the isomers based on their hydrodynamic radii through size exclusion chromatography.

While the starting brominated precursor, **3.8**, was a mixture of geometric isomers; **Het1** was efficiently isolated as exclusively the *trans-N,N'* geometric isomer determined by the absence of other components by <sup>1</sup>H NMR and gel permeation chromatography.

### 3.2.3.9 Synthesis of Het2; Complexation

The  $\mu$ -dichloro-bridged iridium(III) dimer of the 4-bromophenyl-functionalized ligand (**3.5**) was synthesized by a modified Nonoyama route. Cyclometallation of iridium(III) chloride hydrate by **3.5** in aqueous 2-ethoxyethanol occurred with heating in an oil bath at 130°C under an inert atmosphere. After extraction the residues containing the  $\mu$ -dichloro-bridged iridium(III) dimers taken up into 2-ethoxyethanol and chelated by acetylacetonone in the presence of Na<sub>2</sub>CO<sub>3</sub> as a mild base heating in an oil bath at 120°C to give 5-bromophenyl-functionalized heteroleptic iridium complex, **3.9**, in 8 % yield.



Scheme 3.15: Two-step heteroleptic complexation to give **3.9**: The  $\mu$ -dichloro-bridged iridium(III) dimer is formed using the Nonoyama route followed by chelation of the isolated complex by acetylacetonone.

The lower than expected yield obtained for **3.9** is due to its especially high sensitivity to the acidic nature of silica. Iridium(III) complexes are known to readily decompose back to the  $\mu$ -dichloro-bridged complex in the presence of acid halides, including hydrochloric acid and zinc(II) chloride, so it was hypothesized that perhaps minute decomposition of the chlorinated solvents also played a role alongside the silica.<sup>171,172</sup> Unfortunately **3.9** exhibited limited solubility in non-halogenated solvents and the  $\mu$ -dichloro-bridged complex was observed to adsorb virtually irreversibly onto the silica so could not be recovered.

Purification was attempted excluding the use of silica. However, certain impurities could not be removed by any other method attempted. The unsuccessful purification attempts were conducted on portions of the crude and included recrystallization, precipitation, Soxhlet extraction, chromatotron, sublimation and size-exclusion chromatography. Decomposition of **3.9** was the only result of the chromatotron and sublimation attempts; while the recrystallization and Soxhlet extraction were inhibited through the impurity either having similar solubility to **3.9** or through a solubilizing interaction that precluded separation.

Adjusting the pH of the silica through pre-treatment with a pH 7 phosphate buffer or treatment of the packed column with triethylamine, while successful for some materials, provided no improvement for **3.9**. The reported 8 % is the optimized yield using only a single silica column.

The  $^1\text{H}$  NMR spectrum of the 4-bromophenyl-functionalized iridium(III) heteroleptic complex, **3.9**, contained signals indicative of a major geometric isomer with equivalent aromatic ligands and a minor geometric isomer with inequivalent aromatic ligands; in the same fashion as was observed for the 5-bromothiophenyl-functionalized heteroleptic iridium(III) complex, **3.9**.

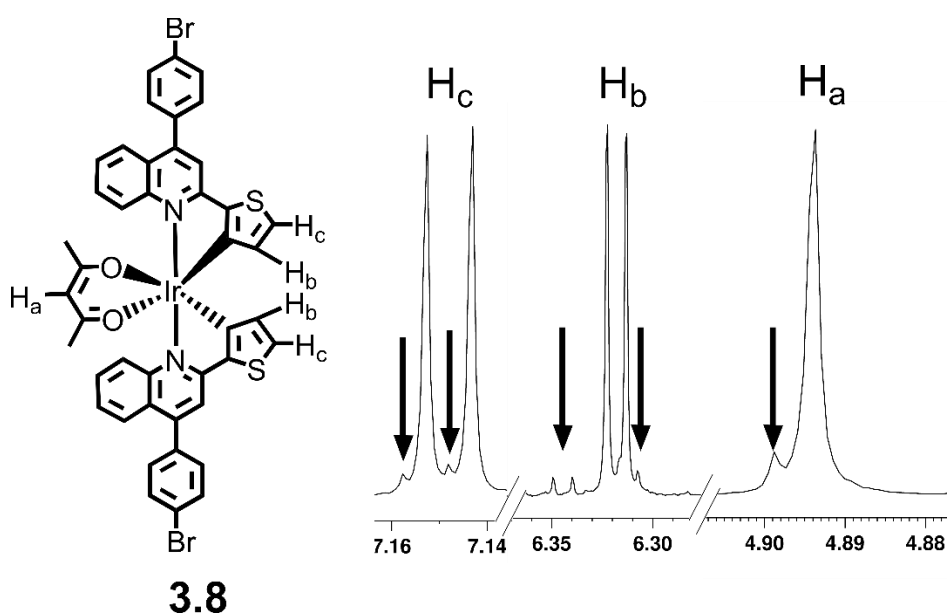


Figure 3.20: Proton NMR signals indicating that **3.9** is a mixture of two heteroleptic iridium(III) complexes. Peak assignments are shown. Signals corresponding to the minor isomer are indicated by arrows.

The proton signals shown in Figure 3.18 correspond to those where the minor isomer is most clearly identifiable. The appearance of the minor geometric isomer signals in the  $^1\text{H}$  NMR spectrum of **3.9** mirrored the other bromide functionalized heteroleptic iridium(III)

complex, **3.8**. The thiophenyl proton alpha to the C-Ir bond (assigned as H<sub>b</sub> in Figure 3.18) of **3.9** was again the most potent diagnostic peak for the presence of multiple geometric isomers.

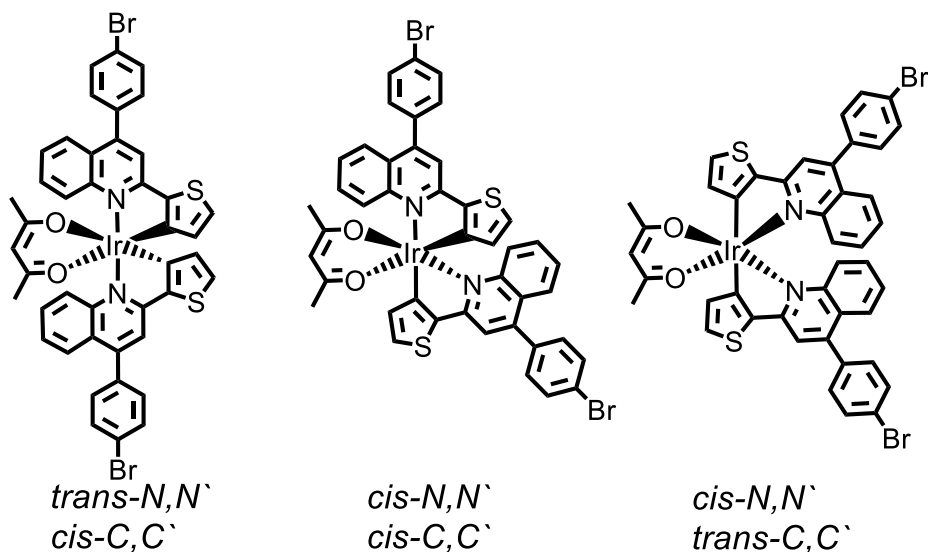


Figure 3.21: Possible geometric isomers of **3.9**.

As in the alternate heteroleptic complex, the intensity of the signals originating from the major geometric isomer (*trans-N,N'*) made it difficult to unambiguously identify the geometry of the minor isomer in **3.9**. It was very likely that the minor isomer was the *cis-N,N'*; *cis-C,C'* isomer as the *trans-C,C'* isomer would be energetically unfavourable. The signals from the minor isomer within the <sup>1</sup>H NMR spectrum of **3.9** also indicate the presence of two inequivalent aromatic ligands which only the *cis-N,N'*; *cis-C,C'* isomer can produce.

Diffraction quality crystals of the heteroleptic 4-bromophenyl-functionalized iridium(III) complex (**3.9**) were grown and analysed by X-ray diffraction. The subsequent structures determined that the crystals contained a single geometric isomer and were solvated by chlorobenzene.



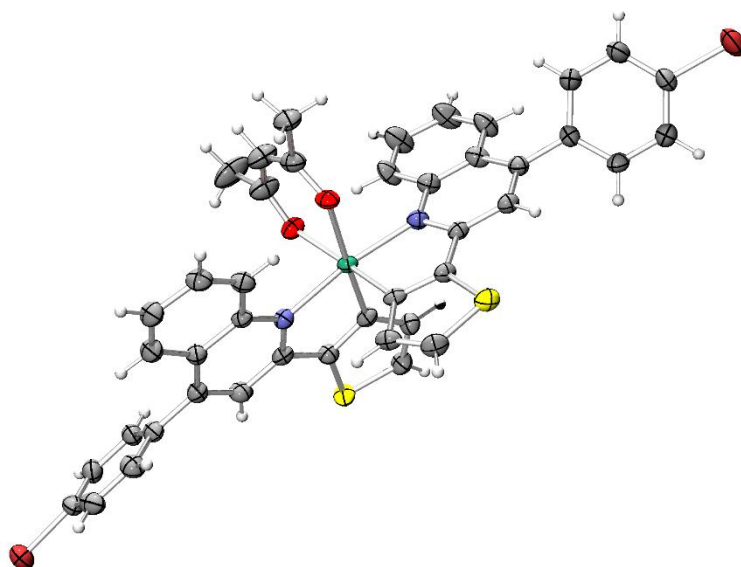


Figure 3.22: Structure of the heteroleptic bromide-functionalized iridium(III) complex, **3.9**.

Table 3.7: Crystallography data summary table; **3.9**

Material	<b>3.9</b>
Empirical Formula	$C_{55}H_{39}Br_2Cl_2IrN_2O_2S_2$
Formula Weight	1246.92
Temperature/K	100(2)
Crystal System	monoclinic
Space Group	$P2_1/c$
a/ Å	16.753(3)
b/ Å	17.524(4)
c/ Å	16.376(3)
$\alpha/^\circ$	90
$\beta/^\circ$	90.64(3)
$\gamma/^\circ$	90
Volume/ Å <sup>3</sup>	4807.4(17)
Z	4
$\rho_{calc}$ g/cm <sup>3</sup>	1.723
$\mu$ / mm <sup>-1</sup>	4.683
F(000)	2448.0
Crystal Size/ mm <sup>3</sup>	0.12 × 0.08 × 0.08
Radiation	synchrotron ( $\lambda = 0.7108$ )
2 $\theta$ range for data collection/ °	2.432 to 56.572
Index ranges	$-22 \leq h \leq 22, -23 \leq k \leq 18, -21 \leq l \leq 13$
Reflections collected	22678
Independent reflections	10997 [ $R_{int} = 0.0416, R_{sigma} = 0.0327$ ]
Data/restraints/parameters	10997/81/638
Goodness-of-fit on F <sup>2</sup>	1.090
Final R indexes [ $ I  > 2\sigma(I)$ ]	$R_1 = 0.0512, wR_2 = 0.1299$
Final R indexes [all data]	$R_1 = 0.0553, wR_2 = 0.1326$
Largest diff. peak/hole / e Å <sup>-3</sup>	2.04/-2.06

In complement with the  $^1\text{H}$  NMR spectroscopy, the crystallography identified the major geometric isomer as being *trans-N,N'*. From the  $^1\text{H}$  NMR spectroscopy it was known that the crystal analysed could not be representative of the bulk as the presence of a second isomer was known. The minor isomer was believed to be in the *cis-N,N'*; *cis-C,C'* geometry which was indicated by the observed inequivalence of the  $^1\text{H}$  NMR signals and unfavourable thermodynamics eliminating the remaining possible isomer (*trans-C,C'*) as a candidate.

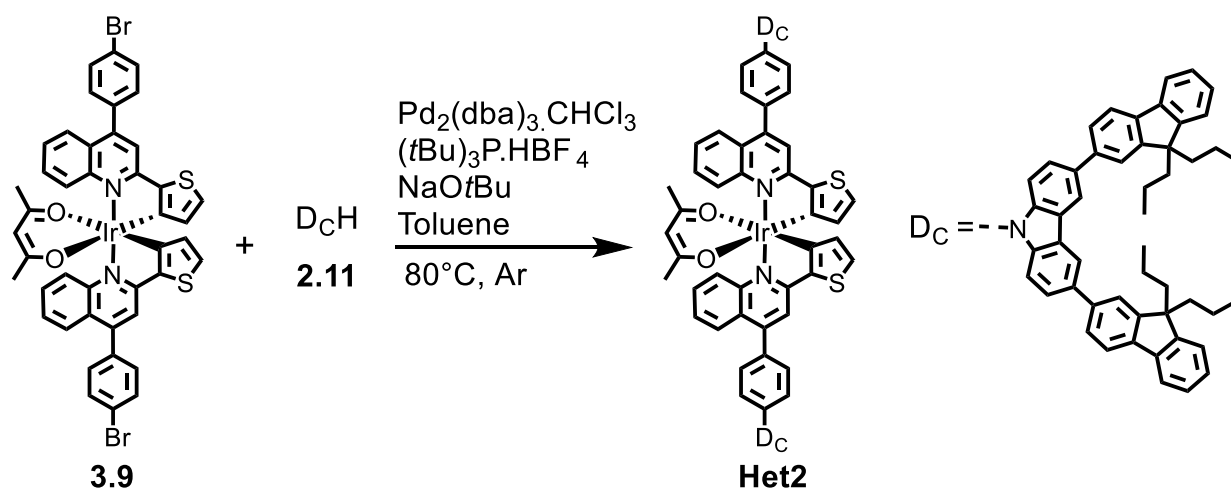
As was observed for **3.8**, the single-crystal X-ray diffraction experiments suggested that crystals containing exclusively the *trans-N,N'* geometric isomer of **3.9** were being obtained. Similarly, recrystallization was found to be ineffective at separating the geometric isomers to any noticeable extent as determined by  $^1\text{H}$  NMR.

From this it was deduced that the geometric isomers of **3.9** were practically inseparable by recrystallization due to exhibiting the same crystallization behaviour as **3.8**. The geometric isomers of **3.9** seem exhibit very similar solubilities and therefore crystallize under very similar conditions. Although the diffractometry suggests that the major geometric isomer is present exclusively within the diffraction quality crystals, the minor geometric isomer is still present within the bulk as inferior quality crystals.

Ultimately, **3.9** was isolated in 8 % yield as a mixture of geometric isomers. The composition of the mixture was estimated by  $^1\text{H}$  NMR to be a ratio of 90:10 of the major: minor isomers, respectively. The major isomer was found to be of the *trans-N,N'* geometry and the minor isomer is strongly suspected to be of the *cis-N,N'*; *cis-C,C'* geometry.

#### **3.2.3.10 Synthesis of Het2; Buchwald-Hartwig Amination**

The Buchwald-Hartwig amination of the heteroleptic iridium(III) complex, **3.9**, was conducted using the same conditions found to be optimal for the previous brominated iridium(III) complexes. A solution of the 4-bromophenyl-functionalized heteroleptic iridium(III) complex, **3.9**, and the carbazolyl-dendron, **2.11**; in the presence of tris(dibenzylideneacetone)dipalladium(0)-chloroform adduct/ tri-*tert*-butylphosphonium tetrafluoroborate as the catalyst/ ligand system and sodium *tert*-butoxide as the base; was heated in an oil bath at 80°C under an inert atmosphere to give **Het2** in 32 % yield.



Scheme 3.16: Buchwald-Hartwig amination of heteroleptic iridium(III) complex, **3.9**, carbazolyldendron, **2.11**.

The dendrimer, **Het2**, was isolated as a pure geometric isomer despite the starting 4-bromophenyl-functionalized heteroleptic iridium(III) complex, **3.9**, containing a mixture of inseparable geometric isomers. As was previously described for **Het1**, the geometric isomers appeared to be easily separable by size exclusion chromatography due to the difference in shape leading to a large difference in hydrodynamic radii.

The dendrimers sharing the dendronized phenyl-ligand, **Hom2** and **Het2**, were both observed to exhibit a crystalline habit. This contrasted strongly with the dendrimers containing the dendronized thiophenyl-ligand, **Hom1** and **Het1**, which macroscopically appeared to form disordered powders or glasses when crystal growth was attempted. Additionally **Het2** exhibited exceptionally low solubility compared to the other dendrimers which was theorised to be an extension of its preference towards crystallization.

Although both dendrimers formed very small crystals which could be identified under an optical microscope, only **Het2** formed crystals of sufficient size for structural analysis. The diffraction pattern of the solvent grown crystals of **Het2** were collected utilizing synchrotron radiation as the source. Even with this intense and focused source of radiation the structure was only resolved by co-refinement patterns from multiple crystals.

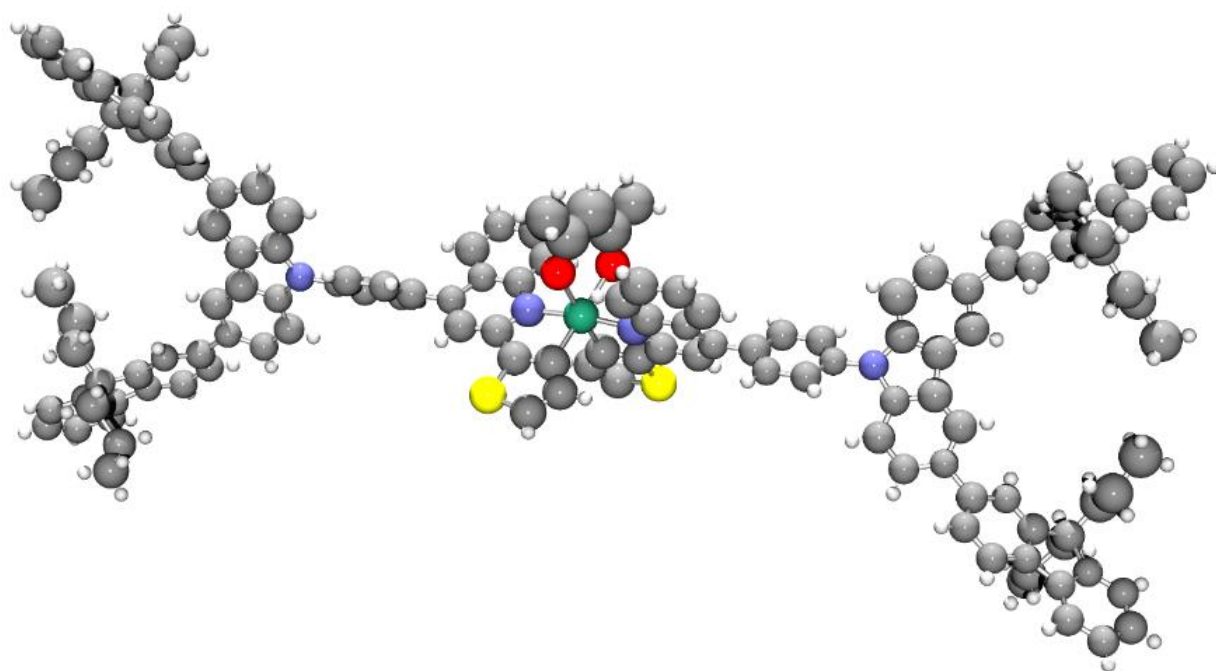


Figure 3.23: Structure of **Het2** as determined by single-crystal X-ray diffraction experiments.

While obtaining sufficient data for structure refinement appeared difficult on the surface, the structure of **Het2** was found to be extremely well ordered and the positions and connectivity of all (non-hydrogen) atoms were extremely well defined. Complementary to the  $^1\text{H}$  NMR spectrum, **Het2** was found to unambiguously exist as the *trans-N,N'* geometric isomer. As only signals corresponding to this geometric isomer were observed in the  $^1\text{H}$  NMR spectrum; the crystal structure was representative of the bulk. This result was not only significant for characterizing the material but also for confirming that the Buchwald-Hartwig amination conditions do not induce isomerism. This was already strongly suspected from the  $^1\text{H}$  NMR but this was the first piece of complementary evidence for confirmation.

Table 3.8: Crystallography data summary table- Heteroleptic Dendrimer

Material	<b>[Ir(tD<sub>CPQ</sub>)<sub>2</sub>(acac)]</b>
Empirical Formula	C <sub>143</sub> H <sub>125</sub> IrN <sub>4</sub> O <sub>2</sub> S <sub>2</sub>
Formula Weight	2187.78
Temperature/K	100(2)
Crystal System	Monoclinic
Space Group	<i>C2/c</i>
a/ Å	49.128(10)
b/ Å	20.939(4)
c/ Å	15.714(3)
α/ °	90
β/ °	104.25(3)
γ/ °	90
Volume/ Å <sup>3</sup>	15667(6)
Z	4
ρ <sub>calc</sub> g/cm <sup>3</sup>	0.928
μ/ mm <sup>-1</sup>	0.920
F(000)	4544.0
Crystal Size/ mm <sup>3</sup>	0.05 × 0.03 × 0.001
Radiation	synchrotron (λ = 0.7108)
2θ range for data collection/ °	1.71 to 50.48
Index ranges	-35 ≤ h ≤ 35, -14 ≤ k ≤ 14, -11 ≤ l ≤ 11
Reflections collected	16247
Independent reflections	2861 [R <sub>int</sub> = 0.1291, R <sub>sigma</sub> = 0.0833]
Data/restraints/parameters	2861/11/222
Goodness-of-fit on F <sup>2</sup>	1.253
Final R indexes [I > 2σ(I)]	R <sub>1</sub> = 0.1558, wR <sub>2</sub> = 0.3815
Final R indexes [all data]	R <sub>1</sub> = 0.1743, wR <sub>2</sub> = 0.4055
Largest diff. peak/hole / e Å <sup>-3</sup>	0.72/-2.48

As shown in Figure 3.21, the thermal ellipsoids of each atom were relatively large and symmetrical. While the observed ellipsoids would encompass the actual thermal motion of the atoms with **Het2**, it is likely that much of the ellipsoids are a result of the weakly diffracting crystal despite using a synchrotron radiation source. While the thermal ellipsoids should be evaluated with caution, the atomic positions and connectivity are extremely well defined.

The dendrimer was surprisingly well ordered despite containing multiple bonds around which free rotation could occur. In aromatic compounds this rotation is often limited by either extended conjugation through which energy is minimized and multiple rings, with freedom of rotation, acquire mutual co-planarity. The only co-planar aromatic moieties within the structure of **Het2** are those that are locked into planarity by covalent or co-ordination bonding; the carbazolyl, fluorenyl and quinoliny-thiophenyl moieties. The *n*-propyl chains attached to the fluorenyl-moieties were particularly interesting as they exhibited strong

preference for a single conformation with relatively little disorder. The alkyl chains appear to prefer the classic staggered conformation of *n*-alkyl chains corresponding to the lowest energy. As the fluorenyl-moieties were rotated with the alkyl chains angled towards the other fluorenyl-moiety of the same dendron, it was likely that the lipophilic London dispersion forces between the alkyl chains are the motivating force for this preference.

No single driving force was observed to describe why **Het2** preferentially forms highly ordered crystals which exhibit poor solubility. A possible explanation would be that the molecules of **Het2** have the ability to pack very neatly with the majority of the molecules surfaces at or near their energy minima. The ability to pack closely may be a combination of the molecules two-fold symmetry and the size relationship between the iridium(III) complex and the carbazoyl-dendrons coincidentally being ideal to minimize void spaces. It was deemed prudent to examine the Ir-Ir distances of **Het2** and its precursor, **3.9**, to examine how this packing may affect material performance.

One of the primary desirable characteristics that dendrons commonly impart upon a iridium(III) complexes is spatial separation of the iridium(III) centres. This is important as the rate of non-radiative triplet-triplet annihilation increases with shorter distance between excited iridium(III) centres. Efficient separation of iridium(III) centres is therefore an essential property for dendronized complexes. This becomes a potential issue for **[Ir(tDcpq)<sub>2</sub>(acac)]** as the bromide intermediate, **3.9**, shows greater Ir-Ir separation than the dendrimer.

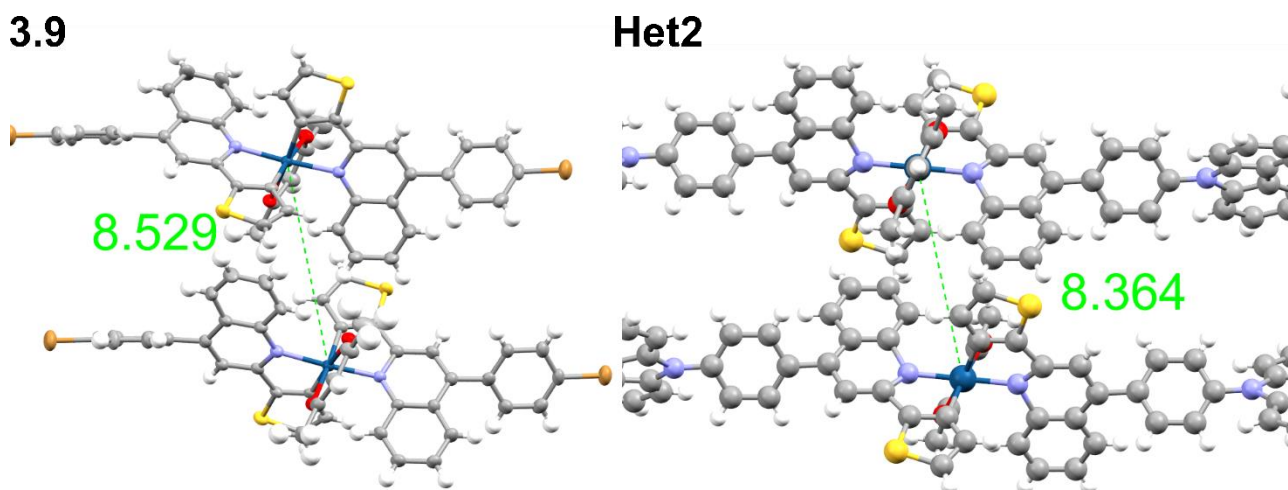


Figure 3.24: Comparison of the Ir-Ir distance in crystals of **3.9** and **Het2**. Much of the dendrons are not included for **Het2** for clarity.

The significance of the precise values for the Ir-Ir distances shown in Figure 3.22 were certainly debatable. While the positions of the heavy iridium(III) centres should be

accurate, even for the weak diffracting **Het2**, it is uncertain whether the observed orientations were indicative of interactions within a solution processed film. What was not debatable was that the dendrons of **Het2** were not improving the separation of iridium(III) centres under all conditions. Combined with the lower than expected solubility it was clear that the dendrons were not endowing **Het2** with the improvements observed in previous materials. This was an important observation as it was the first dendronized substrate within the project to illustrate that the addition of dendrons to a complex will not universally lead to improvements in solubility and decreased interchromophore interactions.

### 3.2.3.11 Iridium(III) complex purification discussion

As alluded to throughout this chapter, all of the iridium(III) complexes appear to experience a detrimental interaction with silica gel. In the cases of the tris-C<sup>N</sup> iridium(III) complexes this typically results in minor losses to yield. The complexes containing the acetylacetonate ligand were found to be exceptionally sensitive to silica. **Het2** and the precursor **3.9** were found to be particularly unstable on silica with almost complete loss of material under column chromatography conditions. Various techniques were attempted to combat this including; pre-treatment of the silica with triethylamine or aqueous pH 7 phosphate buffer, including triethylamine in the eluent system and both flash and gravity feeding to alter the kinetics of the system.

It is believed that many of the yields were considerably higher than reported but losses during purification, particularly the optimization of purification, resulted in the stated values.

Size exclusion chromatography proved instrumental in the isolation of the dendrimers. Following initial purification by column chromatography over silica, size exclusion chromatography through a column of BioRad Laboratories Bio-Beads S-X1 allowed the separation of the similar polarity intermediates; as well as the removal of minor geometric isomers of **Het1** and **Het2**. Because the size exclusion chromatography utilizes a neutral organic substrate it could be conducted repeatedly with little product loss unlike chromatography over silica.

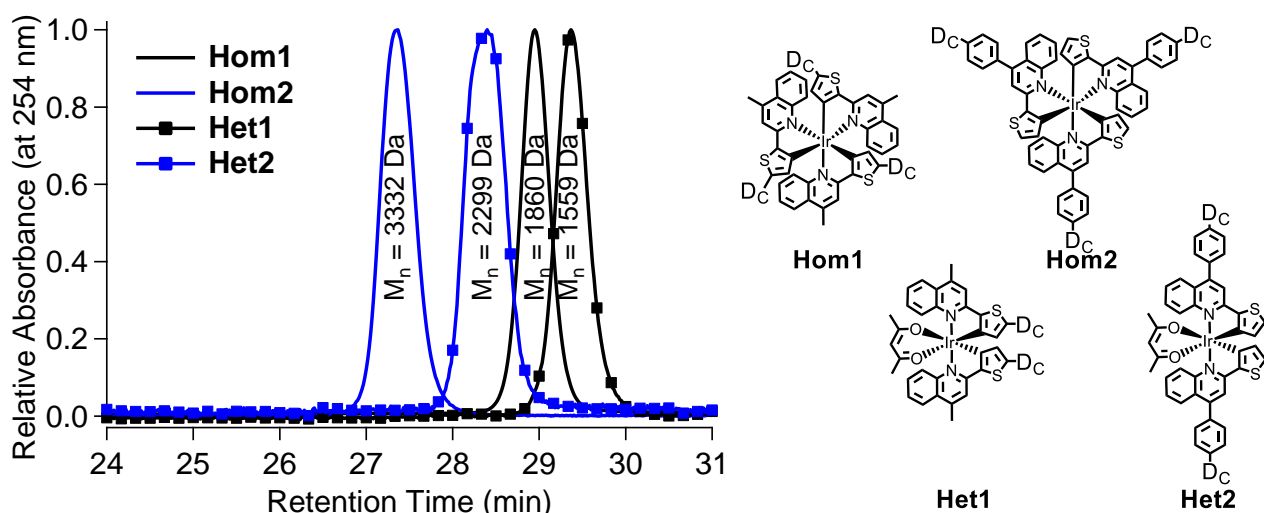


Figure 3.25: Gel permeation chromatography traces of the red-emitting dendrimers demonstrating the large variation in hydrodynamic volume and its structural relationship. The  $M_n$  values for each dendrimer are included for reference.

The effectiveness of the size exclusion chromatography for purification of dendrimers can be understood by examining the gel permeation chromatograms of the four dendrimers. It can be shown that the apparent hydrodynamic volume, the primary molecular property which induces separation by size exclusion chromatography, is strongly dependent upon molecular geometry. The complexes in which the bulky dendron is attached through the thiophenyl-moiety, **Hom1** and **Het1**, have a much smaller hydrodynamic radius as the bulky dendrons are clustered in close proximity to one another. The complexes where the dendrons are attached at the 4-phenyl position, **Hom2** and **Het2**, appear much larger as the dendrons extend away from each other in an almost planar fashion. Because of this the minor geometric isomer in **Het1** and **Het2** would exhibit very different hydrodynamic radii to the major isomer which allows simple separation by size exclusion chromatography.

### 3.3 Re-evaluated Poly(dendrimer)

#### 3.3.1 Design Rationale

The difficulties experienced with the **IT1** and **IT2**; followed by the successes of the dendrimer series would lead to an alternate idea on how a poly(dendrimer) containing a red-emitting iridium(III) complex may be synthesized. With the knowledge that the cracking reaction is effective to form green-emitting complexes and that 4-(4-bromophenyl)-2-(thiophen-2-yl)quinoline (**3.5**) was able to undergo cyclometallation of iridium(III) at high temperatures; it was proposed that the synthetic route used to give **L2**<sup>142</sup> could be utilized



with the substitution of 5-(3-bromophenyl)-1-methyl-3-propyl-1*H*-1,2,4-triazole (**2.2**) with **3.5**. This would result in the red-emitting poly(dendrimer), **PD<sub>c</sub>R**, as shown in Figure 3.26.

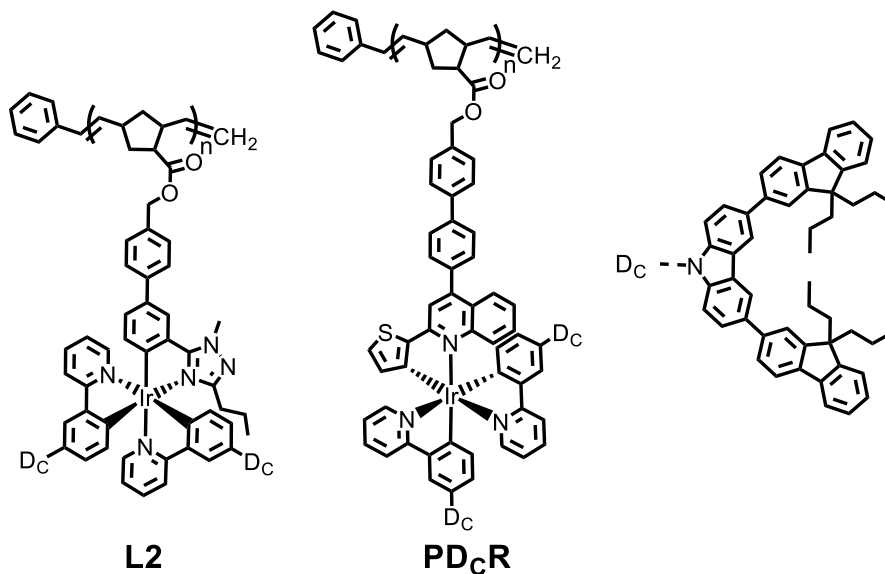


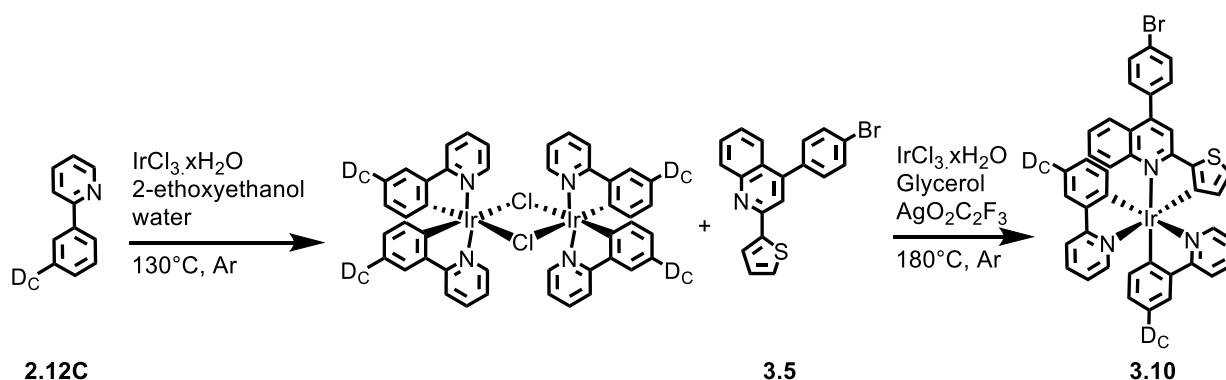
Figure 3.26: Reported green-emitting poly(dendrimer) containing iridium(III) complex (**L2**) and the proposed red-emitting poly(dendrimer (**PD<sub>c</sub>R**) designed by exchanging the non-emissive ancillary ligand with the red-emitting ligand.

### 3.3.2 Synthesis

#### 3.3.2.1 Complexation

The  $\mu$ -dichloro-bridged dimer was formed as per (Scheme 2.6 in section 2.2.5). In a similar fashion to the synthesis of the green-emitting poly(dendrimer)s in chapter 2, the cyclometallation was performed on the dimer without further purification. The initial attempt was performed at the same temperatures conducted for the green-emitting materials: 168°C. Unfortunately only traces of the desired material were formed as indicated by <sup>1</sup>H NMR and mass spectra.

It was hypothesized that the steric hindrance of the quinoline may require higher temperatures to drive the cyclometallation. A complexation was performed, as shown in Scheme 3.17, using 180°C. This temperature was chosen as it proved effective for the one-pot complexations to form the intermediates of **Hom1** and **Hom2** (sections 3.2.3.2 and 3.2.3.5). This proved to be the optimal temperature giving **3.10** in a two-step yield (from the ligands) of 9 %.



Scheme 3.17: Two-step cyclometallation to give red-emitting iridium(III) complex poly(dendrimer) precursor **3.10**.

It was believed that increasing the temperature further may improve the yield of **3.10**. Therefore the reaction in Scheme 3.17 was attempted with the final step being heated at 200°C. Unfortunately only traces of what was believed to be **3.10** by thin layer chromatography, corresponding to ( $n = 2, m = 1$ ) in Figure 3.25.a, was observed to form. From  $^1\text{H}$  NMR and mass spectra the dominant isolated product was discovered to be a different combination of ligands being ( $n = 1, m = 2$ ). It was deduced that the higher temperatures led to more extensive ligand scrambling with the undesired ( $n = 1, m = 2$ ) which is likely thermodynamically more favourable.<sup>173</sup> The reactions were conducted under normal laboratory conditions and as a result the control of temperature was not particularly precise (no greater variation than  $\pm 10^\circ\text{C}$ ), however, it can be concluded that the product required a temperature greater than 168°C to form and that temperatures in the range of 200°C result in deleterious ligand scrambling. Heating in the range of 180°C appears to be the best compromise with **3.10** as the major product.

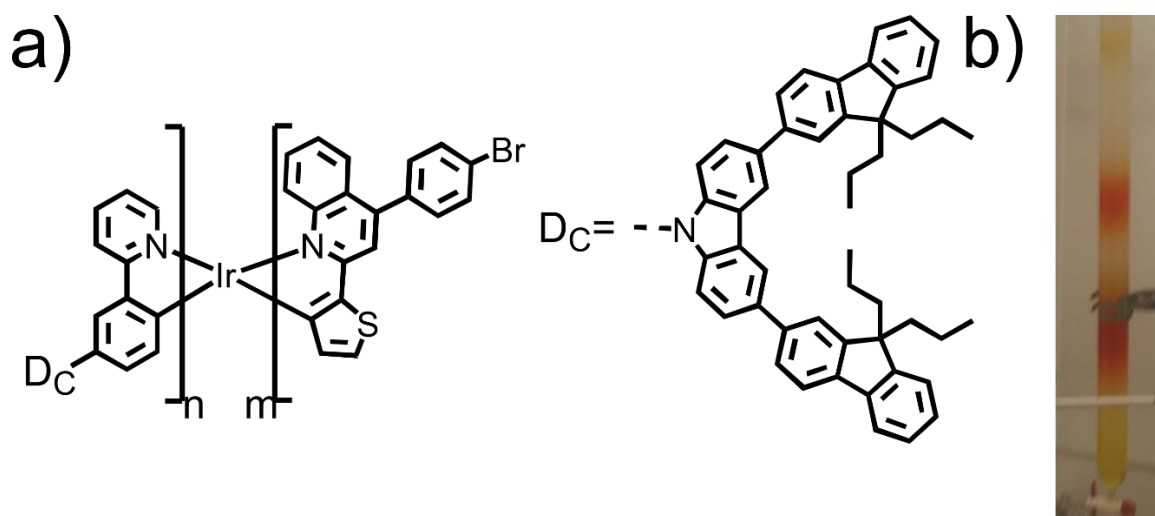


Figure 3.27: a) Possible ligand combinations formed during the reaction in Scheme 3.12 and b) photo of size exclusion chromatography showing what is believed to be each ligand

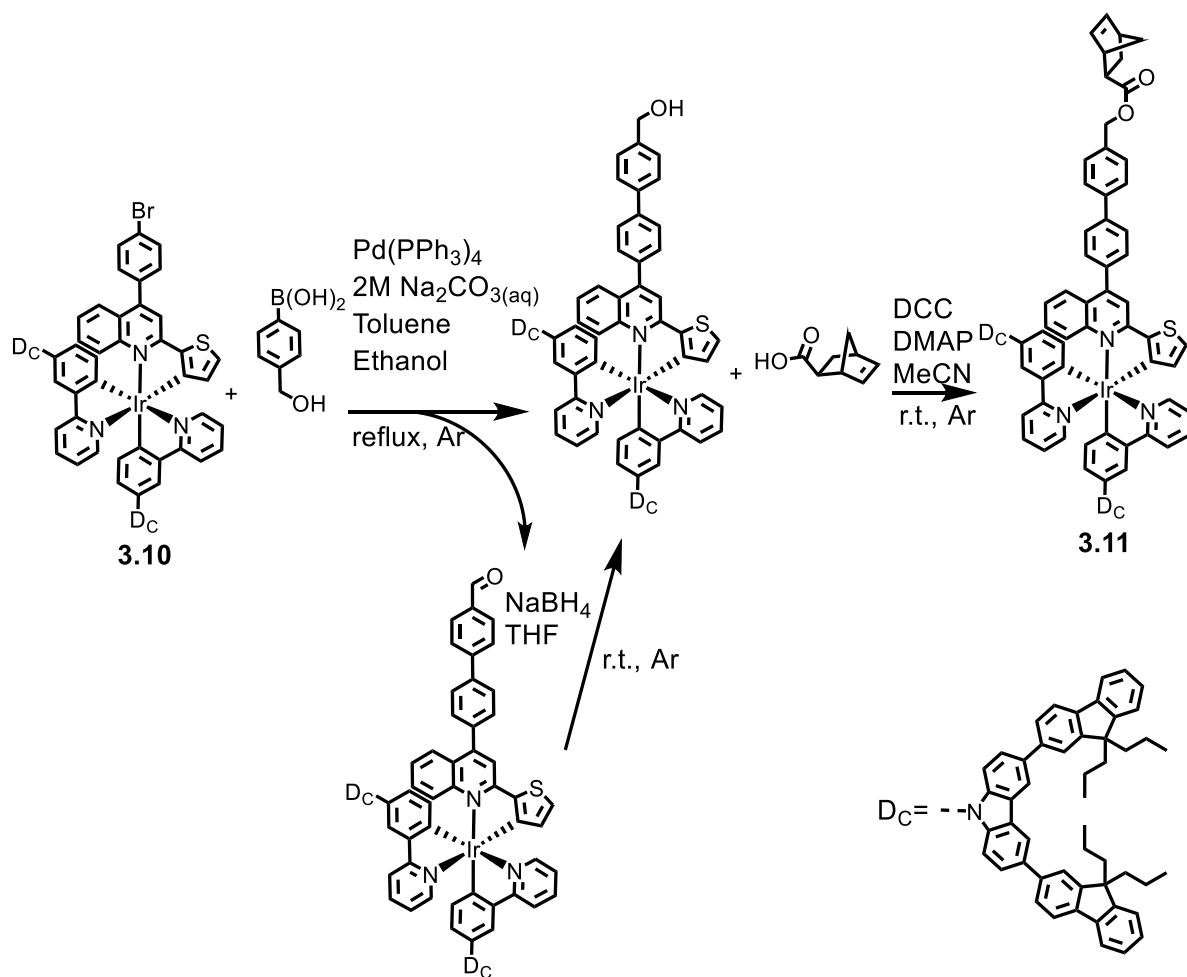
combination eluting separately. The yellow ( $n = 3, m = 0$ ) elutes first being the bulkiest with three dendrons and what is believed to be the faint red-orange ( $n = 0, m = 3$ ; **3.7**) elutes last.

Size exclusion chromatography proved very effective in separating the different complexes (shown in Figure 3.25.b) while chromatography over silica gave no separation of the different ligand combinations. Although easily observed visually during size exclusion chromatography due to their intense visible absorption the quantities of material within the bands other than **3.10** were negligible.

### 3.3.2.2 Synthesis of the monomer

The remaining synthesis followed the route reported for **L2**. Unlike the reported synthesis, the Suzuki coupling of 4-(hydroxymethyl)phenylboronic acid and **3.10** resulted in the formation of two products. These were identified as the desired alcohol and the corresponding benzaldehyde. From this it was concluded that the benzaldehyde was the energetically preferred product and that the benzyl alcohol should be exposed to limited handling. Once separated the alcohol was quickly esterified under Steglich conditions with *exo*-5-norbornenecarboxylic acid (97 % described isomer) to give the monomer (**3.11**) in 42 % yield over two-steps (Scheme 3.18).

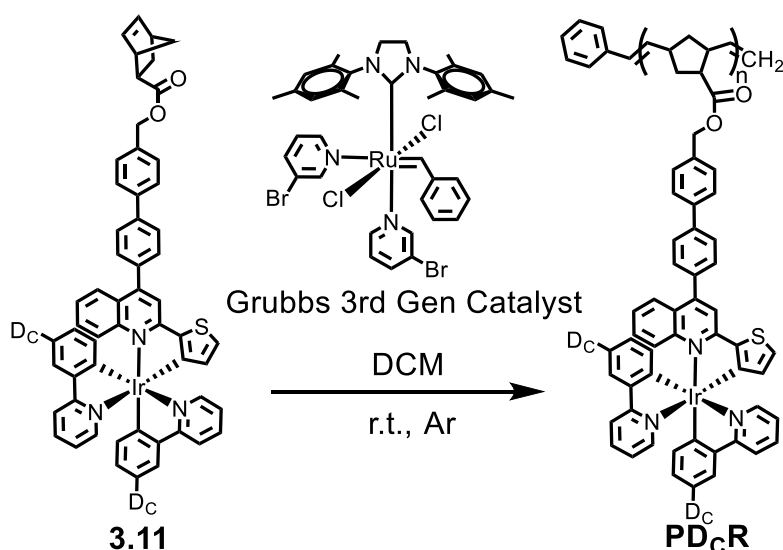
Recovering the aldehyde was desirable to improve the yield, however, it could not be separated from the debrominated starting material. Reduction with sodium borohydride in tetrahydrofuran returned the material to the desired alcohol which could then be esterified to the monomer. Due to the number of steps and the inability to obtain the pure aldehyde the additional mass could not be added to the above yield. The true yield of the two steps is likely considerably higher than the value reported above.



Scheme 3.18: Suzuki coupling and Steglich esterification to give the monomer **3.11**. The benzaldehyde by-product could be reduced and esterified to give more monomer.

### 3.3.2.3 Polymerization

Living ring opening olefin-metathesis polymerization of **3.11** by Grubbs 3<sup>rd</sup> generation catalyst was conducted with only enough material isolated for a single attempt (Scheme 3.19). Commonly polymerizations are conducted at high concentrations as the rate of propagation is lowered during dilution by decreasing the rate of collisions. Higher rates of propagation are key in achieving controlled polymerization. Unfortunately the solubility of the resulting poly(dendrimer) was overestimated resulting in rapid gelation requiring an additional aliquot of solvent to be added as mixing had ceased.



Scheme 3.19: Grubbs 3<sup>rd</sup> generation catalysed ring opening olefin-metathesis polymerization of **3.11** to give **PDcR**.

Ultimately **PDcR** was isolated, however, the dispersity was considerably greater than the value required to consider it truly living (to be living  $\mathcal{D} \leq 1.2$ ). Despite this the polymerization was very successful with **PDcR** isolated in 83 % yield with a number average molecular weight ( $M_n$ ) of 164 kDa and a dispersity ( $\mathcal{D}$ ) of 2.4 (Figure 3.26).

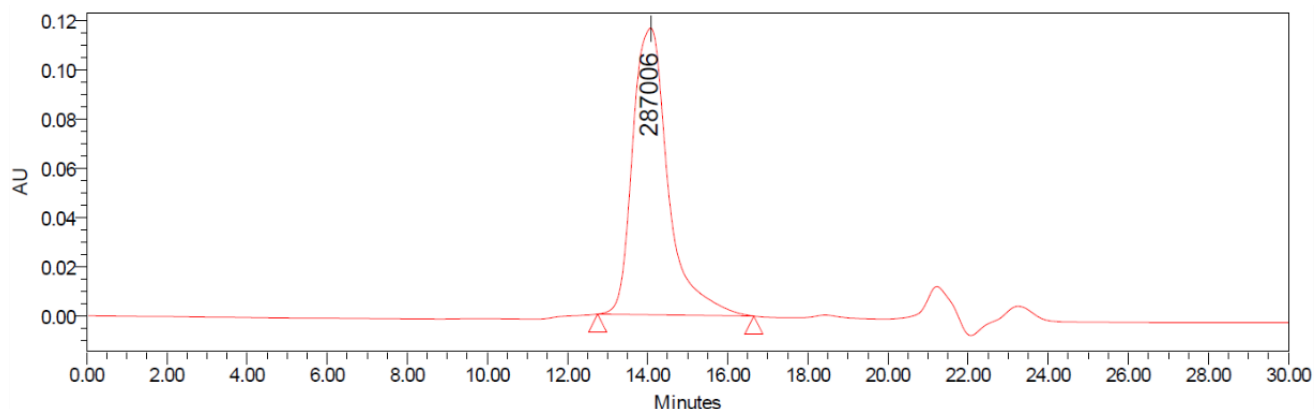


Figure 3.28: Gel-permeation chromatogram of **PDcR**.  $M_n = 164$  kDa,  $\mathcal{D} = 2.4$

Although a controlled living polymerization would have been ideal and may have been possible in this case if the concentration was correct; the synthesized batch of **PDcR** was more than acceptable for photophysical examination and the application as an emitter in organic light-emitting diodes. Most properties of iridium(III) complex containing poly(dendrimer)s remain consistent regardless of molecular weight or dispersity. The optimal processing conditions are an exception and are known to vary considerably with molecular weight. For initial testing of a poly(dendrimer) controlled and reproducible

polymerization was not required as the processing of each batch can be optimized individually. For future integration into commercial products the control over polymerization becomes essential as it would be inefficient to optimise the processing conditions of each batch.

### 3.3.3 Determination of the isomerism of the iridium(III) complex contained within PDcR by $^1\text{H}$ NMR

It has been well documented that the isomer of a cyclometallated iridium(III) complex has a profound effect on the photophysical properties of the material and ultimately its capacity to fabricate efficient organic light-emitting diodes. Upon synthesis of **3.10** it became evident through  $^1\text{H}$  NMR that the two dendronized 2-phenylpyridine ligands were inequivalent.

Due to several possible isomers an evaluation of the possible combinations and suggesting nomenclature for the combinations is required. This will serve as a means of describing the isomer present and as a tool to eliminate all other candidates.

#### 3.3.3.1 Identification of all possible isomers for PDcR and its intermediates

The potential isomers of the homoleptic and heteroleptic iridium(III) complexes were described within section 3.2.1.1 so that the determination of the isolated isomer could be clearly identified and described. While the complexes within the poly(dendrimer) and its intermediates are heteroleptic, as in the cases of **[Ir(Dctmq)<sub>2</sub>(acac)]** and **[Ir(tDcpq)<sub>2</sub>(acac)]**, the asymmetry of the unique ligand adds an additional potential isomer and complicates the available descriptions.

If the stereoisomer nomenclature (*cis* or *trans*) is utilized in isolation the four potential isomers could be described as being *cis-N,N'*, *cis-C,C'*, *cis-N,N<sub>2</sub>*; *trans-N,N'*, *cis-C,C'*, *cis-N,N<sub>2</sub>*; *cis-N,N'*, *trans-C,C'*, *cis-N,N<sub>2</sub>* and *cis-N,N'*, *cis-C,C'*, *trans-N,N<sub>2</sub>*. A more eloquent approach to describing these complexes could be found amalgamating the nomenclature of stereoisomers with that of the homoleptic bidentate complexes. Although there is not two sets of three identical ligands found in complexes of the generic formula  $[\text{ML}_3^{\text{a}}\text{L}_3^{\text{b}}]$ , the bonding elements are pairs of three identical elements with identical formal charges. Therefore the *cis-N,N'*, *cis-C,C'*, *cis-N,N<sub>2</sub>* isomer can be simply referred to as the *facial* isomer while the others are the meridional *trans-N,N'*, meridional *cis-N,N'* or meridional *trans-C,C'* isomers where "N" and "C" refer to the coordinating atoms of the equivalent ligands (Figure 3.27). The advantage of this terminology is that it provides a clearer image of the coordination geometry while also providing some information on how the complexes

are expected to behave. This is due to the hypothesis that the heteroleptic *tris*-(C<sup>^</sup>N) complexes are very likely to behave akin to the homoleptic *tris*-(C<sup>^</sup>N) in terms of energetics. For example the *facial* isomers are believed to be the thermodynamically preferred products in both cases.

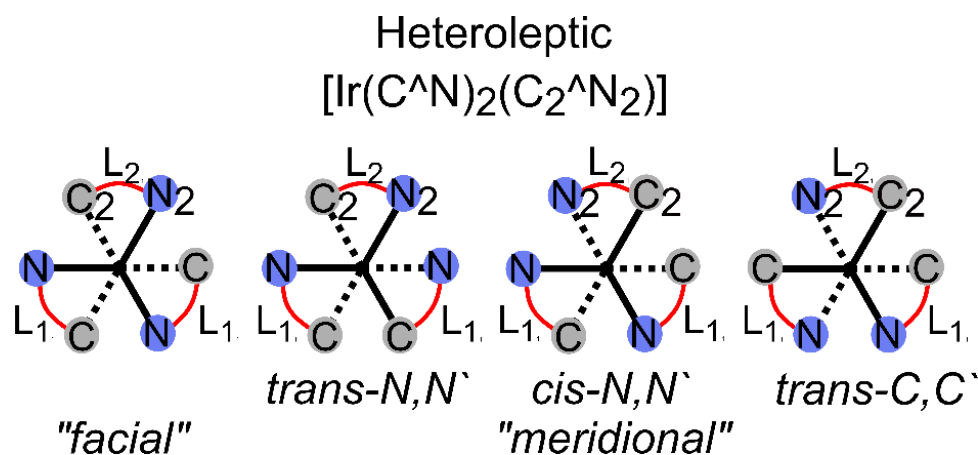


Figure 3.29: Potential isomers of the iridium(III) complexes within **PD<sub>c</sub>R** and its intermediates.

### 3.3.3.2 Overview: Geometry determination iridium(III) complex within PD<sub>c</sub>R

It was essential to identify the geometric isomer of the iridium(III) complexes within **PD<sub>c</sub>R**. As it is known that the photophysical properties of the iridium(III) complexes can change greatly with isomerism; structure identification is paramount for results that can be reliably compared to others within the field and for reproducibility. In previously reported examples the combination of high temperature synthetic conditions and <sup>1</sup>H equivalence of the identical ligands was deemed sufficient to show the formation of the thermodynamic product, the *facial* isomer.

Upon synthesis of **3.10**, however, the <sup>1</sup>H NMR pattern observed signified that all ligands were experiencing different environments resulting in the proton signals being inequivalent.

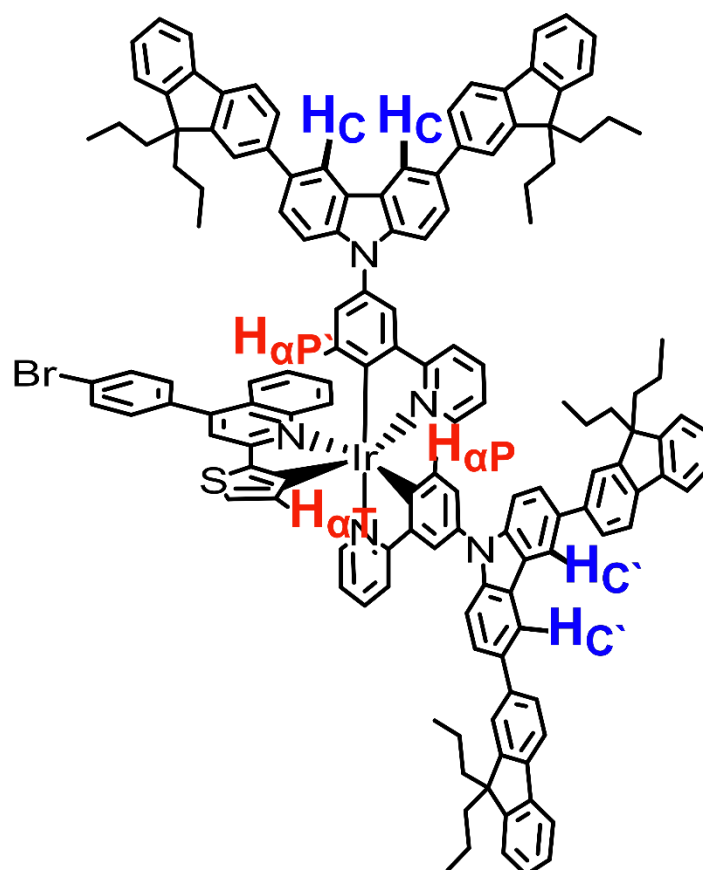
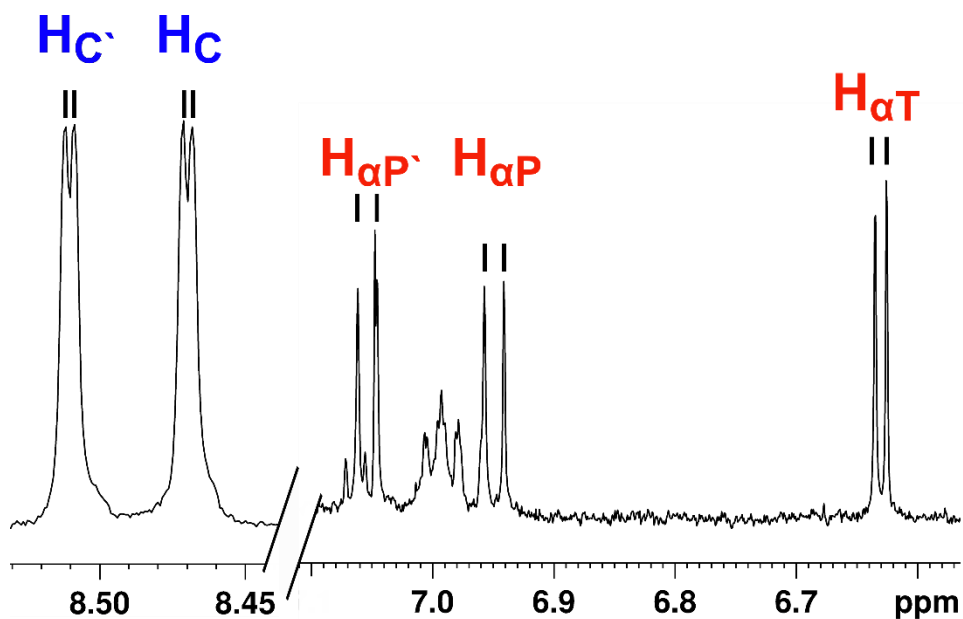


Figure 3.30: Significant aromatic  $^1\text{H}$  NMR (500 MHz,  $\text{CDCl}_3$ ) signals of **3.10** relating to geometry identification. The majority of signals have been removed for clarity as they overlap and provide little information. The important proton signals are labelled as per the included structure (shown as *facial* isomer), however, the signals labelled as prime (') are arbitrary and are interchangeable.



The most obvious indication of the dendronized ligands being inequivalent were the 4,5-carbazolyl proton ( $H_C$  and  $H_{C'}$ ) signals of each ligand appearing at different chemical shifts. (Figure 3.28). Because they were well removed from the remaining aromatic signals it was clear that the two carbazolyl-dendrons; chemical shifts ( $\delta$ ) of 8.47 ppm and 8.51 ppm for  $H_C$  and  $H_{C'}$ , respectively; were experiencing different environments. The thiophenyl-proton alpha to the C-Ir bond ( $H_{\alpha T}$ ) with a chemical shift of 6.63 ppm proved integral in evaluating the geometry as it was also well removed from the other aromatic peaks due to the up-field shift caused by the strongly shielding iridium(III) electron density being in close proximity. The 4,5-carbazolyl-proton doublets were found to integrate equivalently while  $H_{\alpha T}$  was always found to integrate in a ratio that suggested one quinoline-thiophene ligand in the presence of two carbazolyl-dendronized ligands (integration ratios of 1:2:2 for  $H_{\alpha T}$ :  $H_C$ :  $H_{C'}$ , respectively).

Through two-dimensional correlation NMR spectroscopy the signals from the phenyl-protons alpha to the C-Ir bond were also identified and assigned as  $H_{\alpha P}$  and  $H_{\alpha P'}$  with chemical shifts of 6.94 and 7.16 ppm, respectively. While both signals are shifted up-field due to shielding of the nearby iridium(III) electron density, only  $H_{\alpha P}$  is resolved from other nearby signals. The resolved proton,  $H_{\alpha P}$ , was found to integrate equivalently with  $H_{\alpha T}$ . While the peaks of  $H_{\alpha P'}$  could not be separated from those of another proton, the integration suggested it would also be equivalent with  $H_{\alpha T}$  if the convoluted signal also corresponded to a single proton which was likely considering the ratios of the carbazolyl- and thiophenyl-protons.

The integrations strongly suggested that the material was an iridium(III) complex chelated by two chemically inequivalent dendronized ligands and a single quinoline-thiophene ligand. For a mixture of isomers to explain the observed  $^1H$  NMR pattern they would need to be a racemic mixture and both contain a chemically equivalent  $H_{\alpha T}$  which was extremely unlikely. Gel permeation chromatography of the material showed a single non-disperse peak confirming that there was only a single isomer present (excluding the chiral isomers  $\Lambda$  and  $\Delta$  which were known to be indistinguishable by  $^1H$  NMR). It was deduced that the inequivalence of the dendronized ligands must be due to either the complex being in a *meridional* geometry or in a *facial* geometry where the quinoline-thiophene ligand was altering the environment experienced by each dendronized ligand differently.

In order to identify the geometry of iridium(III) complexes within **PDcR** the earliest iridium(III) complex containing intermediate, **3.10**, was analysed. This was deemed acceptable to determine the geometry of the iridium(III) complex within the poly(dendrimer) and **3.11** as all subsequent reaction conditions do not show indications of inducing

isomerization and the ideal analyte, **PDcR**, was incompatible with the techniques available for this determination.

It was previously stated that, asymmetry in the  $^1\text{H}$  NMR spectrum of a *tris*-C<sup>N</sup> cyclometallated iridium(III) complex is associated with the *meridional* isomer. This is certainly the case for homoleptic complexes. However, it is not always so simple for heteroleptic complexes. For example the heteroleptic *tris*-C<sup>N</sup> cyclometallated iridium(III) corresponding to the *facial* isomer is most closely related to the *cis*-N,N', *cis*-C,C' isomer of the acetylacetonate chelated heteroleptic iridium(III) complexes, which is expected to exhibit inequivalence of the cyclometallating ligands.

In an ideal *tris*-C<sup>N</sup> heteroleptic system, containing only one unique ligand, the remaining two ligands should experience the same environment and therefore will exhibit equivalency when characterized by  $^1\text{H}$  NMR in the same way as if it was a homoleptic complex. It is possible though that ligands with particularly intrusive sterics may influence the chemical environment of the other ligands more intensely and possibly even cause distortion of the other ligands about the metal centre.

The important sterics to observe are the bulkiness of the ligand edges *ortho*- to the coordination bonds. These positions project towards the other ligands with the volume occupied by the protons along this edge being responsible for the steric interference. This results in ligands containing quinoline functionality to exert a great deal of steric interference upon another ligand as the benzo-moiety intrudes upon it. Conversely, 5-membered rings such as thiophene tend to result in less steric interference than 6-membered phenyl-rings because the angles within the ring result in the alpha-proton to the C-Ir bond to be angled further from the other ligands.

A combination of the quinoline impinging heavily upon one of the 2-phenylpyridine ligands while the other is unhindered by the thiophenyl moiety will result in significant inequivalence between the seemingly identical ligands due to the disparate environments (Figure 3.29). Additionally the ancillary ligand can exert electronic effects which, although normally relatively weak in octahedral complexes, can alter the coordination environment of the other ligands asymmetrically. It is very possible that the differing bond energies, particularly the divide between the thiophenyl and phenyl moieties, may contribute to the identical ligands exhibiting differing environments.

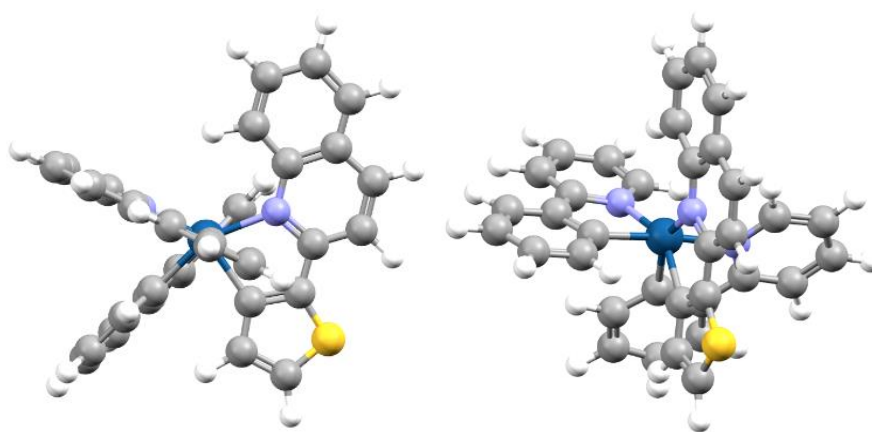


Figure 3.31: A depiction of how the quinoline impinges upon only one 2-phenylpyridine in the iridium(III) complex of **3.10** (*facial*) observed from two angles. Images generated by crude modelling using PerkinElmer Informatics Chem3D using mm2 energy minimization and are only for visualization of the approximate environment.

Since none of the potential isomers detailed in the previous section could be eliminated at this point, it was hypothesized that that **PD<sub>c</sub>R** and its intermediates could contain an iridium(III) complex being the *facial* isomer or any of the three *meridional* isomers. The literature strongly suggests that the most likely isomers would be either the *facial* or *meridional trans-N,N'* as a result of the complexation mechanism in which the *tris-C<sup>N</sup>* heteroleptic complex was formed via the *meridional trans-N,N'*  $\mu$ -dichloro-bridged.

### 3.3.3.3 Techniques: Geometry determination iridium(III) complex within PD<sub>c</sub>R

The techniques available for determination of the geometry of complexes such as **3.10** are limited. As an example one of the preferred techniques, X-ray crystallography, cannot be used as these dendrimers are difficult or perhaps impossible to isolate as crystals. The most promising technique available to the project was a combination the proton nuclear magnetic resonance techniques; correlation spectroscopy (COSY) and exchange nuclear magnetic resonance spectroscopy techniques such as nuclear Overhauser effect spectroscopy (NOESY) or rotating frame nuclear Overhauser effect spectroscopy (ROESY). This began with the assignment of the remaining aromatic proton signals within <sup>1</sup>H NMR spectrum (Figure 3.28).

Three proton signals were identified as being particularly integral for identification of the geometric isomer: H<sub>αT</sub>, H<sub>αP</sub> and H<sub>αP'</sub> with chemical shifts of 6.63, 6.94 and 7.16 ppm, respectively. All three protons are alpha to the C-Ir bond causing their signals to be up-field of the majority of the remaining aromatic peaks. This allows H<sub>αT</sub> and H<sub>αP</sub> to be well resolved while H<sub>αP'</sub> was identifiable and coupling interactions to it can be observed. In addition to this, these protons would be in close proximity to one another if their alpha carbons are

coordinated along the same edge of the complex. This will result in  $H_{\alpha T}$ ,  $H_{\alpha P}$  and  $H_{\alpha P'}$  being able to participate in through-space spin orbital cross-relaxation via the nuclear Overhauser effect during NMR experiments if the complex is in the form of the *facial* geometric isomer. If the molecule is instead in the form of the *meridional* geometric isomer then only one pair of the three will show any through-space cross relaxation. This is illustrated in Figure 3.30.

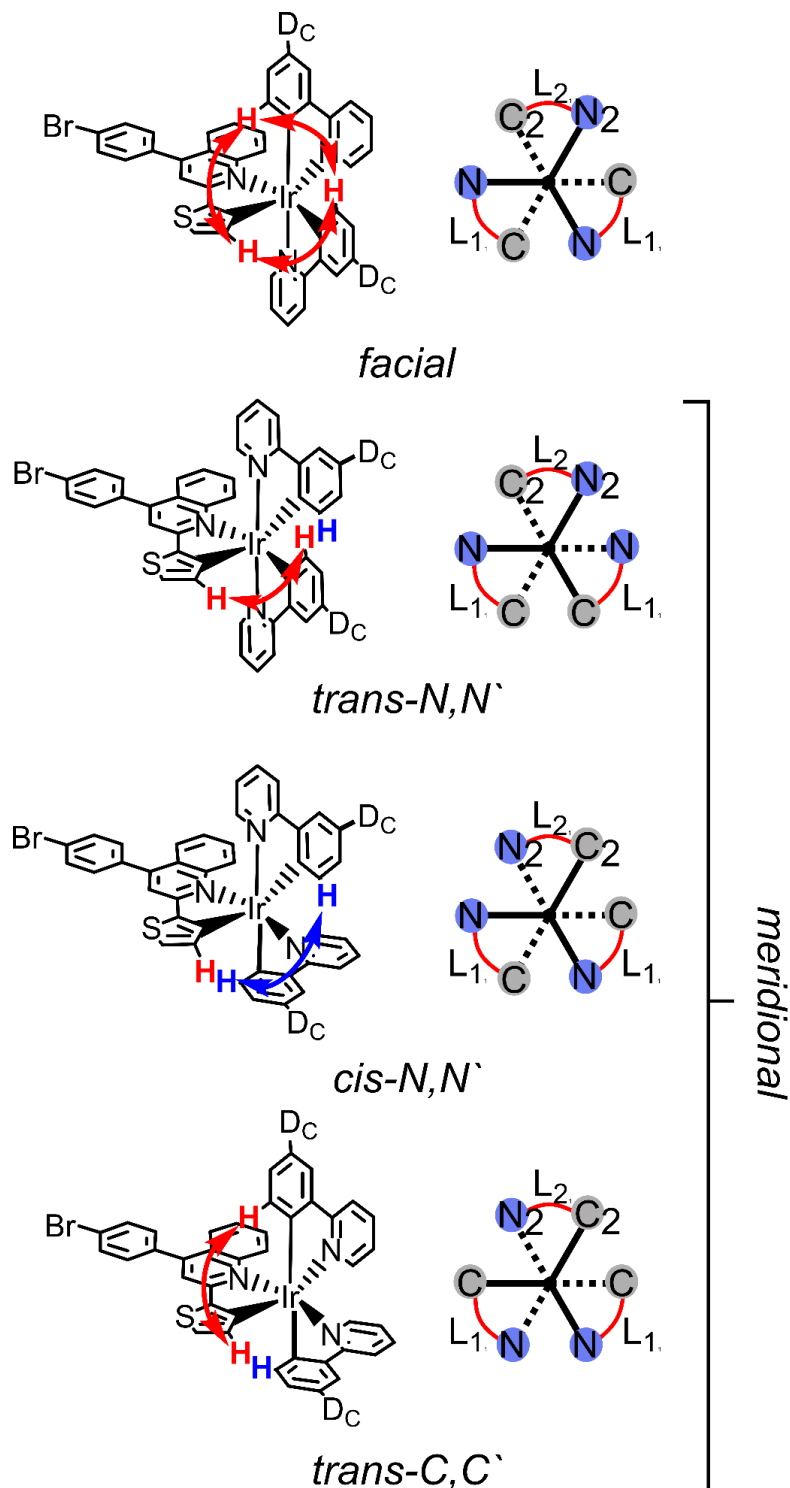


Figure 3.32: All possible geometries for the ligands of **3.10** about the iridium(III) centre with structures and the previously shown pictorial representation of the same geometries. The

possible through-space spin orbital interactions indicated by coloured arrows. Red protons and arrows are towards the reader while blue are facing away.

Prior to NOESY or ROESY experiments, the assignments of  $H_{\alpha T}$ ,  $H_{\alpha P}$  and  $H_{\alpha P'}$  were confirmed through a combination of  $^1H$  COSY analysis to determine through-bond coupling partners, expected chemical shifts of these protons and their coupling partners and a comparison of these results to the previously reported examples. Each exhibits the splitting expected from first order coupling, a doublet, as they each have only a single adjacent proton. The thiophenyl proton alpha to the C-Ir bond was always observed to be the most up-field of the three due to the shielding effect of the heavier sulphur atom's electron cloud. This is supported by the signals and assignments observed in previous materials including **PD<sub>B</sub>** and **PD<sub>C</sub>** of chapter 2 and the dendrimers within this chapter. The identity of  $H_{\alpha T}$ ,  $H_{\alpha P}$  and  $H_{\alpha P'}$  was strongly supported by the available experimental evidence so the material was investigated by ROESY and NOESY spectroscopy.

ROESY was attempted first as it was believed to be the optimal technique for the molecular weight of **3.10**. No useful information was obtained via ROESY so to proceed **3.10** was investigated utilizing one-dimensional (1D) NOESY. The resonance correspond to  $H_{\alpha T}$  ( $\delta$  6.63 ppm, 3328 Hz), was selected for the first 1D-NOESY experiment.

As shown in Figure 3.21a the through bond spin-spin coupling to the neighbouring thiophenyl-proton (negative signal at  $\delta$  7.42 ppm) is observed and through-space cross-relaxation is observed between the thiophene and the alkyl protons of the dendron indicated by the positive signals at  $\delta$  2.01 ppm and 0.68 ppm. No signals corresponding to other aromatic protons were observed.

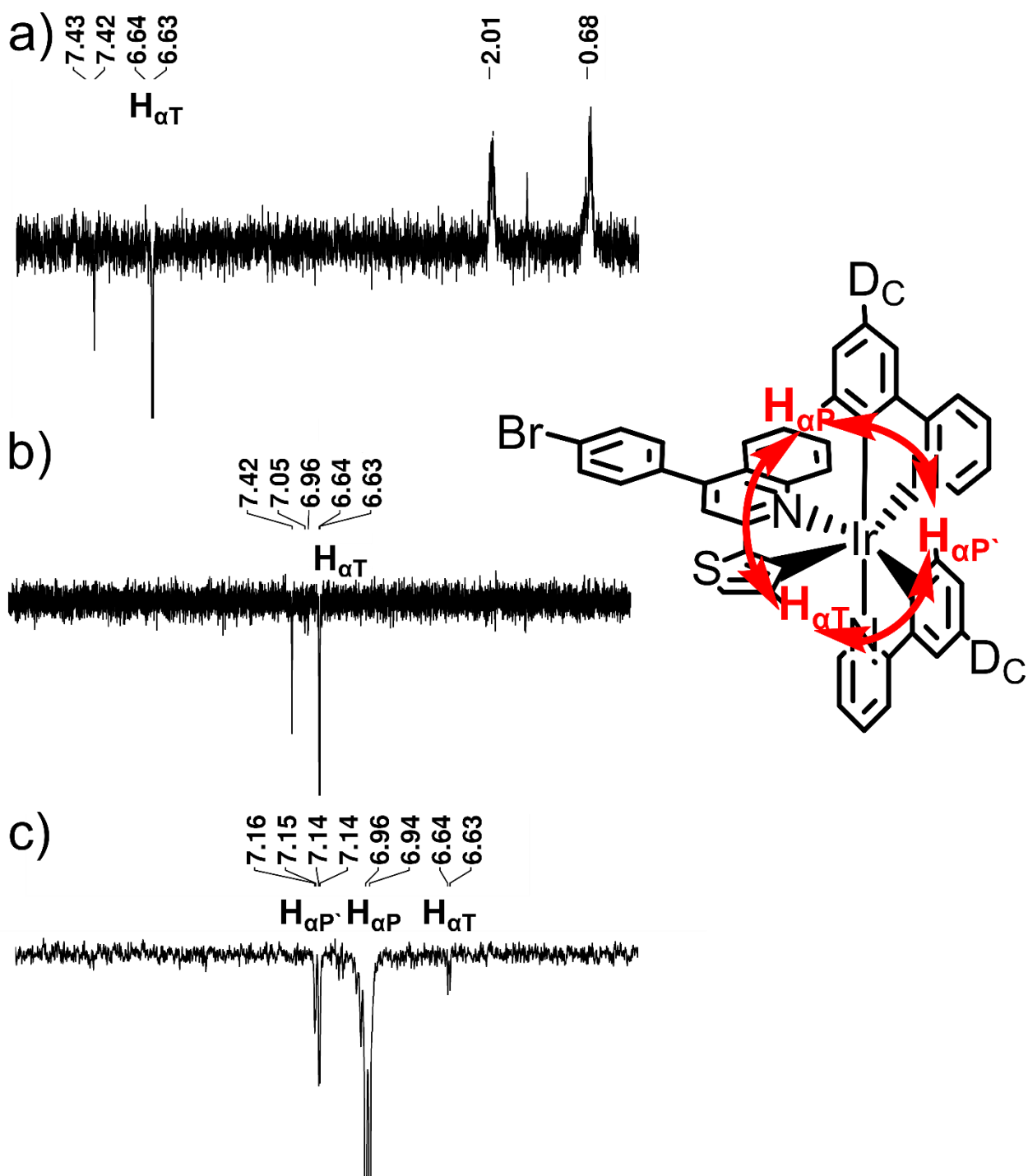


Figure 3.33: 1D NOESY spectra of **3.10**: a) (selected resonance:  $H_{\alpha T}$ ,  $\delta$  6.63 ppm, 3328 Hz) with standard mixing time; b) (selected resonance:  $H_{\alpha T}$ ,  $\delta$  6.63 ppm, 3328 Hz) with longer mixing time, and (selected resonance:  $H_{\alpha P}$ ,  $\delta$  6.94 ppm, 3487 Hz) with longer mixing time. The intense signals from the selected resonances are cut off to better observe the weaker signals. The suggested *facial* isomer of **3.10** is shown with through-space cross-relaxation between the red protons shown by red arrows.

It was theorized that the aromatic protons, which are held much more rigidly experiencing very different cross-relaxation rates than the alkyl groups that the first

experiment was able to observe. To combat this the mixing (correlation) time was increased substantially resulting in the spectrum shown in Figure 3.31b. The increase in mixing time resulted in the thiophenyl/ alkyl cross-relaxation rate constant to be within the region where it is virtually zero and the signals were no longer observed. The through-bond signal at  $\delta$  7.42 ppm was observed again as a negative signal. Additionally two extremely faint negative signals which could correspond to  $H_{\alpha P}$  and  $H_{\alpha P'}$  were observed. Although the signal to noise negated the possibility of any firm conclusion that  $H_{\alpha P}$  and  $H_{\alpha P'}$  were involved through-space cross-relaxation with  $H_{\alpha T}$ , the result did indicate that cross-relaxation may be occurring but the experimental conditions were not optimal to observe them.

In an attempt to obtain a stronger result the one-dimensional NOESY with the increased mixing time was performed with the  $H_{\alpha P}$  signal ( $\delta$  6.94 ppm, 3487 Hz) resonance selected. The equivalent measurement utilizing the  $H_{\alpha P'}$  signal could not be conducted due to interference by an overlapping peak from another proton (Figure 3.28). The obtained spectrum (Figure 3.31c) showed definitive cross-relaxation of the selected resonance,  $H_{\alpha P}$ , with  $H_{\alpha T}$  and  $H_{\alpha P}$ . This provided strong evidence that these protons were on the same face of the octahedral complex and that the isomer is *facial*.

One final complication was that all peaks observed at the increased mixing time were detected as negative signals. The signals resulting from the nuclear Overhauser effect are commonly observed as positive signals due to the cross-relaxation rate being in the positive regime. Additionally all negative signals normally originate from either the selected resonance itself or its spin-spin coupling signals. The positive nuclear Overhauser effect signals are a product of the positive cross-relaxation rate constant associated with such interactions. As the mixing time is increased this rate goes from the positive to the negative regime with a region where the constant is virtually zero. As different molecules, and even different moieties on larger molecules, have different cross-relaxation rates; increasing the mixing time can result in signals moving from positive to negative regime with the central timescales giving no signal due to a near zero rate. As the timescales required to observe any cross-relaxation of the aromatic protons were relatively large the cross-relaxation rate of these signals has moved from near zero in 3.31a to the negative in 3.31b and 3.31c. Although signals indicating an interaction between  $H_{\alpha T}$ ,  $H_{\alpha P}$  and  $H_{\alpha P'}$  are all negative, cross-relaxation via the nuclear Overhauser effect (through-space) is certainly responsible as the results cannot be explained by spin-spin coupling (through-bond).

To confirm the results of the one-dimensional NOESY a two-dimensional (2D) NOESY using the same conditions was conducted. This two-dimensional correlation spectroscopy experiment was also conducted to measure through-bond coupling. By

overlaying the two spectra signals exclusively present within the 2D-NOESY spectrum are through-space interactions (Figure 3.32). The results from the 1D-NOESY were confirmed by the overlaid 2D-COSY/ 2D-NOESY with  $H_{\alpha T}$ ,  $H_{\alpha P}$  and  $H_{\alpha P'}$  all coupling exclusively through-space.

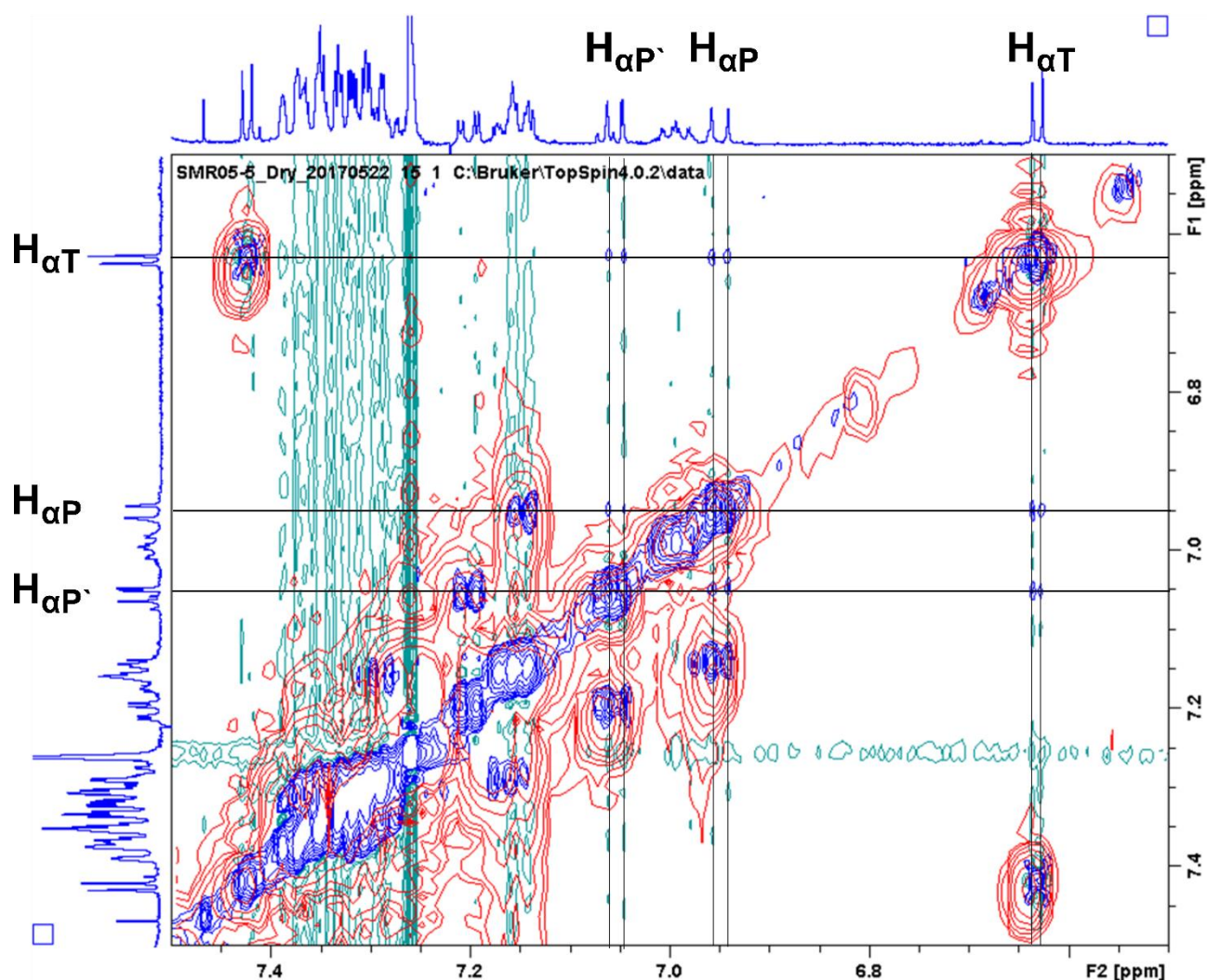


Figure 3.34: NMR spectra: 2D-NOESY of **3.10** (blue and cyan) with 2D-COSY (red) overlay with  $^1\text{H}$  projections on the left and right. The through-space coupling signals of  $H_{\alpha T}$ ,  $H_{\alpha P}$  and  $H_{\alpha P'}$  are highlighted by intersecting lines.

As it is the only iridium(III) complex geometry that allows through-space coupling to occur between all three C-Ir alpha-protons ( $H_{\alpha T}$ ,  $H_{\alpha P}$  and  $H_{\alpha P'}$ ) it can be concluded that **3.10** and the subsequent materials including **PDcR** contain exclusively the *facial* isomer of the iridium(III) complex.



### 3.4 Summary

A small molecule ( $[\text{Ir}(\text{tmq})_3]$ ), four dendrimers (**Hom1**, **Hom2**, **Het1** and **Het2**) and a poly(dendrimer) (**PDcR**) all containing red-emitting iridium(III) complexes were successfully synthesized and characterized. The possible formation of multiple isomers were observed. **Hom1** was isolated as a mixture of regioisomers of which 92 % was estimated to be the desired regioisomer estimated by  $^1\text{H}$  NMR.  $[\text{Ir}(\text{tmq})_3]$  and **Hom2** were isolated as the pure *facial* isomers. Despite the presence of other inseparable geometric isomers in the starting materials; **Het1** and **Het2** were both isolated as the pure *trans-N,N'* isomers. The  $^1\text{H}$  NMR of the intermediates to the poly(dendrimer) indicated that complex had asymmetrical geometry. Despite this it was shown through NOESY experiments that the isolated material was the desired *facial* isomer. The poly(dendrimer), **PDcR**, was isolated in 83 % yield and was found to be a polymer by gel permeation chromatography ( $M_n = 164$  kDa,  $\bar{D} = 2.4$ ).

The successful isolation of the red-emitting iridium(III) complex containing materials allowed for the investigation of their structure-property relationships. Further investigation of the structural properties of many intermediates was conducted by single-crystal X-ray crystallography. Due to their potential application within organic light-emitting diodes, the thermal, photophysical and electrochemical properties of the materials were of great significance and will be discussed in the following chapter.

# Properties of Red-Emitting Dendrimers and Poly(dendrimer) Containing Iridium(III) Complexes

---

*This chapter details and discusses the structural characterization and the application pertinent properties of the materials described in the previous chapter. This will include the thermal, optical and electrochemical properties of the red emitting materials are described while providing discussion on how these values are relevant for OLED technology.*

### 4.1 Introduction

To evaluate the potential of the red-emitting iridium(III) complex containing materials synthesized in chapter 3 for use as the emissive species within organic light-emitting diodes, characterization and evaluation of various material properties was required. In particular, with the exception of the small molecule; **[Ir(tmq)<sub>3</sub>]**, these pertained to the application of solution-processed OLEDs.

In order to act as effective emitters within OLEDs the materials must have sufficient thermal stability to survive fabrication and operating conditions. In the case of solution-processed devices the materials are not expected to be subjected to high temperatures during processing, therefore, stability within the operational temperature range is the primary concern.

The photophysical and electrochemical properties of the materials are paramount to their effectiveness as an emitter within organic light emitting diodes. Additionally, an understanding of these characteristics allows for the progression of future studies. The photoluminescent and electrochemical behaviour of the materials were examined through all available techniques.

### 4.2 Thermal Analysis

It has been shown that the thermal stability of any layer within a device is governed by not only the decomposition temperature but also the presence of any phase transitions which induce interlayer diffusion.<sup>174</sup> To this end the materials were characterized by thermal gravimetric analysis and differential scanning calorimetry. This would uncover the range of temperatures that the materials could withstand during device processing and operation.

#### 4.2.1 Thermal Gravimetric Analysis

Thermal gravimetric analysis was performed on  $[\text{Ir}(\text{tmq})_3]$  and the four dendrimers containing iridium(III) complexes. The obtained results provide the maximum temperatures that the materials can withstand during device fabrication or operation.

As shown in Figure 4.1, all complexes exhibit a decomposition temperature of 5 % mass loss,  $T_d(5\%)$ , of greater than 300°C. The small complex,  $[\text{Ir}(\text{tmq})_3]$ , exhibits a  $T_d(5\%)$  of 426°C. This is important as the device fabrication by vacuum thermal evaporation which  $[\text{Ir}(\text{tmq})_3]$  would require reaches much higher temperatures than the solution processing used for the dendrimers. These results demonstrate that the materials are all stable well above the range of temperatures expected during fabrication and operation.

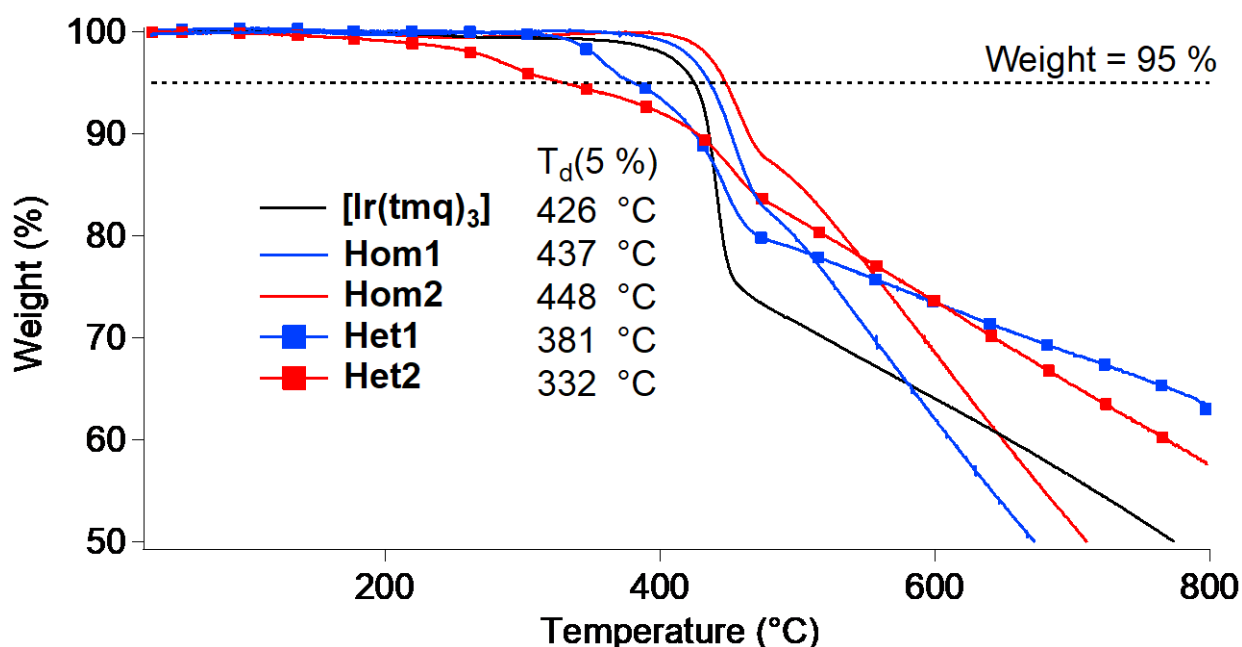


Figure 4.1: Thermal gravimetric analyses

Both iridium(III) complexes employing an acetylacetonate ancillary ligand, **Het1** and **Het2**, were observed to have lower decomposition temperature. Both acacs first decompose ~5 % mass corresponds closely with the loss of the acetylacetonate ligand. All complexes then exhibit a similar weight loss at around 400°C which suggests there is a shared mechanism by which this degradation initiates.

Table 4.1: Comparison of weight loss in complexes occurring around 400°C

	Weight % loss	MW(gmol <sup>-1</sup> ) loss	MW(gmol <sup>-1</sup> ) loss per C <sup>N</sup> ligand
<b>[Ir(tmq)<sub>3</sub>]</b>	25	216	72
<b>Hom1</b>	15	428	143
<b>Hom2</b>	11	334	111
<b>Het1</b>	15	309	155
<b>Het2</b>	11	227	114

As shown in Table 4.1, the material lost to this decomposition appears to vary between the complexes. Due to the large error involved in the single measurement it is impossible to assign any particular decomposition pathway, however, it does appear that the complex sharing identical C<sup>N</sup> ligands lose a similar mass indicating that they decompose via the same mechanism.

In terms of thermal degradation the iridium(III) complexes all appear to be stable to any temperatures they are likely to experience during device fabrication and operation.

#### 4.2.2 Differential scanning calorimetry

Differential scanning calorimetry of the small molecule and dendrimers was performed to investigate any phase transitions. Understanding of these phase transitions was critical to the investigation of the materials for their application as processing or operating temperatures above the glass transition temperature of materials have been linked to deleterious diffusion between layers and the melting of any component would completely compromise the solid-state device.<sup>174</sup> All materials scanned for thermal transitions between at least 0 and 200 °C. Although outside the calibration range of the instrument some materials were analysed beyond this range in hopes of identifying phase transitions.

The calorimetry experiments were performed at 50, 100 and 200 degrees per minute. The results within the calibrated range of 0 and 200 °C show the absence of any thermal phase transitions. The results shown in Figure 4.2 were collected at 200 degrees per minute. This was representative for all heating regimes attempted with no transitions, neither melts nor glass transitions ( $T_g$ ), were observed at any heating rate between 50 and 200 degrees per minute.

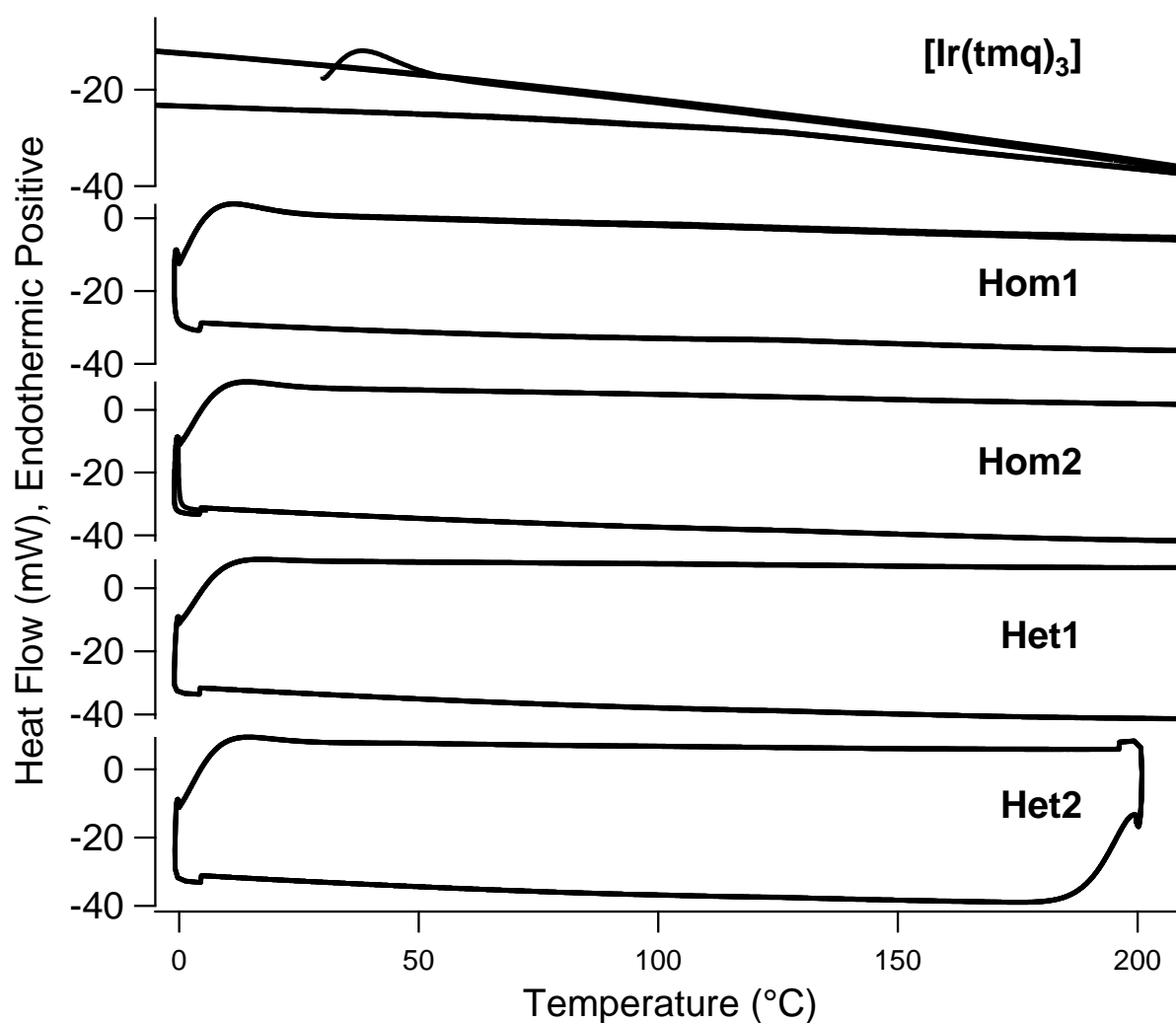


Figure 4.2: Differential scanning calorimetry plots showing the behaviour of the small molecule and dendrimers between 0 and 200 °C when heating and cooling at 200 degrees per minute.

The absence of transitions in dendronized materials is commonly attributed to them being an amorphous glass within the measured range. In the case of **Het2** crystallography indicates that it is likely going to be present in the form of a crystalline solid and therefore must exist below any potential melt or glass transition. This is also the case for **[Ir(tmq)<sub>3</sub>]** and is not surprising as it is not functionalized by dendrons.

The material which exhibited gradual weight loss above 100 °C during thermal gravimetric analysis, **Het2**, did not show noticeable heat flow changes during differential scanning calorimetry. As both techniques are very sensitive it is likely that the observed

weight loss of **Het2** during TGA was caused by environmental variation and the material was stable until the observed decomposition temperature.

The dendrimers containing iridium(III) complexes must either form glassy amorphous solids or they exhibit some form of crystallinity. In both cases the only thermal transition observed was their thermal decompositions and as a result it is difficult to determine which scenario is correct.

#### 4.2.3 Summary of Thermal Properties

The thermal properties of the small molecule and dendrimers containing iridium(III) complexes were analysed. All materials exhibited high resistance to thermal degradation, all  $T_d(5\%) > 300\text{ }^\circ\text{C}$ , and exceptional phase stability with no thermal transitions observed between 0 and 200  $^\circ\text{C}$ . These results indicate that the thermal stability is beyond sufficient for device fabrication and operation.

Whether the materials exist below their glass transition temperature as an amorphous solid or are present as exclusively crystalline species is debateable for most of the materials with the current evidence. It could be possible to examine the materials without crystal structures via techniques such as powder X-ray diffraction to determine whether crystalline domains are present, however, the thin films required for OLEDs are incompatible with powder X-ray crystallography. Additionally, it will be shown later in this chapter, under Section 4.3.5, that these materials all exhibited large non-radiative decays in the neat films due to interchromophore interactions. Because of the sensitivity of these materials to interchromophore interactions, devices approaching optimal efficiencies can only be achieved when a host material is utilized to disperse a low concentration of emissive dendrimer throughout the thin film. From this it was concluded that further investigation of the phase information of the red-emissive iridium(III) containing dendrimers would not be representative of the behaviours of the materials within their intended application.

Thermal investigation of the poly(dendrimer), **PDcR**, was not conducted as only a relatively small portion of product was obtained. It was determined that characterization of **PDcR** as an emitter within devices was of higher priority than determining its thermal properties. The investigation of devices based upon **PDcR** are ongoing and if there is sufficient remaining material afterwards then thermal characterization will be performed.

### 4.3 Investigation of photophysical properties

The photophysical properties of a material constitute the group of related characteristics that are most significant when investigating the suitability of a material for use in organic light-emitting diodes. The absorption and photoluminescence qualities of each material were investigated and observations important to their application are discussed.

#### 4.3.1 UV/Vis absorption and photoluminescence spectroscopy

To investigate the photophysical properties of the materials containing red-emitting iridium(III) complexes, the UV-Vis absorption and photoluminescence spectra of each were measured in solution and as neat films. The photoluminescence spectra of the materials blended with a host material were also examined without the measurement of the UV/Vis absorption spectra as they are dominated by the host material. Dr Anthony Brewer conducted all film preparation and photophysical experimentation, with the exception of **[Ir(tmq)<sub>3</sub>]**.

#### 4.3.2 Solution UV/Vis absorption and photoluminescence spectroscopy

Figure 4.3 shows the solution (toluene) UV/Vis absorption and photoluminescence spectra of **[Ir(tmq)<sub>3</sub>]**, the four red-emitting dendrimers and the poly(dendrimer).

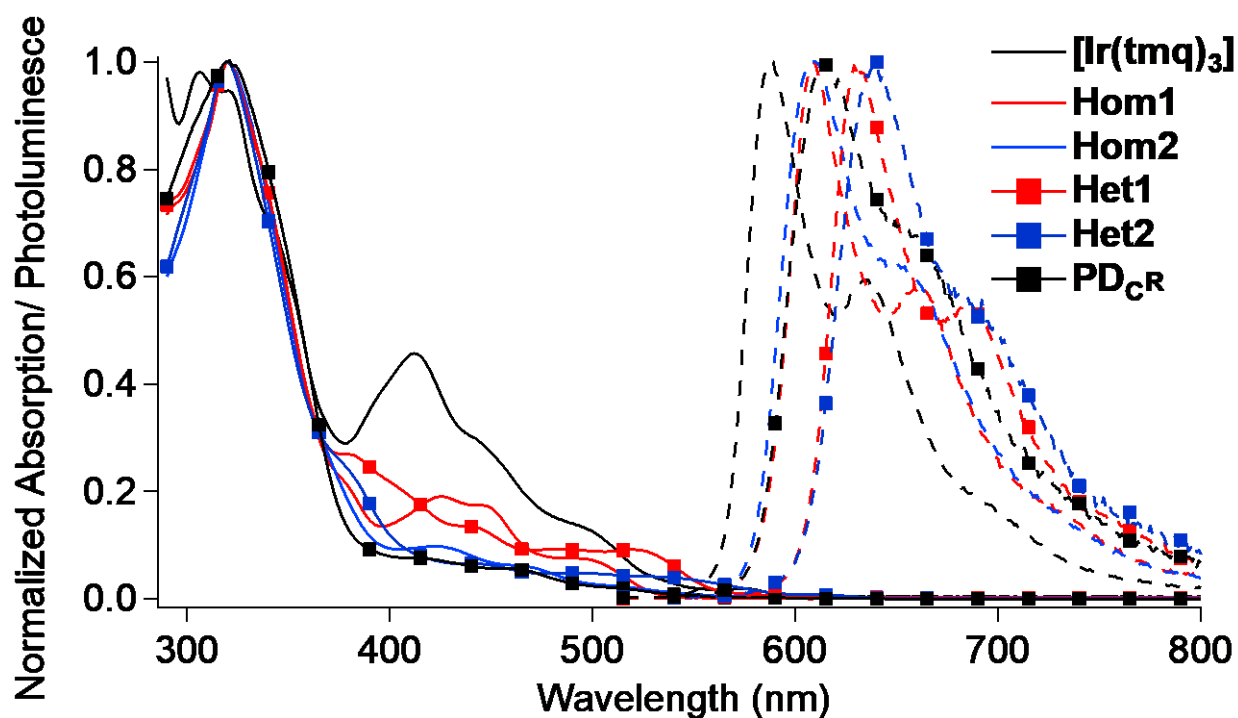


Figure 4.3: Comparison of UV/Vis absorption and photoluminescence spectra of the materials containing red-emitting iridium(III) complexes in degassed toluene. Photoluminescence spectra are expressed using dashed lines.

The observed absorption spectra in solution predominantly results from two types of transitions; either metal-to-ligand charge-transfer (MLCT) transitions or  $\pi$ - $\pi^*$  transitions.

The  $\pi$ - $\pi^*$  transitions, arising from aromaticity within the materials, dominates at the shorter wavelengths below 350 nm. The dendronized materials all show the characteristic fluorenyl absorption as their maxima at 320- 321 nm. While this fluorenyl absorption band is obvious the largest contributor at this point, the absorption spectrum of **[Ir(tmq)<sub>3</sub>]** shows that the ligands also contribute to absorption at this wavelength. In fact the absorption maxima of **[Ir(tmq)<sub>3</sub>]** observed at 286 nm can be seen as either an additional peak or shoulder in the dendrimers. Absorption bands below 350 nm can confidentially be assigned as the result of  $\pi$ - $\pi^*$  transitions with considerable overlap between the aromatic bands of the ligands and the dendrons.

It becomes more difficult to explicitly assign the transitions responsible for absorption modes observed between 350 and 400 nm. The ligands prior to complexation demonstrate absorption tapering out to 400 nm, therefore, it is extremely likely that aromatic  $\pi$ - $\pi^*$  transitions are contributing in this region. At the same time it is common for the MLCT transitions to be seen starting around 350 nm. This results in the portion of the spectrum between 350 and 400 nm comprising of both MLCT transitions and  $\pi$ - $\pi^*$  transitions as one gives way to the other as the dominant mode of photon absorption.



At wavelengths greater than 400 nm the absorption becomes dominated by the metal-to-ligand charge transfer transitions. Multiple MLCT transition bands are observed stretching from 400 nm out to the onset of emission for each complex. Unlike the  $\pi-\pi^*$  transitions which are exclusively observed as spin-allowed transitions between two singlet states, the involvement of the heavy metal permits the occurrence of both spin-allowed singlet and spin-forbidden transitions when metal-to-ligand charge transfer is involved;  $^1\text{MLCT}$  and  $^3\text{MLCT}$ , respectively. The sharper absorption bands between 400 and 475 nm are typically assigned to the  $^1\text{MLCT}$  transition while the broader bands at wavelengths longer than 475 nm are believed to originate from  $^3\text{MLCT}$  transitions.<sup>157,156</sup>

The photoluminescence spectra of the complexes in degassed toluene solution were measured. The small molecule exhibited orange-red emission with a maxima of 589 nm while the dendrimers and poly(dendrimer) containing iridium(III) complexes demonstrated red to deep-red emission with maxima between 609 and 639 nm (Table 4.7).

Each material exhibited an emission band which featured a relatively intense shoulder at lower energy with tailing extending into the near-infrared suggesting the presence of other indistinct shoulders. The shoulder is particularly sharp for the materials utilizing the methyl-substituted ligand; **[Ir(tmq)<sub>3</sub>]**, **Hom1** and **Het1**; compared to those with the phenyl-substituted ligand.

The second emission feature and continuing shoulder into the near-infrared is typically attributed to contribution from a ligand centred  $^3\pi-\pi^*$  transition mixing with the  $^3\text{MLCT}$  transition. The  $^3\pi-\pi^*$  transitions typically exhibit a strong vibronic progression which was shown to be the case for these complexes.<sup>175,176</sup> This featured emission, also commonly labelled as vibrational (or vibronic) fine structure or as exhibiting ligand-character, contrasted strongly with the broad featureless emission typical of emission from purely MLCT transitions; which is sometimes described as exhibiting metal-character.

#### 4.3.3 Film UV/Vis absorption spectroscopy

To further investigate the optical transitions of the red-emitting dendrimeric materials, films of the neat material and blends using CBP as the host were fabricated and their photophysics was compared to the materials in solution.

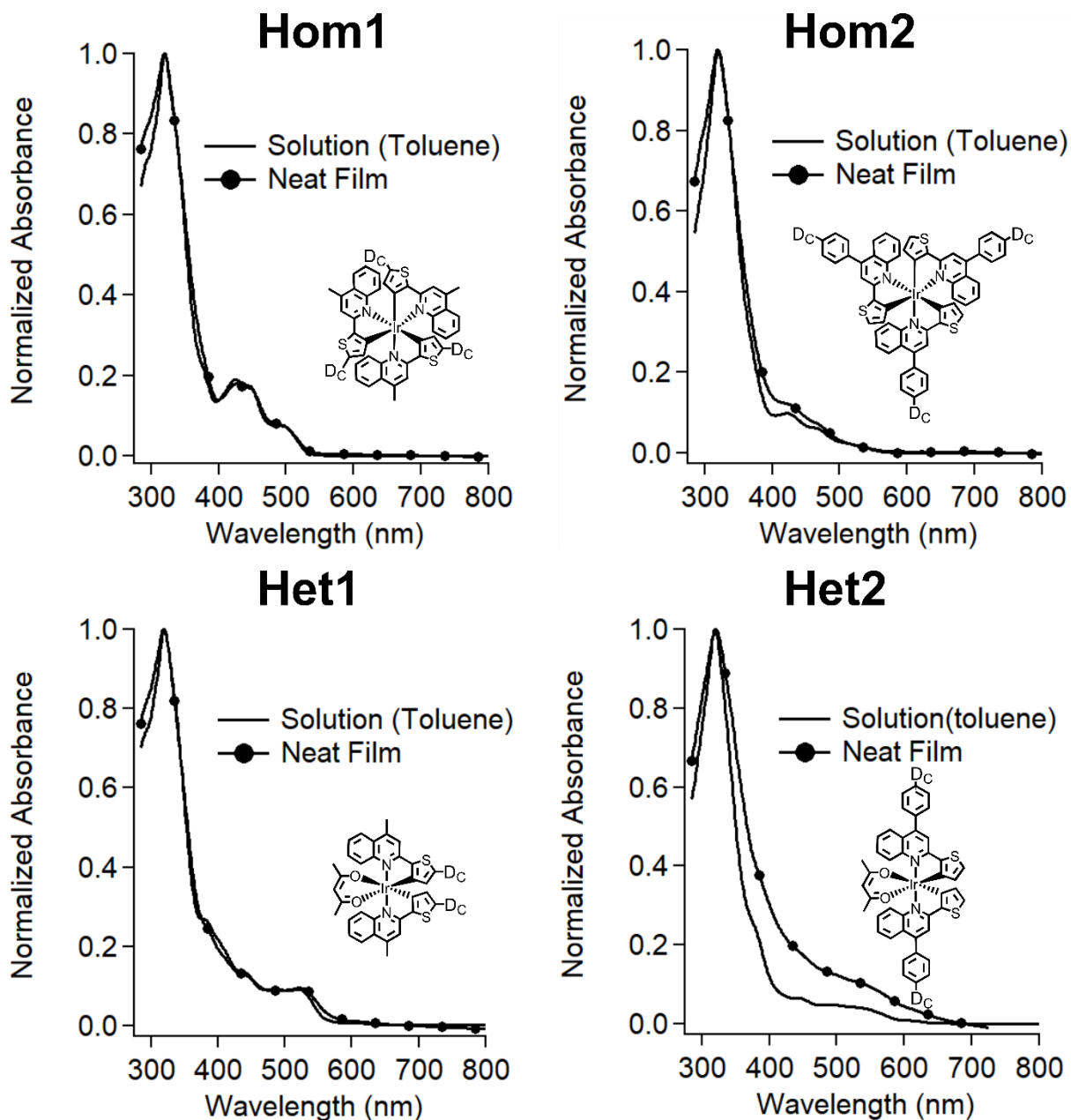


Figure 4.4: UV/Visible absorbance spectra of red-emitting dendrimers: Solution (Toluene) versus neat film comparison.

For UV/Visible absorption spectroscopy shown in Figure 4.4, only the neat films provided significant results as the absorption transitions of CBP overwhelmed the majority of the adsorption bands of the dendrimeric materials. It was found that the spectral shape of all four dendrimers in solution is identical to that of the neat films. The relative intensity of the adsorption bands of all dendrimers, except for **Het2**, were found to be essentially identical across all wavelengths. This indicates that the adsorption transitions occurring within the neat materials, excluding **Het2**, are essentially unchanged whether in solution or in neat film.

In the case of **Het2**, the relative intensities of the adsorption transitions do appear to change at varying wavelength. However, the wavelength of individual spectral features (peaks, shoulders etc) appear unchanged which is inconsistent with the presence of new absorption transition pathways. The relative intensities also appear to increase proportional to the distance from the maxima suggesting that the differences are an optical artefact. The propensity for **Het2** to form opaque films strongly indicates that the differing relative intensity is likely due to scattering and as such the absorption transitions of all dendrimers are essentially unchanged between solution and solid-state.

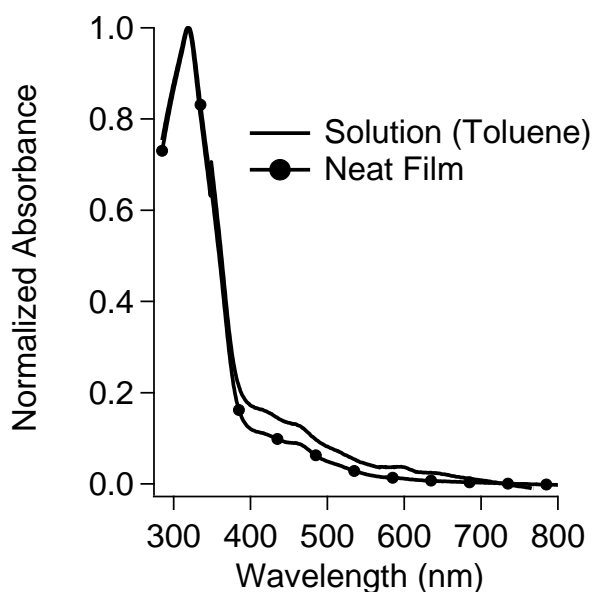


Figure 4.5: UV/Visible absorbance spectra of red-emitting poly(dendrimer), **PDcR**: Solution (Toluene) versus neat film comparison.

The poly(dendrimer), **PDcR**, is shown in Figure 4.5 to behave similarly to the red-emitting dendrimers in that the absorption transitions are essentially unchanged between solution and the solid-state. In all dendrimeric materials the adsorption maxima at  $320 \pm 1$  nm remains unchanged and is assigned as a  $\pi \rightarrow \pi^*$  transition centred on the fluorenyl-moieties of the dendron. Overall it is strongly indicated that any changes in photoluminescence in the solid-state are not the result of a novel excited species and instead originate from changes in available decay pathways.

#### 4.3.4 Film photoluminescence spectroscopy

The photoluminescence spectra of the four dendrimers in solutions (toluene), neat films and 10 wt% in CBP blend films are shown in Figure 4.6. Going from solution into neat film; the photoluminescence spectra of **Hom1** and **Het1** are shown to change only slightly.

The photoluminescence spectra of **Hom1** and **Het1** both show a slight bathochromic shift in their emission maxima; 7 and 10 nm, respectively; as well as a small increase in contribution from the longer wavelength vibronic radiative transition in the neat film. These differences are relatively insignificant compared to the stronger changes exhibited by **Hom2** and **Het2** when moving from solution to neat films.

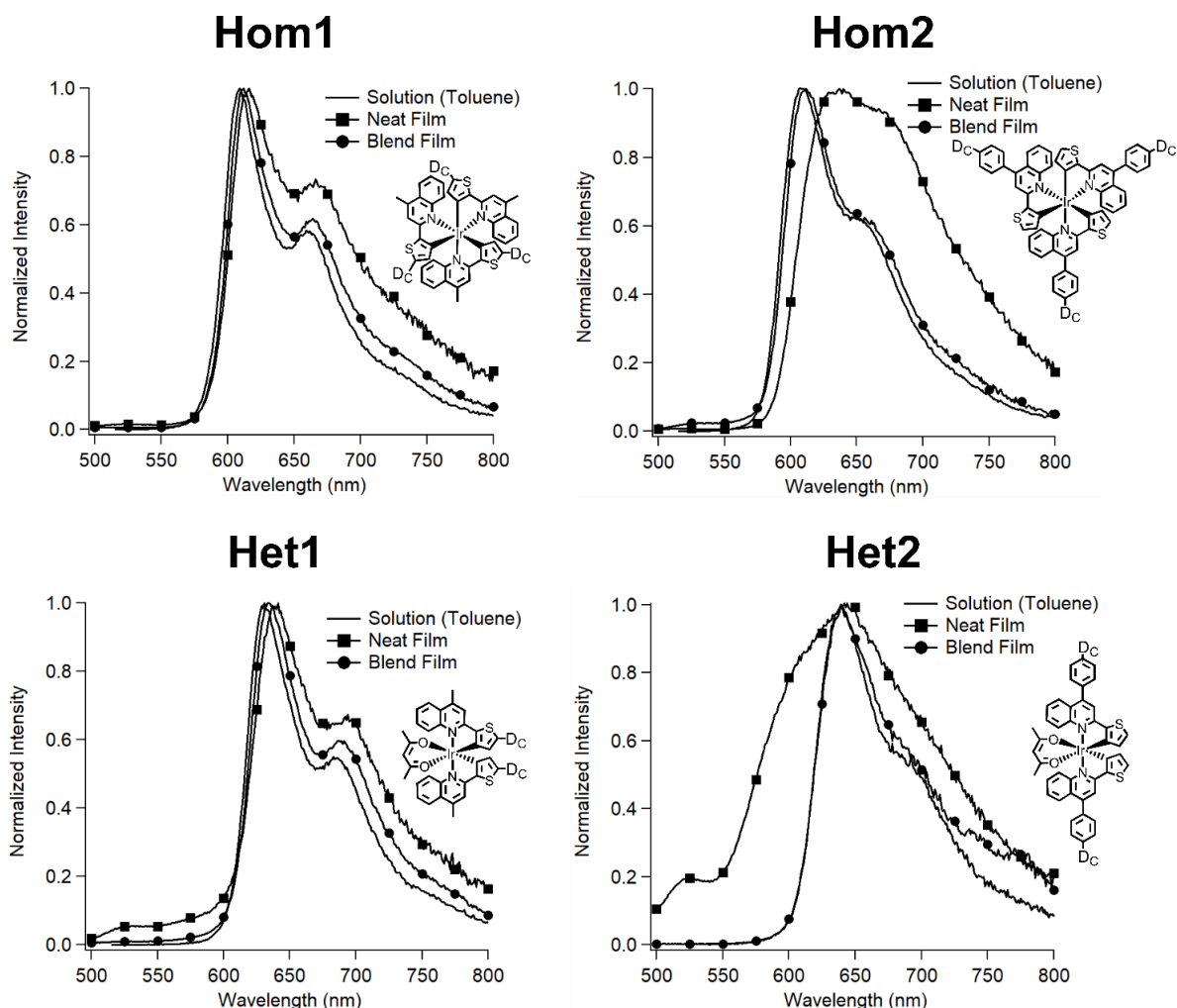


Figure 4.6: Photoluminescence spectra of dendrimers a containing red-emitting iridium(III) complex in solution (toluene), neat film and 10 wt% in CBP blend film.

The emission maxima of **Hom2** experiences a bathochromic shift of 28 nm as a neat film in respect to the solution photoluminescence. Additionally, the relative intensity of the shoulder band has increased greatly in solid-state.

The solid-state photoluminescence of **Het2** exhibits a very different spectral shape compared to in solution. The neat film emission maxima of **Het2** has a much smaller bathochromic shift (9 nm) compared to that observed for **Hom2**; however, the emission shape is vastly different, being far broader and losing its defined vibronic shoulder.

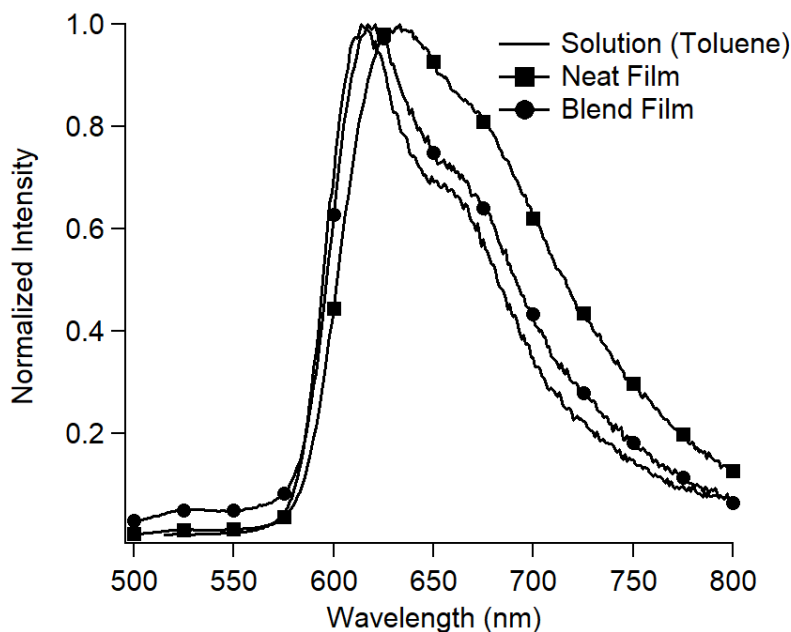


Figure 4.7: Photoluminescence spectra of poly(dendrimer) a containing red-emitting iridium(III) complex, **PDcR**, in solution (toluene), neat film and 10 wt% in CBP blend film.

The photoluminescence spectra of **PDcR** as a neat film shows a bathochromic shift of 18 nm as well as broadening of the emission bands. This is consistent with the behaviour shown by most of the red-emitting dendrimers.

The photoluminescence spectra of blends using red-emitting dendrimers and polydendrimer (10 wt%) in CBP host showed insignificant differences from their respective solution photoluminescence spectra.

#### 4.3.5 Film photoluminescence spectroscopy: Quantum yields

To further characterize the photoluminescence spectra, a comparison the photoluminescent quantum yields of each material in solution (toluene), neat film and blend film was conducted and the results are displayed in Table 4.2. The solution and neat film photoluminescent quantum yield of **[Ir(tmq)<sub>3</sub>]** was also included for comparison.

Table 4.2. Summary table of photoluminescent quantum yield of red-emitting iridium(III) complexes.

	Solution <sup>a</sup>		Neat Film		Blend Film <sup>c</sup>	
	$\lambda_{\max}^{\text{Em}}$ (nm)	$\Phi_{\text{PL}}^{\text{b}}$ (%)	$\lambda_{\max}^{\text{Em}}$ (nm)	$\Phi_{\text{PL}}$ (%)	$\lambda_{\max}^{\text{Em}}$ (nm)	$\Phi_{\text{PL}}$ (%)
<b>[Ir(tmq)<sub>3</sub>]</b>	589	92 ± 9	634	1.9 ± 0.6		
<b>Hom1</b>	609	74 ± 7	616	19 ± 2	612	78 ± 9
<b>Hom2</b>	609	86 ± 9	637	7.1 ± 1.3	611	87 ± 10
<b>Het1</b>	631	66 ± 7	641	2.8 ± 1.0	633	45 ± 5
<b>Het2</b>	639	61 ± 6	648	8.6 ± 1.5	640	20 ± 3
<b>PDcR</b>	615	72 ± 7	633	35 ± 4	617	69 ± 8

<sup>a</sup>Solution photoluminescent (PL) spectra and quantum yields were recorded in toluene at a optically dilute ( $A \approx 0.10$  A.U.  $\equiv T \approx 79\%$  at excitation wavelength) concentrations. <sup>b</sup>Solution quantum yield measurements were recorded against rhodamine 6G in ethanol as external standard ( $\Phi_{\text{PL}} = 95\%$ ,  $\lambda_{\text{exc}} = 500\text{nm}$ ), <sup>c</sup>Blend films were 10 wt% dopant in CBP.

The solution photoluminescent quantum yield of the red-emitting iridium(III) complex containing dendrimeric materials was very high at between 61 % and 86 %. The orange-red emitting small molecule iridium(III) complex also gave an impressive solution photoluminescent quantum yield of 92 %. The red-emitting dendrimers all exhibited a large reduction in phosphorescent quantum yield when deposited as a neat film indicative of non-radiative inter-chromophore interactions.

The structures of the four dendrimers are shown in Figure 4.8 so that the structural relationship to these results can be made clear. Within each pair, (**Hom1** and **Het1**) or (**Hom2** and **Het2**), the materials share the same ligand structure and dendron connectivity while the homoleptic (**Hom1** and **Hom2**) or heteroleptic (**Het1** and **Het2**) contain the same coordination connectivity about the iridium(III) centre.

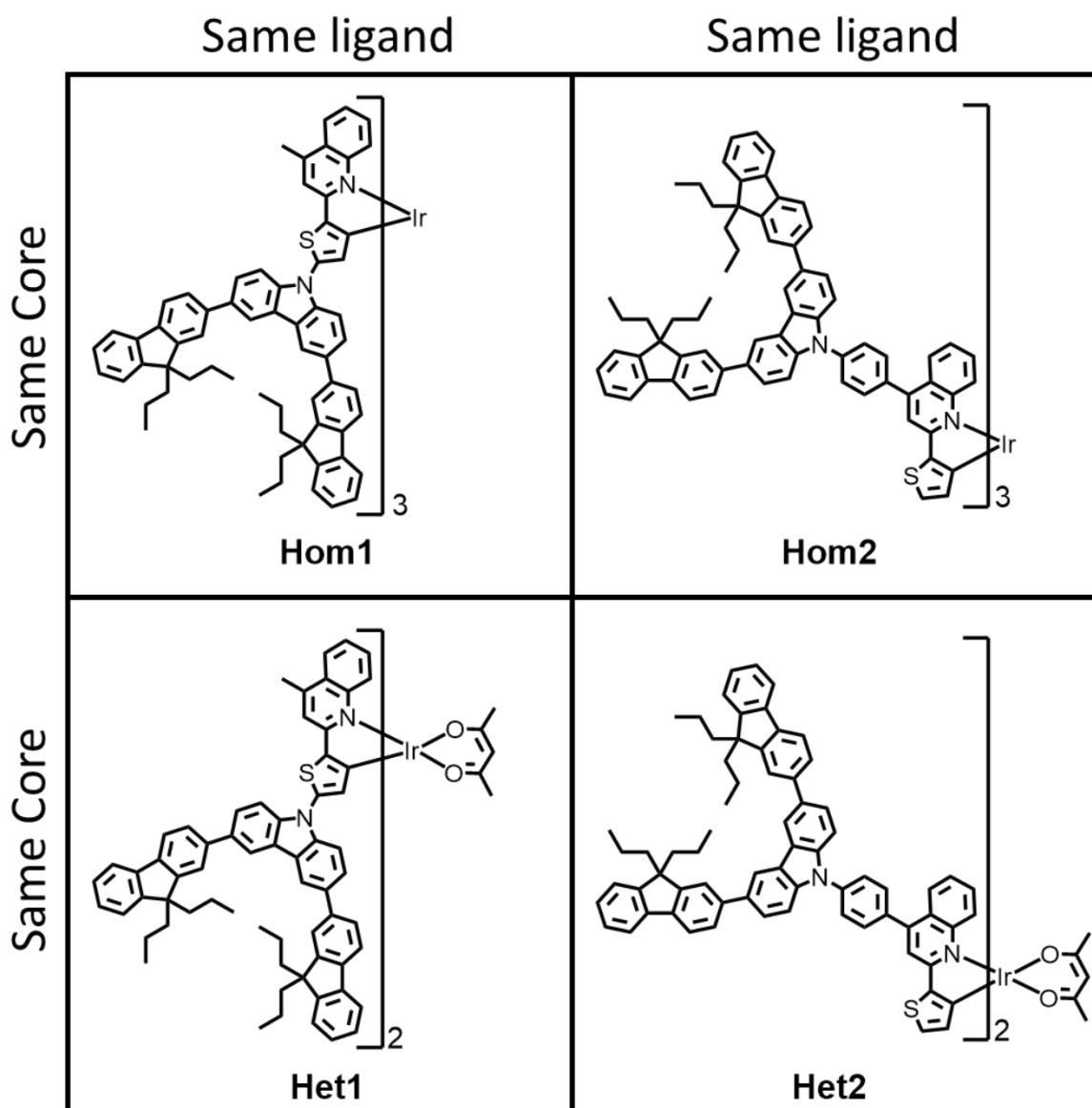


Figure 4.8: Structural relationship of target red-emitting dendrimers. The materials in the same row contain the same emissive iridium(III) complex, either homoleptic or heteroleptic, while those sharing a column contain the same dendronized ligand.

The homoleptic dendrimer, **Hom1**, showed the smallest loss of quantum yield in the neat film which suggests the dendrons are more effective at separating the chromophores when they are arranged closely in space. Because of this the outstretched dendrons of **Hom2** are less effective at providing chromophore separation. However, the photoluminescent quantum yield of **Het1** decreases more significantly when transitioning to the neat film than does **Het2**. This shows that the position of dendron attachment may play a significant role in chromophore separation, however, it is not the exclusive contributor.

All red-emitting dendrimeric materials, except for **Het2**, were observed to exhibit phosphorescent quantum efficiencies comparable to their solution values when blended in

a host material. Under commonly used processing techniques **Het2** consistently produced poor quality (opaque) blend films. This is believed to be related to its propensity to crystallize and low solubility described in chapter 3. It is believed that **Het2** is prone to phase separation during processing and further optimization of the conditions would be required to utilize the material.

#### 4.3.6 Photoluminescence spectroscopy: emission lifetimes

The emission lifetimes of red-emitting iridium(III) complexes were investigated by time-correlated single-photon counting spectroscopy and the results are shown in Table 4.3. Due to an instrumental fault, **PDcR** (10 wt%) in CBP was the only blend film able to be collected. Collection of the remaining decays is expected once repairs are completed.

Table 4.3: Observed photoluminescence lifetime of red-emitting iridium(III) complexes by TCSPC.

	$\tau_1$ ( $\mu\text{s}$ )	$\tau_2$ ( $\mu\text{s}$ )	$\tau_3$ ( $\mu\text{s}$ )
<b>[Ir(tmq)<sub>3</sub>]</b>			
Solution	3.2		
<b>Hom1</b>			
Solution	1.7		
Neat	0.05 (46 %)	0.37 (46 %)	2.1 (8 %)
<b>Hom2</b>			
Solution	1.8		
Neat	0.02 (42 %)	0.13 (44 %)	0.41 (13 %)
<b>Het1</b>			
Solution	4.0		
Neat	0.04 (47 %)	0.24 (49 %)	1.9 (4 %)
<b>Het2</b>			
Solution	1.5		
Neat	0.04 (67 %)	0.25 (27 %)	1.9 (7 %)
<b>PDcR</b>			
Solution	0.53 (16 %)	2.0 (84 %)	
Neat	0.31 (38 %)	0.88 (62 %)	
Blend	1.8 (100 %)		

Calculated errors were all less than an order of magnitude lower than the significant figures in Table 4.3. Please refer to Figure 4.9 and Figure 4.10 below to view the quality of the fits.



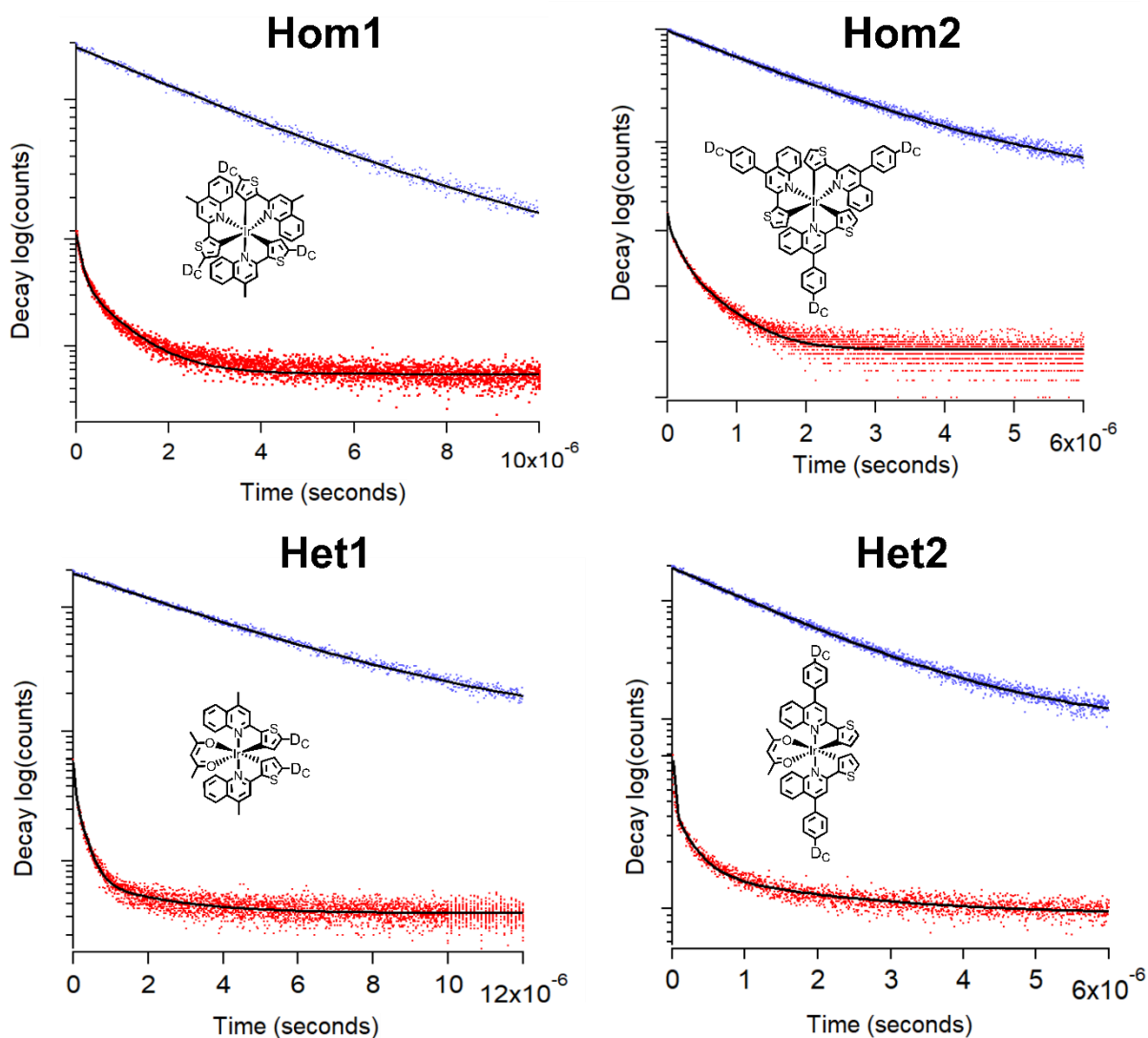


Figure 4.9: TCSPC decays of the red-emitting dendrimers in toluene (blue) and as neat films (red) showing fit curves (black).

All four dendrimers showed the mono-exponential decay with observed lifetimes on the order of a microsecond when in dilute solution. This suggests that the dendrimers are behaving as expected: i.e. without quenching by inter-chromophore interactions (as the solution is dilute) and occurring on timescales indicative of phosphorescence. Transitioning into the neat film, all dendrimers show at least three decay components indicating significant non-radiative decay via inter-chromophore interactions such as triplet-triplet annihilation.

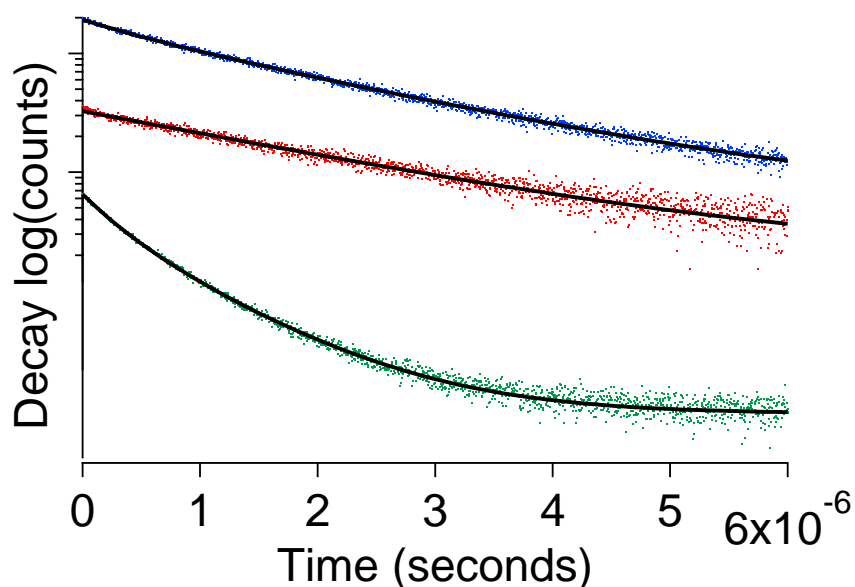


Figure 4.10: TCSPC decays of the red-emitting poly(dendrimer) in toluene (blue) as a neat film (red) and 10 wt% in CBP blend film (green); including fit curves (black).

As shown in Table 4.3 and Figure 4.10, **PDcR** exhibits excited state lifetime behaviour differing substantially from the dendrimers. In solution there is at least two decay components suggesting at least some non-radiative decay arising from intra-chain, inter-chromophore interactions. When transitioning to the neat film the emissive lifetime is observed to get shorter indicating stronger quenching likely via inter-chain, interchromophore interactions. Compared to the dendrimers, **PDcR** shows significantly less contribution of non-radiative processes in the observed lifetime. The observed lifetimes of **PDcR** are longer and only two components are observed compared to the three for all dendrimers.

The poly(dendrimer) also exhibits an unusual property when transitioning into the blend. Only a single decay component is observed in the blend film. This suggests that the additional decay component from quenching via intra-chain, inter-chromophore interactions which was observed in solution is absent in the blend. This suggests that the intra-chain, interchromophore interactions of **PDcR** decrease to become negligible when the polymer is in a host matrix. This phenomenon is generally attributed to limiting molecular movement (vibrational, rotational, librational etc) or limiting possible conformations while the molecule is in a solid matrix; deactivating a non-radiative decay pathway that was present in solution.<sup>177,178</sup>

### 4.3.7 Discussion

In combination the photoluminescence spectra, quantum yields and excited state lifetimes allow for thorough characterization of the emissive chromophores and their behaviour when in solution, neat and blend films.

One clear observation is that significant quenching due to interchromophore interactions occurs for all dendrimers in the neat film. This is evident by the decrease in photoluminescence quantum yields along with the additional and shorter observed emission lifetimes of all dendrimers when moving to the neat solid. Additionally all dendrimers showed a bathochromic shift to their emission spectra, with that of **Hom2** being particularly pronounced, which is commonly ascribed to be caused by aggregation of the emissive species.<sup>116,179,180</sup> This behaviour is comparable to that observed for the structurally related green-emitting dendrimer, **L3**, shown in Figure 4.11. It has been reported that **L3** also exhibited a decreased photoluminescence quantum yield from 82 % to 20 % while the photoluminescence lifetime decreased and became multiexponential as the dendrimer moved from solution into the neat film.<sup>142</sup>

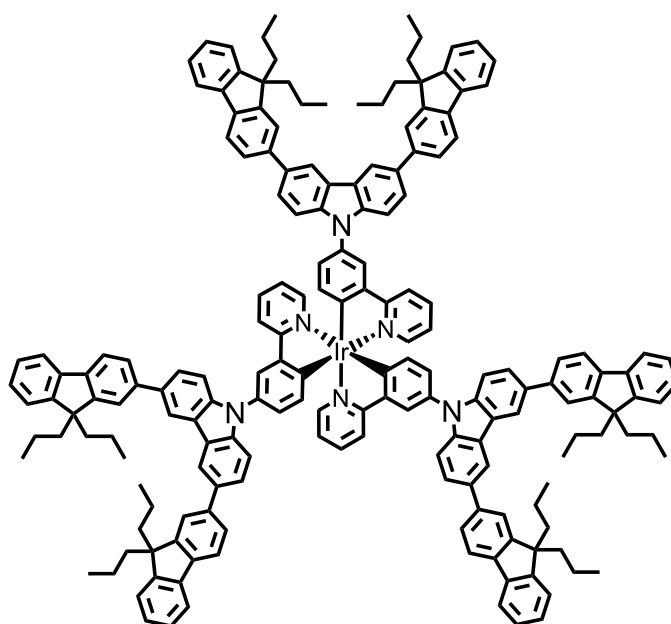


Figure 4.11. Structure of the related green-emissive iridium(III) complex containing dendrimer, **L3**.<sup>111</sup>

With the exception of **Hom1**, the red-emitting iridium(III) complex containing dendrimers experienced more deleterious interchromophore interactions in the neat film than the reported green-emitting dendrimer, **L3**. This indicates that the dendrons of **Hom2**, **Het1** and **Het2** are not achieving sufficient levels of chromophore separation to be used in host-free OLEDs. The inability for the dendrons of **Hom2**, **Het1** and **Het2** to separate

neighbouring chromophores probably stems from the position and directionality of their dendrons. The green-emitting dendrimer, **L2**, and **Hom1** both have dendrons attached to one face of their octahedral complex resulting in a large portion of the metal complex being tightly surrounded by the protective moieties. In contrast the dendrons of **Hom2** are further in distance from the complex and in a pseudo-trigonal planar arrangement which leaves much of the complex unprotected. The heteroleptic complexes, **Het1** and **Het2**, suffer from even less protection by their dendrons as the ancillary ligand does not bare any sterically bulky groups. While all four dendrimers are of great interest for use in blend systems, it is clear that if the goal is to produce dendrimers for host-free emissive layers then thought must be given to the position of dendrons and how their topology will be capable of segregating the emissive moieties.

The photoluminescence quantum yield of the poly(dendrimer), **PDcR**, was found to decrease by approximately 50 %, from 72 % to 32 %, when deposited as a neat film. While there is a significant decrease in photoluminescence quantum yield, **PDcR** experiences far less quenching than the dendrimers with the quantum yield of the next best dendrimer decreasing by 74 % (**Hom1**: 74 % to 19 %) when going from solution to the neat film. While the photoluminescence lifetimes of **PDcR** did decrease in the neat film; unlike the dendrimers there was no large, very short decay component. The photoluminescence properties of **PDcR** are very consistent with those shown for the related green-emitting poly(dendrimer), **L2** (Figure 4.12). The photoluminescence quantum yield of **L2** was reported to decrease from 72 % to 30 % when moving from solution to neat film, respectively.<sup>142</sup> This strongly suggests that, in spite of the emissive chromophores being held in close proximity along the backbone, the steric bulk of the dendrons are very effective at spatially separating the pendant groups. Additionally, both poly(dendrimer)s appear to exhibit less quenching from interchromophore interactions in the neat film than their respective dendrimers. Ultimately, it has been shown that the poly(dendrimer) architecture is a potent approach to improving the neat film photoluminescent properties of phosphorescent emitters.

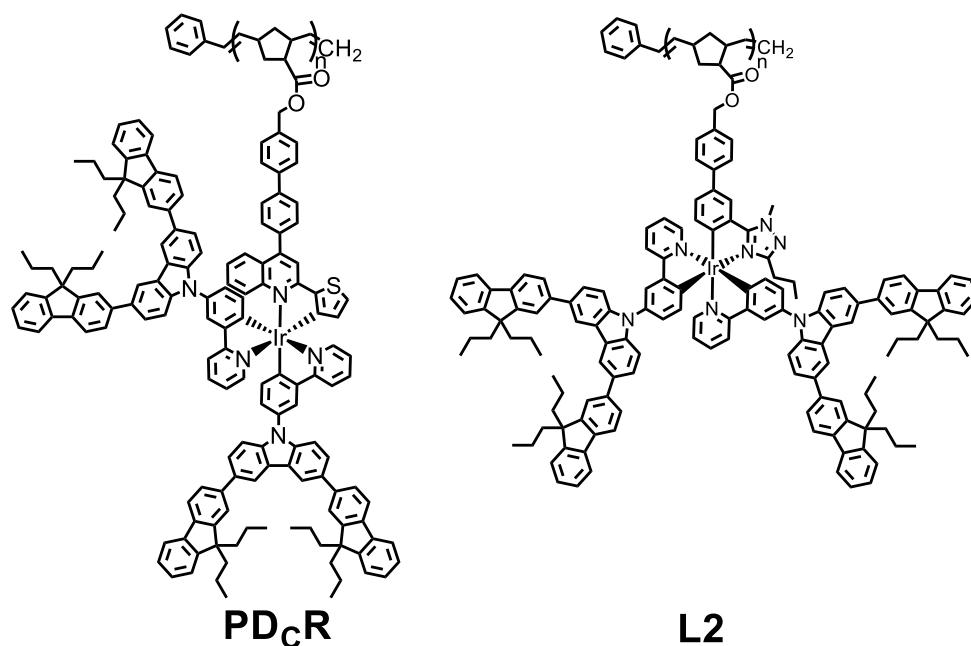


Figure 4.12: Structures of the related red-emitting (**PD<sub>c</sub>R**) and green-emitting (**L2**) poly(dendrimer)s.

As described previously, with the exception of **Het2**, all of the red-emitting dendrimeric materials are shown to have comparable phosphorescent quantum yields in solution and 10 wt% in CBP blend films. To the best of my knowledge **Hom2** has the highest solution and blend film photoluminescent quantum yields achieved as of April 2018 for a solution processable deep-red phosphorescent emitter. Prior to a recent publication in which a phosphorescent small molecule deep-red emitter was reported to have a solution photoluminescent quantum yield of 100 %<sup>79</sup>; **Hom2** was believed to have achieved the highest phosphorescent quantum yield of any phosphorescent deep-red emissive material. As of April 2018, all five phosphorescent deep-red emitting materials show phosphorescent quantum yields comparable to the highest reported.

While the two heteroleptic dendrimers, **Het1** and **Het2**, have lower phosphorescent quantum yields than their homoleptic analogues; their emission is also a deeper red. This is particularly interesting as the photoluminescence quantum yields, and subsequent device efficiencies, are known to decrease sharply as emission wavelength increases through the red-region of the visible spectrum. This phenomenon is known as the energy-gap law and is due to non-radiative decay pathways via vibrational (heat) mechanisms becoming more efficient (thus more probable) as the energy gap between the lowest electronic transition approaches the highest vibrational transition.<sup>181,182,183</sup>

Even more interesting is that the emission colour of **Het1** and **Het2** are both suitable for use in UHDTV (or Rec.2020 or BT.2020) gamut displays having CIE 1931 coordinates

of approximately (0.70, 0.30).<sup>184</sup> To the best of my knowledge, **Het1** exhibits the highest photoluminescence quantum yield of any material capable of reaching the colour requirements for Rec.2020 displays.

These high photoluminescent quantum yields are also interesting as phosphorescent iridium(III) complexes employing sulfur-containing moieties within their ligands were often reported to exhibit low phosphorescent quantum yields compared with analogous iridium(III) complexes featuring sulfur-free ligands.<sup>66,185</sup> It was posited by the authors that non-radiative decay of the excited population in sulfur-containing species could be occurring through a thermally driven transition to the low-lying  $n\pi^*$  excited state, which typically has low radiative quantum efficiencies. The research within this chapter, along with multiple recent publications<sup>156,186</sup>, demonstrate that high phosphorescent quantum yields can be achieved using sulfur-containing ligands; suggesting that the former observations are not a general property of iridium(III) complexes with sulfur-containing ligands.

In summary, all red-emitting dendrimeric materials explored during this project exhibit high photoluminescence quantum yields when used as a 10 % dopant in CBP blend films. With the exception of **Het2**, all dendrimeric materials show blend film photoluminescence quantum yields comparable to solution photoluminescence quantum yields indicating that the deleterious interchromophore interactions observed in the neat films are mitigated by dispersal through the CBP host. It is believed **Het2** has a high affinity towards aggregation which is likely driving phase separation during preparation of the blend film with the result of reduced quantum yields.

#### 4.3.8 Photoluminescence spectroscopy: Excitation versus Emission

To investigate whether the energy transfer from the carbazolyl-dendrons into the emissive iridium(III) core is efficient, the solution excitation spectrum (intensity of photoluminescence at a fixed emission wavelength and varying excitation wavelength) of the red-emitting dendrimeric materials were collected. When compared to the solution adsorption spectra, the emission spectra should show similar relative intensities if there is efficient energy transfer from the adsorption transition to the radiative transition. Figure 4.13 shows the comparison of the solution excitation spectrum versus the absorption spectrum of the small molecule, **[Ir(tmq)<sub>3</sub>]**.

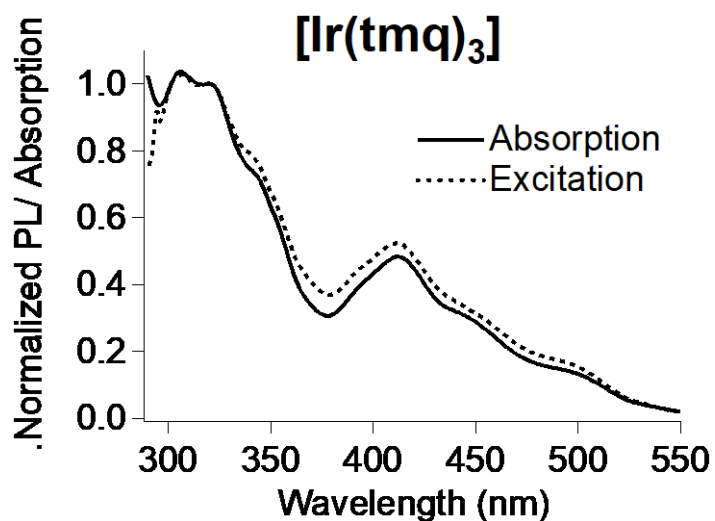


Figure 4.13: Comparison of the absorption and excitation spectra of **[Ir(tmq)<sub>3</sub>]** in degassed toluene. The excitation spectrum was collected at the emission maxima.

The comparison of the adsorption and excitation spectra of **[Ir(tmq)<sub>3</sub>]** indicate that all absorption transitions greater than 300 nm transfer their energy into the emissive species with equivalent efficiency. Therefore any adsorption bands giving a lower quantum yield within the dendrimers must result from the dendron moieties.

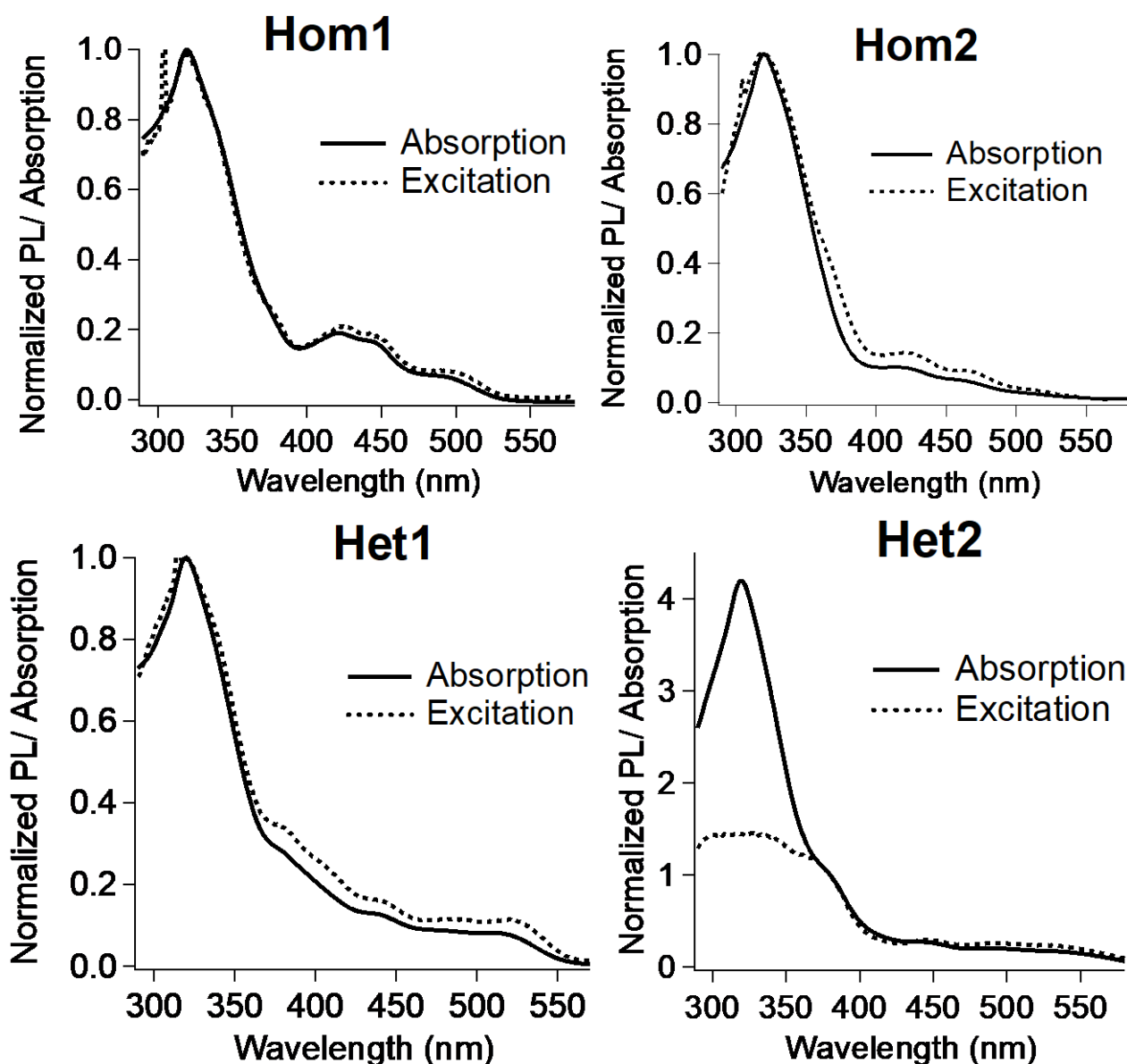


Figure 4.14: Comparison of the absorption and excitation spectra of the homoleptic dendrimers, **Hom1** and **Hom2**, and the heteroleptic dendrimers, **Het1** and **Het2**, in degassed toluene. The excitation spectrum was collected at the emission maxima. The expected  $\lambda/2$  diffraction peak can be seen as a sharp peak in some excitation spectra.

As shown in Figure 4.14., **Hom1**, **Hom2** and **Het1** all displayed efficient energy transfer between all absorption transitions and emission. There is no significant indication that energy transfer to the emissive chromophore from any moiety within these three dendrimers is in any way hindered. Therefore, it is expected that the dendrons will be effective in transporting exciton species to the emissive cores in these three dendrimers.

The emission spectrum of **Het2** was very different from the other dendrimers. In the plot shown in Figure 4.14, both spectra are normalized to 380 nm, above which there is no significant deviation between the adsorption and excitation spectra. At shorter wavelengths



there is significant deviation with significantly reduced photoluminescence being seen. From the wavelength of the low quantum yield adsorption transitions, it can be deduced that they are the singlet  $\pi \rightarrow \pi^*$  transitions of the fluorenyl- and/or carbazolyl-moieties. As there is no reason for either Förster or Dexter energy transfer from the dendron to the emissive chromophore to be inefficient (as evident for the other dendrimers); the loss of excited species is likely due to a very fast non-radiative process available to the excited dendrons. The dendrons of **Het2** are known to have the highest freedom of movement as they project away from each other and the emissive chromophore in a linear fashion. It is believed that this additional freedom may create efficient non-radiative vibrational-rotational decay pathways not seen in the other dendrimers.

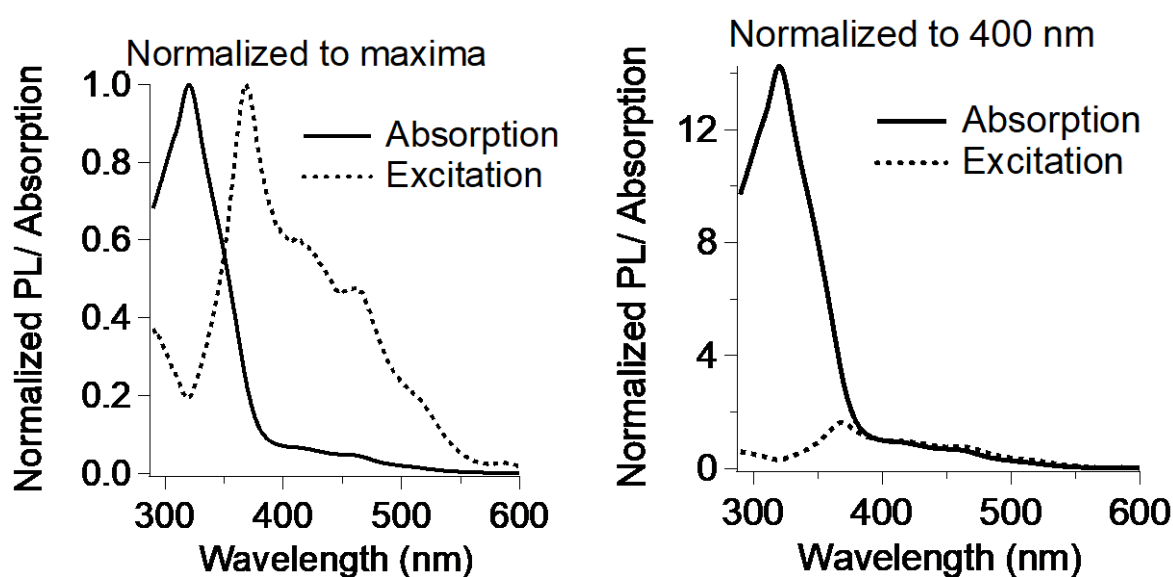


Figure 4.15: Comparison of the absorption and excitation spectra of **PDcR**.

The solution excitation and absorption spectra of **PDcR** are compared in Figure 4.15. The poly(dendrimer) shows equivalent photoluminescent quantum yield for all excitation wavelengths above approximately 400 nm, however, the photoluminescence is remarkably attenuated at shorter wavelengths. The greatest difference between the two coincides with the fluorenyl- adsorption band at 319 nm. As was the case for **Het2**, it is apparent that photo-excitation of the dendrons of **PDcR** leads to non-radiative decay, albeit to a much greater degree for the poly(dendrimer). The attenuation also appears to continue to a longer wavelength than shown in **Het2** and it is likely that any adsorption transition of the phenylpyridinyl ligand or dendron will experience a greater rate non-radiative decay.

While the phenylpyridine ligands of **PDcR** were believed to be non-emissive due to Kasha's law, the inefficient red-emission from excitation of the dendronized ligands brought

this assumption into question. To check for any additional radiative processes within the materials, the solution emission versus excitation spectra of the dendrimeric materials in were collected. If only one radiative process is involved, it is expected that the emission spectra will maintain the same shape but with intensity varying proportional to the excitation spectra. The small molecule and dendrimers were also assessed.

The solution emission versus excitation spectra of **[Ir(tmq)<sub>3</sub>]** are shown as a contour plot in Figure 4.16. The emission and excitation/ adsorption plots are shown as projections of the axis for comparison. **[Ir(tmq)<sub>3</sub>]** displays the ideal behaviour of an emissive material with the intensities within the contour plot always being a product of the one-dimensional emission and excitation spectra.

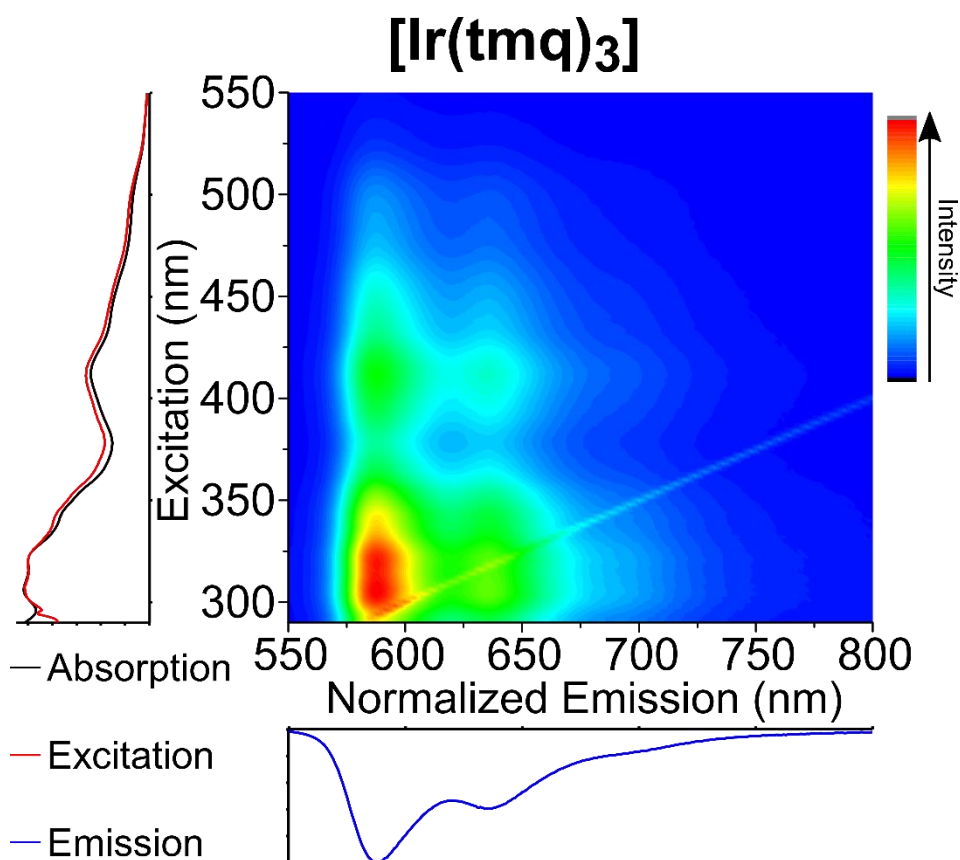


Figure 4.16: Emission versus excitation contour plot of **[Ir(tmq)<sub>3</sub>]** in solution (toluene). One-dimensional emission, excitation and adsorption spectra are shown as axis projections for comparison.

The dendrimers were all shown to behave as expected from their emission and excitation spectra. As shown in Figure 4.17, no additional radiative processes were present and the contour plots were the product of the emission and excitation spectra. This confirmed that the difference between the excitation and adsorption spectra of **Het2** were stemming from at least one additional non-radiative process which is accessible through

excitation of the dendron. As the cause may be due to molecular movement, it is possible that confining the molecule to a solid matrix, as it would be within an OLED, would result in deactivation of this additional non-radiative process. Unfortunately it was not possible to investigate this further at this point as **Het2** appears to separate from common hosts during film preparation. The resulting non-radiative decay from aggregation of **Het2** in the blend films could not be separated from other non-radiative decay mechanisms.

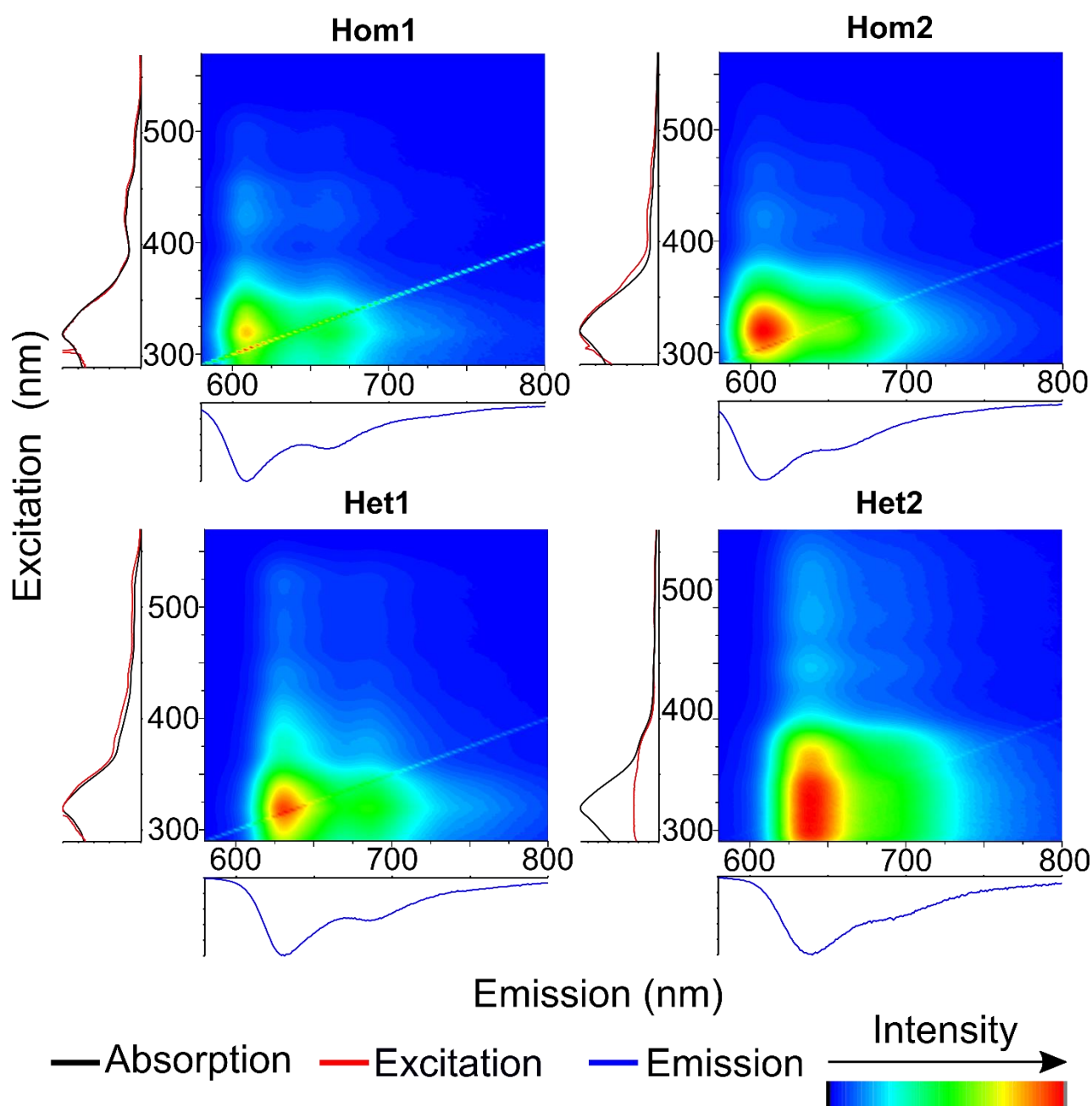


Figure 4.17: Emission versus excitation contour plots of the four red-emitting dendrimers in solution (toluene). One-dimensional emission, excitation and adsorption spectra are shown as axis projections for comparison.

The remaining dendrimers; **Hom1**, **Hom2** and **Het1**; produce emission versus excitation contour plots which are directly proportional to the product of the one-dimensional emission versus excitation spectra. This indicates that, for these three dendrimers, the attachment of the dendrons is not creating any additional non-radiative decay pathways and that energy transfer from the dendron to the emissive chromophore is very efficient.

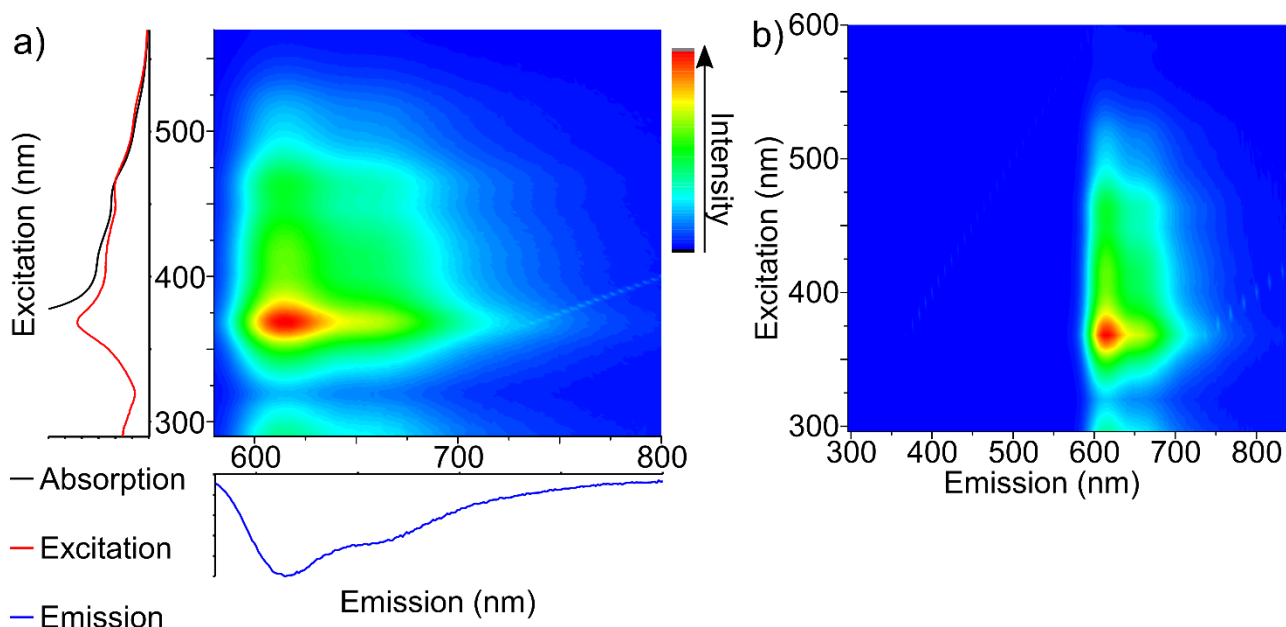


Figure 4.18: Emission versus excitation contour plots of **PDcR** in solution (toluene). One-dimensional emission, excitation and adsorption spectra are shown as axis projections for comparison. Plots collected over a) same range as other materials and b) wider emission range.

As shown in Figure 4.18, the poly(dendrimer) behaves as expected from the one-dimensional solution emission and excitation spectra. The emission shows extensive attenuation when excited at wavelengths corresponding to absorption transitions localized on the dendronized ligand. Importantly the emission profile does not vary with wavelength and, as with the small molecule and dendrimers, it is equivalent to the product of the one-dimensional emission and excitation spectra of the material in solution. The emission range of the solution emission versus excitation spectrum of **PDcR** was increased to ensure the absence of higher energy radiative transitions resulting from the dendronized phenylpyridine ligands.

#### 4.3.9 Summary of photophysical investigations

The photophysical properties of the small molecule, four dendrimers and poly(dendrimer) containing red-emitting iridium(III) complexes were thoroughly investigated. The UV/visible absorption spectra of all materials were consistent with expectations. All materials were shown to exhibit very high solution photoluminescence quantum yields with all materials, excluding the small molecule, being saturated emissive chromophores. The photoluminescence quantum yields were shown to decrease substantially when transitioning to the neat film indicating that the dendrons were not sufficient for highly efficient host-free OLEDs. The neat film photoluminescence lifetimes were consistent with increased non-radiative decay via interchromophore interactions. The photoluminescence quantum yields of the dendrimeric materials incorporated into a 10 wt% blend in CBP were equivalent to their solution values, with **Het2** being a notable exception.

The solution emission and excitation properties of the complexes were examined to investigate the presence of any non-radiative or additional radiative transitions. The small molecule, **[Ir(tmq)<sub>3</sub>]**, along with three dendrimers; **Hom1**, **Hom2** and **Het1**, were found to produce emission spectra consistent with a single radiative process. The intensity of the emission for these materials were directly proportional to the absorption across the examined wavelengths.

The  $^1\pi\rightarrow\pi^*$  transitions localized on the dendron were observed to undergo increased non-radiative decay, respective to other absorption transitions, for the remaining dendrimer (**Het2**) and the poly(dendrimer) (**PDcR**). Whether these additional non-radiative decay processes also occurs in the film was not investigated. Instead, these results may be used as a starting point for investigating the origin of any unusual performance observed in the subsequent devices.

#### 4.4 Electrochemistry

The electrochemistry of the small molecule and iridium(III) complexes were investigated by cyclic voltammetry to provide an insight into their frontier orbital energies. All reduction cycles were collected in my absence by Dr Dani Stoltzfus, with the oxidation cycles being collected by myself. A compilation of the oxidation and reduction cycles of the iridium(III) complexes is shown in Figure 4.19 with the numerical values reported in Table 4.4. The electrochemistry of the poly(dendrimer), **PDcR**, was not collected due to limited quantities of material and precedence being given to its use in device fabrication.

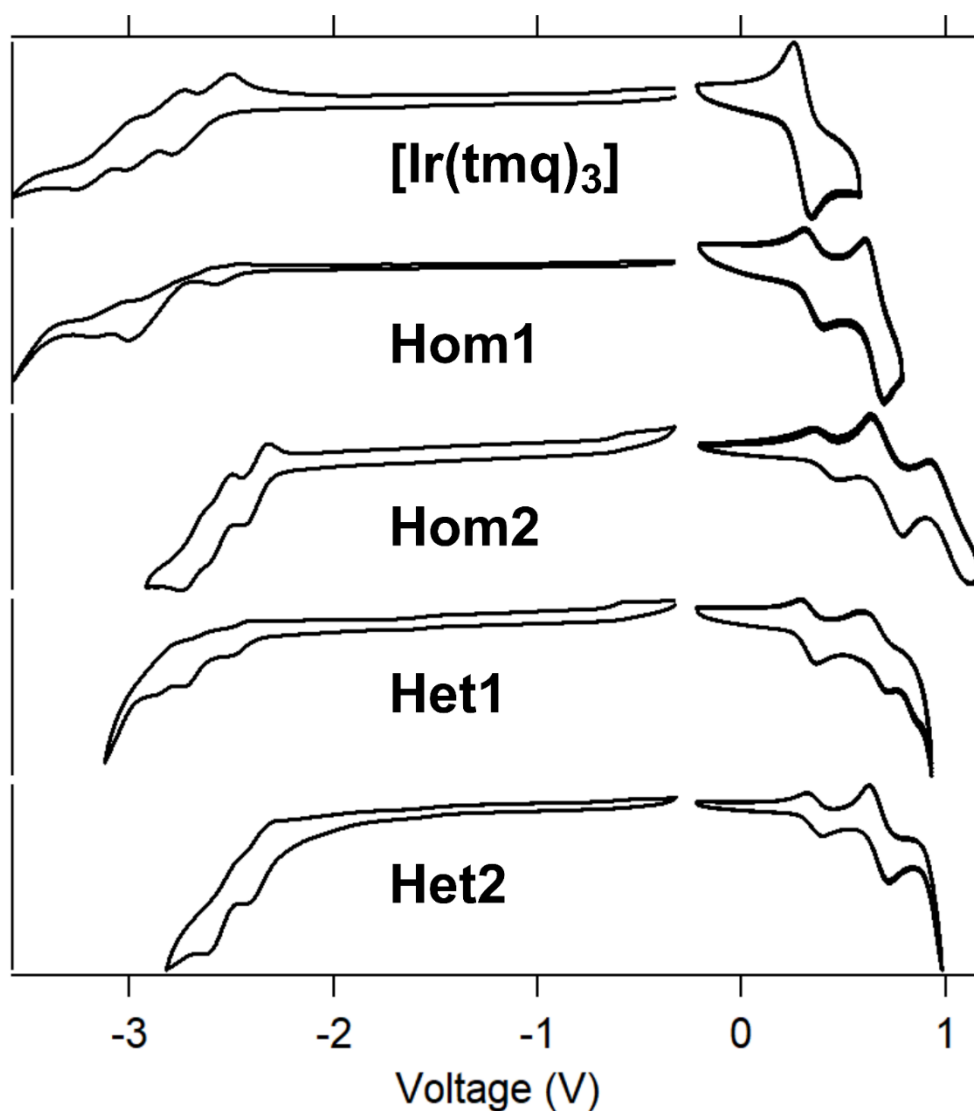


Figure 4.19: Cyclic voltammograms of red-emitting iridium(III) complexes versus Fc/Fc<sup>+</sup> redox couple. Oxidations were performed in anhydrous dichloromethane while reductions were in anhydrous tetrahydrofuran. Tetrabutylammonium perchlorate was utilized as the electrolyte with a glassy carbon working electrode, platinum counter electrode and silver/silver(I) nitrate in acetonitrile reference electrode.

Table 4.4: Redox couplings calculated from cyclic voltammetry. Values in brackets indicate the coupling was irreversible. Greyed values indicate a coupling was not observed. Calculated versus Fc/Fc<sup>+</sup> couple.

	E <sub>1/2</sub> Oxidation (eV)			E <sub>1/2</sub> Reduction (eV)			ΔE (eV)
	+1	+2	+3	-1	-2	-3	
<b>[Ir(tmq)<sub>3</sub>]</b>	0.3			-2.6	-2.9	-3.1	2.9
<b>Hom1</b>	0.4	0.7		(-2.5)	(-2.8)	(-3.1)	2.9
<b>Hom2</b>	0.4	0.7	1.0	-2.4	-2.6	-2.7	2.8
<b>Het1</b>	0.3	0.7		(-2.5)	(-2.7)	(-2.8)	2.8
<b>Het2</b>	0.4	0.7		-2.4	-2.5		2.8

The small molecule was found to undergo one fully reversible one-electron oxidation and three fully reversible reductions. The dendrimers with the carbazoyl-dendron attaching through the 5-thiophenyl-position, **Hom1** and **Het1**, were observed to one fully reversible one-electron oxidation, one fully reversible two-electron oxidation and multiple irreversible reductions. **Het2** was observed to undergo one fully reversible one-electron oxidation, one fully reversible two-electron oxidations and two fully reversible reductions of equal electron number. The other dendrimer containing phenyl-functionalized dendrons, **Hom2**, behaved in a similar manner to **Het2**, however, an additional fully reversible two-electron oxidation and a fully reversible reduction were observed.

The first one-electron oxidation observed for all materials is attributed to the metal centred Ir(III)/Ir(IV) redox couple while the remaining oxidations are attributed to dendron localized redox couples. As the reductions always occurred in equal amplitude they are known to involve the same number of electrons. The irreversibility of **Hom1** and **Het1** reductions supports the assignment of the reductions being localized to the ligands.

Table 4.5: Energy level estimation from cyclic voltammetry. Values in brackets estimated using irreversible process.

	Ionization Potential (eV)	Electron Affinity (eV)	$\Delta E$ (eV)
<b>[Ir(tmq)<sub>3</sub>]</b>	5.1	2.2	2.9
<b>Hom1</b>	5.2	(2.3)	(2.9)
<b>Hom2</b>	5.2	2.4	2.8
<b>Het1</b>	5.1	(2.3)	(2.8)
<b>Het2</b>	5.2	2.4	2.8

From the oxidation and reduction couples, the ionization potential (IP) and electron affinity (EA) can be estimated (Table 4.5). It should be emphasized that estimation of energy levels from cyclic voltammetry should also be treated with caution as they are conducted in an environment that is considerably different to that experienced by the molecules within a device.<sup>24</sup> Additionally, **Hom1** and **Hom2** did not undergo reversible reduction and the calculated electron affinities and electrochemical gaps should be examined cautiously.

From cyclic voltammetry the energy levels of all red-emitting dendrimers were shown to have similar ionization potentials (5.1 to 5.2 eV), electron affinities (2.3 to 2.4 eV) and electrochemical gaps (2.8 to 2.9 eV). It is notable that the difference between the IP and EA of the materials is far larger than their estimated triplet energy of approximately 2 eV. A portion of this discrepancy can be explained by the exciton binding energy which is not involved in the phosphorescence transition. This suggests that, while the materials should

have low triplet energies, OLEDs should be fabricated using materials with relatively large electrochemical gaps to allow efficient charge transfer.

## 4.5 Device performance

Organic light-emitting diodes utilizing the dendrimeric materials containing red-emissive iridium(III) complexes as the emissive species were fabricated and tested by Dr Anthony Brewer.

The general device structure used for the preliminary red-emitting dendrimeric materials was as follows: indium tin oxide (100nm)/ PEDOT:PSS (35 nm)/ emissive layer)/ 1,3,5,-tris(2-N-phenylbenzimidazolyl)benzene (70 nm)/ lithium fluoride (1 nm)/ aluminium (100 nm).

The results described below are for dendrimers utilizing tris(4-carbazoyl-9-ylphenyl)amine (TCTA) as a host and the poly(dendrimer) using 4,4'-bis(N-carbazoyl)-1,1'-biphenyl (CBP) as the host with emissive layers being approximately 40 nm in thickness. The device characteristics are summarized for comparison in Table 4.6.

Table 4.6: Average device characteristics for red-emitting OLEDs. Doping concentration for each material is shown in brackets.

	$\eta_{\text{ext}}$ (%)	$\eta^*$ lm/W	Turn-on Voltage† (V)	Luminance cd/m <sup>2</sup>
<b>Hom1 (20 %)</b>	5.7 ± 0.1	4.3 ± 0.1	4.0	3.8 ± 0.2
<b>Hom2 (20 %)</b>	11.0 ± 0.4	8.4 ± 0.1	3.9 ± 0.1	8.4 ± 5.5
<b>Het1 (15 %)</b>	4.2 ± 0.3	1.5 ± 0.1	3.8 ± 0.3	21 ± 5
<b>Het2 (15 %)</b>	2.1	0.5	5.8	43
<b>PDcR (15 %)</b>	10.0 ± 0.2	8.7 ± 0.4	3.4 ± 0.1	5.2 ± 2.6

†Defined as a brightness of 1 cd/m<sup>2</sup>. In most cases the sample size is small and further experiments are required.

Typical device characteristics for organic light-emitting diodes utilizing homoleptic complexes, **Hom1** and **Hom2**, are shown in Figure 4.20.



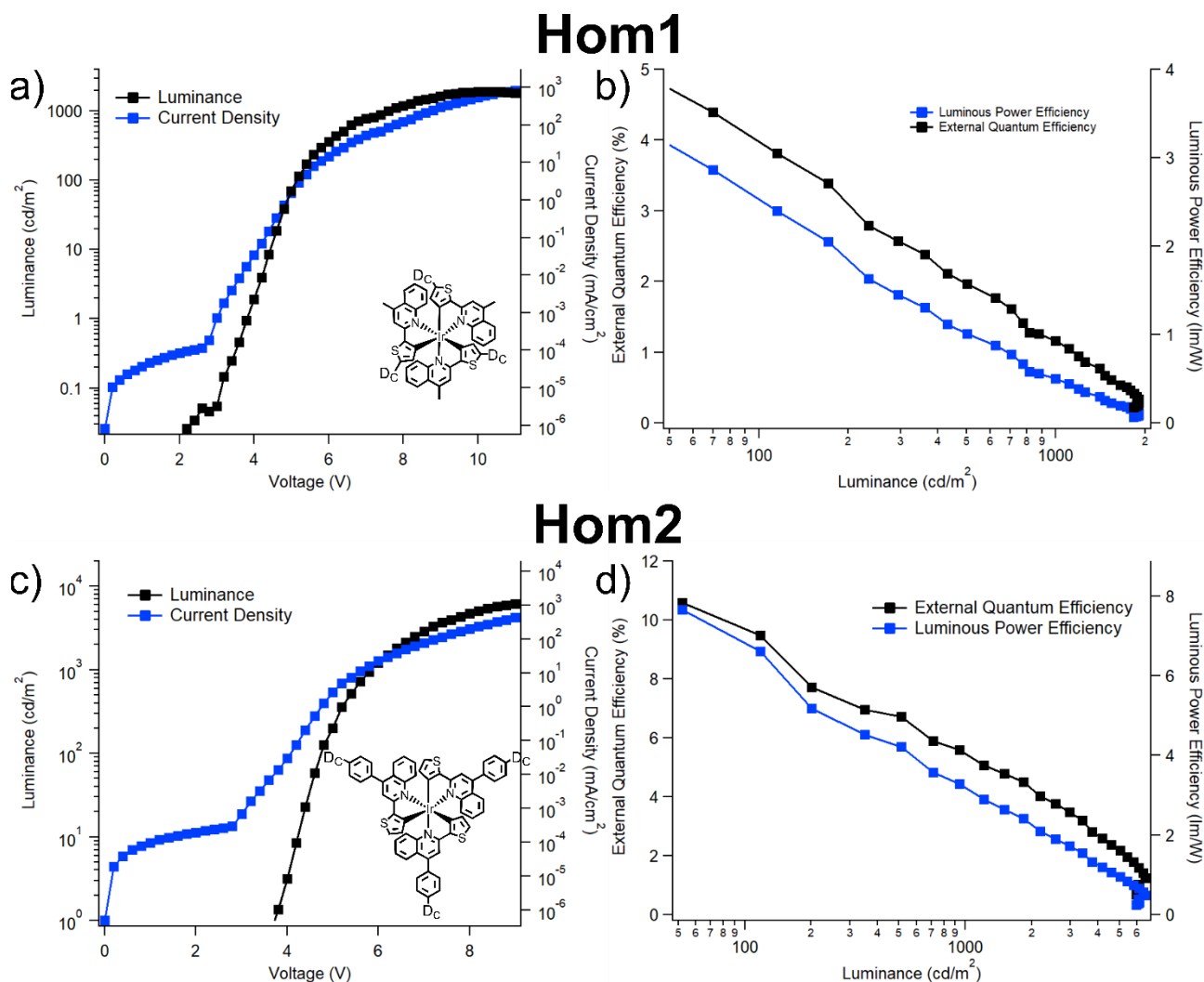


Figure 4.20: Typical device characteristics for OLEDs using **Hom1** or **Hom2** as the emissive dopant. The current-voltage-luminance curves (a and c) as well as the external quantum efficiency and power efficiency versus luminance (b and d) are shown with the structure of the relevant dendrimer inset for reference.

Devices using **Hom1** (20 wt% in TCTA) as the emissive layer gave a decent turn on voltage of 4.0 V and a maximum external quantum efficiency of  $5.7 \pm 0.1$  %. For devices using **Hom2** (20 wt% in TCTA) as the emissive layer the turn-on voltage was found to be comparable at  $3.9 \pm 0.1$  V, while an impressive external quantum efficiency of  $11.0 \pm 0.4$  % was observed. Higher luminance was also observed for devices incorporating **Hom2** being able to reach approximately 6000 cd/m<sup>2</sup> compared to the **Hom1** devices falling just short of 2000 cd/m<sup>2</sup>. For both materials there was a significant efficiency decrease corresponding with increasing luminance. Due to this the reported maximum external quantum efficiencies of **Hom1** and **Hom2** devices being at the low luminances of  $3.8 \pm 0.2$  cd/m<sup>2</sup> and  $8.4 \pm 5.5$  cd/m<sup>2</sup>, respectively.

Typical device characteristics for organic light-emitting diodes utilizing heteroleptic complex **Het1** are shown in Figure 4.21. The best device performance for an OLED utilizing **Het2** is also shown in Figure 4.21. The devices using **Het2** displayed extremely poor reproducibility stemming from the poor quality films produced when using it as a dopant. As such only one pixel is described in this preliminary work with the intent of improving upon it with further optimization.

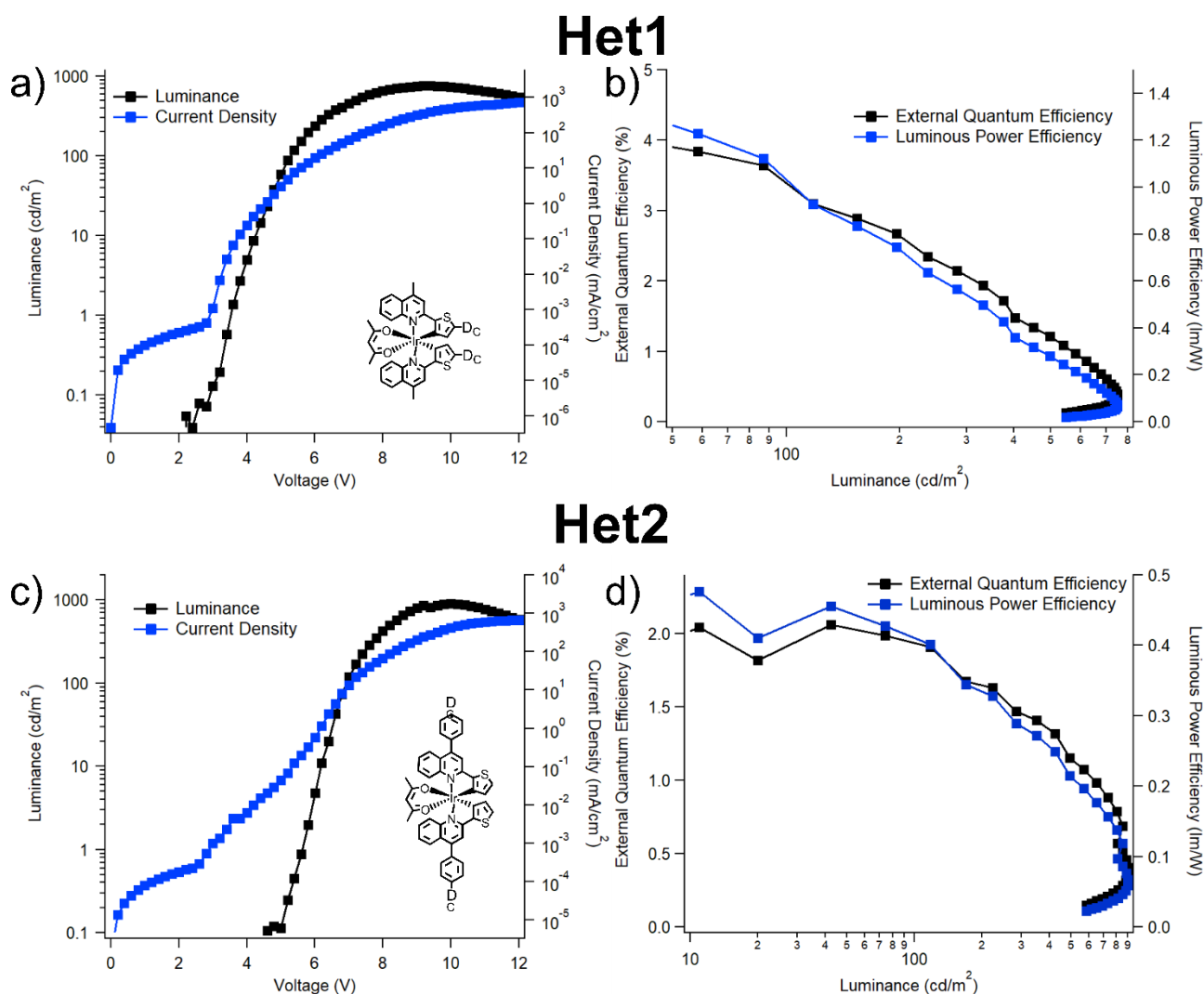


Figure 4.21: Typical device characteristics for OLEDs using **Het1** or **Het2** as the emissive dopant. The current-voltage-luminance curves (a and c) as well as the external quantum efficiency and power efficiency versus luminance (b and d) are shown with the structure of the relevant dendrimer inset for reference.

Devices using **Het1** (15 wt% in TCTA) as the emissive were found to have a turn-on voltage similar to the homoleptic complexes at  $3.8 \pm 0.3$  V. The external quantum efficiency of these devices were found to have an average maximum of  $4.2 \pm 0.3$  % at a

luminance of  $21 \pm 5 \text{ cd/m}^2$ . For the single device using **Het2** (15 wt% in TCTA) as the emissive layer the external quantum efficiency was found to reach a maximum of 2.1 % with a luminance of  $43 \text{ cd/m}^2$ . This device exhibited a poor turn-on voltage of 5.8 V and is an indication of the poor electrical properties observed for all devices utilizing **Het2** due to its habit of crystallizing. Devices using both heteroleptic complexes struggle to achieve high luminance with a roll-off observed before reaching  $1000 \text{ cd/m}^2$ .

Upon collecting the electroluminescence spectra of the dendrimers they were compared to the respective photoluminescence spectra of the blend films. The comparisons are shown in Figure 4.22.

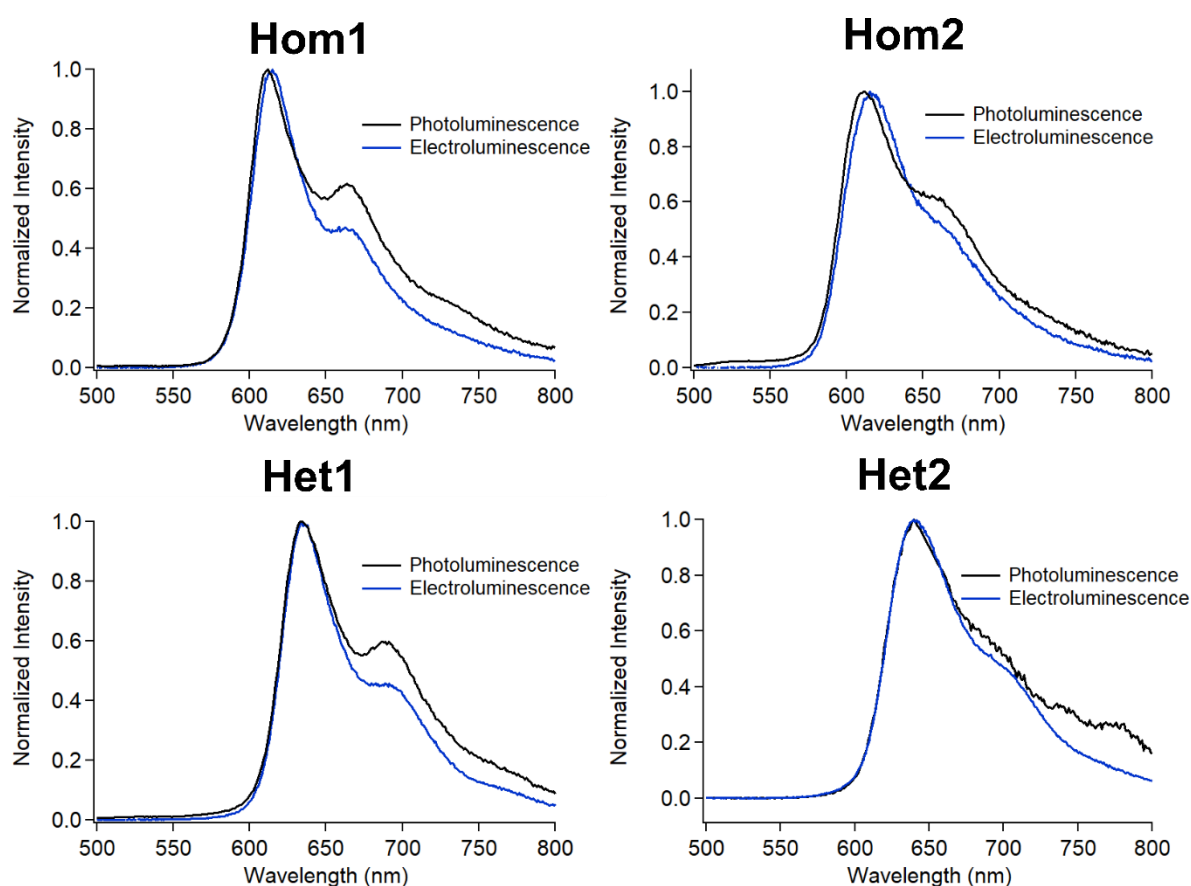


Figure 4.22: Comparison of the blend photoluminescence and electroluminescence spectra of the red-emitting dendrimers.

The photoluminescence and electroluminescence spectra of all dendrimers are shown to behave in a similar fashion. The maximum emission bands appear to be identical for photoluminescence and electroluminescence. The vibronic bands, however, appear to have decreased in intensity. The difference appears particularly large for the dendrimers exhibiting the more pronounced vibronic band, **Hom1** and **Het1**. As these results are recent

results further investigation is required to determine if this is due to an optical phenomenon in the films or devices as opposed to an alteration of the radiative transition upon application of an electric field; although as the difference appears correlated to the molecular structure is more likely to be the latter.

Organic light-emitting diodes utilizing the poly(dendrimer), **PDcR**, as a dopant were likewise characterized with the typical device characteristics shown in Figure 4.23.

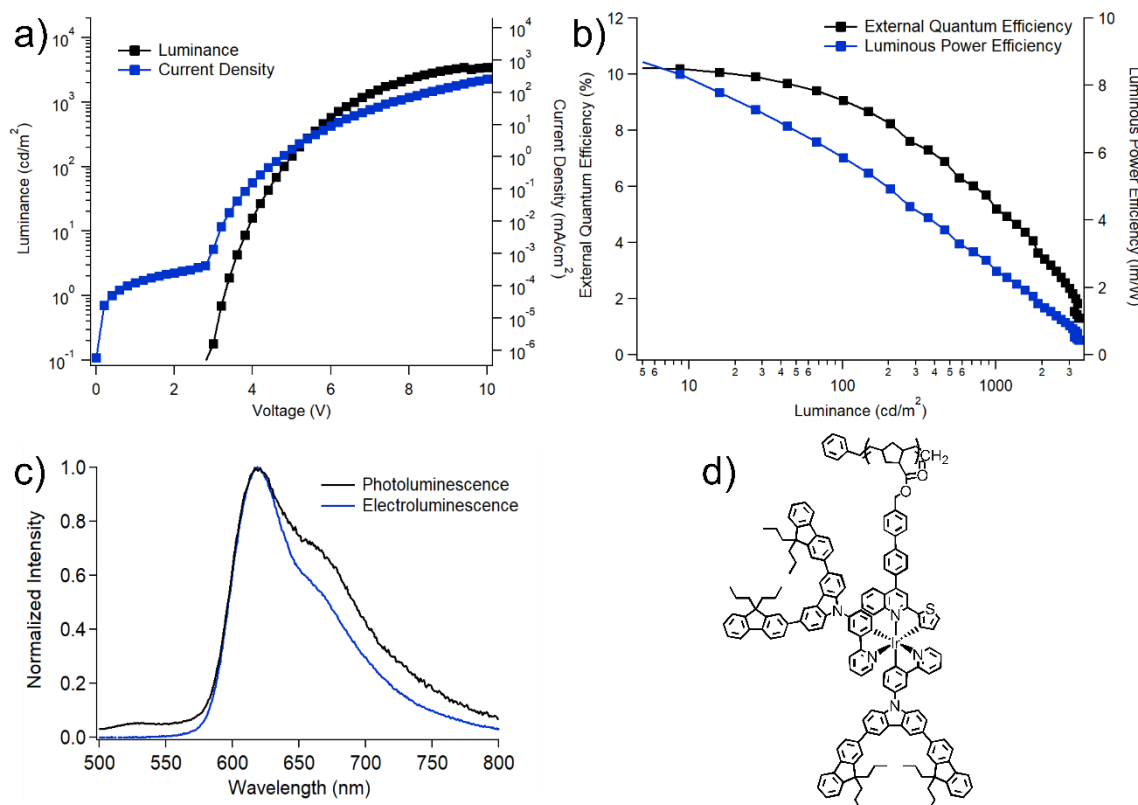


Figure 4.23: Typical device characteristics for OLEDs using **PDcR** as the emissive dopant. The a) current-voltage-luminance curve as well as the b) external quantum efficiency and power efficiency versus luminance are shown along with c) the comparison of photoluminescence and electroluminescence and d) the structure of the material.

Devices incorporating **PDcR** (10 wt% in CBP) as the emissive layer exhibited a very good turn-on voltage of  $3.4 \pm 0.1$  V as well as achieving a respectable average maximum external quantum efficiency of  $10 \pm 0.2$  % at  $5.2 \pm 2.6$  cd/m<sup>2</sup>. In contrast to the high turn-on voltage of **Het2**, the low turn-on voltage exhibited by the devices using the poly(dendrimer) may result from the excellent quality films it was found to produce. Similar to the devices incorporating the dendrimers, significantly reduced efficiency was obtained as luminance was increased. The poly(dendrimer) devices achieved maximum luminance of approximately 3500 cd/m<sup>2</sup>. A comparison of the photoluminescence and

electroluminescence of the poly(dendrimer) observed a similar phenomenon of reduced intensity of the vibronic bands relative to the maxima.

As mentioned the device results presented herein are preliminary work. It is known that the electrical characteristics of these devices are not optimal. For example, significant leakage current can be seen below the turn-on voltage (refer to Figures 4.20, 4.21 and 4.23) It was also observed that the dendrimers experience considerable non-radiative decay at the concentrations used for devices which corresponds to a significant loss of photoluminescence quantum yield. One of the first modifications being investigated is reducing the dopant concentrations, however, this generally decreases the film quality as the hosts are generally crystalline.

Table 4.7: Chromaticity of dendrimeric materials containing red-emitting iridium(III) complexes

	$\lambda_{emmax}$ (nm)	CIE 1931 coordinates
<b>Hom1</b>	615	(0.66, 0.33)
<b>Hom2</b>	616	(0.66, 0.34)
<b>Het1</b>	634	(0.69, 0.30)
<b>Het2</b>	639	(0.68, 0.30)
<b>PDcR</b>	621	(0.66, 0.34)

As shown in Table 4.7, all dendrimeric emitters were found to be saturated red in colour. **Hom1**, **Hom2** and **PDcR** were found to have CIE 1931 coordinates very close to the ideal red required for the sRGB gamut of (0.66, 0.33). Interestingly, the electroluminescence of both heteroleptic complexes was found to be a deeper red with CIE 1931 coordinates almost achieving the level required for the Rec.2020 (UHDTV) gamut of (0.71, 0.29). While still requiring significant optimization, devices utilizing **Het1** may be able to achieve efficiencies considerably higher than previously reported emitters with a similarly deep red emission.

In summary, all four dendrimers and the poly(dendrimer) were employed as dopants within the emissive layer of organic light-emitting diodes. The best performing materials were **Hom2** and **PDcR** were with external quantum efficiencies reaching  $11.0 \pm 0.4 \%$  at  $8.4 \pm 5.5$   $\text{cd/m}^2$  and  $10 \pm 0.2 \%$  at  $5.2 \pm 2.6$   $\text{cd/m}^2$ , respectively. All devices were observed to experience decreasing performance with increasing luminance from just above the turn-on voltage. Devices utilizing **Hom2** were capable of achieving a luminance of  $6000 \text{ cd/m}^2$  while the next brightest devices were those utilizing **PDcR** achieving approximately  $3500 \text{ cd/m}^2$ .

All materials were found to possess saturated red-emission suitable for applications using sRGB gamut. While the preliminary devices utilizing **Het1** did not achieve the performances suggested by its blend film photoluminescence quantum yield, it is hoped that further optimization will lead to devices that can make use of its deep red emission which is very close to the ideal red of Rec. 2020 gamut.

## 4.6 Summary

The thermal, photophysical, electrochemical and device properties of the red-emitting dendrimeric materials, whose synthesis was described in chapter 3, were investigated to determine suitability for their application as emitters within organic light-emitting diodes.

The dendrimers were found to be thermally stable over the temperature ranges likely to be experienced during device fabrication and operation. No glass transition temperatures or melting points were observed for the dendrimers indicating that they were either a stable glass or crystal.

All dendrimers and poly(dendrimers) exhibited high solution phosphorescence quantum yields in the range of 61-87 %, with **Hom2** being the highest. With the exception of **Het2**, all materials achieved photoluminescence quantum yields comparable to their solution values when blended within a host.

The dendrimers were found to undergo red photoluminescence through a single radiative process in solution. Additional decay components and decreased radiative lifetimes were observed in the neat films indicating new non-radiative pathways through interchromophore interactions. These lifetime changes corresponded to significantly reduced photoluminescence quantum yields, indicating that the first generation dendrons were not sufficient to inhibit intermolecular interchromophore interactions. The observed emission lifetime of the poly(dendrimer) in solution indicated the presence of at least some non-radiative decay via intra-chain, interchromophore interactions. When processed as a neat film the poly(dendrimer) exhibited increased non-radiative decay and decreased phosphorescent quantum yield due to introduced inter-chain, interchromophore interactions. However, it was shown that the poly(dendrimer) suffered these detrimental interactions significantly less than any of the dendrimers. When blended into a host, the observed lifetime of the poly(dendrimer) was found to only have one decay component indicating suppression of the intra-chain, interchromophore interactions present in solution.

The electrochemistry of the dendrimers was examined via cyclic voltammetry. All dendrimers exhibited a similar first oxidation which was fully reversible at 0.3 eV to 0.4 eV versus Fc/Fc<sup>+</sup> couple. Only the materials with dendrons coupled through the phenyl moiety,

**Hom2** and **Het2**, were observed to have a reversible reduction at -2.4 eV versus Fc/Fc<sup>+</sup> couple. However; the dendrimers with alternative dendron connectivity, **Hom1** and **Het1**, were shown to undergo an irreversible reduction at approximately the same voltage. From this the ionization potential and electron affinities of all dendrimers were estimated to be between 5.1 eV to 5.2 eV and 2.3 eV to 2.4 eV, respectively.

Preliminary devices with emissive layers containing blends of the four dendrimers and poly(dendrimer) within a common host material were fabricated and characterized. Both **Hom2** and **PDcR** were found to produce devices with decent characteristics with maximum external quantum efficiencies of  $11.0 \pm 0.4 \%$  at  $8.4 \pm 5.5 \text{ cd/m}^2$  and  $10 \pm 0.2 \%$  at  $5.2 \pm 2.6 \text{ cd/m}^2$ , respectively. The devices with **Hom2** as an emitter also reached a good luminance of  $6000 \text{ cd/m}^2$ . All materials were found to produce electroluminescence suitable for application in displays using sRGB gamut, while **Het1** may even be suitable for displays using the Rec. 2020 gamut. This is particularly interesting as the deep red OLEDs required for Rec. 2020 gamut displays is very difficult to achieve. Ultimately, these preliminary devices demonstrate that these materials possess the properties necessary for application as emitters in OLEDs for displays or lighting.

# Chapter 5

## Experimental

---

### 5.1 General experimental

Carbazole was obtained from ACROS Organic and was used as received. 3'-Bromoacetophenone, 3-bromobenzoyl chloride, 4-bromophenol, 1-bromopropane, 3-bromopyridine, butyronitrile, 1,3-diaminopropane, *trans,trans*-dibenzylideneacetone, 1-fluoro-4-nitrobenzene, 1-hexanol, hydrazine hydrate, isopropoxyboronic acid, *cis*-5-norbornene-*exo*-2,3-dicarboxylic anhydride and sodium *tert*-butoxide were obtained from Alfa Aesar and were used as received. Trimethylborate was obtained from Alfa Aesar and distilled from the sodium-benzophenone ketyl radical and used fresh or stored over 4 Å molecular sieves. Potassium acetate was obtained from AMRESCO and was used as received. 4-Dimethylaminopyridine and methyl hydrazine were obtained from Fluka and were used as received. Bis(pinacolato)diboron, 2-bromofluorene, [1,1'-Bis(diphenylphosphino)ferrocene]dichloropalladium(II) dichloromethane adduct, silver triflate and 1,3,5-tribromobenzene were obtained from Matrix Scientific and were used as received. 2-Ethoxyethanol and triethylamine were obtained from Merck KGaA and were used as received. Iridium (III) chloride hydrate and Palladium (II) chloride were obtained from Precious Metals Online and were used as received. Iron powder was obtained from Riedel-de Haen and was used as received. 2'-aminoacetophenone was obtained from SAFC and was used as received. Copper (II) sulphate pentahydrate was obtained from Scharlau and was used as received. 2-Acetylthiophene, bromobenzene, *N*-bromosuccinimide, 4,4'-dibromophenyl, *N,N'*-dicyclohexylcarbodiimide, diethylene glycol butyl ether, *N,N'*-dimethylacetamide (anhydrous), 1,4-dioxane, diphenylamine, 2-ethylhexylbromide, ethyl vinyl ether, glycerol, Grubbs catalyst second generation, iron (III) chloride, 2 M isopropylmagnesium chloride in tetrahydrofuran, *exo*-5-norbornenecarboxylic acid, oxalyl chloride, Proton-sponge® (*N,N,N',N'*-Tetramethyl-1,8-naphthalenediamine), silver trifluoroacetate, sodium borohydride, sodium hydride 60 % in mineral oil, triflic acid, triphenylphosphine and *p*-toluenesulphonic acid monohydrate were obtained from Sigma-Aldrich and were used as received. Tri-*tert*-butylphosphonium tetrafluoroborate was obtained from Strem Chemicals and was used as received. Anhydrous diethyl ether, anhydrous *N,N*-dimethylformamide, anhydrous tetrahydrofuran and anhydrous toluene were



obtained by passage of the commercial solvents through a LC Technology Solutions Inc SPBT-104 solvent purification system prior to use. The following catalysts were prepared in house from commercial materials using literature procedures and used without further characterization;

tetrakis(triphenylphosphine)palladium(0),  
tris(dibenzylideneacetone)dipalladium(0) chloroform adduct and dichloro[1,3-bis(2,4,6-trimethylphenyl)-2-imidazolidinylidene](benzylidene)bis(3-bromopyridine)ruthenium(II) (Grubb's 3<sup>rd</sup> generation catalyst).

Column chromatography was performed with Davisil LC60A 40–63 micron silica gel or Merck KGaA silica gel 60 (0.040-0.063 mm) as received unless otherwise noted. When pH 7 buffer treated silica gel was noted the stationary phase was the above silica gel which had been previously prepared according to the literature method described by Armarego *et al*; 200 g of silica was stirred in in pH 7 phosphate buffer (17g potassium phosphate monohydrate and 3 g sodium hydride made up to 1 L with water) for half an hour, filtered and reactivated at above 110°C for at least 16 hours.<sup>187</sup>

Size exclusion chromatography was performed with BioRad Laboratories Bio-Beads S-X1 Support #1522151 as the stationary phase.

Thin layer chromatography (TLC) was performed using aluminum backed silica gel 60 F254 plates.

<sup>1</sup>H and <sup>13</sup>C NMR were performed using Bruker Avance (AV-300, AV-400, AV-500 MHz) or Bruker Ascend (AS-500 MHz) spectrometers in deuterated chloroform solution or deuterated dichloromethane solution and chemical shifts ( $\delta$ ) were referenced to 7.26 ppm and 77.16 ppm or 5.32 ppm and 53.84 ppm for the proton and carbon spectra, respectively. Multiplicities are reported as singlet (s), doublet (d), triplet (t), multiplet (m) and *para*-aromatic systems (AA`BB`) and coupling constants (*J*) are in Hertz and quoted to the nearest 0.5 Hz. The following notations indicate peak assignments: -CH<sub>3</sub> = methyl proton, -CH<sub>2</sub> = methylene proton, -CH = methane proton, -OCH<sub>2</sub> = ether methylene proton, -NCH<sub>3</sub> = *N*-amine methyl proton, -CH<sub>2</sub>OH = methylene proton of benzyl alcohol moiety, -CH<sub>2</sub>OOC = methylene proton of benzyl ester moiety, LCH<sub>3</sub> = methyl proton of lepidine (4-methylquinoline) moiety, -OH = alcohol proton, -NH<sub>2</sub> = primary amine proton, -NH = secondary amine proton, EH = 2-ethylhexyl proton (followed by group assignment), *n*Pr = *n*-propyl proton (followed by group assignment), NB = norbornenyl proton, CP = cyclopentanyl proton, V = vinyl proton, BiPh = aromatic proton on biphenyl dendron moiety, L= aromatic proton on 2-phenylpyridinyl or phenyltriazole ligand moieties, Fl = aromatic proton on fluorenyl moiety, Cbz = aromatic proton on carbazole moiety, T = biphenyl tether

proton, Th = aromatic proton on thiophenyl moiety, Q = aromatic proton on quinolinyl moiety, QPh = aromatic proton phenyl attached to quinolinyl moiety.

UV-visible spectroscopy was performed using a Cary 5000 UV-Vis spectrophotometer as either a thin film on quartz substrates or as a solution in dichloromethane or toluene using 10 × 10 mm quartz cuvettes.  $\lambda_{\text{max}}$  values were quoted in nm and shoulders denoted as “sh”. Photoluminescence spectra were measured using a Jobin-Yvon Horiba Fluoromax-4 in steady-state mode using a xenon lamp as the excitation source. Solution photoluminescent quantum yields ( $\Phi_{\text{PL}}$ ) were measured by a relative method utilizing either quinine sulfate in 0.5 M sulfuric acid ( $\Phi_{\text{PL}} = 55\%$ ) or rhodamine 6G in ethanol ( $\Phi_{\text{PL}} = 95\%$ ) as standards for the green- or red-emitting materials respectively. Sample materials were dissolved in distilled toluene and freeze-pump-thaw degassed. The solutions of standard and sample were made to concentrations where the optical densities were both comparable and dilute ( $\sim 0.1$  A.U.). The accuracy of these measurements is estimated to be  $\pm 10\%$  of the stated value. Measurements for film  $\Phi_{\text{PL}}$  calculations were obtained using an integrating sphere under a nitrogen purge<sup>188</sup> in a Hamamatsu C9920-02 luminescence measurement system. Time-resolved luminescence measurements were performed using the time-correlated single photon counting (TCSPC) technique on a Jobin-Yvon Fluorolog 3, with excitation at 441 nm from a pulsed LED (Horiba NanoLED) and the instrument response was about 1 ns. FT-IR spectroscopy was performed on solid samples using a Perkin-Elmer Spectrum 100 FT-IR spectrometer with ATR attachment. Electrochemistry was performed using a BAS Epsilon electrochemistry station, a standard three-electrode system, at room temperature using a solution comprising approximately 1 mM of sample and 0.1 M tetra-*n*-butylammonium perchlorate (TBAP, Alfa Aesar, electrochemical grade) as electrolyte in distilled (from CaH<sub>2</sub>) dichloromethane using either a glassy carbon or Pt wire working electrode, a Pt wire counter electrode and a Ag/AgNO<sub>3</sub> solution as the reference electrode at various scan rates of between 10 and 200 mV/s to obtain the optimal voltammogram. The solutions were sparged with argon and measured under an argon atmosphere. Melting points (MPs) were measured in a glass capillary on a Büchi B-545 melting point apparatus and are uncorrected. Elemental microanalyses were performed using a modified classical Pregl and Dumas methodology with either a Carlo Erba NA 1500 Elemental Analyzer or Thermo Scientific FLASH 2000 CHNS/O Analyzer.

Mass spectra were recorded utilising the following instrumentation setups with sample results quoting the acronyms in brackets corresponding to the method of data collection followed by the recorded pattern giving  $m/z$  values and relative peak intensities.

For samples not requiring accurate mass spectra were recorded using either a Bruker Esquire HCT (High Capacity 3D ion trap) instrument with a Bruker ESI source (ESI-HCT) or a ABSciex QTRAP 5500 mass spectrometer using atmospheric pressure chemical ionisation (APCI-QTRAP). Other low resolution spectra were recorded using matrix-assisted laser desorption ionization time-of-flight (MALDI-TOF) on a Bruker Autoflex III, Applied Biosystems Voyager-DE STR or on an Applied Biosystems 4700 Proteomics Analyzer. Samples were suspended in 2,5-dihydroxybenzoic acid (DHB), 1,8-dihydroxy-9,10-dihydroanthracen-9-one (DIT) or *trans*-2-[3-(4-*tert*-Butylphenyl)-2-methyl-2-propenylidene]malononitrile (DCTB) as the matrix and spectra were collected in positive reflection mode.

Samples requiring accurate mass spectra were recorded using a Bruker micrOTOF-Q (quadrupole – Time of Flight) instrument with a Bruker ESI source (ESI-micrOTOF-Q) or using an ABSciex Orbitrap Elite MS using a heated electrospray source (HESI-Orbitrap). ESI-micrOTOF-Q accurate mass measurements were carried out with direct infusion of 10 nM to 10  $\mu$ M solutions of sample in methanol and with external calibration using Agilent Tune Mix as the reference. HESI-Orbitrap accurate mass measurements were carried out on samples in dichloromethane: methanol (50:50) at approximately 10  $\mu$ M directly infused at 3  $\mu$ L per minute. Data was collected in positive mode being acquired for 3 minutes across the *m/z* range (varied between 150 and 4000 depending on sample). HESI source parameters included a heater temperature at 50°C; sheath gas flow 6; ISV at 3.5 kV and S-lens at 60%, ion transfer tube temperature at 50°C. Fourier transform mass spectrometer parameters included resolution range 60-240K (resolution was adjusted as required); spectral averaging across 8 microscans with a maximum ion injection time of 200 ms.

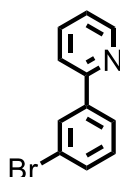
Thermal transitions were determined by using a Perkin–Elmer Diamond Differential Scanning Calorimeter. Thermal gravimetric analysis was undertaken using a Perkin–Elmer STA 6000 Simultaneous Thermal Analyzer. Thermal decomposition values [ $T_{d(5\%)}$ ] were reported as the temperature corresponding to a 5% mass reduction.

Estimation of molecular weights by gel permeation chromatography (GPC) was carried out using either a Polymer Laboratories PL-GPC 50 or a Waters GPC 1515 system equipped with Empower software to operate the system. All measurements of non-polymeric large molecules were carried out on the Polymer Laboratories PL-GPC 50 equipped with PLgel Mixed-A columns (600 mm + 300 mm lengths, 7.5 mm diameter) from Polymer Laboratories, calibrated with polystyrene narrow standards ( $\bar{M}_p = 162$  to 47,190  $\text{g mol}^{-1}$ ) and run in series in tetrahydrofuran with toluene as flow marker. The tetrahydrofuran pumped at a rate of 0.5  $\text{cm}^3\text{min}^{-1}$  with the columns maintained at 40 °C. The gel permeation chromatography of

measurements of polymeric materials were carried out using the Waters GPC 1515 system utilized Styrag HT-6E ( $M_w$  5000 to 10 million Da) maintained at 40 °C and a flow rate of 1 mL/min of tetrahydrofuran and a UV detector. The Waters GPC 1515 was calibrated using Shodex narrow polystyrene standards (Range:  $M_w$  1350 to 1.3 million Da). All samples were filtered with a 0.45 micro PTFE filter before GPC analysis.

Photoelectron spectroscopy in air (PESA) was performed by Dr. Dani Stoltzfus on  $\approx$ 100 nm thick films on glass using a Riken Kekei AC-2 spectrometer.

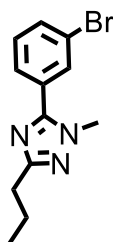
## 5.2 Synthetic procedures



### 2-(3-bromophenyl)pyridine (2.1)

2-(3-bromophenyl)pyridine (**2.1**) was synthesized using a literature procedure.<sup>189</sup> A solution of *n*-butyllithium in hexane (1.6 M, 21.8 cm<sup>3</sup>, 34.9 mmol) was added dropwise over 20 min to a solution of 2-bromopyridine (3 cm<sup>3</sup>, 31.02 mmol) in dry tetrahydrofuran (120 cm<sup>3</sup>) under argon that had been cooled to -78 °C in a dry ice/acetone bath with stirring. Upon addition stirring of the mixture continued for a further 30 min. Tri-*n*-butylstannyl chloride (8.6 cm<sup>3</sup>, 32.0 mmol) was added dropwise to the solution. The mixture was kept in the dry ice/ acetone bath for a further 30 min before removal to allow warming to room temperature. Diethyl ether (100 cm<sup>3</sup>) and water (100 cm<sup>3</sup>) were added to the mixture and the aqueous layer was removed and extracted with diethyl ether (100 cm<sup>3</sup>). The combined organic layers were washed with brine (100 cm<sup>3</sup>), dried over anhydrous magnesium sulphate, filtered and the solvent removed. The crude, a dark orange oil (14.5 g), was used in the next step without further purification. The crude, 1,3-dibromobenzene (9.09 g, 38.5 mmol) and tetrakis(triphenylphosphine)palladium(0) (0.43 g, 12 %) were dissolved in toluene (200 cm<sup>3</sup>) and *N,N*-dimethylformamide (50 cm<sup>3</sup>) and the mixture was deoxygenated with argon for 30 minutes. The mixture was heated at reflux under argon for 30 h. After cooling to room temperature, potassium fluoride ( $\sim$ 1 g) was added and the mixture was heated at reflux for 1 hour to sequester remaining organotin compounds. The mixture was allowed to cool to room temperature, filtered and dichloromethane (100 cm<sup>3</sup>) and water (200 cm<sup>3</sup>) were added. The organic layer was separated and the aqueous layer was extracted with dichloromethane (1 x 100 cm<sup>3</sup>, 4 x 50 cm<sup>3</sup>). The combined organic layers were dried over anhydrous

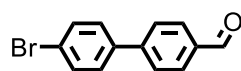
magnesium sulfate, filtered, and the solvent removed. The residue was purified by column chromatography over silica using dichloromethane: petroleum ether (1:3 to 1:0) to dichloromethane: ethyl acetate (1:0 to 0:1) as eluent to give **2.1** as a light yellow oil (4.62 g, 63%). <sup>1</sup>H NMR (300 MHz, CDCl<sub>3</sub>) δ: 7.26 (1 H, m), 7.34 (1 H, t), 7.53 (1 H, m), 7.68-7.80 (2 H, m), 7.91 (1 H, m), 8.17 (1 H, t), 8.70 (1 H, m); <sup>13</sup>C NMR (75 MHz, CDCl<sub>3</sub>) δ: 120.5, 123.0, 125.4, 130.0, 130.2, 131.8, 136.9, 141.3, 149.7, 155.7. The <sup>1</sup>H NMR and <sup>13</sup>C NMR spectra were consistent with the literature values.<sup>189,190</sup>



### 5-(3-bromophenyl)-1-methyl-3-propyl-1H-1,2,4-triazole (**2.2**)

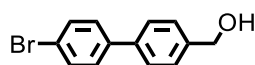
5-(3-bromophenyl)-1-methyl-3-propyl-1H-1,2,4-triazole (**2.2**) was synthesized according to a literature procedure.<sup>191</sup> To 3-bromobenzoyl chloride (33.0 g, 0.150 mmol) and ethyl butyrimidate hydrochloride (23.0 g, 0.152 mmol) in chloroform (200 cm<sup>3</sup>), triethylamine (45 cm<sup>3</sup>, 0.323 mmol) was added dropwise with stirring. The reaction is vigorously exothermic and requires a condenser. After being allowed to stir overnight the solvent was removed. Dichloromethane (300 cm<sup>3</sup>) and water (300 cm<sup>3</sup>) were added and separation occurred. The aqueous layer was washed with dichloromethane (2 x 100 cm<sup>3</sup>) and the combined organic fractions were washed with water (100 cm<sup>3</sup>) and brine (100 cm<sup>3</sup>), dried over anhydrous sodium sulphate, filtered and solvent removed. The resulting residue was used without further purification. The residue was dissolved in chloroform (200 cm<sup>3</sup>) and placed under a nitrogen atmosphere. With stirring, methylhydrazine (8 cm<sup>3</sup>, 0.152 mmol) was added dropwise slowly. The reaction is vigorously exothermic and requires a condenser. Upon addition the reaction was stirred for a further 64 hours. The solvent was removed and the residue was taken up into dichloromethane (400 cm<sup>3</sup>) and water (400 cm<sup>3</sup>) and, separation occurred. The aqueous layer was washed with dichloromethane (3 x 50 cm<sup>3</sup>) and the combined organic layer was washed with water (3 x 100 cm<sup>3</sup>) and brine (100 cm<sup>3</sup>), dried over anhydrous sodium sulphate, filtered and solvent removed. The residue was purified by column chromatography over silica using a dichloromethane increasing to dichloromethane: ethyl acetate mixture (9:1) as eluent to give **2.2** as a colourless oil (29.6 g, 71 %) that slowly discolours on standing. <sup>1</sup>H NMR (300 MHz, CDCl<sub>3</sub>) δ: 1.00 (3 H, t, *J* = 7.5 Hz), 1.80 (2 H, m), 2.71 (2 H, t, *J* = 7.5 Hz), 3.93 (3 H, s), 7.34-7.40 (1 H, m), 7.57-7.63 (2 H, m), 7.83-7.85 (1

H, m);  $m/z$  (HESI-Orbitrap;  $[MH]^+$ ) 280.0458; calcd for  $C_{12}H_{14}N_3Br + H^+$ : 280.0444. The  $^1H$  NMR and ESI-MS spectra were consistent with the literature values.<sup>191</sup>



#### 4'-bromo-1,1'-biphenyl-carboxaldehyde (**2.3**)

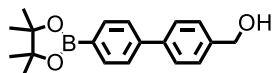
4'-bromo-1,1'-biphenyl-carboxaldehyde (**2.3**) was synthesized using a modified literature procedure.<sup>192</sup> A mixture of 1-bromo-4-iodobenzene (0.28 g, 0.99 mmol), 4-formylphenylboronic acid (0.198 g, 1.33 mmol), caesium fluoride (0.520 g, 3.45 mmol) and tetrakis(triphenylphosphine)palladium(0) (0.083 g, 0.072 mmol) in dry tetrahydrofuran (7  $cm^3$ ) was deoxygenated with nitrogen for 30 min. The mixture was heated to reflux under nitrogen for 41 hours. The mixture was allowed to cool to room temperature. Dichloromethane (50  $cm^3$ ) and water (50  $cm^3$ ) was added. The organic layer was separated and the aqueous layer was extracted by dichloromethane (2 x 50  $cm^3$ ). The combined organic layers were extracted with water (2 x 50  $cm^3$ ) and brine (50  $cm^3$ ), dried over anhydrous magnesium sulphate, filtered and solvent removed. The residue was purified by column chromatography over silica using a dichloromethane: petroleum ether mixture (1: 1) as eluent to give **2.3** as an off white solid (0.189 g, 73 %).  $^1H$  NMR (300 MHz,  $CDCl_3$ )  $\delta$ : 7.48-7.52 (2 H, AA'BB',  $J = 8.5$  Hz), 7.60-7.63 (2 H, AA'BB',  $J = 8.0$  Hz), 7.70-7.73 (2 H, AA'BB',  $J = 9.0$  Hz), 7.94-7.97 (2 H, AA'BB', 9.0 Hz), 10.06 (1 H, s); IR:  $\bar{\nu}$  solid/ $cm^{-1}$  = 3031, 2819, 1692, 1602, 808;  $m/z$  (APCI-QTRAP;  $[MH]^+$ ) 260.1; calcd for  $C_{13}H_9BrO + H^+$ : 260.1. The  $^1H$  NMR, FTIR and mass spectra were consistent with literature values.<sup>193</sup>



#### 4'-bromo-1,1'-biphenyl-4-methanol (**2.4**)

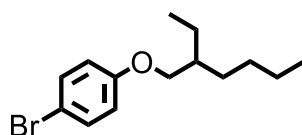
4'-bromo-1,1'-biphenyl-4-methanol (**2.4**) was synthesized according to a modified literature procedure.<sup>194</sup> Lithium aluminium hydride (0.615 g, 16.2 mmol) was added to a solution of **2.3** (1.60 g, 6.14 mmol) in tetrahydrofuran (40  $cm^3$ ). The solution was allowed to stir overnight and was quenched by chilled water (40  $cm^3$ ). Diethyl ether (50  $cm^3$ ) was added to the mixture and the organic layer was separated, dried over anhydrous magnesium sulphate, filtered and solvent removed. The residue was then purified by via column chromatography over silica using a ethyl acetate: petroleum ether mixture (1:3) as eluent to

give **2.4** (0.702 g, 28 %) as a colourless crystalline waxy solid.  $^1\text{H NMR}$  (300 MHz,  $\text{CDCl}_3$ )  $\delta$ : 1.65 (1 H, t,  $J = 5.5$  Hz), 4.75 (2 H, d,  $J = 5.5$  Hz), 7.43-7.48 (4 H, AA'BB'), 7.54-7.59 (4 H, AA'BB');  $m/z$  (ESI-HCT;  $[\text{MK}^+]$ ) 300.9; calcd for  $\text{C}_{13}\text{H}_{11}\text{BrOK}^+$ ; 300.9. The  $^1\text{H NMR}$  and mass spectra were consistent with the literature values.<sup>194</sup>



#### 4'-((4,4,5,5-tetramethyl-1,3,2-dioxaborolan-2-yl)-[1,1'-biphenyl]-4-ylmethanol (**2.5**)

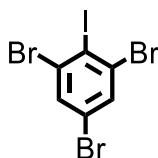
A mixture of **2.4** (0.201 g, 0.764 mmol), bis(pinacollato)diboron (0.585 g, 2.30 mmol),  $[1,1'$ -bis(diphenylphosphino)ferrocene]dichloropalladium(II) (0.056 g, 10.1 %) and potassium acetate (0.756 g, 7.70 mmol) in 1,4-dioxane (19  $\text{cm}^3$ ) that had been sparged with argon was heated to reflux overnight under argon. The mixture was quenched with an aqueous saturated ammonium chloride solution (25  $\text{cm}^3$ ) and extracted with water (25  $\text{cm}^3$ ) and dichloromethane (50  $\text{cm}^3$ ) and the aqueous fraction was washed with dichloromethane (2 x 50  $\text{cm}^3$ ). The combined organic fractions were washed with brine (50  $\text{cm}^3$ ) and dried over anhydrous magnesium sulphate before filtration. The solvent was removed from the produce the crude material. The crude was dissolved in dichloromethane, passed through a celite plug and the solvent was removed in vacuo. The residue was purified via automated flash column chromatography over silica using an ethyl acetate: petroleum ether (0:1 to 1:0) mixture to give **2.5** (53 mg, 22%) as a colourless solid. IR:  $\bar{\nu}$  solid/ $\text{cm}^{-1}$  = 808, 820, 858, 962, 1005, 1018, 1031, 1093, 1108, 1139, 1167, 1211, 1271, 1306, 1324, 1359, 1390, 1445, 1476, 1507, 1530, 1549, 1608, 1728, 2869, 2928, 2977, 3429. UV-Vis:  $\lambda_{\text{max}}(\text{CH}_2\text{Cl}_2)/\text{nm}$ : 266 ( $\log \epsilon/\text{dm}^3\text{mol}^{-1}\text{cm}^{-1}$  4.46).  $^1\text{H NMR}$  (300 MHz,  $\text{CDCl}_3$ ):  $\delta$  1.37 (11H, s,  $\text{MeCH}_3$ ), 1.66 (1H, t,  $J = 6$ , OH), 4.76 (2H, d,  $J=6$ ,  $\text{CH}_2\text{-OH}$ ), 7.46 (2H,  $J_2=8.5$ , Ar-H), 7.61 (2H,  $J_2=5$ , Ar-H), 7.64 (2H,  $J_2=5$ , Ar-H), 7.89 (2H,  $J_2= 8.5$ , Ar-H).



#### 1-Bromo-4-(2-ethylhexyloxy)benzene (**2.6**)

1-Bromo-4-(2-ethylhexyloxy)benzene (**2.6**) was synthesized according to a literature procedure.<sup>195</sup> A solution of 4-bromophenol (50.7g, 293 mmol), sodium hydroxide pellets

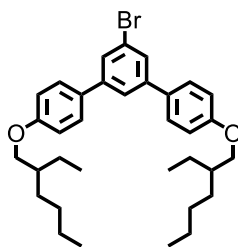
(11.5 g, 288 mmol) in ethanol (210 cm<sup>3</sup>) and 2-ethylhexylbromide (34.5 cm<sup>3</sup>, 194 mmol). The solution was heated at reflux under nitrogen for 65 h. The mixture was allowed to cool to room temperature and the solvent was removed. The residue was dissolved in diethyl ether (200 cm<sup>3</sup>) and aqueous sodium hydroxide (2M, 200 cm<sup>3</sup>). The organic layer was separated extracted with aqueous sodium hydroxide (2M, 200 cm<sup>3</sup>), dried over anhydrous magnesium sulphate, filtered and solvent removed. The residue did not require further purification and **2.6** was obtained as a colourless oil (42.2 g, 76%). The <sup>1</sup>H NMR (300 MHz, CDCl<sub>3</sub>) and <sup>13</sup>C NMR (75 MHz, CDCl<sub>3</sub>) spectra were consistent with the literature values. <sup>1</sup>H NMR (300 MHz, CDCl<sub>3</sub>) δ: 0.87-0.97 (6 H, m), 1.25-1.52 (8 H, m), 1.65-1.75 (1 H, m), 3.80 (2 H, d, *J* = 6.0), 6.75-6.81 (2 H, AA':BB', *J*<sub>ortho</sub> = 9.0, *J*<sub>meta</sub> = 2.0 Hz), 7.32-7.39 (2 H, AA':BB', *J*<sub>ortho</sub> = 9.0, *J*<sub>meta</sub> = 2.0 Hz); <sup>13</sup>C NMR (75 MHz, CDCl<sub>3</sub>) δ: 11.2, 14.2, 23.2, 24.0, 29.2, 30.6, 39.5, 70.9, 112.6, 116.5, 132.2, 158.7; The <sup>1</sup>H NMR and <sup>13</sup>C NMR were consistent with literature values.<sup>196</sup>



### 1,3,5-Tribromo-2-iodobenzene (2.7)

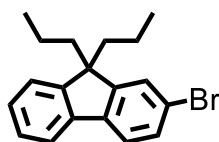
1,3,5-tribromo-2-iodobenzene (**2.7**) was synthesized according to a literature procedure.<sup>197</sup> To a stirred slurry of 1,3,5-tribromo-aniline (22.9 g, 69.3 mmol) in concentrated hydrochloric acid (61 cm<sup>3</sup>) cooled in an ice-water bath, a solution of sodium nitrite (4.99 g, 72.3 mmol) in water (22.5 cm<sup>3</sup>) was added dropwise. The mixture was allowed to warm to room temperature over 30 minutes and subsequently added dropwise to a solution of potassium iodide (115.12 g, 693 mmol) in water (171 cm<sup>3</sup>). Upon completion of addition the mixture was allowed to stir for 1 hour. Dichloromethane (300 cm<sup>3</sup>) and an aqueous solution of sodium metabisulphite (0.5 M, 30 cm<sup>3</sup>) were added. The organic layer was separated and the aqueous layer was extracted with dichloromethane (2 x 100 cm<sup>3</sup>). The combined organic fractions were extracted with water (100 cm<sup>3</sup>) and brine (100 cm<sup>3</sup>), dried over anhydrous magnesium sulphate, filtered and the solvent removed. The residue was purified by recrystallization from dichloromethane to produce **2.7** (15.6 g, 51 %) as large colourless needles. <sup>1</sup>H NMR (300 MHz, CDCl<sub>3</sub>) δ: 7.70 (2 H, s). <sup>13</sup>C NMR (75 MHz, CDCl<sub>3</sub>) δ: 133.7, 132.0, 123.1, 108.2. The <sup>1</sup>H NMR and <sup>13</sup>C NMR spectra were consistent with those reported in the literature.<sup>197</sup>





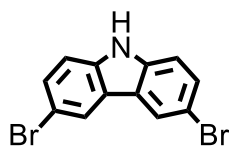
### 5'-Bromo-4,4''-bis[(2-ethylhexyl)oxy]-1,1':3',1''-terphenyl (**2.8**)

5'-Bromo-4,4''-bis[(2-ethylhexyl)oxy]-1,1':3',1''-terphenyl (**2.8**) was synthesized according to a modified literature procedure.<sup>154</sup> A solution **2.6** (10.1 g, 35.5 mmol) in dry tetrahydrofuran (15 cm<sup>3</sup>) was added dropwise to magnesium shavings (0.974 g, 40.0 mmol) under nitrogen flow. The mixture was allowed to stir for 1 hour after initiation of the Grignard reagent which was signified by a colour change to green-grey and heat liberation. A solution of **2.7** (2.58 g, 5.85 mmol) in dried tetrahydrofuran (25 cm<sup>3</sup>) was added dropwise to the Grignard solution while the vessel was submerged in an ice-water bath. After addition was completed the solution was heated at reflux for 3 hours. The mixture was allowed to cool to room temperature and hydrochloric acid (3M, 20 cm<sup>3</sup>) was added dropwise. Dichloromethane (50 cm<sup>3</sup>) and water (50 cm<sup>3</sup>) were added. The organic layer was separated and extracted with water (30 cm<sup>3</sup>) and brine (30 cm<sup>3</sup>), dried over anhydrous magnesium sulfate, filtered and solvent removed. The residue was purified by column chromatography over silica using a dichloromethane: petroleum ether mixture (1:10) as eluent to give **2.8** as a pale yellow oil (0.66 g, 20 %). <sup>1</sup>H NMR (300 MHz, CDCl<sub>3</sub>) δ: 0.93-0.98 (12 H, m), 1.34-1.36 (16 H, m), 1.74-1.76 (2 H, m), 3.89-3.99 (4 H, m), 6.97-7.00 (4 H, AA`BB`), 7.51-7.54 (4 H, AA`BB`), 7.62 (3 H, m). <sup>13</sup>C NMR (75 MHz, CDCl<sub>3</sub>) δ: 11.28, 14.25, 23.22, 24.04, 29.25, 30.70, 39.55, 70.78, 115.06, 123.31, 124.03, 127.91, 128.32, 132.18, 143.43, 159.62. <sup>1</sup>H NMR (300 MHz, CDCl<sub>3</sub>) δ: 7.70 (2 H, s). The <sup>1</sup>H NMR and <sup>13</sup>C NMR spectra were consistent with those reported in the literature.<sup>198</sup>



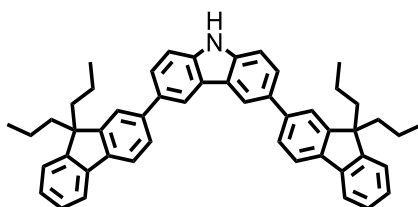
### 2-bromo-9,9-dipropyl-9H-fluorene (**2.9**)

2-bromo-9,9-dipropyl-9*H*-fluorene (**2.9**) was synthesized using a modified literature procedure.<sup>199</sup> A solution of sodium hydroxide (261.9 g, 6.55 mol) in water (250 cm<sup>3</sup>) was added to a solution of 2-bromo-9*H*-fluorene (54.52 g, 222.4 mmol) and tetrabutylammonium bromide (51.2 g, 159 mmol) in toluene (400 cm<sup>3</sup>) under argon with stirring. The mixture was heated at 50°C for 2 h. 1-bromopropane (63 cm<sup>3</sup>, 659 mmol) was added to the mixture and heating continued for 2 days. The mixture was allowed to cool to room temperature. The organic layer was separated and extracted with water (2 x 200 cm<sup>3</sup>) and brine (200 cm<sup>3</sup>), dried over anhydrous sodium sulphate, filtered and solvent removed. The residue was purified via column chromatography over silica using a petroleum ether as eluent to give **2.9** (70.95 g, 97 %) as a colourless crystalline solid. <sup>1</sup>H NMR (300 MHz, CDCl<sub>3</sub>) δ: 0.67 (10 H, m), 1.90-1.95 (4 H, m), 7.29-7.34 (3 H, m), 7.42-7.48 (2 H, m), 7.53-7.57 (1 H, m), 7.62-7.68 (1 H, m); 152.2; *m/z* (APCI-QTRAP; [M]<sup>+</sup>):= 328.1; calcd for C<sub>19</sub>H<sub>21</sub>Br<sup>+</sup>: 328.1. The <sup>1</sup>H NMR and mass spectroscopy spectra were consistent with literature values.<sup>199</sup>



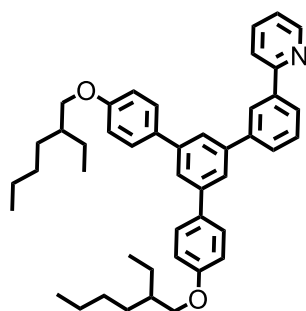
### 3,6-dibromo-9*H*-carbazole (**2.10**)

3,6-dibromo-9*H*-carbazole (**2.10**) was synthesized according to the method described in Simon-Sheng Yen Chen's thesis.<sup>200</sup> Under ambient conditions but with protection from light; *N*-bromosuccinimide (4.28 g, 24.0 mmol) was added over 30 minutes in 3 portions to a stirred solution of carbazole (1.99 g, 11.9 mmol) in tetrahydrofuran (12.4 cm<sup>3</sup>). Upon complete addition the solution was stirred for a further 1 hour. Water (6 cm<sup>3</sup>) was added and the organic layer was separated and extracted with water (3 x 6 cm<sup>3</sup>), dried over anhydrous magnesium sulphate, filtered, and solvent removed. The residue was recrystallized from dichloromethane and ethanol to give **2.10** as an off-white solid (3.11 g, 80%). <sup>1</sup>H NMR (300 MHz, CDCl<sub>3</sub>) δ: 7.31 (2 H, dd, *J*<sub>1</sub>= 8.5 and *J*<sub>2</sub>= 0.5 Hz), 7.52 (2 H, dd, *J*<sub>1</sub>= 8.5 and *J*<sub>2</sub>= 2.0 Hz), 8.14 (3 H, m); <sup>13</sup>C NMR (75 MHz, CDCl<sub>3</sub>) δ: 112.2, 112.6, 123.3, 124.1, 129.3, 138.4; The <sup>1</sup>H NMR and <sup>13</sup>C NMR were consistent with literature values.<sup>201</sup>



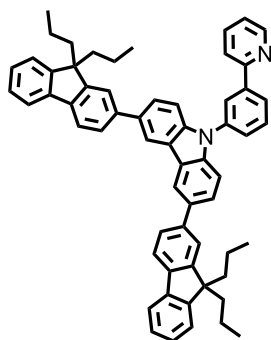
### 3,6-bis(9,9-dipropyl-9H-fluoren-2-yl)-9H-carbazole (**2.11**)

5'-Bromo-4,4''-bis[(2-ethylhexyl)oxy]-1,1':3',1''-terphenyl (**2.11**) was synthesized according to a modified literature procedure.<sup>202</sup> To a stirred solution of **2.9** (59.8 g, 182 mmol) in dry tetrahydrofuran (600 cm<sup>3</sup>) under an argon atmosphere and cooled in a dry ice/ acetone bath; *n*-butyllithium in hexanes (137 cm<sup>3</sup>, 1.6 M, 219 mmol) was added dropwise. After stirring for 1 hour trimethylborate (61 cm<sup>3</sup>, 547 mmol) was added. The solution was allowed to warm before addition the of 3 M hydrochloric acid (250 cm<sup>3</sup>). After stirring for 2 hours separation occurred and the aqueous phase was extracted with diethyl ether (3 × 250 cm<sup>3</sup>). The combined organic fractions were extracted with water (250 cm<sup>3</sup>) and brine (250 cm<sup>3</sup>), dried over anhydrous magnesium sulphate, filtered and solvent removed. The residue was dissolved in toluene (490 cm<sup>3</sup>), ethanol (280 cm<sup>3</sup>) and aqueous sodium carbonate (2 M, 175 cm<sup>3</sup>). **2.10** (22.7 g, 69.8 mmol) and tetrakis(triphenylphosphine)palladium(0) (2.40 g, 2.08 mmol) were added and the mixture was sparged with argon for 30 minutes. The mixture was heated at reflux for 36 hours before allowing to cool. Dichloromethane (250 cm<sup>3</sup>) and water (250 cm<sup>3</sup>) were added and separation occurred. The aqueous layer was extracted with dichloromethane (2 × 250 cm<sup>3</sup>). The combined organic fractions were extracted with water (250 cm<sup>3</sup>) and brine (250 cm<sup>3</sup>), dried over anhydrous magnesium sulfate, filtered and solvent removed. The residue was purified by column chromatography over silica using a dichloromethane: petroleum spirit 40-60 mixture (1:2) as eluent. The residue was recrystallized from ethyl acetate: petroleum spirit 40-60 (1:9) mixture to give **2.11** (16.1 g, 35 %) as a colourless, fluffy solid. <sup>1</sup>H NMR (300 MHz, CDCl<sub>3</sub>) δ: 0.65-0.88 (20 H, m), 2.00-2.12 (8 H, m), 7.27-7.40 (6 H, m), 7.53-7.58 (2 H, m), 7.67-7.82 (10 H, m), 8.16 (1 H, s), 8.43 (2 H, m); *m/z* (HESI-Orbitrap; [MH]<sup>+</sup>) 663.3866; calcd for C<sub>50</sub>H<sub>49</sub>N<sup>+</sup>; 663.6860. The <sup>1</sup>H NMR and mass spectra were consistent with those reported in the literature.<sup>202</sup>



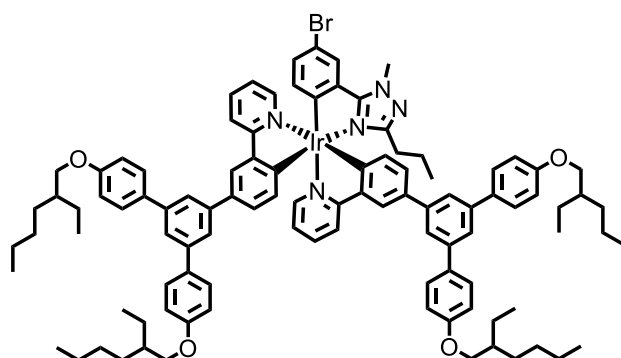
### 2-(3-(3,5-bis[4-(2-ethylhexyloxy)phenyl]phenyl)phenyl)pyridine (**2.12B**)

2-(3-(3,5-bis[4-(2-ethylhexyloxy)phenyl]phenyl)phenyl)pyridine (**2.12B**) was synthesized according to a literature procedure.<sup>198</sup> To a solution of **2.8** (2.77 g, 4.8 mmol) in dry tetrahydrofuran (20 cm<sup>3</sup>) cooled in a dry ice/ acetone bath, *n*-butyllithium in hexane (1.3 M, 7.6 cm<sup>3</sup>, 9.88 mmol) was added dropwise under argon. The mixture was stirred for 2 hours before trimethylborate (1.7 cm<sup>3</sup>, 15.0 mmol) was rapidly added. The mixture was allowed to warm to room temperature overnight. Hydrochloric acid (3M, 80 cm<sup>3</sup>) was added and stirred for 2 hours. The organic layer was separated and the aqueous layer was extracted with diethyl ether (2 x 25 cm<sup>3</sup>). The combined organic fractions were dried over anhydrous sodium sulphate, filtered and solvent removed. The residue and **2.1** (1.73 g, 7.40 mmol) were dissolved in toluene (10 cm<sup>3</sup>), ethanol (3 cm<sup>3</sup>) and aqueous sodium carbonate (2 M, 3 cm<sup>3</sup>) and sparged with argon for 30 minutes. Tetrakis(triphenylphosphine)palladium(0) (408 mg, 0.353 mmol) was added and the reaction mixture was heated at reflux with stirring under argon for 20 hours. The mixture was allowed to cool to room temperature and diethyl ether (50 cm<sup>3</sup>) and water (50 cm<sup>3</sup>) were added. The organic layer was separated and the aqueous layer was extracted with diethyl ether (2 x 50 cm<sup>3</sup>). The combined organic fractions were extracted with water (50 cm<sup>3</sup>) and brine (50 cm<sup>3</sup>), dried over anhydrous sodium sulphate, filtered and solvent removed. The residue was purified by column chromatography over silica using a dichloromethane: toluene mixture (2:1) as eluent to give **2.12B** as a viscous very pale yellow oil (2.14 g, 68 %). <sup>1</sup>H NMR (300 MHz, CDCl<sub>3</sub>) δ: 0.87-1.00 (12 H, m), 1.29-1.51 (16 H, m), 1.70-1.82 (2 H, m), 3.90 (4 H, m), 7.00-7.03 (4 H, AA`BB`), 7.18 (1 H, m), 7.60-7.67 (5 H, AA`BB` & m), 7.73 (1 H, m), 7.79-8.07 (6 H, m), 8.34 (1 H, m), 8.79 (1 H, m); *m/z* (HESI-Orbitrap; [MH]<sup>+</sup>) 640.4188; calcd for C<sub>45</sub>H<sub>53</sub>NO<sub>2</sub> + H<sup>+</sup>: 640.4149. The <sup>1</sup>H NMR and mass spectra were consistent with the literature values.<sup>198</sup>



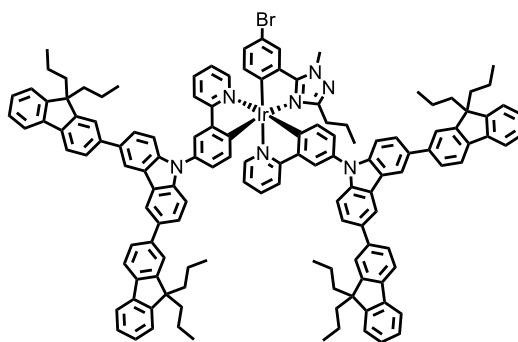
### 3,6-bis(9,9-dipropyl-9H-fluoren-2-yl)-9-(3-(pyridin-2-yl)phenyl)-9H-carbazole (**2.12C**)

3,6-bis(9,9-dipropyl-9H-fluoren-2-yl)-9-(3-(pyridin-2-yl)phenyl)-9H-carbazole (**2.12C**) was synthesized according to a literature procedure.<sup>142</sup> A mixture of **2.1** (1.05 g, 4.49 mmol), **2.11** (3.71 g, 5.59), tris(dibenzylideneacetone)dipalladium(0)-chloroform adduct (0.486 g, 0.732 mmol), tri-*tert*-butylphosphonium tetrafluoroborate (1.28g, 4.41 mmol) and sodium *tert*-butoxide (2.23 g, 23.2 mmol) in xylenes (140 cm<sup>3</sup>) was sparged with argon for 30 minutes. The mixture was heated at reflux with stirring under an argon atmosphere for 3 days and allowed to cool. Water (200 cm<sup>3</sup>) was added and separation occurred. The aqueous layer was extracted with diethyl ether (3 × 250 cm<sup>3</sup>) and the combined organic fractions were dried over anhydrous sodium sulphate, filtered, and solvent removed. The residue was purified by column chromatography over silica using dichloromethane: petroleum spirit 40-60 (1:1) mixture as eluent to give **2.12C** as a colourless powder (3.15 g, 86 %). <sup>1</sup>H NMR (300 MHz, CDCl<sub>3</sub>) δ: 0.64-0.84 (20 H, m), 2.00-2.16 (8 H, m), 7.30-7.41 (7 H, m), 7.56-7.60 (2 H, m), 7.68-7.85 (12 H, m), 8.17 (1 H, m), 8.31 (1 H, m), 8.51 (2 H, m), 8.75 (6 H, m); *m/z* (HESI-Orbitrap; [MH]<sup>+</sup>) 817.4537; calcd for C<sub>61</sub>H<sub>56</sub>N<sub>2</sub> + H<sup>+</sup>: 817.4516. The <sup>1</sup>H NMR and mass spectra were consistent with the literature values.<sup>142</sup>



### [4-bromo-2-(1-methyl-3-propyl-1*H*-1,2,4-triazol-5-yl-κ<sup>N4</sup>)phenyl-κ<sup>C</sup>]bis{4''-[(2-ethylhexyloxy)-5''-{4-[(2-ethylhexyl)oxy]phenyl}-3-(2-pyridinyl-κ<sup>N</sup>)[1,1':3',1''-terphenyl]-4-yl-κ<sup>C</sup>}iridium(III) (**2.13B**)

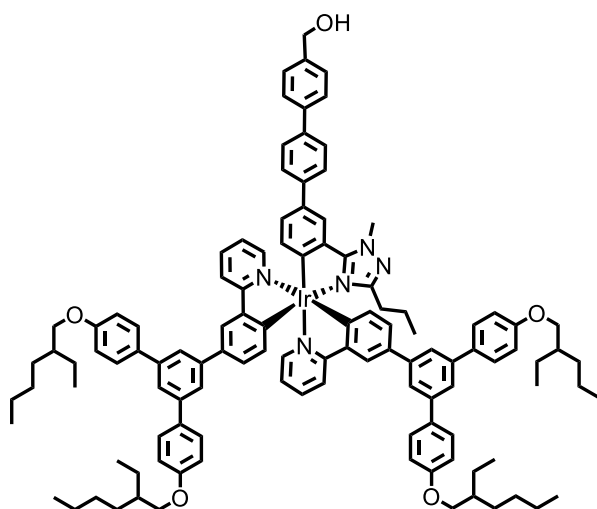
**2.13B** was synthesized according to a modified literature procedure.<sup>140</sup> **2.12B** (1.42 g, 2.22 mmol) and iridium(III) chloride hydrate (0.331 g, 1.11 mmol) in 2-ethoxyethanol (28 cm<sup>3</sup>) and water (8.5 cm<sup>3</sup>) was sparged with argon for 3 hours. The mixture was heated in an oil bath set at 130°C for 2 days with stirring under argon. The canary yellow suspension was allowed to cool to ambient temperature before being dissolved in dichloromethane (50 cm<sup>3</sup>) and water (50 cm<sup>3</sup>). The aqueous layer was washed with dichloromethane (2 x 50 cm<sup>3</sup>) and the combined organic fractions were washed with water (100 cm<sup>3</sup>) and brine (100 cm<sup>3</sup>), dried over anhydrous sodium sulphate, filtered, and solvent removed. Without further purification the residue was combined with 5-(3-bromophenyl)-1-methyl-3-propyl-1H-1,2,4-triazole (1.57 g, 5.593 mmol), Proton sponge (0.279 g, 1.30 mmol) and silver(I) triflate (0.523 g, 2.04 mmol) and the mixture was heated with stirring under argon for 14 hours in an oil bath set at 168°C. The residue was purified by column chromatography over silica using dichloromethane: petroleum ether 40-60 mixture, 1:1 as eluent to give **2.13B** (0.270 g, 14 %) as a bright yellow powder. <sup>1</sup>H NMR (300 MHz, CDCl<sub>3</sub>) δ: 0.57 (3 H, s), 0.80-1.00 (24 H, m), 1.24-1.66 (34 H, m), 1.73-1.96 (6 H, m), 3.90 (8 H, m), 4.23 (3 H, s), 6.87-7.05 (14 H, m), 7.27 (1 H, m), 7.54-7.86 (20 H, m), 7.96-8.05 (4 H, m),; *m/z* (HESI-Orbitrap; [M]<sup>+</sup>) 1748.7958, calcd for C<sub>102</sub>H<sub>117</sub>BrIrN<sub>5</sub>O<sub>4</sub><sup>+</sup>: 1748.7934. <sup>1</sup>H NMR and mass spectra were consistent with literature values.<sup>140</sup>



**[4-bromo-2-(1-methyl-3-propyl-1H-1,2,4-triazol-5-yl-κN<sup>4</sup>)phenyl-κC]bis{4-[3,6-bis(9,9-dipropyl-9H-fluoren-2-yl)-9H-carbazol-9-yl]-2-(pyridine-2-yl-κM)-phenyl-κC}iridium (III) (2.12C)**

**2.13C** was synthesized according to a modified literature procedure.<sup>142</sup> **2.12C** (1.03 g, 1.26 mmol) and iridium(III) chloride hydrate (0.186 g, 0.623 mmol) in 2-ethoxyethanol (16 cm<sup>3</sup>) and water (4.7 cm<sup>3</sup>) were sparged with argon for 30 minutes. The mixture was heated in an oil bath set at 130°C for 64 hours with stirring under nitrogen flow. The canary yellow suspension was allowed to cool to ambient temperature before brine (20 cm<sup>3</sup>) was added to

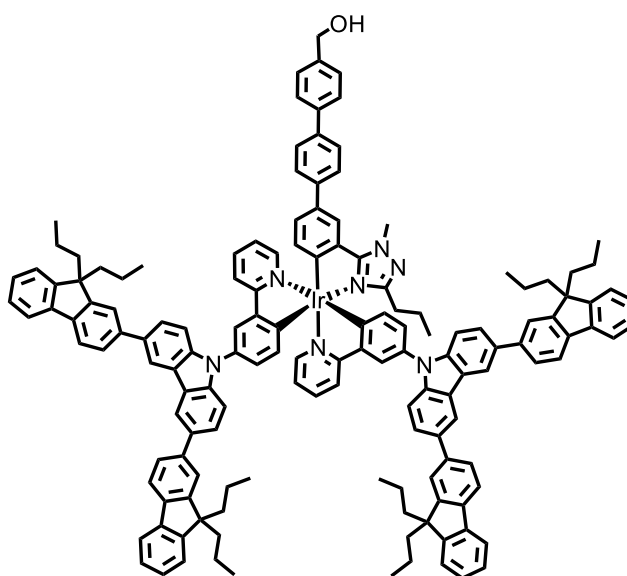
ensure complete precipitation. The residue was collected by vacuum filtration and washed with water. Without further purification the residue was combined with 5-(3-bromophenyl)-1-methyl-3-propyl-1*H*-1,2,4-triazole (2.31 g, 8.24 mmol), Proton sponge (0.111 g, 0.518 mmol) and silver(I) triflate (0.278 g, 1.08 mmol) and the mixture was heated with stirring under argon for 15 hours in an oil bath set at 168°C. The residue was purified by column chromatography over silica using dichloromethane: petroleum ether 40-60 mixture, 1:1 as eluent to give **2.13B** (0.261 g, 23 %) as a bright yellow powder. <sup>1</sup>H NMR (300 MHz, CDCl<sub>3</sub>) δ: 0.60-0.93 (45 H, m), 1.25-1.43 (24 H, m), 1.90-2.11 (16 H, m), 4.32 (3 H, s), 6.90-7.23 (6 H, m), 7.29-7.45 (12 H, m), 7.46-7.62 (4 H, m), 7.63-7.86 (26 H, m), 7.86-8.10 (5 H, m), 8.50 (4 H, m); *m/z* (MALDI-TOF: DCTB; [M+H]<sup>+</sup>) 2103.9, calcd for C<sub>134</sub>H<sub>123</sub>BrIrN<sub>7</sub>+H<sup>+</sup>: 2103.9. <sup>1</sup>H NMR and mass spectra were consistent with literature values.<sup>142</sup>



**bis(4''-[(2-ethylhexyl)oxy]-5'-{4-[(2-ethylhexyl)oxy]phenyl}-3-(2-pyridinyl-κM)[1,1':3',1''-terphenyl-4-yl-κC])[4''-hydroxymethyl-3-(1-methyl-3-propyl-1*H*-1,2,4-triazol-5-yl-κN<sup>4</sup>)[1,1':4',1''-terphenyl]-4-yl-κC]iridium(III) (2.14B)**

A mixture of **2.13B** (149 mg, 85.2 μmol), **2.5** (77.9 mg, 251 μmol) and tetrakis(triphenylphosphine)palladium(0) (46.6 mg, 40.3 μmol) in toluene (1.5 cm<sup>3</sup>), ethanol (0.6 cm<sup>3</sup>) and 2 M aqueous potassium carbonate (0.5 cm<sup>3</sup>) which had been deoxygenated via sparging with argon was heated to reflux under argon for 18 hours. After being allowed to cool to ambient temperature, dichloromethane (10 cm<sup>3</sup>) and water (10 cm<sup>3</sup>) were added. The aqueous fraction was washed with dichloromethane (2 × 10 cm<sup>3</sup>) and the combined organic fractions were washed with water (10 cm<sup>3</sup>), brine (10 cm<sup>3</sup>). The brine extraction emulsified slightly and another portion of dichloromethane (10 cm<sup>3</sup>) was added to aid separation. The organic phase was dried over anhydrous sodium sulphate, filtered and the

solvent was removed in vacuo. The residue was purified by column chromatography over silica with dichloromethane: methanol (200: 1) mixture as eluent to give **2.14B** (109 mg, 69 %) as a bright yellow powder. Mp. 154-156°. Found: C, 74.5; H, 7.0; N, 3.7.  $C_{115}H_{128}IrN_5O_5$  requires C, 74.6; H, 7.0; N, 3.8%; IR:  $\bar{\nu}$  solid/ $cm^{-1}$  = 808, 824, 872, 1004, 1027, 1064, 1110, 1176, 1235, 1282, 1396, 1423, 1464, 1510, 1561, 1599, 2859, 2926, 2957, 3033, 3567. UV-Vis:  $\lambda_{max}(CH_2Cl_2)/nm$ : 271 ( $\log \epsilon/dm^3mol^{-1}cm^{-1}$  5.25), 285 sh (5.22), 327 sh (4.77), 384 sh (4.33), 415 sh (4.03).  $^1H$  NMR (500 MHz,  $CD_2Cl_2$ ): 0.60 (3H, t,  $J=7.5$ , Pr  $CH_3$ ), 0.92-0.98 (26 H, m, EH  $CH_3$ ), 1.34-1.55 (35H, m, EH  $CH_2$ , Pr  $CH_2$ ), 1.73-1.81 (4H, m, EH CH), 1.84-1.93 (2H, m, Pr  $CH_2$ ), 3.90 (8H, d,  $J= 5.5$ ,  $OCH_2$ ), 4.32 (3H, s,  $NCH_3$ ), 4.76 (2H, s,  $CH_2-OH$ ), 6.86-6.90 (1H, m, LH), 6.94-7.07 (12H, m, SPH, LH), 7.17-7.23 (2H, m, LH), 7.29 (1H, d,  $J= 2$ , LH), 7.45 (2H, d,  $J= 8.5$ , BP), 7.58-7.73 (20H, m, SPH, LH, G1-BPH), 7.75 and 7.78 (4H, AA' BB', LPH), 7.83 (2H, d,  $J=2$ , G1-BPH), 7.95-8.08 (5H, m, G1-BPH, LH).  $m/z$  (MALDI: DIT) calcd for  $C_{115}H_{128}IrN_5O_5$ , 1850.0 (39%), 1851.0 (50%), 1852.0 (98%), 1853.0 (100%), 1854.0 (61%), 1855.0 (26%), 1856.0 (8%), 1857.0 (2%); found, 1850.8 (38%), 1851.7 (48%), 1852.6 (96%), 1853.6 (100%), 1854.5 (63%), 1855.4 (26%), 1856.5 (12%), 1857.4 (5%).

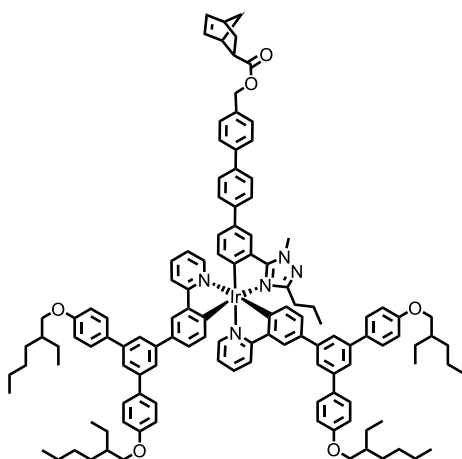


**bis{4-[3,6-bis(9,9-dipropyl-9H-fluoren-2-yl)-9H-carbazol-9-yl]-2-(pyridinyl- $\kappa M$ )phen-4-yl- $\kappa C$ }[4''-hydroxymethyl-3-(1-methyl-3-propyl-1H-1,2,4-triazol-5-yl- $\kappa N^4$ )] [1,1':4',1''-terphenyl]-4-yl- $\kappa C$ }iridium(III) (**2.14C**)**

A mixture of **2.4** (0.0408 g, 0.115 mmol), bis(pinacolato)diboron (0.113 g, 0.450 mmol), [1,1'-bis(diphenylphosphino)ferrocene]dichloropalladium(II) dichloromethane (0.0264 g, 0.0324

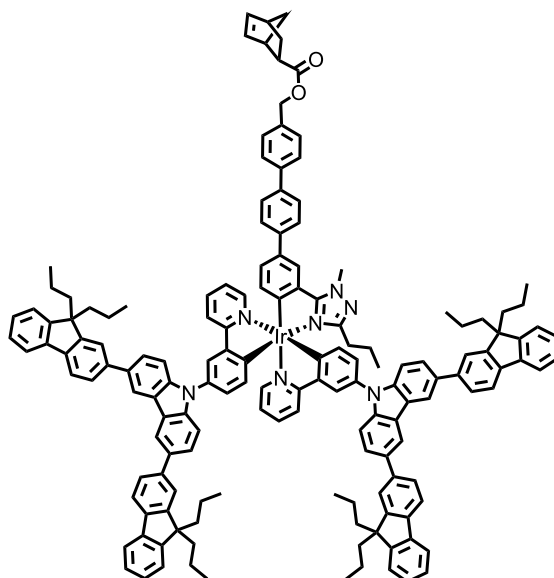


mmol) and potassium acetate (0.197 g, 2.01 mmol) in anhydrous 1,4-dioxane (2.2 cm<sup>3</sup>) was deoxygenated by the freeze-pump-thaw technique (two cycles) and returned to nitrogen atmosphere. The mixture was heated at 100°C for 22 hours with stirring under a nitrogen flow. The mixture was allowed to cool to temperature and diethyl ether (10 cm<sup>3</sup>) and water (10 cm<sup>3</sup>) were added. Separation occurred and the aqueous layer was washed with diethyl ether (10 cm<sup>3</sup>, two repeats). The combined organic layer was washed with water (10 cm<sup>3</sup>) and brine (10 cm<sup>3</sup>), dried over anhydrous sodium sulphate, filtered and solvent removed. The excess bis(pinacolato)diboron was removed via sublimation under vacuum and the crude boronic ester was used without further purification. A suspension of the crude **2.4** and **2.12C** (0.102 g, 0.0483 mmol) in a mixture of toluene (0.65 cm<sup>3</sup>), ethanol (0.30 cm<sup>3</sup>) and 2 M sodium carbonate (0.3 cm<sup>3</sup>) was subjected to sparging by argon for 15 minutes. Tetrakis(triphenylphosphine)palladium(0) (0.0116 g, 0.0100 mmol) was added and the mixture was heated at reflux under the argon atmosphere with stirring for two hours. The mixture was allowed to cool and water (5 cm<sup>3</sup>) was added and the phases were allowed to separate. The aqueous layer was extracted by dichloromethane (3 × 5 cm<sup>3</sup>). The combined organic layer was washed with water (5 cm<sup>3</sup>) and brine (5 cm<sup>3</sup>). The combined organic layer was dried over anhydrous sodium sulphate, filtered and the solvent was removed under reduced pressure to afford the yellow-brown crude. The residue was purified by column chromatography over silica gel using dichloromethane: ethyl acetate (20:1) mixture as eluent to give **2.14C** (0.0599 g, 0.0271 mmol, approximately 57 %) as an intense yellow powder. Isolation of a high purity sample for analysis proved impossible. The following characterization correspond to the sample as isolated and was used without further purification and the yield of the next step is calculated over three steps. Mpt: 145 °C; Found: C, 77.7; H, 6.0; N, 4.4. C<sub>147</sub>H<sub>134</sub>IrN<sub>7</sub>O requires C, 80.0; H, 6.1; N, 4.4 %; IR:  $\bar{\nu}$  solid/cm<sup>-1</sup>= 3568 (O-H), 3027, 2954, 2928, 2869, 1600, 1476, 1465, 1447, 1230, 1029, 809, 782, 736; UV-Vis:  $\lambda_{\text{max}}$ (CH<sub>2</sub>Cl<sub>2</sub>)/nm: 321 (log  $\epsilon$ /dm<sup>3</sup>mol<sup>-1</sup>cm<sup>-1</sup> 5.18), 270 (4.98), 301 sh (5.08), 454 sh (3.49); <sup>1</sup>H NMR (500 MHz, CDCl<sub>3</sub>):  $\delta$  0.60-0.87 (43 H, m, *n*Pr CH<sub>2</sub> and CH<sub>3</sub>), 1.64 (1H, t, *J* = 6 Hz, OH), 1.89-2.11 (20 H, m, *n*Pr CH<sub>2</sub>), 4.42 (3 H, s, NCH<sub>3</sub>), 4.75 (2 H, d, *J* = 6 Hz, CH<sub>2</sub>OH), 7.01-7.06 (1 H, m, L), 7.11-7.23 (6 H, m, L), 7.28-7.40 (16 H, m, Cbz, FI and T), 7.41-7.50 (4 H, m, L), 7.52-7.83 (28 H, m, Cbz, FI, L and T), 7.91-7.97 (5 H, m, L and T), 8.04 (1 H, m, L), 8.51 (4 H, m, Cbz).; m/z (HESI-Orbitrap; [M]<sup>2+</sup>): 1102.0138 (29 %), 1102.5156 (47 %), 1103.0159 (84 %), 1103.5169 (100 %), 1104.0185 (72 %), 1104.5201 (35 %), 1105.0216 (14 %), 1105.5232 (4 %). calcd for C<sub>147</sub>H<sub>134</sub>IrN<sub>7</sub>O<sup>2+</sup>: 1102.0122 (29 %), 1102.5134 (47 %), 1103.0143 (87 %), 1103.5155 (100 %), 1104.0169 (73 %), 1104.5185 (37 %), 1105.0201 (15 %), 1105.0233 (1 %).



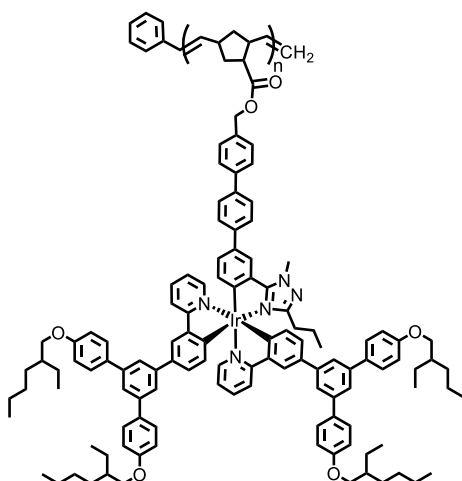
**{4'-[(bicyclo[2.2.1]hept-5-en-2-ylcarbonyl)oxy]methyl-3-(1-methyl-3-propyl-1*H*-1,2,4-triazol-5-yl- $\kappa N^A$ )[1,1':4',1''-terphenyl]-4-yl- $\kappa C$ ]bis(4''-[(2-ethylhexyl)oxy]-5'-{4-[(2-ethylhexyl)oxy]phenyl)-3-(2-pyridinyl- $\kappa M$ )[1,1':3',1''-terphenyl-4-yl- $\kappa C$ ]iridium(III) (2.15B)**

A mixture of **2.14B** (55.7 mg, 30.0  $\mu\text{mol}$ ) and *exo*-5-norbornene-2-carboxylic acid (6.4 mg, 46  $\mu\text{mol}$ ) and 4-dimethylaminopyridine (4.7 mg, 38  $\mu\text{mol}$ ) in distilled dichloromethane (2  $\text{cm}^3$ ) that had been passed over activated alumina and sparged for 30 minutes with argon, was added a solution of *N,N'*-dicyclohexylcarbodiimide (11.7 mg, 57.0  $\mu\text{mol}$ ) in similarly purified dichloromethane (0.4  $\text{cm}^3$ ). The reaction mixture was stirred for 20 hours under argon. The solvent was removed in vacuo and the residue was purified via automated flash column chromatography over silica using a dichloromethane: petroleum ether 40-60 (0:1 to 1:0) mixture to give **2.15B** (23.0 mg, 38%) as a yellow powder. Found: C, 74.6; H, 6.9; N, 3.5.  $\text{C}_{123}\text{H}_{136}\text{IrN}_5\text{O}_6$  requires C, 74.9; H, 7.0; N, 3.6%; IR:  $\bar{\nu}$  solid/ $\text{cm}^{-1}$  = 1728 (C=O, ester); UV-Vis:  $\lambda_{\text{max}}(\text{CH}_2\text{Cl}_2)/\text{nm}$ : 274 (log  $\epsilon/\text{dm}^3\text{mol}^{-1}\text{cm}^{-1}$  4.87), 268 sh (4.85), 323 (4.45), 378 sh (3.99), 452 (3.22);  $^1\text{H}$  NMR (500 MHz,  $\text{CD}_2\text{Cl}_2$ ): 0.60 (3H, t,  $J=7.5$ , *nPr*  $\text{CH}_3$ ), 0.88-0.97 (26 H, m, EH  $\text{CH}_3$ ), 1.24-1.58 (38H, m, EH  $\text{CH}_2$ , Pr  $\text{CH}_2$ , NB- $\text{CH}_2$ ), 1.71-1.89 (4H, m, EH CH), 1.81-1.98 (3H, m, Pr  $\text{CH}_2$ , NB- $\text{CH}_2$ ), 2.27-2.31 (1H, m, NB-CH), 2.92 (1H, s, NB-CH), 3.07 (1H, s, NB-CH), 3.88-3.94 (8H, m,  $J=5$ , OCH<sub>2</sub>), 4.31 (3H, s, NCH<sub>3</sub>), 5.16 (2H, s, COOCH<sub>2</sub>), 6.11-6.16 (2H, m, V H), 6.88-7.03 (12 H, m, BiPh, PhPy), 7.08-7.31 (4 H, m, PhPy), 7.43-7.45 (2H, m, BiPh), 7.62-7.81 (23 H, m, BiPh, T), 7.88 (1H, m, PhPy), 7.88 (1H, d,  $J=2$ , BiPh), 7.96-8.14 (5H, m, BiPh, PhPy). *m/z* (MALDI: DCTB) 1969.3 (36 %), 1970.3 (55 %), 1971.3 (89 %), 1972.3 (100 %), 1973.3 (68 %), 1974.3 (34 %), 1975.3 (14 %); calcd for  $\text{C}_{123}\text{H}_{136}\text{IrN}_5\text{O}_6$ : 1970.0 (35 %), 1971.0 (50 %), 1972.0 (95 %), 1973.0 (100 %), 1974.0 (65 %), 1975.0 (29 %), 1976.0 (10 %), 1977.0 (3 %).



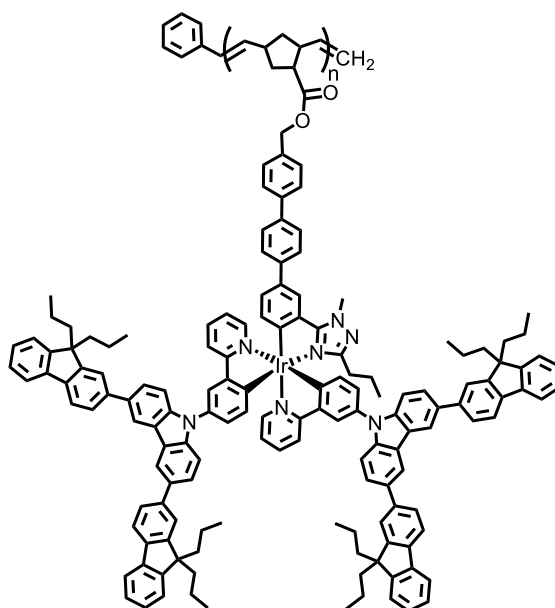
**{4'-[(bicyclo[2.2.1]hept-5-en-2-ylcarbonyl)oxy]methyl-3-(1-methyl-3-propyl-1*H*-1,2,4-triazol-5-yl- $\kappa$ N<sup>A</sup>)[1,1':4',1''-terphenyl]-4-yl- $\kappa$ C}bis bis{4-[3,6-bis(9,9-dipropyl-9*H*-fluoren-2-yl)-9*H*-carbazol-9-yl]-2-(pyridinyl- $\kappa$ M)phen-4-yl- $\kappa$ C}iridium(III) (2.15C)**

A solution of *N,N*-dicyclohexylcarbodiimide (0.146 g, 0.707 mmol) in dichloromethane (1 cm<sup>3</sup>) was added to a solution of **2.14C**, *exo*-5-norbornene-2-carboxylic acid (0.0163 g, 0.118 mmol) and 4-dimethylaminopyridine (0.0454 g, 0.372 mmol) in dichloromethane (1 cm<sup>3</sup>) and was deoxygenated by argon. The solution was stirred for 24 hours at room temperature. The solvent was removed and the residue was purified by column chromatography over silica using dichloromethane:petroleum ether (4:1) mixture as eluent to give **2.15C** (0.033 g, 51 %) as an intense yellow solid. Yield calculated over two-steps from **2.13C**. Mp. 200-202°C. Found: C, 80.0; H, 6.2; N, 3.9. C<sub>156</sub>H<sub>142</sub>IrN<sub>7</sub>O<sub>2</sub> requires C, 80.0; H, 6.2; N, 4.2; IR:  $\bar{\nu}$  solid/cm<sup>-1</sup> = 1725 (C=O, ester); UV-Vis:  $\lambda_{\max}$ (CH<sub>2</sub>Cl<sub>2</sub>)/nm: 321 (log  $\epsilon$ /dm<sup>3</sup>mol<sup>-1</sup>cm<sup>-1</sup> 5.27), 270 (5.08), 408 sh (3.95), 451 sh (3.47); <sup>1</sup>H NMR (500 MHz, CDCl<sub>3</sub>):  $\delta$  0.60-0.87 (43 H, m, *n*Pr -CH<sub>2</sub> and -CH<sub>3</sub>), 1.37 (4H, m, *n*Pr CH<sub>2</sub> and NB CH<sub>2</sub>), 1.94 (3 H, m, NB CH), 1.99-2.13 (16 H, m, *n*Pr CH<sub>2</sub>), 2.29 (1 H, m, NB CH<sub>2</sub>), 2.92 (1 H, s, NB CH<sub>2</sub>), 3.07 (1 H, s, NB CH), 4.40 (3 H, s, NCH<sub>3</sub>), 5.16 (2 H, s, COOCH<sub>2</sub>), 6.10-6.17 (2 H, m, NB V), 7.08 (1 H, m, L), 7.12-7.21 (3 H, m, L), 7.25 (2 H, m, Cbz), 7.28-7.42 (12 H, m, Cbz, FI and T), 7.42-7.48 (4 H, m, L), 7.53-7.64 (5 H, m, L), 7.64-7.72 (5 H, m, L and T), 7.72-7.84 (22 H, m, Cbz and FI), 7.88 (1 H, m, L), 7.97-8.05 (5 H, m, L), 8.08 (1 H, m, L), 8.56 (4 H, m, Cbz). *m/z* (MALDI: DCTB) calcd for C<sub>156</sub>H<sub>142</sub>IrN<sub>7</sub>O<sub>2</sub>, 2324.1 (26 %), 2325.1 (46 %), 2326.1 (83 %), 2327.1 (100 %), 2328.1 (78 %), 2329.1 (43 %), 2330.1 (18 %) 2331.1 (6 %) ; found, 2323.8 (34 %). 234.8 (56 %), 2325.8 (98 %), 2326.8 (94 %), 2327.8 (100 %), 2328.8 (62 %), 2329.8 (23 %).



**{4'-[(bicyclo[2.2.1]hept-5-en-2-ylcarbonyl)oxy]methyl-3-(1-methyl-3-propyl-1*H*-1,2,4-triazol-5-yl- $\kappa N^4$ )[1,1':4',1''-terphenyl]-4-yl- $\kappa C$ )}bis(4''-[(2-ethylhexyl)oxy]-5'-{4-[(2-ethylhexyl)oxy]phenyl}-3-(2-pyridinyl- $\kappa N$ )[1,1':3',1''-terphenyl-4-yl- $\kappa C$ ])iridium(III) homopolymer (PD<sub>B</sub>)**

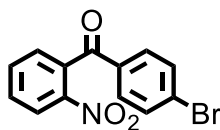
Anhydrous dichloromethane was prepared by distillation from calcium hydride followed by subjection to three cycles of freeze-pump-thaw backfilling to argon. Subsequent solutions were also subjected to three cycles of vacuum backfilling to argon prior to reaction initiation. A solution of 3.7 mM Grubb's 3<sup>rd</sup> generation catalyst (0.12 cm<sup>3</sup>, 0.44  $\mu$ mol) in anhydrous dichloromethane was added rapidly to a solution of **2.16B** (84.8 mg, 43  $\mu$ mol) in anhydrous dichloromethane (0.13 cm<sup>3</sup>) with stirring. After 40 minutes, ethyl vinyl ether (0.1 cm<sup>3</sup>, 1.04 mmol) was added. The solution was poured onto methanol (10 cm<sup>3</sup>) and the precipitate was collected by centrifugation. The residue was purified by dissolution in dichloromethane and precipitation with methanol to give **PD<sub>B</sub>** (61 mg, 72 %) as a bright yellow solid. UV-Vis:  $\lambda_{\text{max}}$ (Toluene)/nm: 326, 295 sh, 395 sh. IR:  $\bar{\nu}$  solid/cm<sup>-1</sup>= 1728 (C=O, ester); <sup>1</sup>H NMR (500 MHz, CD<sub>2</sub>Cl<sub>2</sub>): 0.45 (3 H, m, *n*Pr CH<sub>3</sub>), 0.81-0.97 (26 H, m, EH CH<sub>3</sub>), 1.18-1.51 (38 H, m, EH CH<sub>2</sub>, Pr CH<sub>2</sub>, NB-CH<sub>2</sub>), 1.62-1.85 (4 H, m, EH CH), 1.93-2.19 (2 H, m, Pr CH<sub>2</sub>, NB-CH<sub>2</sub>), 3.77-4.22 (13 H, m, NB-CH and OCH<sub>2</sub>), 4.84-5.54 (5 H, m, NCH<sub>3</sub> and COOCH<sub>2</sub>), 6.45-7.18 (2 H, m, V H, BiPh, PhPy), 7.28-8.14 (32 H, m, BiPh, PhPy and T), GPC: M<sub>n</sub> = 35,691 Da, M<sub>w</sub> = 97,126 Da, Đ = 2.72.



**{4'-[(bicyclo[2.2.1]hept-5-en-2-ylcarbonyl)oxy]methyl-3-(1-methyl-3-propyl-1*H*-1,2,4-triazol-5-yl-κ*N*<sup>4</sup>)[1,1':4',1''-terphenyl]-4-yl-κ*C*}bis      bis{4-[3,6-bis(9,9-dipropyl-9*H*-fluoren-2-yl)-9*H*-carbazol-9-yl]-2-(pyridinyl-κ*N*)phen-4-yl-κ*C*}iridium(III) (PDc)**

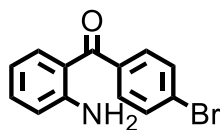
Anhydrous dichloromethane was prepared by distillation from calcium hydride followed by subjection to three cycles of freeze-pump-thaw backfilling to argon. A solution of 3.7 mM Grubb's 3<sup>rd</sup> generation catalyst (0.055, 0.20 μmol) in anhydrous dichloromethane was added rapidly to a solution of **2.16C** (48.8 mg, 21 μmol) in anhydrous dichloromethane (0.13 cm<sup>3</sup>) with stirring. After 20 minutes an addition aliquot of dichloromethane (0.4 cm<sup>3</sup>) was added. After stirring for 66 hours, ethyl vinyl ether (0.1 cm<sup>3</sup>, 1.04 mmol) was added. The solution was poured onto methanol (10 cm<sup>3</sup>) and the precipitate was collected by filtration to give **PDc** (19 mg, 39 %) as a light yellow solid. IR:  $\bar{\nu}$  solid/cm<sup>-1</sup>= 1730 (C=O, ester); UV-Vis:  $\lambda_{\text{max}}$ (Toluene)/nm: 321. <sup>1</sup>H NMR (500 MHz, CDCl<sub>3</sub>): δ 0.53-1.08 (43 H, m, *n*Pr -CH<sub>2</sub> and -CH<sub>3</sub>), 1.85-2.14 (16 H, m, *n*Pr CH<sub>2</sub>), 3.67 (3 H, s, NCH<sub>3</sub>), 6.70-8.06 (56 H, m, L, T, Cbz and Fl), 8.48 (4 H, m, Cbz). GPC: M<sub>n</sub> = 77,165 Da, Da, Đ = 3.86.

### (4-Bromophenyl)(2-nitrophenyl)methanone (3.1)



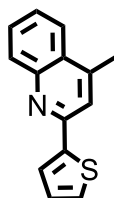
(4-Bromophenyl)(2-nitrophenyl)methanone (**3.1**) was synthesized according to a modified literature procedure.<sup>203</sup> Oxalyl chloride (20.5 cm<sup>3</sup>, 235 mmol) was added dropwise with stirring to a suspension of 2-nitrobenzoic acid (20.06 g, 120 mmol) in anhydrous dichloromethane (420 cm<sup>3</sup>) and anhydrous *N,N*-dimethylformamide (0.4 cm<sup>3</sup>) that had been cooled in an ice bath under nitrogen. The solution was kept in the ice bath for 30 min after the addition was complete and then the solution was allowed to warm to room temperature. After the reaction had gone to completion, indicated by the solution becoming clear and the evolution of gas having ceased, the solvent was removed under reduced pressure to give the acyl chloride as a slightly yellow oil. The oil was redissolved in 1,2-dichloroethane (45 cm<sup>3</sup>) and bromobenzene (20 cm<sup>3</sup>, 191 mmol) was added under an argon atmosphere. The stirred mixture was cooled again in an ice bath and iron(III) chloride (16.9 g, 104 mmol) was added portion-wise over 30 min (three portions). After being allowed to react for an additional hour the mixture was carefully poured onto ice/ water mixture (250 cm<sup>3</sup>) to quench the reaction. The mixture was extracted with diethyl ether (250 cm<sup>3</sup>) and then hydrochloric acid (37%, 100 cm<sup>3</sup>) was added to the aqueous layer to destabilise any colloidal iron particles. The aqueous phase was further extracted with diethyl ether (6 x 250 cm<sup>3</sup>) and the combined organic phases were washed with "acidic brine" solution [a mixture of brine (250 cm<sup>3</sup>) and hydrochloric acid (3M, 250 cm<sup>3</sup>)]. The crude product was purified by column chromatography over silica using a dichloromethane:petroleum ether 40-60 fraction mixture (1:2) as eluent. The desired product was collected and then recrystallized from a dichloromethane/petroleum ether 40-60 mixture to give **3.1** (9.43 g, 30.8 mmol, 26 %) as off-white crystals. <sup>1</sup>H NMR (300 MHz, CDCl<sub>3</sub>): 7.48 (1 H, dd, *J*<sub>ortho</sub> = 7.5 Hz, *J*<sub>meta</sub> = 1.6 Hz), 7.60 (4 H, m), 7.68-7.73 (1 H, ddd, *J*<sub>ortho1</sub> = 8.6 Hz, *J*<sub>ortho2</sub> = 7.1 Hz, *J*<sub>meta</sub> = 1.6 Hz), 7.77-7.83 (1 H, td, *J*<sub>ortho</sub> = 7.5 Hz, *J*<sub>meta</sub> = 1.3 Hz) 8.23-8.27 (1 H, dd, *J*<sub>ortho</sub> = 8.2 Hz, *J*<sub>meta</sub> = 1.3 Hz), *m/z* (ESI-TOF ES<sup>+</sup>; [MNa]<sup>+</sup>) 327.7; calcd for C<sub>13</sub>H<sub>8</sub>BrNO<sub>3</sub>Na<sup>+</sup>: 328.0. The <sup>1</sup>H NMR and mass spectra were consistent with those reported in the literature.<sup>203</sup>

### (2-Aminophenyl)(4-bromophenyl)methanone (3.2)



(2-Aminophenyl)(4-bromophenyl)methanone (**3.2**) was synthesized according to a modified literature procedure.<sup>203</sup> To a stirred refluxing suspension of **3.1** (5.54 g, 18.1 mmol) and iron metal powder (10.11 g, 181 mmol) in ethyl acetate (10 cm<sup>3</sup>) and water (50 cm<sup>3</sup>) under a nitrogen flow, acetic acid (35 cm<sup>3</sup>) was added slowly. The heat was maintained for a further two hours before cooling. The mixture was extracted with ethyl acetate (200 cm<sup>3</sup>) and 2M aqueous sodium hydroxide (200 cm<sup>3</sup>). The aqueous fraction was washed further with ethyl acetate (2 x 200 cm<sup>3</sup>) and diethyl ether (200 cm<sup>3</sup>). The combined organic fraction was washed with diluted brine (100 cm<sup>3</sup> of brine with 100 cm<sup>3</sup> of water) before being dried over anhydrous magnesium sulphate, filtering and removing the solvent under reduced pressure. The crude was purified by column chromatography over silica using dichloromethane: petroleum ether 40-60 fraction (4 : 1) as the mobile phase. The material was then recrystallized from 2-propanol to give **3.2** (4.53 g, 16.4 mmol, 91 %) as yellow crystals. <sup>1</sup>H NMR (300 MHz, CD<sub>2</sub>Cl<sub>2</sub>): 6.10 (2 H, s), 6.57-6.63 (1 H, dd,  $J_{ortho} = 7.6$  Hz, ,  $J_{meta} = 1.2$  Hz ), 6.74-6.78 (1 H, dd,  $J_{ortho} = 8.4$  Hz,  $J_{meta} = 1.1$  Hz), 7.28-7.34 (1 H, dd,  $J_{ortho} = 7.6$  Hz,  $J_{meta} = 1.4$  Hz), 7.37-7.40 (1 H, dd,  $J_{ortho} = 7.9$  Hz,  $J_{meta} = 1.5$  Hz), 7.48-7.53 (2 H, td,  $J_{ortho} = 8.6$  Hz,  $J_{meta} = 2.0$  Hz), 7.59-7.64 (2 H, td,  $J_{ortho} = 8.6$  Hz,  $J_{meta} = 2.0$  Hz); m/z (ESI-TOF ES<sup>+</sup>; [MNa]<sup>+</sup>) found 298.0 (100 %), 299.0 (15 %), 299.9 (98 %), 300.9 (14 %) 301.9 (1 %); calcd for C<sub>13</sub>H<sub>10</sub>BrNONa<sup>+</sup>: 298.0 (100 %), 299.0 (15 %), 300.0 (99 %), 301.0 (15 %), 302.0 (1 %). The <sup>1</sup>H NMR and mass spectra were consistent with those reported in the literature.<sup>203</sup>

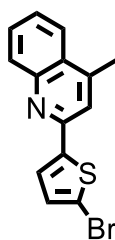
### 4-Methyl-2-(thiophen-2-yl)quinoline (3.3)



4-Methyl-2-(thiophen-2-yl)quinoline (**3.3**) was synthesized using a modified literature procedure.<sup>159</sup> *p*-Toluenesulphonic acid monohydrate (7.63 g, 40.1 mmol) was dried at 100 °C under vacuum for four h in the reaction flask. After placing under nitrogen, 2'-

aminoacetophenone (2.30 cm<sup>3</sup>, 20.0 mmol), 2-acetylthiophene (2.10 cm<sup>3</sup>, 19.7 mmol) and anhydrous toluene (200 cm<sup>3</sup>) were added. The stirred mixture was sparged with argon for 30 min before being heated in an oil bath set at 95 °C for 18 h under a nitrogen atmosphere. The mixture was then heated at reflux for 96 h under Dean-Stark conditions to remove water by its toluene azeotrope. After being allowed to cool, aqueous sodium hydroxide (2 M, 100 cm<sup>3</sup>) was added to the mixture. The organic layer was collected and the aqueous phase was extracted with dichloromethane (3 x 100 cm<sup>3</sup>). The combined organic phases were washed with water (100 cm<sup>3</sup>) and brine (100 cm<sup>3</sup>), dried over anhydrous sodium sulphate, filtered and the solvent was removed under reduced pressure. The crude was purified by column chromatography over silica with a dichloromethane:petroleum ether 40-60 mixture (1:1) as eluent to give **3.3** (3.00 g, 13.3 mmol, 68 %) as a pale yellow oil which very slowly solidifies to an off white waxy solid. Diffraction quality crystals were grown from hot petroleum ether 40-60 solution. Mp. 69°C; T<sub>d</sub>(5%) = 210°C; <sup>1</sup>H NMR (300 MHz, CDCl<sub>3</sub>) δ: 2.74 (1 H, d, J = 2.0 Hz), 7.16 (1 H, dd, J<sub>ortho</sub> = 5.0 Hz, J<sub>meta</sub> = 3.5 Hz), 7.44-7.53 (2 H, m), 7.64-7.74 (3 H, m), 7.95 (1 H, ddd, J<sub>ortho</sub> = 8.0 Hz), 8.08 (1 H, ddd, J<sub>ortho</sub> = 8.5 Hz), <sup>13</sup>C NMR (75 MHz, CDCl<sub>3</sub>) δ: 19.1, 118.4, 123.8, 125.8, 126.0, 127.5, 128.2, 128.5, 129.6, 130.0, 144.8, 145.7, 148.1, 152.2; m/z (ESI-HCT; [MH]<sup>+</sup>) 226.1; calcd for C<sub>14</sub>H<sub>12</sub>NS<sup>+</sup>: 226.1. The <sup>1</sup>H NMR, <sup>13</sup>C NMR and mass spectroscopy were consistent with literature values.<sup>204</sup>

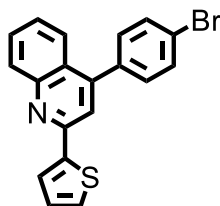
#### 4-methyl-2-(5-bromothiophen-2-yl)quinoline (3.4)



A mixture of 2'-aminoacetophenone (1.7 cm<sup>3</sup>, 14.8 mmol), 2-acetyl-5-bromothiophene (3.00 g, 14.6 mmol) and *p*-toluenesulphonic acid monohydrate (5.16 g, 27.16 mmol) in toluene (200 cm<sup>3</sup>) was heated with stirring at reflux for 24 h under a nitrogen atmosphere under Dean-Stark conditions. After being allowed to cool 2M aqueous sodium hydroxide (200 cm<sup>3</sup>) was added to the mixture. Separation occurred and the aqueous phase was washed further with dichloromethane (4 portions of 200 cm<sup>3</sup>). The combined organic phase was washed with water (200 cm<sup>3</sup>) and brine (200 cm<sup>3</sup>), dried over anhydrous magnesium sulphate, filtered and the solvent was removed under reduced pressure. The crude product was purified by column chromatography over silica using a dichloromethane:petroleum ether 40-



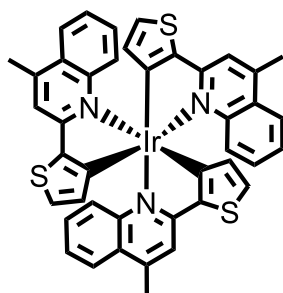
60 fraction mixture (0:1 to 1:4) as eluent to give **3.4** (4.17 g, 13.6 mmol, 94 %) as a pale yellow waxy solid. Diffraction quality crystals were grown by evaporation from a saturated petroleum ether 40-60 solution. Mp. 119°C;  $T_d(5\%) = 216^\circ\text{C}$ ; Found: C, 55.1; H, 3.5; N, 4.6.  $\text{C}_{14}\text{H}_{10}\text{NSBr}$  requires C, 55.3; H, 3.3; N, 4.6; %; IR:  $\bar{\nu}$  solid/ $\text{cm}^{-1}$  = 1596, 1550, 1464, 1427, 964, 852, 794, 766, 756, 685, 659; UV-Vis:  $\lambda_{\text{max}}(\text{CH}_2\text{Cl}_2)/\text{nm}$ : 284 ( $\log \epsilon/\text{dm}^3\text{mol}^{-1}\text{cm}^{-1}$  4.39), 276 sh (4.35), 313 sh (4.13), 324 (4.22), 337 (4.33), 352 (4.33);  $^1\text{H}$  NMR (500 MHz,  $\text{CD}_2\text{Cl}_2$ )  $\delta$ : 2.74 (d,  $J = 1.0$ ,  $-\text{CH}_3$ , 3 H); 7.13-7.14 (d,  $J = 3.9$ , Th-H, 1 H), 7.47-7.48 (d,  $J = 3.9$ , Th-H, 1 H), 7.52-7.55 (ddd,  $J_{\text{ortho}} = 8.3$  Hz,  $J_{\text{ortho}} = 6.9$  Hz,  $J_{\text{meta}} = 1.3$  Hz, Q-H, 1H), 7.61 (d,  $J = 1.0$ ,  $-\text{CH}_3$ , 1 H), 7.68-7.72 (ddd,  $J_{\text{ortho}} = 8.5$  Hz,  $J_{\text{ortho}} = 6.9$  Hz,  $J_{\text{meta}} = 1.4$  Hz, Q-H, 1H), 7.97-8.00 (m, Q-H and Th-H, 2 H);  $^{13}\text{C}$  NMR (125 MHz,  $\text{CD}_2\text{Cl}_2$ )  $\delta$ : 19.1, 116.2, 117.5, 124.2, 125.9, 126.5, 127.9, 129.8, 130.1, 131.5, 145.7, 147.8, 148.2, 151.4; m/z (microTOF-Q ES<sup>+</sup>; MNa<sup>+</sup>) 303.9796 (99 %), 304.9829 (16 %), 305.9777 (100 %), 306.9807 (16 %), 307.9752 (5 %); calcd for  $\text{C}_{14}\text{H}_{11}\text{NSBr}^+$ , 303.9790 (97 %), 304.9821 (16 %), 305.9770 (100 %), 306.9800 (17 %), 307.9752 (6 %)



#### 4-(4-Bromophenyl)-2-(thiophen-2-yl)quinoline (**3.5**)

A stirred suspension of **3.2** (5.01 g, 18.1 mmol), 1-(thiophen-2-yl)ethan-1-one (1.93 cm<sup>3</sup>, 18.1 mmol) and *p*-toluenesulphonic acid monohydrate (3.43 g, 18.1 mmol) in xylene (200 cm<sup>3</sup>) was heated at reflux under a nitrogen atmosphere under Dean-Stark conditions. After 32 h the mixture was allowed to cool and then washed with aqueous sodium hydroxide (2 M, 200 cm<sup>3</sup>). The organic layer was separated and the aqueous layer was extracted with diethyl ether (2 x 200 cm<sup>3</sup>). Brine (200 cm<sup>3</sup>) was added to the aqueous phase and was further extracted with diethyl ether (3 x 200 cm<sup>3</sup>). The combined organic fractions were washed with brine (100 cm<sup>3</sup>) diluted with water (100 cm<sup>3</sup>) before being dried over anhydrous sodium sulphate, filtered and removal of solvent under vacuum. The crude material was purified by column chromatography over silica using an ethyl acetate:petroleum ether 40-60 mixture (1: 9) as eluent followed by recrystallization using a dichloromethane/methanol mixture to give **3.5** (4.86 g, 13.3 mmol, 73 %) as pale yellow crystals. Diffraction quality crystals were grown from dichloromethane evaporation from a dichloromethane/methanol

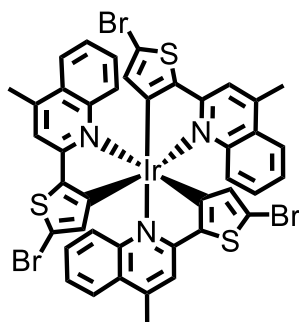
mixture. Mp. 113-114°C. Found: C, 62.3; H, 3.3; N, 3.7. C<sub>16</sub>H<sub>12</sub>NSBr requires C, 62.3; H, 3.3; N, 3.8; %; IR:  $\bar{\nu}$  solid/cm<sup>-1</sup>= 1595, 1545, 1485, 1063, 1010, 834, 823, 816, 758, 700, 583; UV-Vis:  $\lambda_{\text{max}}$ (CH<sub>2</sub>Cl<sub>2</sub>)/nm: 286 (log  $\epsilon$ /dm<sup>3</sup>mol<sup>-1</sup>cm<sup>-1</sup> 4.43), 259 sh (4.24), 322 (4.01), 339 (4.06), 353 (4.07), 385 (3.59). <sup>1</sup>H NMR (300 MHz, CDCl<sub>3</sub>)  $\delta$ : 7.15-7.18 (dd,  $J_1$  = 5.1 Hz,  $J_2$  = 3.7 Hz, Th-H, 1 H), 7.41-7.46 (m, Th-H + Q-H + Ph-H, 3 H), 7.68-7.72 (m, Q-H + Ph-H, 3H), 7.73-7.75 (m, Th-H, 1 H), 7.76-7.80 (m, Q-H, 1 H), 8.14-8.17 (m, Q-H, 1 H); <sup>13</sup>C NMR (100 MHz, CDCl<sub>3</sub>)  $\delta$ : 117.9, 123.0, 125.4, 125.7, 126.1, 126.5, 128.3, 128.9, 129.9, 130.0, 131.3, 132.0, 137.2, 145.3, 148.8, 152.0; m/z (microTOF-Q ES<sup>+</sup>; MH<sup>+</sup>) 365.9948 (96 %), 366.9973 (21 %), 367.9930 (100 %), 368.9955 (21 %), 369.9916 (6 %); calcd for C<sub>16</sub>H<sub>12</sub>NSBrH<sup>+</sup>; 365.9947 (96 %), 366.9978 (22 %), 367.9927 (100 %), 368.9957 (22 %), 369.9922 (6 %), 370.9932 (1 %).



### tris[2-(4-methyl-2-quinolinyl- $\kappa$ N)-3-thienyl- $\kappa$ C]iridium(III), [Ir(tmq)<sub>3</sub>]

A mixture of **3.3** (2.50 g, 11.1 mmol), iridium (III) chloride hydrate (0.336 g, 1.11 mmol) and silver trifluoroacetate (0.997 g, 4.50 mmol) in glycerol (25 cm<sup>3</sup>) was deoxygenated by evacuating over two hours, backfilling to argon. The mixture was heated at 180°C for 24 hours with stirring under an argon atmosphere. The mixture was allowed to cool to room temperature before the addition of water (200 cm<sup>3</sup>). The precipitate was collected by filtration and taken up into dichloromethane before passing through a silica gel plug. The collected material was further purified by recrystallization from initially from toluene and finally from dichloromethane with petroleum spirit 40-60 fraction to give [Ir(tmq)<sub>3</sub>] (0.244 g, 25 %) as a deep red powder. Further purification by train sublimation under vacuum (300°C at  $\approx 10^{-6}$  mbar) was used to obtain samples for analysis. Diffraction quality crystals were grown through vapour diffusion of petroleum ether 40-60 into a dichloromethane solution. Diffraction quality crystals containing only [Ir(tmq)<sub>3</sub>] were also grown during sublimation.

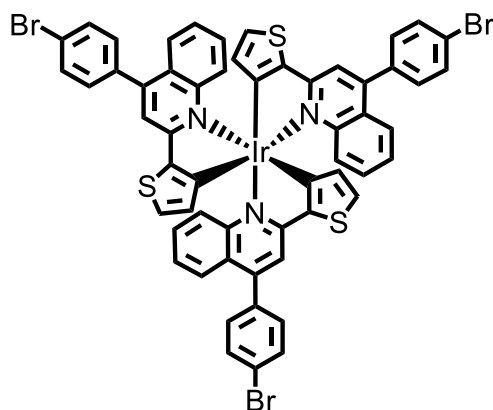
Mp. >350°C;  $T_d(5\%) = 425\text{ }^\circ\text{C}$ ; Found: C, 58.1; H, 3.2; N, 4.6.  $\text{C}_{42}\text{H}_{30}\text{IrN}_3\text{S}_3$  requires C, 58.3; H, 3.5; N, 4.9 %; IR:  $\bar{\nu}$  solid/ $\text{cm}^{-1} = 690, 690, 726, 730, 753, 758, 865, 874, 1423, 1452, 1603$ ; UV-Vis:  $\lambda_{\text{max}}$  (Toluene)/nm: 306 (log  $\epsilon/\text{dm}^3\text{mol}^{-1}\text{cm}^{-1}$  4.62), 320 (4.60), 347 sh (4.43), 395 sh (4.20) 413 (4.28), 448 sh (4.07), 501 sh (3.70), 544 sh (2.91), 579 (2.74).  $^1\text{H NMR}$  (500 MHz,  $\text{CD}_2\text{Cl}_2$ )  $\delta$ : 2.78 (9 H, d,  $J = 1.0$  Hz,  $\text{LCH}_3$ ), 5.95-5.96 (3 H, d,  $J = 5.0$  Hz, Th), 6.71-6.75 (3 H, ddd,  $J_{\text{ortho}} = 8.5$  Hz,  $J_{\text{ortho}} = 7.0$  Hz,  $J_{\text{meta}} = 1.5$  Hz, Q), 7.11-7.12 (3 H, d,  $J = 5.0$  Hz, Th), 7.20-7.24 (3 H, ddd,  $J_{\text{ortho}} = 8.0$  Hz,  $J_{\text{ortho}} = 7.0$  Hz,  $J_{\text{meta}} = 1.3$  Hz, Q), 7.56-7.57 (3 H, d, 1.0 Hz, Q), 7.84-7.87 (3 H, dd,  $J_{\text{ortho}} = 8.0$  Hz,  $J_{\text{meta}} = 1.0$  Hz, Q), 7.92-7.94, (3 H, dd,  $J_{\text{ortho}} = 8.5$  Hz,  $J_{\text{meta}} = 1.0$  Hz, Q);  $m/z$  (microTOF-Q;  $\text{MNa}^+$ ) 886.1111 (54 %), 887.1143 (25 %), 888.1129 (100 %), 889.1258 (46 %), 890.1137 (22 %), 891.1141 (7 %), 892.1134 (2 %); calcd for  $\text{C}_{42}\text{H}_{30}\text{IrN}_3\text{S}_3\text{Na}^+$ , 886.1100 (52 %), 887.1130 (26 %), 888.1121 (100 %), 889.1250 (48 %), 890.1128 (24 %), 891.1133 (8 %), 892.1124 (2 %).



### tris[5-bromo-2-(4-methyl-2-quinolinyl- $\kappa\text{M}$ )-3-thienyl- $\kappa\text{C}$ ]iridium(III), (3.6)

**[Ir(tmq)<sub>3</sub>]** (0.0199 g, 0.023 mmol) was dissolved in *N,N*-dimethylformamide (60 cm<sup>3</sup>) under an argon atmosphere and cooled in an ice bath. With continuous stirring, *N*-bromosuccinimide (0.0245 g, 0.138 mmol) in *N,N*-dimethylformamide (5 cm<sup>3</sup>) was added dropwise slowly with both solutions being protected from light. After the addition was complete the solution was allowed to warm to ambient temperature naturally. The mixture was again cooled in an ice bath before the addition of acetone (1 cm<sup>3</sup>) to stop the reaction. Brine (30 cm<sup>3</sup>) which had been cooled in the ice bath was added to the solution before being allowed to warm to room temperature. Water (70 cm<sup>3</sup>) and dichloromethane (50 cm<sup>3</sup>) were added; and separation occurred. The aqueous phase was washed with dichloromethane (50 cm<sup>3</sup> x 2) and the combined organic phase was washed with water (5 x 100 cm<sup>3</sup>) and brine (100 cm<sup>3</sup>). The solution was dried over anhydrous sodium sulphate, filtered and the solvent was removed. The residue was further purified by recrystallization from toluene. The solid was recrystallized from a dichloromethane: methanol mixture and a dichloromethane:

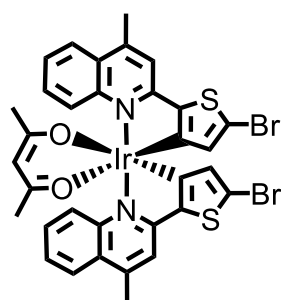
petroleum spirit (40-60 fraction) mixture to give **3.6** (0.0098 g, 0.0089 mmol, 39 %) as a bright orange-red powder. Diffraction quality crystals were grown through vapour diffusion of petroleum ether 40-60 into a dichloromethane solution. Mp. >350°C. Found: C, 45.4; H, 2.5; N, 3.8. C<sub>42</sub>H<sub>27</sub>IrN<sub>3</sub>S<sub>3</sub>Br<sub>3</sub> requires C, 45.8; H, 2.5; N, 3.8; IR:  $\bar{\nu}$  solid/cm<sup>-1</sup>= 1603, 1512, 1466, 1457, 1421, 1375, 1330, 1073, 754; UV-Vis:  $\lambda_{\text{max}}$ (CH<sub>2</sub>Cl<sub>2</sub>)/nm: 312 (log  $\epsilon$ /dm<sup>3</sup>mol<sup>-1</sup>cm<sup>-1</sup> 4.69), 292 (4.63), 324 sh (4.68), 340 sh (4.58), 393 sh (4.32), 410 (4.42), 435 sh (4.24), 483 sh (3.91), 539 sh (2.68), 559 sh (2.22), 581 (2.31). <sup>1</sup>H NMR (500 MHz, CD<sub>2</sub>Cl<sub>2</sub>)  $\delta$ : 2.79 (d,  $J$  = 1.0 Hz, -CH<sub>3</sub>, 9 H), 6.0391 (s, Q-H, 3 H), 6.70-6.74 (ddd,  $J_{\text{ortho}}$  = 8.7 Hz,  $J_{\text{ortho}}$  = 6.7 Hz,  $J_{\text{meta}}$  = 1.5 Hz, Q-H, 3H), 7.23-7.26 (ddd,  $J_{\text{ortho}}$  = 8.2 Hz,  $J_{\text{ortho}}$  = 7.3 Hz,  $J_{\text{meta}}$  = 1.2 Hz, Q-H, 3H), 7.44 (d, 1.0 Hz, Q-H, 3 H), 7.79-7.81 (dd,  $J_{\text{ortho}}$  = 8.2 Hz,  $J_{\text{meta}}$  = 1.5 Hz, Q-H, 3 H), 7.87-7.89 (dd,  $J_{\text{ortho}}$  = 8.3 Hz,  $J_{\text{meta}}$  = 1.4 Hz, Q-H, 3 H); m/z (microTOF-Q ES<sup>+</sup>; MNa<sup>+</sup>) 1119.8380 (12 %), 1120.8416 (6 %), 1121.8380 (56 %), 1122.8415 (28 %), 1123.8368 (100 %), 1124.8395 (47 %), 1125.8360 (85 %), 1126.8384 (39 %), 1127.8351 (36 %), 1128.8369 (16 %), 1129.8342 (6 %), 1130.8359 (2 %) calcd for C<sub>42</sub>H<sub>27</sub>IrN<sub>3</sub>S<sub>3</sub>Br<sub>3</sub>Na<sup>+</sup>, 1119.8416 (11 %), 1120.8446 (6 %), 1121.8412 (54 %), 1122.8441 (27 %), 1123.8405 (100 %), 1124.8319 (48 %), 1125.8396 (87 %), 1126.8420 (40 %), 1127.83889 (36 %), 1128.8406 (15 %), 1129.8388 (6 %), 1130.8391 (2 %).



### tris{2-[4-(4-bromophenyl)-2-quinolinyl- $\kappa$ N]-3-thienyl- $\kappa$ C}iridium(III), (**3.7**)

A mixture of **3.5** (4.01 g, 11.0 mmol), iridium (III) chloride hydrate (0.400 g, 1.34 mmol) and silver(I) trifluoroacetate (1.38 g, 6.25 mmol) were suspended in glycerol (120 cm<sup>3</sup>). The mixture was subjected to evacuation for one hour with continuous stirring before backfilling with argon. The mixture was heated at 200°C for 43 hours with stirring under an argon atmosphere. The mixture was allowed to cool to room temperature before the addition of diluted of water (400 cm<sup>-1</sup>) and dichloromethane (200 cm<sup>-1</sup>). Both phases were filtered to

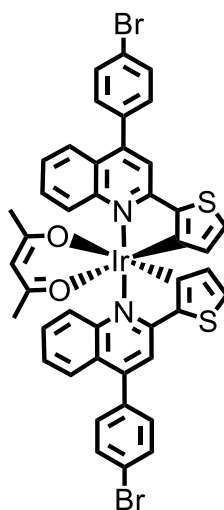
remove inorganic solid. The residue was washed with further water (100 cm<sup>-1</sup>) and dichloromethane (100 cm<sup>-1</sup>). The aqueous fractions were extracted with dichloromethane (100 cm<sup>-1</sup> × 5). The combined organic phase was washed with water (250 cm<sup>-1</sup> × 3), dried over anhydrous sodium sulphate, filtered and solvent was removed. The crude was first purified by column chromatography over silica using dichloromethane: petroleum ether 40-60 mixture (1: 1 to 1: 2) with 1 % triethylamine as eluent. The collected fractions were further purified by subsequent recrystallizations from dichloromethane using methanol and petroleum ether 40-60 to give **3.7** (0.240 g, 0.186 mmol, 14 %) as a deep red powder. Diffraction quality crystals were grown from a dichloromethane: dimethyl sulfoxide solution through the evaporation of dichloromethane. Mp. >350°C.  $T_{d(5\%)} = 416$  °C; Found: C, 53.4; H, 2.8; N, 3.2. C<sub>57</sub>H<sub>33</sub>IrN<sub>3</sub>S<sub>3</sub>Br<sub>3</sub> requires C, 53.2; H, 2.6; N, 3.3; %; IR:  $\bar{\nu}$  solid/cm<sup>-1</sup>= 1487, 1461, 1451, 1425, 1010, 877, 826, 764, 737, 697; UV-Vis:  $\lambda_{max}(\text{CH}_2\text{Cl}_2)/\text{nm}$ : 312 (log  $\epsilon/\text{dm}^3\text{mol}^{-1}\text{cm}^{-1}$  4.53), 263 (4.42), 292 (4.49), 356 sh (4.23), 419 (4.08), 456 sh (3.92), 505 sh (3.57), 581 (3.17); <sup>1</sup>H NMR (500 MHz, CD<sub>2</sub>Cl<sub>2</sub>): 6.03 (3 H, d,  $J = 5.0$  Hz, Th), 6.81-6.84 (3 H, ddd,  $J_{ortho} = 8.5$  Hz,  $J_{ortho} = 7.0$  Hz,  $J_{meta} = 1.5$  Hz, Q), 7.18-7.22 (6 H, m, Th and Q), 7.47-7.50 (6 H, AA`BB`,  $J = 8.5$  Hz, Ph), 7.64 (3 H, s, Q), 7.69-7.74 (9 H, m, Q and Ph), 8.06 (3 H, d,  $J = 8.5$  Hz, Q); m/z (microTOF-Q ES<sup>+</sup>; MNa<sup>+</sup>) 1305.89 (14 %), 1306.90 (10 %), 1307.89 (54 %), 1308.89 (36 %), 1309.89 (100 %), 1310.89 (60 %), 1311.88 (93 %), 1312.89 (51 %), 1313.89 (43 %), 1314.89 (21 %), 1315.90 (11 %); calcd for C<sub>57</sub>H<sub>33</sub>IrN<sub>3</sub>S<sub>3</sub>Br<sub>3</sub>Na<sup>+</sup>, 1305.89 (11 %), 1306.89 (7 %), 1307.89 (53 %), 1308.89 (34 %), 1309.89 (100 %), 1310.89 (62 %), 1311.89 (92 %), 1312.89 (52 %), 1313.89 (42 %), 1314.89 (20 %), 1315.89 (9 %).



### **bis[5-bromo-2-(4-methyl-2-quinolinyl- $\kappa$ N)-3-thienyl- $\kappa$ C]iridium(III), (3.8)**

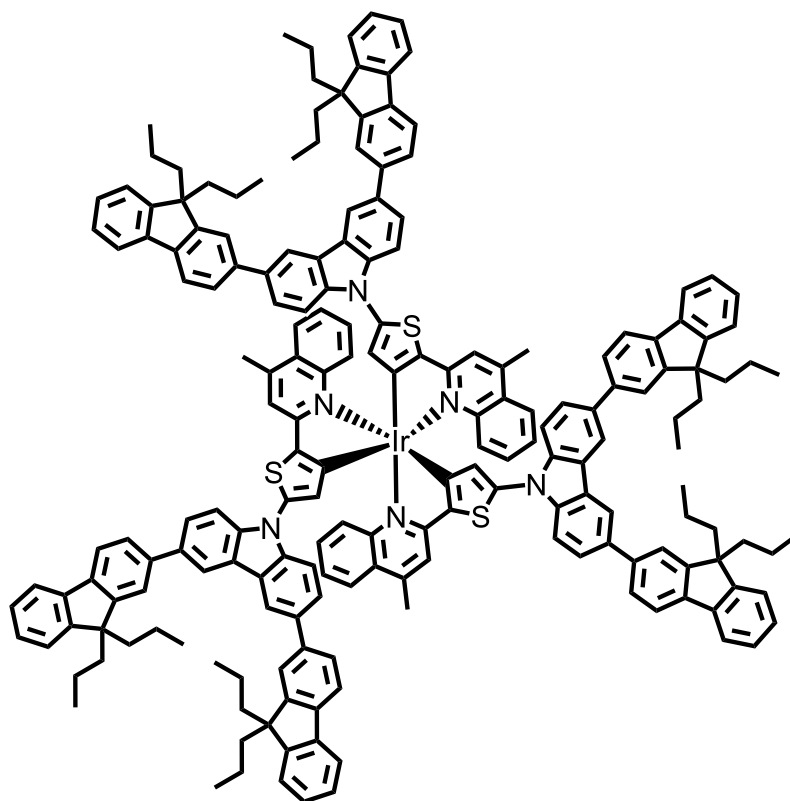
A mixture of **3.4** (0.704 g, 2.31 mmol) and iridium (III) chloride hydrate (0.150 g, 5.39 mmol) were suspended in 2-ethoxyethanol (24 cm<sup>3</sup>) and water (7 cm<sup>3</sup>). The mixture was subjected to three freeze-pump-thaw cycles backfilling with argon. The mixture was heated with stirring in an oil bath set at 130°C for 17 hours. The mixture was allowed to cool to room temperature before being added slowly to a stirred brine solution (100 cm<sup>3</sup>). The precipitate was collected by filtration and washed with water, methanol and diethyl ether. Without further purification

the residue was combined with anhydrous sodium carbonate (0.616 g, 5.81 mmol) and acetylacetone (0.20 cm<sup>3</sup>, 1.95 mmol) in 2-ethoxyethanol (2.5 cm<sup>3</sup>). The mixture was subjected to three freeze-pump-thaw cycles backfilling to argon and heated in an oil bath set at 120°C for 20 hours. The mixture was allowed to cool and precipitation occurred upon addition of petroleum ether 40-60. The residue was dissolved in dichloromethane and passed through a bed of silica. The product was further recrystallized from dichloromethane with methanol and again from dichloromethane with petroleum ether 40-60 to give **3.8** (207 mg, 0.680 mmol, 43 %) as a deep red crystalline material (Estimated from <sup>1</sup>H NMR; 94:6: *trans-N,N*: *cis-N,N*). Diffraction quality crystals were grown through layer diffusion of methanol into a dichloromethane solution. Mp. >310°C; *T*<sub>d(5%)</sub> = 310°C; C, 43.7; H, 3.1; N, 2.9; S, 7.1. C<sub>33</sub>H<sub>25</sub>IrN<sub>2</sub>O<sub>2</sub>S<sub>2</sub>Br<sub>2</sub> requires C, 44.2; H, 3.1; N, 2.9; S, 7.1; %; IR:  $\bar{\nu}$  solid/cm<sup>-1</sup> = 1605, 1582, 1512, 1455, 1424, 1399, 1373, 971, 755, 732; UV-Vis:  $\lambda_{\text{max}}$ (CH<sub>2</sub>Cl<sub>2</sub>)/nm: 294 (log  $\epsilon$ /dm<sup>3</sup>mol<sup>-1</sup>cm<sup>-1</sup> 4.61), 353 (4.44), 429 (3.85), 469 (3.95), 498 (3.92), 596 (2.65); <sup>1</sup>H NMR (500 MHz, CD<sub>2</sub>Cl<sub>2</sub>)  $\delta$ : 1.66 (6 H, s, -CH<sub>3</sub>), 2.89 (6 H, d, *J* = 1 Hz, -CH<sub>3</sub>), 4.94 (1 H, s, enolate-H), 6.14 (2 H, s, Th), 7.47 (2 H, d, *J* = 1 Hz, Q), 7.49-7.53 (4 H, m, Q), 7.93-7.98 (2 H, m, Q), 8.25-8.30 (2 H, m, Q); *m/z* (micrOTOF-Q ES<sup>+</sup>; MNa<sup>+</sup>) 916.9216 (21 %), 917.9251 (8 %), 918.9218 (76 %), 919.9246 (29 %), 920.9214 (100 %), 921.9964 (55 %), 922.9230 (46 %), 923.9226 (17 %), 924.9202 (7 %), 1049.9523 (5 %); calcd for C<sub>33</sub>H<sub>25</sub>IrN<sub>2</sub>O<sub>2</sub>S<sub>2</sub>Br<sub>2</sub>Na<sup>+</sup>, 916.9222 (21 %), 917.9253 (8 %), 918.9253 (78 %), 919.9253 (30 %), 920.9217 (100 %), 921.9246 (38 %), 922.9211 (48 %), 923.9234 (17 %), 924.9213 (8 %), 925.9220 (2 %)



**bis[2-(4-(4-bromophenyl)-2-quinolinyl- $\kappa$ N)-3-thienyl- $\kappa$ C]acetylacetonatoiridium(III), (3.9)**

A mixture of **3.5** (0.482 g, 1.32 mmol) and iridium(III) chloride hydrate (0.147 g, 0.492 mmol) were suspended in 2-ethoxyethanol (24 cm<sup>3</sup>) and water (7 cm<sup>3</sup>). The mixture was subjected to three freeze-pump-thaw cycles backfilling argon. The mixture transferred to a nitrogen atmosphere and heated with stirring in an oil bath set to 130°C for 14.5 hours. The mixture was allowed to cool to room temperature before being added slowly to a stirred brine solution (100 cm<sup>3</sup>). The precipitate was filtered and washed with water, methanol and diethyl ether. The remaining precipitate was dissolved in dichloromethane (100 cm<sup>3</sup>) and filtered. The solvent was removed from the filtrate and anhydrous sodium carbonate (0.476 g, 4.47 mmol), acetylacetone (0.13 cm<sup>3</sup>, 4.47 mmol) and 2-ethoxyethanol (5 cm<sup>3</sup>) were added. The mixture was subjected to three freeze-pump-thaw cycles backfilling to argon and heated in an oil bath set at 120°C for 14.5 hours. The mixture was allowed to cool and precipitation occurred upon addition of water (20 cm<sup>3</sup>). The material was filtered and washed with water (100 cm<sup>3</sup>) and methanol (20 cm<sup>3</sup>) before being dissolved in dichloromethane and passed through a celite plug. The crude product was purified by column chromatography over silica using a dichloromethane:petroleum ether 40-60 fraction mixture (1:2) as eluent. The collected fractions were further recrystallized in dichloromethane/ methanol and dichloromethane/ petroleum ether 40-60 to give **3.9** (41.6 mg, 0.404 mmol, 8 %) as a deep red crystalline material (Estimated from <sup>1</sup>H NMR; 90:10: *trans-N,N*: *cis-N,N*). Single-crystals were grown through layer diffusion of methanol into a dichloromethane solution. Diffraction quality crystals were grown through vapour diffusion of petroleum ether 40-60 into a chlorobenzene solution. Mp. >310°C;  $T_{d(5\%)}$  = 310°C; Found: C, 50.3; H, 3.1; N, 2.8. C<sub>43</sub>H<sub>29</sub>IrN<sub>2</sub>O<sub>2</sub>S<sub>2</sub>Br<sub>2</sub> requires C, 50.5; H, 2.9; N, 2.7; %; IR:  $\bar{\nu}$  solid/cm<sup>-1</sup>= 1450, 1429, 1390, 1010, 824, 760, 738, 731, 714, 690, 582; UV-Vis:  $\lambda_{\max}(\text{CH}_2\text{Cl}_2)/\text{nm}$ : 295 (log  $\epsilon/\text{dm}^3\text{mol}^{-1}\text{cm}^{-1}$  4.65), 268 sh (4.45), 305 sh (4.62), 359 (4.47), 440 (3.88), 485 (3.90), 523 sh (3.84), 596 sh (3.05). <sup>1</sup>H NMR (500 MHz, CD<sub>2</sub>Cl<sub>2</sub>)  $\delta$ : 1.73 (s, -CH<sub>3</sub>, 6 H), 5.01 (s, enolate-H, 1 H), 6.31 (d,  $J$ = 4.8 Hz, Th-H, 2 H), 7.20 (d,  $J$ = 4.8 Hz, Th-H, 2 H), 7.42-7.44 (ddd,  $J_{\text{ortho}}$  = 8.2 Hz,  $J_{\text{ortho}}$  = 6.9 Hz,  $J_{\text{meta}}$  = 1.3 Hz, Q-H, 2H), 7.50-7.53 (ddd,  $J_{\text{ortho}}$  = 8.7 Hz,  $J_{\text{ortho}}$  = 7.5 Hz,  $J_{\text{meta}}$  = 1.5 Hz, Q-H, 2H), 7.54-7.57 (AA`BB`,  $J$ = 8.6 Hz, Ph-H, 4H), 7.75-7.79 (m, Q-H and Ph-H 6 H.), 8.41-8.43 (d,  $J$ = 9.5 Hz, Q-H 2 H); m/z (microTOF-Q ES<sup>+</sup>; MNa<sup>+</sup>) 1040.9506 (22 %), 1041.9535 (11 %), 1042.9515 (79 %), 1043.9541 (40 %), 1044.9508 (100 %), 1045.9539 (48 %), 1046.9505 (52 %), 1047.9529 (23 %), 1048.9519 (10 %), 1049.9523 (5 %); calcd for C<sub>43</sub>H<sub>29</sub>IrN<sub>2</sub>O<sub>2</sub>S<sub>2</sub>Br<sub>2</sub>Na<sup>+</sup>, 1040.9535 (20 %), 1041.9567 (10 %), 1042.9536 (77 %), 1043.9567 (38 %), 1044.9533 (100 %), 1045.9560 (47 %), 1046.9530 (51 %), 1047.9550 (22 %), 1048.9541 (8 %), 1049.9544 (2 %).

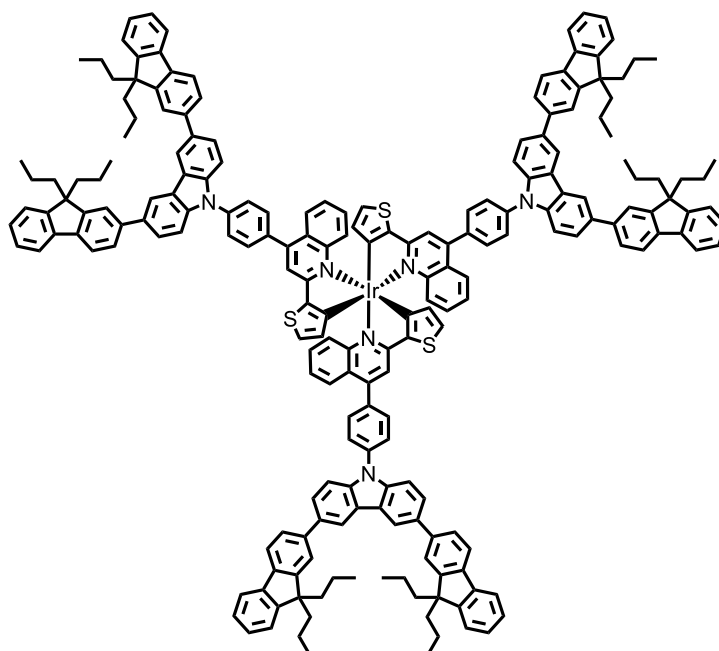


**tris(5-[3,6-bis(9,9-dipropyl-9H-fluoren-2-yl)-9H-carbazol-9-yl]-2-(4-methyl-2-quinolinyl-κM)-3-thienyl-κC}iridium(III) (Hom1)**

A mixture of **3.6** (0.323 g, 0.293 mmol), 3,6-bis(9,9-dipropyl-9H-fluoren-2-yl)-9H-carbazole **2.11** (2.41 g, 3.64 mmol), tris(dibenzylideneacetone)dipalladium(0)-chloroform adduct (0.190 g, 0.181 mmol), tri-*tert*-butylphosphonium tetrafluoroborate (0.107 g, 369 μmol) and sodium *tert*-butoxide (0.415 g, 4.32 mmol) were dissolved in anhydrous toluene (150 cm<sup>3</sup>). The solution was subjected to three cycles of freeze-pump-thaw backfilling with argon. Under continual nitrogen flow the mixture was heated in an oil bath set to 80 °C for 100 hours. After being allowed to cool, dichloromethane (150 cm<sup>3</sup>) and water (150 cm<sup>3</sup>) were added. Separation occurred and the aqueous layer was washed with dichloromethane (3 x 150 cm<sup>3</sup>). The combined organic phase was washed with water (150 cm<sup>3</sup>) and brine (150 cm<sup>3</sup>), dried over anhydrous sodium sulphate, filtered and the solvent was removed under vacuum to afford the crude. The crude material purified over silica gel (pre-treated with a pH 7 aqueous phosphate buffer) using toluene: petroleum ether 40-60 (1: 2) as eluent. The fractions containing the desired material were collected and the solvent was removed. The residue was then passed through a size exclusion chromatography column (Stationary phase: BioRad Laboratories Bio-Beads S-X1 Support #1522151; Mobile phase: toluene). The residue was precipitated from dichloromethane with methanol and the residue was

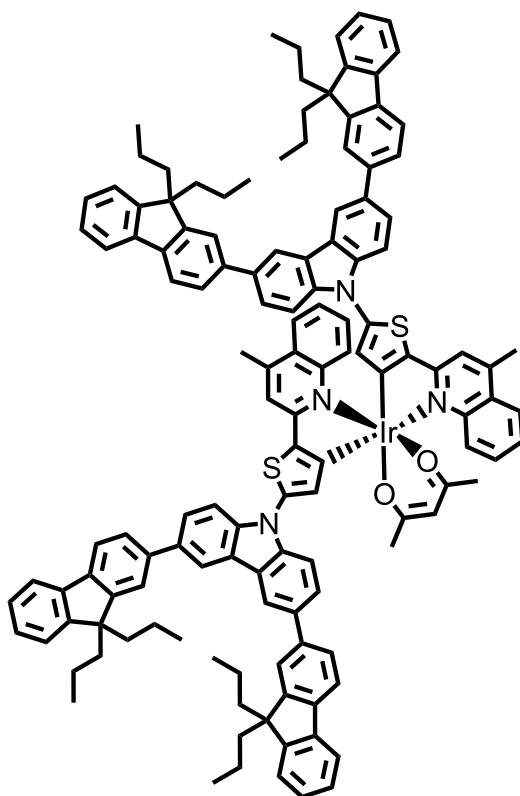


redissolved in dichloromethane and re-precipitated with petroleum ether 40-60 to give **Hom1** (0.164 g, 0.0575 mmol, 20 % over two steps from **[Ir(tmq)<sub>3</sub>]**) as bright orange powder that was a mixture of inseparable regioisomers, predominantly the structure described (no less than 92% described isomer estimated by <sup>1</sup>H NMR). Mp. >350°C; T<sub>d</sub>(5%) = 437 °C. IR:  $\bar{\nu}$  solid/cm<sup>-1</sup>= 1605, 1513, 1463, 1424, 1138, 1071, 871, 756, 731, 697; UV-Vis:  $\lambda_{\text{max}}$  (CH<sub>2</sub>Cl<sub>2</sub>)/nm: 320 (log  $\epsilon$ /dm<sup>3</sup>mol<sup>-1</sup>cm<sup>-1</sup> 5.40), 275 sh (5.17), 295 sh (5.28), 422 (4.68), 438 sh (4.63), 485 sh (4.24). <sup>1</sup>H NMR (500 MHz, CDCl<sub>3</sub>)  $\delta$ : 0.50-0.88 (60 H, m, *n*Pr -CH<sub>2</sub> and -CH<sub>3</sub>), 1.86-2.05 (24 H, m, *n*Pr -CH<sub>2</sub>), 2.88 (9 H, d, *J* = 0.5 Hz, *n*Pr -CH<sub>3</sub>), 6.71 (3 H, s, Th), 6.90-6.94 (3 H, ddd, *J*<sub>ortho</sub> = 8.5 Hz, *J*<sub>ortho</sub> = 7 Hz, *J*<sub>meta</sub> = 1.5 Hz, Q), 7.28-7.37 (21 H, m, Q, Cbz and/or Fl), 7.45 (12 H, m, Fl), 7.50-7.54 (6 H, m, Cbz and/or Fl), 7.59 (3 H, d, *J* = 0.5 Hz, Q), 7.63-7.66 (12 H, m, Cbz and/or Fl), 7.69-7.72 (6 H, m, Cbz and/or Fl), 7.95-7.97 (3 H, dd, *J*<sub>ortho</sub> = 8.5 Hz, *J*<sub>meta</sub> = 1 Hz, Q), 8.20 (3 H, d, *J* = 8.5 Hz, Q), 8.37 (6 H, d, *J* = 1.5 Hz, Cbz); *m/z* (HESI-Orbitrap; M<sup>2+</sup>): 1423.6176 (18 %), 1424.1194 (39 %), 1424.6202 (73 %), 1425.1211 (100 %), 1425.6217 (96 %), 1426.1224 (69 %), 1426.6232 (39 %), 1427.1239 (18 %), 1427.6247 (8 %), 1428.1256 (3 %), calcd for C<sub>192</sub>H<sub>171</sub>IrN<sub>6</sub>S<sub>3</sub><sup>2+</sup>, 1423.6161 (17 %), 1424.1178 (38 %), 1424.6184 (74 %), 1425.1194 (100 %), 1425.6205 (97 %), 1426.1216 (71 %), 1426.6225 (42 %), 1427.1234 (21 %), 1427.6242 (9 %), 1428.1251 (3 %); GPC: M<sub>n</sub> = 1870 Da, Đ = 1.004.



**tris[2-(4-{4-[3,6-bis(9,9-dipropyl-9H-fluoren-2-yl)-9H-carbazol-9-yl]phenyl}quinolin-2-yl-κN)thiophen-3-yl-κC]iridium(III) (Hom2)**

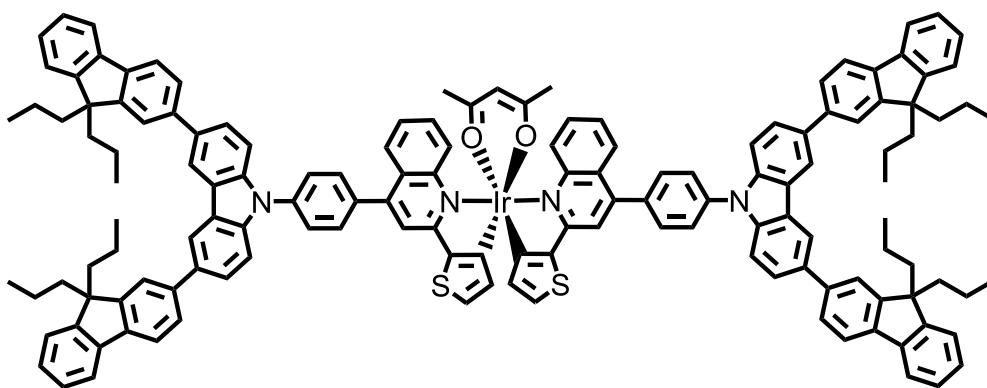
A mixture of **3.7** (0.290 g, 0.225 mmol), **2.11** (0.622g, 0.937 mmol), tris(dibenzylideneacetone)dipalladium(0)-chloroform adduct (0.0150 g, 0.144 mmol), tri-*tert*-butylphosphonium tetrafluoroborate (0.083 g, 0.29 mmol) and sodium *tert*-butoxide (0.192 g, 2.00 mmol) were dissolved in anhydrous toluene (25 cm<sup>3</sup>). The solution was subjected to three cycles of freeze-pump-thaw backfilling to argon. The mixture was heated with stirring under an argon atmosphere in an oil bath set at 80 °C for 44 hours. After being allowed to cool, diethyl ether (25 cm<sup>3</sup>) and water (50 cm<sup>3</sup>) were added. Separation occurred and the aqueous layer was further washed with diethyl ether (3 x 25 cm<sup>3</sup>) and finally dichloromethane (25 cm<sup>3</sup>). The combined organic phase was washed with water (50 cm<sup>3</sup>) and brine (50 cm<sup>3</sup>), dried over anhydrous sodium sulphate filtered, and solvent was removed under vacuum to afford the crude. The residue was passed through a plug of silica using toluene as eluent. The filtrate was collected and the solvent removed. The residue was passed through a size exclusion chromatography column (Stationary phase: BioRad Laboratories Bio-Beads S-X1 Support #1522151; Mobile phase: toluene) followed re-precipitation from dichloromethane with methanol and the residue was redissolved in dichloromethane and re-precipitated with petroleum ether 40-60 to give **Hom2** (0.326 g, 0.107 mmol, 48 %) as bright orange-red powder. Mp. >350°C; T<sub>d</sub>(5%) = 448 °C. IR:  $\bar{\nu}$  solid/cm<sup>-1</sup> = 1599, 1506, 1451, 1356, 1281, 1227, 878, 808, 737, 694; UV-Vis:  $\lambda_{\max}$ (CH<sub>2</sub>Cl<sub>2</sub>)/nm: 320 (log  $\epsilon$ /dm<sup>3</sup>mol<sup>-1</sup>cm<sup>-1</sup> 5.45), 272 (5.20), 292 sh (5.29), 415 (4.46), 461 sh (4.26), 512 sh (3.85). <sup>1</sup>H NMR (500 MHz, CDCl<sub>3</sub>)  $\delta$ : 0.55-0.94 (60 H, m, *n*Pr -CH<sub>2</sub> and -CH<sub>3</sub>), 1.97-2.14 (24 H, m, *n*Pr -CH<sub>2</sub>), 6.20 (3 H, d, *J* = 5 Hz, Th), 6.91-6.95 (3 H, ddd, *J*<sub>ortho</sub> = 8.5 Hz, *J*<sub>ortho</sub> = 7.0 Hz, *J*<sub>meta</sub> = 1.5 Hz, Q), 7.27-7.41 (24 H, m, Q, Th, Cbz and/or FI), 7.69-7.76 (24 H, m, Q, Cbz and/or FI), 7.80-7.84 (15 H, m, Cbz and/or FI), 7.88-7.91 (6 H, AA'BB', *J*<sub>ortho</sub> = 8.5 Hz, Ph), 7.92-7.95 (6 H, AA'BB', *J*<sub>ortho</sub> = 8.5 Hz, Ph), 7.97-8.00 (3 H, dd, *J*<sub>ortho</sub> = 8.5 Hz, *J*<sub>meta</sub> = 1.0 Hz, Q), 8.21-8.24 (3 H, d, *J* = 9 Hz, Q), 8.54 (6 H, d, *J* = 1.5 Hz, Cbz); m/z HESI-Orbitrap; M<sup>2+</sup>): 1516.6394 (13 %), 1517.1410 (34 %), 1517.6418 (72 %), 1518.1428 (97 %), 1518.6440 (100 %), 1519.1450 (75 %), 1519.6462 (42 %), 1520.1473 (23 %), 1520.6481 (11 %), 1521.1497 (4 %); calcd for C<sub>207</sub>H<sub>177</sub>IrN<sub>6</sub>S<sub>3</sub><sup>2+</sup>, 1516.6396 (16 %), 1517.1412 (37 %), 1517.6419 (72 %), 1518.1429 (100 %), 1518.6440 (100 %), 1519.1451 (76 %), 1519.6461 (47 %), 1520.1470 (24 %), 1520.6479 (11 %), 1521.1488 (4 %); GPC: M<sub>n</sub> = 3332 Da, Đ = 1.005.



**bis{5-[3,6-bis(9,9-dipropyl-9H-fluoren-2-yl)-9H-carbazol-9-yl]-2-(4-methyl-2-quinolinyl-κN)-3-thienyl-κC}(acetylacetonato)iridium(III) (Het1)**

A mixture of **3.8** (0.188 g, 0.209 mmol), **2.11** (0.367 g, 0.553 mmol), tris(dibenzylideneacetone)dipalladium(0)-chloroform adduct (0.0435 g, 0.420 mmol), tri-*tert*-butylphosphonium tetrafluoroborate (0.026 g, 0.897 mmol) and sodium *tert*-butoxide (0.125 g, 1.30 mmol) were dissolved in anhydrous toluene (10 cm<sup>3</sup>). The solution was subjected to three cycles of freeze-pump-thaw backfilling with argon. Under argon atmosphere the mixture was heated with stirring in an oil bath set to 80 °C for 46 hours. After being allowed to cool, dichloromethane (20 cm<sup>3</sup>) and water (20 cm<sup>3</sup>) were added. Separation occurred and the aqueous layer was washed with dichloromethane (2 x 20 cm<sup>3</sup>). The combined organic phase was washed with water (20 cm<sup>3</sup>) and brine (20 cm<sup>3</sup>), dried over anhydrous sodium sulphate, filtered and the solvent was removed under vacuum to afford the crude. The crude material passed through a bed of silica in toluene. The collected residue was separated using size exclusion chromatography (Stationary phase: BioRad Laboratories Bio-Beads S-X1 Support #1522151; Mobile phase: toluene: triethylamine, 19:1). The residue was re-precipitated from dichloromethane with methanol and the residue was redissolved in dichloromethane and re-precipitated with petroleum ether 40-60 to give **Het1** (0.143 g, 0.0693 mmol, 33 %) as deep-red powder. Mp. >350°C, T<sub>d</sub>(5%) = 381 °C. UV-Vis: λ<sub>max</sub>

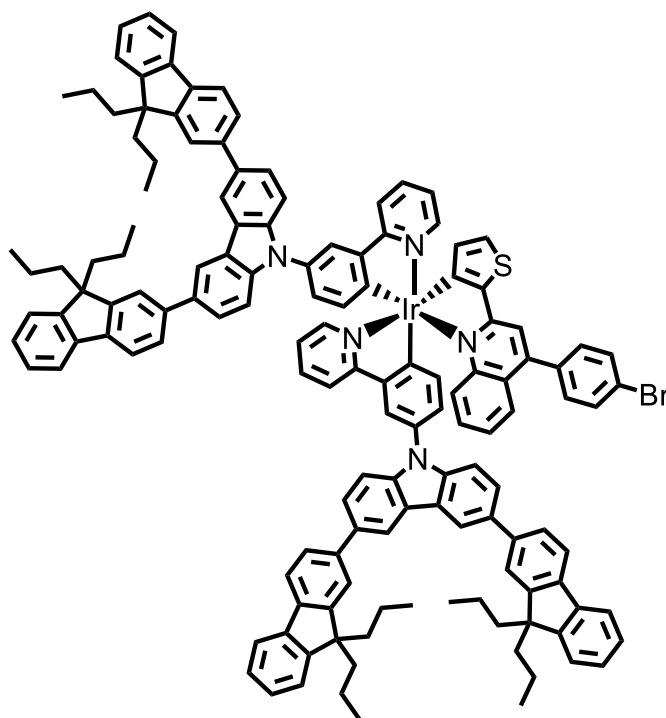
(CH<sub>2</sub>Cl<sub>2</sub>)/nm: 320 (log  $\epsilon$ /dm<sup>3</sup>mol<sup>-1</sup>cm<sup>-1</sup> 5.22), 273 sh (4.96), 294 sh (5.09), 3.78 (4.68), 431 sh (4.34), 481 sh (4.16), 510 (4.13). IR:  $\bar{\nu}$  solid/cm<sup>-1</sup>= 1606, 1581, 1507, 1460, 1435, 1404, 1377, 811, 756, 738; <sup>1</sup>H NMR (500 MHz, CD<sub>2</sub>Cl<sub>2</sub>)  $\delta$ : 0.63-0.86 (40 H, m, *n*Pr -CH<sub>2</sub> and -CH<sub>3</sub>), 1.86 (6 H, s, -CH<sub>3</sub>), 1.98-2.10 (16 H, m, *n*Pr -CH<sub>2</sub>), 2.90 (6 H, d, *J* = 0.5 Hz, -CH<sub>3</sub>), 5.10 (1 H, s, enolate-*H*), 6.52 (2 H, s, Th), 7.30-7.37 (8 H, m, Q, Cbz and/or FI), 7.38-7.41 (4 H, m, Q, Cbz and/or FI), 7.61-7.72 (20 H, m, Q, Cbz and/or FI), 7.73-7.76 (4 H, m, Cbz and/or FI), 7.79-7.73 (6 H, m, Cbz and/or FI), 8.01-8.03 (2 H, dd, *J*<sub>ortho</sub> = 8.5 Hz, *J*<sub>meta</sub> = 1.0 Hz, Q), 8.41 (4 H, d, *J* = 1.5 Hz, Cbz), 8.71 (2 H, d, *J* = 8.5 Hz, Q); *m/z* (HESI-Orbitrap; M<sup>2+</sup>) 1030.4266 (31 %), 1030.9282 (45 %), 1031.4286 (92 %), 1031.9294 (100 %), 1032.4306 (71 %), 1032.9315 (37 %), 1033.4323 (15 %), 1033.9331 (5 %), 1034.4336 (2 %); calcd for C<sub>133</sub>H<sub>121</sub>IrN<sub>4</sub>O<sub>2</sub>S<sub>2</sub><sup>2+</sup>: 1030.4263 (32 %), 1030.9279 (47 %), 1031.4282 (91 %), 1031.9293 (100 %), 1032.4304 (72 %), 1032.9314 (39 %), 1033.4322 (17 %), 1033.9323 (6 %), 1034.4338 (2 %); GPC: M<sub>n</sub> = 1599 Da, Đ = 1.006.



**bis[2-(4-{4-[3,6-bis(9,9-dipropyl-9H-fluoren-2-yl)-9H-carbazol-9-yl]phenyl}quinolin-2-yl-κM)thiophen-3-yl-κC](acetylacetonato)iridium(III) (Het2)**

A mixture of **3.9** (185 mg, 181 μmol), **2.11** (325 mg, 489 μmol), tris(dibenzylideneacetone)dipalladium(0)-chloroform adduct (40.3 mg, 39.0 μmol), tri-*tert*-butylphosphonium tetrafluoroborate (25 mg, 86 μmol) and sodium *tert*-butoxide (98 mg, 1.0 μmol) were dissolved in anhydrous toluene (8 cm<sup>3</sup>). The solution was subjected to three cycles of freeze-pump-thaw backfilling to argon. The mixture was heated with stirring under an argon atmosphere in an oil bath set at 80 °C for 2.5 hours. After being allowed to cool the solvent was removed and the residue was taken up into dichloromethane (100 cm<sup>3</sup>) and water (100 cm<sup>3</sup>). Separation occurred and the aqueous layer was further washed with dichloromethane (100 cm<sup>3</sup> x 2). The combined organic phase was washed with water (100 cm<sup>3</sup>) and brine (100 cm<sup>3</sup>), dried over anhydrous sodium sulphate, filtered, and solvent was

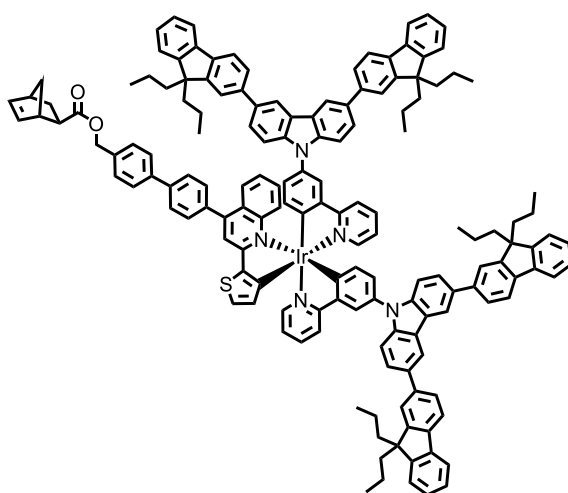
removed under vacuum. Residue was dissolved in a minimum volume of the mobile phase solution desired for the next step (toluene: triethylamine, 19: 1) and passed through a plug of Celite, eluting with additional mobile phase until the eluent became colourless, solvent removed under vacuum. The collected residue was separated in small portions ( $\approx 50$  mg to achieve sufficient separation) using size exclusion chromatography (Stationary phase: BioRad Laboratories Bio-Beads S-X1 Support #1522151; Mobile phase: toluene: triethylamine (19:1)). Following recrystallization from dichloromethane with methanol and additional precipitation from dichloromethane and with petroleum ether 40-60 **Het2** (128 mg, 58.5  $\mu\text{mol}$ , 32 %) was isolated as a dark-red crystalline powder. Diffraction quality crystals were grown by vapour diffusion of methanol into a solution of neat **Het2** in toluene giving extremely reddish-pink, thin rhombus-shaped plates. Mp.  $>332^\circ\text{C}$ ;  $T_d(5\%) = 332^\circ\text{C}$ . UV-Vis:  $\lambda_{\text{max}}(\text{CH}_2\text{Cl}_2)/\text{nm}$ : 319 ( $\log \epsilon/\text{dm}^3\text{mol}^{-1}\text{cm}^{-1}$  5.26), 272 (4.95), 372 sh (4.73), 439 (4.04), 486 (3.99), 522 sh (3.92), 596 sh (3.15). IR:  $\bar{\nu}$  solid/ $\text{cm}^{-1}$  = 2954, 1595, 1511, 1452, 1361, 1277, 1229, 879, 809, 739;  $^1\text{H NMR}$  (500 MHz,  $\text{CD}_2\text{Cl}_2$ ): 0.58-0.92 (40 H, m,  $n\text{Pr}-\text{CH}_2$  and  $-\text{CH}_3$ ), 1.81 (6 H, s,  $-\text{CH}_3$ ), 2.02-2.16 (16 H, m,  $n\text{Pr}-\text{CH}_2$ ), 5.09 (1 H, s, enolate- H), 6.42 (2 H, d,  $J = 5.0$  Hz, Th), 7.28 (2 H, d,  $J = 5.0$  Hz, Th), 7.32-7.35 (4 H, td,  $J_{\text{ortho}} = 7.0$  Hz,  $J_{\text{meta}} = 1.0$  Hz, FI), 7.35-7.39 (4 H, td,  $J_{\text{ortho}} = 7.0$  Hz,  $J_{\text{meta}} = 1.0$  Hz, FI), 7.40-7.44 (4 H, m, FI), 7.53-7.58 (2 H, ddd,  $J_{\text{ortho}} = 8.0$  Hz,  $J_{\text{ortho}} = 7.5$  Hz,  $J_{\text{meta}} = 1.0$  Hz, Q), 7.59-7.63 (2 H, ddd,  $J_{\text{ortho}} = 8.5$  Hz,  $J_{\text{ortho}} = 7.5$  Hz,  $J_{\text{meta}} = 1.5$  Hz, Q), 7.76-7.78 (4 H, m, Cbz), 7.78-7.82 (12 H, m, FI), 7.84-7.887 (6 H, m, Q and FI), 7.88-7.91 (4 H, dd,  $J_{\text{ortho}} = 8.5$  Hz,  $J_{\text{meta}} = 1.5$  Hz, Cbz), 7.95-7.99 (4 H, AA'BB',  $J = 8.5$  Hz, Ph), 8.00-8.03 (4 H, AA'BB',  $J = 8.5$  Hz, Ph), 8.06-8.10 (2 H, dd,  $J_{\text{ortho}} = 8.0$  Hz,  $J_{\text{meta}} = 1.5$  Hz, Q), 8.52-8.55 (2 H, dd,  $J_{\text{ortho}} = 8.5$  Hz,  $J_{\text{meta}} = 1.0$  Hz, Q), 8.62 (4 H, d,  $J = 1.5$  Hz, Cbz).  $m/z$  (HESI-Orbitrap;  $\text{M}^{2+}$ ): 1092.4443 (27 %), 1092.9458 (43 %), 1093.4457 (86 %), 1093.9459 (100 %), 1094.4462 (72 %), 1094.9468 (43 %), 1095.4476 (19 %), 1095.9487 (7 %), 1096.4500 (2 %).; calcd for  $\text{C}_{143}\text{H}_{125}\text{IrN}_4\text{O}_2\text{S}_2^{2+}$ : 1092.4419 (38 %), 1092.9436 (59 %), 1093.4431 (64 %), 1093.9448 (100 %), 1094.4465 (76 %), 1094.9481 (39 %), 1095.4498 (14 %), 1095.9515 (4 %), 1096.4477 (1 %). GPC:  $M_n = 2299$  Da,  $\text{Đ} = 1.007$ .



**{2-[4-(4-bromophenyl)-2-quinolinyl- $\kappa$ N]-3-thienyl- $\kappa$ C}bis{4-[3,6-bis(9,9-dipropyl-9H-fluoren-2-yl)-9H-carbazol-9-yl]-2-(pyridine-2-yl- $\kappa$ M)phenyl- $\kappa$ C}iridium(III) (3.10)**

A mixture of **2.12C** (1.25 g, 1.53 mmol) and iridium(III) chloride hydrate (0.246 g, 0.824 mmol) were suspended in 2-ethoxyethanol (27 cm<sup>3</sup>) and water (7 cm<sup>3</sup>). The mixture was subjected to three freeze-pump-thaw cycles backfilling with argon. The mixture was heated with stirring in an oil bath set at 130°C for 41 hours. The mixture was allowed to cool to room temperature before being added slowly to a stirred brine solution (100 cm<sup>3</sup>). The precipitate was collected by filtration and washed with water (100 cm<sup>3</sup>). The residue was dissolved in dichloromethane (50 cm<sup>3</sup>) and washed with water (50 cm<sup>3</sup>). The aqueous layer was further washed with dichloromethane until fully taken into the organic layer (3 x 50 cm<sup>3</sup>). The combined organic layers were washed with water (3 x 50 cm<sup>3</sup>), dried over anhydrous sodium sulphate, filtered, and solvent removed. Without further purification the residue was combined with **3.5** (3.20 g, 8.74 mmol), silver(I) trifluoroacetate (0.225 g, 1.02 mmol) and "Proton Sponge" (76 mg, 0.355 mmol), and the mixture was subjected to evacuation for 30 minutes backfilling to argon. The mixture was heated in an oil bath set at 180°C with stirring for 21 hours while being monitored by gel-permeation chromatography. Product formation appeared to cease so upon cooling an additional portion of silver(I) trifluoroacetate (0.247 g, 1.118 mmol) was added, the mixture was subjected to evacuation for 30 minutes backfilling to argon and again heated in an oil bath set at 180°C with stirring for a further 22 hours. The mixture was allowed to cool. The residue purified by column chromatography

over silica using a dichloromethane:petroleum ether 40-60 fraction mixture (1:1) as eluent. The collected residue was separated using size exclusion chromatography (Stationary phase: BioRad Laboratories Bio-Beads S-X1 Support #1522151; Mobile phase: toluene) followed precipitation from dichloromethane with methanol and the residue was redissolved in dichloromethane and precipitated with petroleum ether 40-60 to give to give **(3.10)** (157 mg, 71.8  $\mu\text{mol}$ , 9 %) as a deep red crystalline material. Mp. 281-282°C (decomp.). IR:  $\bar{\nu}$  solid/ $\text{cm}^{-1}$  = 1599, 1454, 1268, 1229, 1063, 1027, 878, 811, 781, 739; UV-Vis:  $\lambda_{\text{max}}(\text{CH}_2\text{Cl}_2)/\text{nm}$ : 320 ( $\log \epsilon/\text{dm}^3\text{mol}^{-1}\text{cm}^{-1}$  5.31), 272 (5.05), 408 sh (4.15), 454 (4.00), 493 sh (3.66);  $^1\text{H}$  NMR (500 MHz,  $\text{CDCl}_3$ )  $\delta$ : 0.60-0.90 (40 H, m, *n*Pr - $\text{CH}_2$  and - $\text{CH}_3$ ), 1.95-2.10 (16 H, m, *n*Pr - $\text{CH}_2$ ), 6.63 (1 H, d,  $J = 5.0$  Hz, Th), 6.95 (1 H, d,  $J = 8$  Hz, L), 6.97-7.01 (1 H, m, Q), 7.04-7.07 (1 H, m, L), 7.13-7.18 (3 H, m, Q and L), 7.19-7.22 (1 H, dd,  $J_{\text{ortho}} = 8\text{Hz}$ ,  $J_{\text{meta}} = 2$  Hz, L), 7.27-7.39 (14 H, m, Cbz and Fl), 7.42 (1 H, d,  $J = 5.0$  Hz, Th), 7.49-7.57 (5 H, m, Cbz, Fl and L), 7.57-7.87 (27 H, m, Cbz, Fl, Ph and Q), 7.90-7.93 (3 H, m, L), 7.95-7.98 (2 H, m, L), 8.02-8.06 (1 H, m, Q), 8.47 (2 H, d,  $J = 1.5$  Hz, Cbz), 8.51 (2 H, d,  $J = 1.5$  Hz, Cbz);  $m/z$  (HESI-Orbitrap;  $\text{M}^{2+}$ ) 1092.9036 (15 %), 1093.4052 (29 %), 1093.9056 (76 %), 1094.4064 (100 %), 1094.9068 (98 %), 1095.4073 (83 %), 1095.9083 (56 %), 1096.4091 (23 %), 1096.9100 (4 %); calcd for  $\text{C}_{141}\text{H}_{121}\text{IrN}_5\text{SBr}_2^{2+}$ : 1092.9061 (19 %), 1093.4077 (30 %), 1093.9073 (74 %), 1094.4084 (91 %), 1094.9086 (100 %), 1095.4092 (85 %), 1095.9101 (54 %), 1096.4111 (27 %), 1096.9121 (11 %), 1097.4132 (3 %); GPC:  $M_n = 1726$  Da,  $\text{Đ} = 1.008$ .

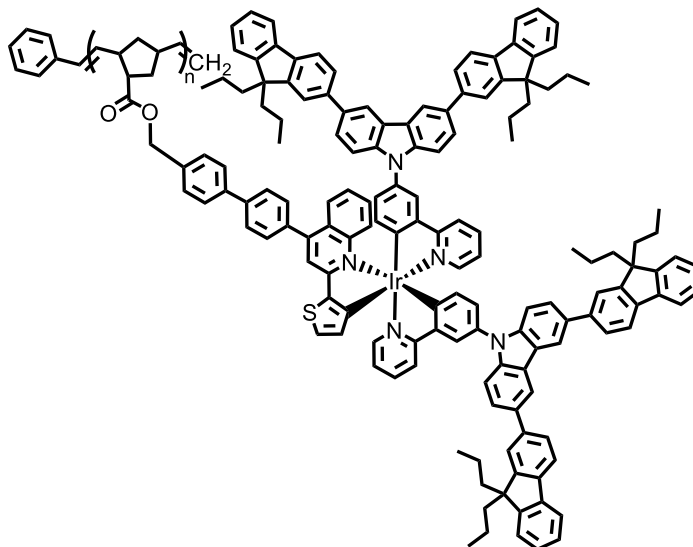


**[4-(4'-{[(bicyclo[2.2.1]hept-5-en-2-ylcarbonyl)oxy]methyl-[1,1'-biphenyl]-4-yl)-2-quinolinyl- $\kappa\text{N}$ }-3-thienyl- $\kappa\text{C}$ ]bis{4-[3,6-bis(9,9-dipropyl-9H-fluoren-2-yl)-9H-carbazol-9-yl]-2-(pyridine-2-yl- $\kappa\text{N}$ )phenyl- $\kappa\text{C}$ }iridium(III) (3.11)**

A mixture of **3.10** (120 mg, 54.8  $\mu\text{mol}$ ) and 4-(hydroxymethyl)phenylboronic acid (18 mg, 119  $\mu\text{mol}$ ) and in toluene (5  $\text{cm}^3$ ), ethanol (2.5  $\text{cm}^3$ ) and 2 M aqueous potassium carbonate (2.5  $\text{cm}^3$ ) was subjected to two cycles of freeze-pump-thaw backfilling with argon. After addition of tetrakis(triphenylphosphine)palladium(0) (10.8 mg, 9.35  $\mu\text{mol}$ ) under a continuous flow of argon, the mixture was subjected to a further two cycles of freeze-pump-thaw backfilling to argon. The mixture was heated under an argon atmosphere at reflux with stirring for 19 hours. After being allowed to cool to ambient temperature water (50  $\text{cm}^3$ ) was added and separation occurred. The aqueous phase was washed with dichloromethane (2  $\times$  50  $\text{cm}^3$ ). The combined organic fractions were washed with water (50  $\text{cm}^3$ ) and brine (50  $\text{cm}^3$ ); dried over anhydrous sodium sulphate, filtered and, solvent removed. The residue was purified via column chromatography over silica using a dichloromethane: petroleum ether 40-60: triethylamine (80:20:1 to 90:10:1) mixture to give the alcohol intermediate (approximately 68.4 mg, 45 %) as a bright red powder. The alcohol was used without further purification due to the observation of oxidation to the aldehyde during handling. To a solution of the isolated alcohol, exo-5-norbornene-2-carboxylic acid (15.2 mg, 110  $\mu\text{mol}$ ) and 4-dimethylaminopyridine (3.9 mg, 31.9  $\mu\text{mol}$ ) in acetonitrile (9  $\text{cm}^3$ , distilled from anhydrous potassium carbonate); a solution of *N,N*'-dicyclohexylcarbodiimide (59.2 mg, 287  $\mu\text{mol}$ ) in acetonitrile (0.5  $\text{cm}^3$ , distilled from anhydrous potassium carbonate) was added dropwise. The mixture was sparged with argon for 30 minutes. The mixture was allowed to stir for 24 hours before the solvent was removed in vacuo. The residue was separated using size exclusion chromatography (Stationary phase: BioRad Laboratories Bio-Beads S-X1 Support #1522151; Mobile phase: toluene followed by column chromatography over silica that had been previously treated with a pH 7 aqueous phosphate buffer using dichloromethane: petroleum ether 40-60 (2: 1) as eluent. Further precipitation from dichloromethane with methanol and again with petroleum ether 40-60 liberated **3.11** as a bright red solid that was observed to fluorescence (optical phenomenon) strongly under ambient light (53.2 mg, 42 %, 2-steps). Mp. 267-268°C (decomp.). IR:  $\bar{\nu}$  solid/ $\text{cm}^{-1}$ = 1723 (C=O, ester); UV-Vis:  $\lambda_{\text{max}}(\text{CH}_2\text{Cl}_2)/\text{nm}$ : 320 (log  $\epsilon/\text{dm}^3\text{mol}^{-1}\text{cm}^{-1}$  5.30), 271 (5.05), 409 sh (4.15), 453 (4.01), 498 sh (3.64);  $^1\text{H}$  NMR (500 MHz,  $\text{CD}_2\text{Cl}_2$ ): 0.53-0.80 (40 H, m, *nPr* - $\text{CH}_2$  and - $\text{CH}_3$ ), 1.37-1.45 (2 H, m, NB - $\text{CH}_2$ ), 1.93-2.13 (18 H, m, *nPr* - $\text{CH}_2$  and NB - $\text{CH}$ ), 2.94 (1 H, m, NB - $\text{CH}$ ), 3.09 (1 H, m, NB - $\text{CH}$ ), 5.20 (2 H, s,  $\text{COOCH}_2$ ), 6.12-6.18 (2 H, m, NB V), 6.63 (1 H, d,  $J = 5.0$  Hz, Th), 6.98-7.00 (1 H, d,  $J = 8.0$  Hz, L), 7.03-7.07 (1 H, ddd,  $J_{\text{ortho}} = 7.0$  Hz,  $J_{\text{ortho}} = 6.0$  Hz,  $J_{\text{meta}} = 1.0$  Hz, Q), 7.10 (1 H, d,  $J = 8.0$  Hz, L), 7.14-7.17 (1 H, dd,  $J_{\text{ortho}} = 8$  Hz,  $J_{\text{meta}} = 2$  Hz, L), 7.18-7.24 (3 H, m, Q and L), 7.28-7.42 (14 H, m, Cbz and Fl), 7.43 (1 H, d,  $J = 5.0$  Hz, Th), 7.50-7.60 (5 H, m, Cbz, Fl and L), 7.67-7.89 (31 H, m, Cbz, Fl, Ph and Q), 7.91-7.96 (1



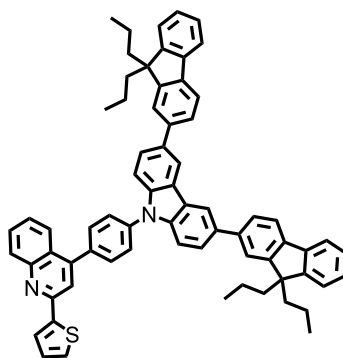
H, dd,  $J_{ortho} = 8.5 \text{ Hz}$ ,  $J_{meta} = 1.5 \text{ Hz}$ , Q), 7.97-8.02 (3 H, m, L), 8.02-8.06 (2 H, m, L), 8.10-8.12 (1 H, dd,  $J_{ortho} = 6.0 \text{ Hz}$ ,  $J_{meta} = 1.0 \text{ Hz}$ , Q), 8.52 (2 H, d,  $J = 1.5 \text{ Hz}$ , Cbz), 8.57 (2 H, d,  $J = 1.5 \text{ Hz}$ , Cbz); m/z (HESI-Orbitrap;  $M^{2+}$ ) 1167.0030 (27 %), 1167.5049 (47 %), 1168.0052 (88 %), 1168.5063 (100 %), 1169.0076 (82 %), 1169.5087 (46 %), 1170.0098 (20 %), 1170.5111 (7 %), 1171.0124 (2 %); calcd for  $C_{156}H_{136}IrN_5O_2S^{2+}$ : 1167.0005 (26 %), 1167.5021 (45 %), 1168.0026 (83 %), 1168.5037 (100 %), 1169.0050 (78 %), 1169.5063 (45 %), 1170.0075 (20 %), 1170.5087 (7 %), 1171.0099 (2 %); GPC:  $M_n = 2031 \text{ Da}$ ,  $\bar{D} = 1.006$ .



**[4-(4'-{[(bicyclo[2.2.1]hept-5-en-2-ylcarbonyl)oxy]methyl-[1,1'-biphenyl]-4-yl)-2-quinolinyl-κM)-3-thienyl-κC]bis{4-[3,6-bis(9,9-dipropyl-9H-fluoren-2-yl)-9H-carbazol-9-yl]-2-(pyridine-2-yl-κM)phenyl-κC}iridium(III), homopolymer (PDcR)**

The dried components were prepared in separate vessels which were subjected to three cycles of evacuation and backfilling to argon prior to the addition of solvent. The solvent was dichloromethane which was freshly distilled from calcium hydride and in a separate vessel subjected to three cycles of freeze-pump-thaw backfilling to argon. To a solution of Grubb's 3<sup>rd</sup> generation catalyst (0.10 cm<sup>3</sup>, 3.00 mM, 0.30 μmol) in dichloromethane under argon, a solution of **3.11** (69.0 mg, 29.5 μmol) in dichloromethane (0.3 cm<sup>3</sup>) was added by cannula with vigorous stirring. The reaction mixture appeared to rapidly form insoluble aggregates indicating insufficient solubility to complete polymerization at this concentration; therefore, a further portion of dichloromethane (0.6 cm<sup>3</sup>) was used to transfer any residual monomer into the reaction vessel and aid solubility. After 22 hours of stirring under an argon atmosphere ethyl vinyl ether (0.1 cm<sup>3</sup>, 887 μmol) was injected rapidly with continued stirring and after 30 minutes solvent was removed in vacuo. The residue was sequentially redissolved in

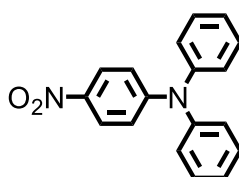
dichloromethane and precipitated with methanol, acetone and, petroleum spirits 40-60 to give **PDcR** as a vibrant red powder (57.1 mg, 83 %). IR:  $\bar{\nu}$  solid/cm<sup>-1</sup>= 1735 (C=O, ester); UV-Vis:  $\lambda_{\text{max}}$ (CH<sub>2</sub>Cl<sub>2</sub>)/nm: 320, 271, 407 sh, 454 sh, 505 sh; <sup>1</sup>H NMR (500 MHz, CD<sub>2</sub>Cl<sub>2</sub>): 0.45-0.78 (40 H, m, *n*Pr CH<sub>2</sub>, CH<sub>3</sub>), 1.83-2.10 (16 H, m, *n*Pr CH<sub>2</sub>), 2.4-2.7 (2 H, m, NB), 6.55-6.70 (1 H, m, Th), 6.89-8.09 (64 H, m, Fl, Cbz, T, Th, Q, PhPy) 8.42-8.60 (4 H, m, Cbz), other norbornenyl-proton signals lost in baseline; GPC: M<sub>n</sub> = 164 kDa, Đ = 2.4.



### 3,6-bis(9,9-dipropyl-9H-fluoren-2-yl)-9-(4-(2-(thiophen-2-yl)quinolin-4-yl)phenyl)-9H-carbazole (tDcpq)

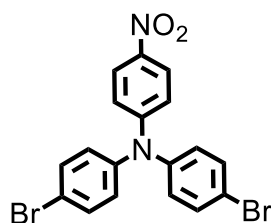
A mixture of **3.5** (0.216 g, 0.589 mmol), **2.11** (0.407 g, 0.739 mmol), tris(dibenzylideneacetone)dipalladium(0)-chloroform adduct (0.076 g, 0.0734 mmol), tri-*tert*-butylphosphonium tetrafluoroborate (0.052 g, 0.179 mmol) and sodium *tert*-butoxide (0.501 g, 5.21 mmol) were dissolved in anhydrous toluene (10 cm<sup>3</sup>). The solution was sparged with argon for 30 minutes. The mixture was heated with stirring an oil bath set at 80 °C for 75 hours. After being allowed to cool ethyl acetate (20 cm<sup>3</sup>) and water (20 cm<sup>3</sup>) were added. Separation occurred and the aqueous layer was further washed with ethyl acetate (3 x 20 cm<sup>3</sup>). The combined organic phase was washed with water (20 cm<sup>3</sup>) and brine (20 cm<sup>3</sup>), dried over anhydrous sodium sulphate filtered, and solvent was removed under vacuum. The crude material was purified by column chromatography over silica using an ethyl acetate: petroleum ether 40-60 mixture (6: 94) as eluent to give **tDcpq** (0.349 g, 0.368 mmol, 62 %) as a very pale yellow solid. Mp. 243-244°C. T<sub>d(5%)</sub> = 442°C. Found: C, 87.1; H, 6.1; N, 3.0. C<sub>69</sub>H<sub>60</sub>N<sub>2</sub>S requires C, 87.3; H, 6.4; N, 3.0; %; IR:  $\bar{\nu}$  solid/cm<sup>-1</sup>= 1600, 1511, 1452, 1367, 1271, 1231, 829, 803, 737, 706; UV-Vis:  $\lambda_{\text{max}}$ (CH<sub>2</sub>Cl<sub>2</sub>)/nm: 321 (log  $\epsilon$ /dm<sup>3</sup>mol<sup>-1</sup>cm<sup>-1</sup> 4.95), 274 (4.75), 290 (4.82), 334 sh (4.92); <sup>1</sup>H NMR (300 MHz, CDCl<sub>3</sub>)  $\delta$ : 0.65-0.92 (20 H, m, *n*Pr CH<sub>2</sub>H<sub>3</sub>), 2.0-2.16 (8 H, m, *n*Pr CH<sub>2</sub>), 7.20-7.24 (1 H, dd, J<sub>1</sub>= 5.0 Hz, J<sub>2</sub>= 3.0 Hz, Th), 7.30-7.42 (6 H, m, Cbz and/ or Fl), 7.52-7.60 (2 H, m, Cbz), 7.68-7.91 (19 H, m, Th, Q, Ph, Cbz

and Fl), 8.01-8.06 (1 H, d,  $J = 8.5$  Hz, Q), 8.20-8.31 (1 H, m, Q), 8.55 (2 H, d,  $J = 1.5$  Hz, Cbz).  $m/z$  (HESI-Orbitrap;  $M+H^+$ ) 949.4575 (100 %), 950.4602 (78 %), 951.4618 (32 %), 952.4633 (9 %); calcd for  $C_{69}H_{60}N_2SH^+$ ; 949.4550 (100 %), 950.4583 (79%), 951.4602 (35 %), 952.4616 (11 %).



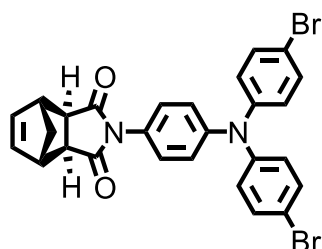
#### 4-nitrotriphenylamine (**5.1**)

4-nitrotriphenylamine (**5.1**) was synthesized according to a literature procedure.<sup>205</sup> Diphenylamine (0.502 g, 2.97 mmol) was added to a mixture of 60 % sodium hydride in paraffin oils (0.260 g, 6.50 mmol) in dry *N,N*-dimethylacetamide (3 cm<sup>3</sup>) under argon and stirred for 30 min. The mixture was cooled in an ice bath and 4-fluoro-1-nitrobenzene (0.4 cm<sup>3</sup>, 3.77 mmol) was added dropwise. The mixture was heated at 100°C for 1 h. The mixture was allowed to cool to room temperature and poured onto chilled 3M hydrochloric acid solution (20 cm<sup>3</sup>) and filtered. The filtrate was purified by column chromatography over silica using a dichloromethane: petroleum ether mixture (1:2) as eluent to give **5.1** (0.820 g, 95%) as a bright yellow solid. <sup>1</sup>H NMR (300 MHz, CDCl<sub>3</sub>)  $\delta$ : 6.90-6.97 (2 H, AA'BB',  $J_{AB} = 9.5$  Hz,  $J_{AB'} = 3.5$  Hz,  $J_{AA'} = 2.0$  Hz), 7.16-7.25 (6 H, m), 7.34-7.41 (4 H, m), 8.01-8.08 (2 H, AA'BB',  $J_{AB} = 9.5$  Hz,  $J_{AB'} = 3.5$  Hz,  $J_{AA'} = 2.0$  Hz); <sup>13</sup>C NMR (75 MHz, CDCl<sub>3</sub>)  $\delta$ : 118.3, 125.6, 125.9, 126.7, 130.1, 145.81, 153.6;  $m/z$  (ESI-HCT;  $[MNa]^+$ ) 313.2; calcd for  $C_{18}H_{14}N_2O_2Na^+$ ; 313.1. The <sup>1</sup>H NMR <sup>13</sup>C NMR and mass spectra were consistent with the literature values.<sup>206</sup>



### ***N,N*-bis(4-bromophenyl)-4-nitrophenylamine (5.2)**

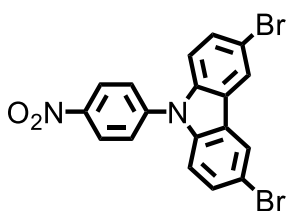
*N,N*-bis(4-bromophenyl)-4-nitrophenylamine (**5.2**) was synthesized according to a literature procedure.<sup>207</sup> A solution of *N*-bromosuccinimide (1.29 g, 7.23 mmol) in *N,N*-dimethylformamide (4 cm<sup>3</sup>) was added dropwise to a solution of **5.1** (1.00 g, 3.45 mmol) in *N,N*-dimethylformamide (7 cm<sup>3</sup>) with stirring. The mixture was stirred for two days. Water (20 cm<sup>3</sup>) was added to the mixture and **5.2** (1.52 g, 98%) was obtained as a bright orange solid via filtration. Further purification was not required. <sup>1</sup>H NMR (300 MHz, CDCl<sub>3</sub>) δ: 6.93-6.99 (2 H, AA'BB', *J*<sub>AB</sub> = 9.5 Hz, *J*<sub>AB'</sub> = 3.5 Hz, *J*<sub>AA'</sub> = 2.0 Hz), 7.00-7.06 (4 H, AA'BB', *J*<sub>AB</sub> = 9.0 Hz, *J*<sub>AB'</sub> = 3.0 Hz, *J*<sub>AA'</sub> = 2.0 Hz), 7.44-7.51 (4 H, AA'BB', *J*<sub>AB</sub> = 9.0 Hz, *J*<sub>AB'</sub> = 3.0 Hz, *J*<sub>AA'</sub> = 2.0 Hz), 8.04-8.10 (2 H, AA'BB', *J*<sub>AB</sub> = 9.5 Hz, *J*<sub>AB'</sub> = 3.5 Hz, *J*<sub>AA'</sub> = 2.0 Hz); *m/z* (ESI-HCT; [MNa]<sup>+</sup>) 470.7; calcd for C<sub>18</sub>H<sub>12</sub>N<sub>2</sub>O<sub>2</sub>Br<sub>2</sub>Na<sup>+</sup>; 470.9. The <sup>1</sup>H NMR and mass spectra were consistent with the literature values.<sup>208</sup>



### **(3aR,4R,7S,7aS)-2-{4-[bis(4-bromophenyl)amino]phenyl}-3a,4,7,7a-tetrahydro-1H-4,7-methanoisoindole-1,3(2H)-dione (5.3)**

A mixture of **5.2** (0.138 g, 0.308 mmol), *cis*-5-norbornene-*exo*-2,3-dicarboxylic anhydride (0.0509 g, 0.310 mmol) and iron powder (0.0997g, 1.79 mmol) in acetic acid (10 cm<sup>3</sup>) was heated at reflux with stirring under a nitrogen flow for two hours. After cooling to room temperature the light grey precipitate was collected by filtration and washed thoroughly with water. The precipitate was dissolved in dichloromethane (10 cm<sup>3</sup>) and washed with water (10 cm<sup>3</sup>). The aqueous layer was further extracted with dichloromethane (10 cm<sup>3</sup>, twice) and the combined organic layers were washed with water (10 cm<sup>3</sup>) and brine (10 cm<sup>3</sup>). The

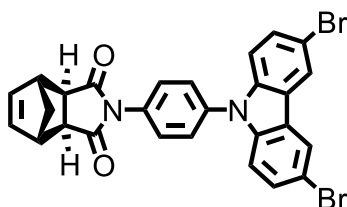
organic layers were tried over anhydrous magnesium sulphate, filtered and the solvent was removed. The crude was purified by column chromatography over silica gel using ethyl acetate: petroleum ether (1:3) as eluent to give **5.3** (0.151 mg, 87%) as a colourless solid. Mp. 162-163°. Found: C, 57.6; H, 3.6; N, 4.9.  $C_{27}H_{20}N_2O_2Br_2$  requires C, 57.5; H, 3.6; N, 5.0 %; IR:  $\bar{\nu}$  solid/cm<sup>-1</sup> = 1706 (imide, C=O); UV-Vis:  $\lambda_{max}(CH_2Cl_2)/nm$ : 311 (log  $\epsilon/dm^3mol^{-1}cm^{-1}$  4.41). <sup>1</sup>H NMR (300 MHz, CDCl<sub>3</sub>): 1.42-1.49 (1 H, m, NB CH<sub>2</sub>), 1.58-1.66 (1 H, m, NB CH<sub>2</sub>), 2.85 (2 H, d,  $J = 1$  Hz, NB CH), 3.40 (2 H, m, NB CH), 6.35 (2 H, t,  $J = 1.5$  Hz, NB V), 6.94-7.00 (4 H, AA'BB',  $J_{AB} = 9.5$ ,  $J_{AB'} = 3.0$  Hz,  $J_{AA'} = 2.0$  Hz, Ph), 7.06-7.11 (2 H, AA'BB',  $J_{AB} = 9.0$ ,  $J_{AB'} = 2.5$  Hz,  $J_{AA'} = 2.0$  Hz, Ph), 7.12-7.17 (2 H, AA'BB',  $J_{AB} = 9.0$ ,  $J_{AB'} = 2.5$  Hz,  $J_{AA'} = 2.0$  Hz, Ph), 7.33-7.40 (4 H, AA'BB',  $J_{AB} = 9.5$ ,  $J_{AB'} = 3.0$  Hz,  $J_{AA'} = 2.0$  Hz, Ph); <sup>13</sup>C NMR (75 MHz, CDCl<sub>3</sub>): 43.1, 46.0, 48.0, 116.5, 123.8, 126.2, 126.6, 127.5, 132.7, 138.1, 146.1, 147.2, 177.4.  $m/z$  (microTOF-Q ES<sup>+</sup>; MNa<sup>+</sup>) 584.9760 (53 %), 585.9797 (16 %), 586.9743 (100 %), 587.9774 (30 %), 588.9732 (54 %), 589.9758 (16 %); calcd for  $C_{27}H_{20}N_2O_2Br_2Na^+$ , 584.9790 (51 %), 585.9822 (15 %), 586.9769 (100 %), 587.9802 (30 %), 588.9749 (49 %), 589.9782 (15 %).



### 3,6-dibromo-9-(4-nitrophenyl)-9H-carbazole (**5.4**)

3,6-dibromo-9-(4-nitrophenyl)-9H-carbazole (**5.4**) was synthesized according to a literature procedure.<sup>209</sup> A mixture of **2.10** (0.522 g, 1.61 mmol), 4-fluoro-1-nitrobenzene (0.7 cm<sup>3</sup>, 6.60 mmol) and potassium carbonate (1.11 g, 8.05 mmol) in dry *N,N*-dimethylformamide was heated to reflux under argon for 2 days. The mixture was allowed to cool to room temperature. The mixture was poured onto warm water (40°C, 40 cm<sup>3</sup>) and allowed to stir for 1 h. Dichloromethane was added (20 cm<sup>3</sup>) and the organic layer was separated. The aqueous layer was extracted with dichloromethane (2 × 20 cm<sup>3</sup>) and the combined organic layers were extracted with water (5 × 20 cm<sup>3</sup>), dried over anhydrous sodium sulfate, filtered and solvent removed. The residue was purified by column chromatography over silica using toluene: petroleum ether (2: 3) as eluent to give **5.4** (0.590 g, 82%) as a bright yellow solid. <sup>1</sup>H NMR (300 MHz, CDCl<sub>3</sub>)  $\delta$ : 7.31-7.36 (2 H, dd,  $J_{ortho} = 8.5$  Hz,  $J_{meta} = 0.5$  Hz), 7.53-7.59 (2 H, dd,  $J_{ortho} = 9.0$  Hz,  $J_{meta} = 2.0$  Hz), 7.71-7.77 (2 H, AA'BB',  $J_{AB} = 9.5$  Hz,  $J_{AB'} = 3.0$  Hz,

$J_{AB} = 2.0$  Hz), 8.21-8.23 (2 H, dd,  $J_{para} = 2.0$  Hz,  $J_{meta2} = 0.5$  Hz), 8.48-8.53 (2 H, AA'BB',  $J_{AB} = 9.5$  Hz,  $J_{AB'} = 3.0$  Hz,  $J_{AB''} = 2.0$  Hz);  $m/z$  (HESI-Orbitrap; MCl<sup>-</sup>): 478.8774 (43 %), 479.8812 (8 %), 480.8754 (100 %), 481.8785 (20 %), 482.8732 (70 %), 483.8763 (14 %), 484.8709 (15 %); calcd for C<sub>18</sub>H<sub>10</sub>N<sub>2</sub>O<sub>2</sub>Br<sub>2</sub>Cl<sup>-</sup>: 478.8797 (44 %), 479.8830 (9 %), 480.8775 (100 %), 481.8808 (20 %), 482.8753 (70 %), 483.8786 (14 %), 484.8728 (14 %). The <sup>1</sup>H NMR and mass spectra were consistent with the literature values.<sup>209</sup>



**(3aR,4R,7S,7aS)-2-[4-(3,6-dibromo-9H-carbazol-9-yl)phenyl]-3a,4,7,7a-tetrahydro-1H-4,7-methanoisoindole-1,3(2H)-dione (5.6)**

To a refluxing, stirred slurry of **3.4** (0.406 g, 0.910 mmol) in aqueous hydrochloric acid (37 %, 10 cm<sup>3</sup>) and ethanol (13 cm<sup>3</sup>); iron powder (0.706 g, 12.6 mmol) was added while maintaining a constant nitrogen flow. After three hours of refluxing, with stirring under a nitrogen atmosphere, the mixture the reaction had not progressed to completion; concluded from thin-layer chromatography and the absence of a complete colour change (vibrant yellow to colourless). An additional portion of iron powder (1.13 g, 20.3 mmol) and ethyl acetate (5 cm<sup>3</sup>) was added maintaining a constant nitrogen flow. The stirred mixture was refluxed under a nitrogen atmosphere for two hours and then allowed to cool. Much of the iron powder was being lost on the solvent wet glass so a final portion of iron powder (1.37 g, 24.6 mmol) wrapped in aluminium foil (80 mg, 3.0 mmol). The aluminium aided in rapid addition of the iron powder and is also a known reducing agent for some nitroaromatics and may have participated as well. Upon refluxing for a further two hours with stirring under a nitrogen atmosphere the reaction reached completion and was cooled. Aqueous sodium hydroxide (100 cm<sup>3</sup>) and dichloromethane (100 cm<sup>3</sup>) were added. The collected aqueous phase was washed with dichloromethane (3 × 100 cm<sup>3</sup>). The combined organic layer was washed with water (100 cm<sup>3</sup>), dried over anhydrous sodium sulphate, filtered, and solvent removed. The crude, a colourless powder, was used without further purification. The crude amine and *cis*-5-norbornene-*exo*-2,3-dicarboxylic anhydride (0.154 g, 0.937 mmol) were dissolved together in *N,N'*-dimethylformamide (2 cm<sup>3</sup>) and stirred under argon at ambient temperature for four hours. Acetic anhydride (0.35 cm<sup>3</sup>, 3.7 mmol) and pyridine (0.6 cm<sup>3</sup>,

7.4 mmol) were added to the mixture. Stirring at room temperature was maintained for one hour followed by heating at 90°C for 17 hours. After being allowed to cool the reaction mixture was directly transferred and purified by column chromatography over silica using ethyl acetate: petroleum ether 40-60 (1:3 to 2:3) as eluent. Recrystallization from dichloromethane with methanol and petroleum ether 40-60 to give **5.6** (98.7 mg, 0.176 mmol, Y = 19 %) as a colourless powder. Mp. 286-288°C (decomp.). Found: C, 57.2; H, 3.1; N, 4.8.  $C_{27}H_{18}Br_2N_2O_2$  requires C, 57.7; H, 3.2; N, 5.0 %. IR:  $\bar{\nu}$  solid/cm<sup>-1</sup> = 1703 (C=O, imide); UV-Vis:  $\lambda_{max}$ (CH<sub>2</sub>Cl<sub>2</sub>)/nm: 244 (log  $\epsilon$ /dm<sup>3</sup>mol<sup>-1</sup>cm<sup>-1</sup> 4.71), 236 sh (4.68), 271 (4.39), 296 (4.37), 302 (4.44), 330 sh (3.41), 342 (3.58), 356 (3.61). <sup>1</sup>H NMR (500 MHz, CD<sub>2</sub>Cl<sub>2</sub>): 1.48-1.52 (1 H, d,  $J$  = 10.0 Hz, NB CH<sub>A</sub>H<sub>B</sub>), 1.63-1.66 (1 H, dt,  $J_{ipso}$  = 10.0 Hz,  $J_{alpha}$  = 1.5 Hz, NB CH<sub>B</sub>H<sub>A</sub>), 2.91 (2 H, d,  $J$  = 1.0 Hz, NB CH), 3.41 (2 H, t,  $J$  = 1.5 Hz, NB CH), 6.93 (2 H, t,  $J$  = 1.5 Hz, NB V), 7.34-7.36 (2 H, d,  $J$  = 9.0 Hz, Cbz), 7.53-7.59 (4 H, m, Cbz and Ph), 7.63-7.67 (2 H, AA'BB',  $J_{AB}$  = 9.0 Hz,  $J_{AB'}$  = 2.5 Hz,  $J_{AA'}$  = 2.0 Hz, Ph), 8.22 (2 H, d,  $J$  = 2.0 Hz, Cbz). <sup>13</sup>C NMR (125 MHz, CD<sub>2</sub>Cl<sub>2</sub>). 43.2, 46.2, 48.2, 111.8, 113.4, 123.4, 124.3, 127.5, 128.3, 129.7, 131.8, 136.8, 138.2, 139.9, 177.0.  $m/z$  (microTOF-Q ES<sup>+</sup>; MNa<sup>+</sup>) 582.9636 (52 %), 584.9617 (100 %), 585.9649 (32 %), 586.9602 (53 %), 587.9628 (15 %); calcd for  $C_{27}H_{18}Br_2N_2O_2 + Na^+$ , 582.9633 (51 %), 583.9666 (15 %), 584.9612 (100 %), 585.9645 (30 %), 586.9592 (49 %), 587.9625 (14 %), 588.9656 (2 %).

## Conclusions and Future Outlook

---

The work presented within this thesis has demonstrated that dendrimer and poly(dendrimer) architectures provide a synthetic route to highly efficient solution processable organic light-emitting diodes for displays or lighting applications. To advance the scientific understanding of organic, dendrimeric semiconductors for organic light-emitting diodes; a series of new poly(dendrimer)s and dendrimers containing phosphorescent iridium(III) complexes were designed, synthesized and characterized.

Building upon the foundation laid by previously reported materials, two poly(dendrimer)s containing green-emissive phosphorescent iridium(III) complexes were synthesized with the aim of improving control of the polymerization reaction by increasing the length of the tether which connects the emissive pendants to the polymer backbone. While both poly(dendrimer)s, **PD<sub>B</sub>** and **PD<sub>C</sub>**, were found to be solution processable emitters with decent photoluminescence quantum yields ( $55 \pm 6\%$  and  $56 \pm 6\%$ , respectively); both exhibited quenching resulting from intra-chain interchromophore interactions not present in the reported materials. Additionally, neither showed improved polymerization control with both poly(dendrimer)s being isolated with large dispersity indices.

Unexpectedly, when employed as the emissive species within OLEDs, the carbazolyl-dendronized **PD<sub>C</sub>** showed very high maximum external quantum efficiencies (19%). It was determined that, for the measured photoluminescence quantum yields ( $\Phi_{\text{PL}}$ ), the outcoupling efficiency of the devices utilizing **PD<sub>C</sub>** were greater than that expected of an isotropic emitter. This was particularly interesting as solution processed organic light-emitting diodes were reported as having only randomly distributed emissive species leading to an overall isotropic emission. The ability to fabricate devices with improved outcoupling efficiency is also shared by the related poly(dendrimer) **L2** strengthening the conclusion that poly(dendrimer)s of this structure may participate in preferential alignment leading to increased outcoupling efficiency and therefore increased external quantum efficiencies.

While both poly(dendrimer)s and dendrimers containing green-emissive iridium(III) complexes have been explored thoroughly; there were not any thorough investigations into whether their reported advantages would transfer to saturated red-emissive iridium(III) complexes. To investigate this a series of structurally related dendrimers utilizing first generation carbazolyl-dendrons were designed and synthesized. In order to derive



information through comparison, each dendrimer was structurally related to another by either having identical dendronized ligand structure or sharing the same coordination complex (i.e. *tris*-bidentate *facial* homoleptic complex versus *N,N'*-*trans*, *cis*-*C,C'* heteroleptic complex with acetylacetonato ancillary ligand). This gave four interrelated dendrimers with either the first ligand type where the carbazoyl-dendron coupled to the thiophene moiety of the ligand (**Hom1** and **Het1**) or the second ligand type where the carbazoyl-dendron has been coupled through a phenyl moiety (**Hom2** and **Het2**).

All red-emitting dendrimers were found to exhibit excellent photophysical properties for their application in organic light-emitting diodes. In solution **Hom1**, **Hom2**, **Het1** and **Het2** were found to have photoluminescence quantum yields of  $74 \pm 7 \%$ ,  $86 \pm 9 \%$ ,  $66 \pm 7 \%$  and  $61 \pm 6 \%$ , respectively. When deposited as neat films the photoluminescence quantum yields were found to decrease substantially from the introduction of non-radiative decay pathways through inter-molecular interchromophore interactions. The obtained neat film photoluminescence quantum yields;  $7.1 \pm 1.3 \%$ ,  $2.8 \pm 1.0 \%$  and  $8.6 \pm 1.5 \%$  for **Hom2**, **Het1** and **Het2**, respectively; were much lower in respect to their solution values when compared to the previously reported green-emissive dendrimer **L3**. On the other hand, **Hom1** showed a decrease from  $74 \%$  to  $19 \pm 2 \%$  which was quite comparable to that reported for the green-emitting dendrimer from  $82 \pm 8 \%$  to  $20 \pm 3 \%$ ; when transitioning from solution to neat film, respectively. This provided insight into how dendrons effectiveness at separating the phosphorescent chromophores to impede interchromophore quenching is dependent upon dendron position. It is believed that in **Hom1** the dendrons are in close proximity to one another creating a large volume in which other molecules cannot approach. In contrast, the dendrons of **Hom2** are believed to project outward from the complex along a shared like a three-bladed fan. Neighbouring chromophores may approach **Hom2** closely from either direction perpendicular to the plane of the dendrons. The heteroleptic iridium(III) complexes, **Het1** and **Het2**, allow for very close interchromophore distances due to the volume surrounding the acetylacetonate ligand being unprotected by the dendrons. These neat film photoluminescence quantum yields suggested that the dendrons were not sufficiently reducing interchromophore interactions for the materials to produce efficient host-free OLEDs. However, when distributed throughout a common host the photoluminescence quantum yield of the blend films were found to be comparable to the excellent values obtained in solution; with the notable exception of **Het2**.

Throughout the project the heteroleptic complex, **Het2**, was observed to have unusually low solubility for a dendrimer as well as a propensity towards crystallization. This

property was exploited for purification and growth of a crystal from which the structure was determined by single-crystal X-ray diffraction. Unfortunately, this property was also deleterious for the intended application of the material as the high affinity it had shown for itself led to phase separation when blend films were attempted. This was initially observed in the very opaque films produced using **Het2** and was found to cascade into the comparable low blend film photoluminescence quantum yield and poor device performance which was exacerbated by difficulties in reproducibility.

While **Het2** appeared to have limited value in terms of application, it provided great insight into the effect of structural properties on the performance of dendrimers. The crystal structure of **Het2** showed no evidence of any particularly strong intermolecular interactions that would result in its insolubility and the highly ordered crystals appear to be a culmination of many weaker intermolecular interactions. The dendrons of **Het2** project outward from the iridium(III) complex in a perfectly linear fashion leading to a herringbone-like packing which greatly reduces the effectiveness of the dendrons in inhibiting interchromophore interactions and imbuing solubility. From this it was concluded that functionalization with dendrons should not be through such highly symmetrical positions. Additionally, the packing could likely be inhibited if the dendrons were of a higher generation or, if a symmetrical position is to be functionalized, the use of bulkier dendrons should minimise the risk of aggregation.

While still preliminary, the results of organic light-emitting diode utilizing a solution processed emissive layer containing **Hom2** appear very promising with a maximum external quantum efficiency of  $11.0 \pm 0.4 \%$  at  $8.4 \pm 5.5 \text{ cd/m}^2$  with the ability to reach a brightness of  $6000 \text{ cd/m}^2$ . The devices still require extensive optimization and it is expected that these values, as well as the mediocre results from devices using **Hom1** and **Het1**, will improve significantly when certain fabrication difficulties are resolved.

The preliminary organic light-emitting diodes containing a solution processed emissive layers utilizing the dendrimers all exhibited saturated red-emission. The homoleptic dendrimers, **Hom1** and **Hom2**, were observed to produce electroluminescence with CIE 1931 coordinates of (0.66, 0.33) and (0.66, 0.34), respectively; making them ideal for applications utilizing the sRGB gamut with a pure red defined as (0.64, 0.33). The electroluminescence of the heteroleptic complexes, **Het1** and **Het2**, are further red-shifted with CIE 1931 coordinates of (0.69, 0.30) and (0.68, 0.30), respectively; which is very close to the pure red as defined by the Rec.2020 gamut or (0.71, 0.29). The high photoluminescence observed for these dendrimers is especially exciting when their emission is considered with reported photoluminescence quantum yields of materials with

comparable emission colour are typically very low due to non-radiative decay governed by the energy gap rule.

In addition to the dendrimer series, a poly(dendrimer) containing a red-emissive iridium(III) complex was designed and synthesized. With a very good photoluminescence quantum yield of in solution  $72 \pm 7 \%$  and a decent neat film value of  $35 \pm 4 \%$ ; the red-emitting poly(dendrimer), **PDcR**, was found to behave in a similar fashion to the previously reported and structurally similar green-emitting poly(dendrimer) **L2** (solution  $\Phi_{\text{PL}} = 72 \%$ , neat film  $\Phi_{\text{PL}} = 30 \%$ ) which suggests that the emissive chromophores are behaving similarly when incorporated into a poly(dendrimer) architecture. As was the case for the majority of the red-emissive dendrimers and the reported green-emitting dendrimer and poly(dendrimer); the photoluminescence quantum yield of **PDcR** was found to differ insignificantly between solution and as a blended dopant in film. When incorporated into OLEDs as the emissive dopant, maximum external quantum efficiencies of  $10.0 \pm 0.2 \%$  at a luminance of  $5.2 \pm 2.6 \text{ cd/m}^2$  were observed. While nearly as efficient as devices utilizing **Hom2**, the OLEDs with **PDcR** were only able to achieve luminances up to approximately  $3500 \text{ cd/m}^2$ . The poly(dendrimer) produced electroluminescence with CIE 1931 coordinates identical to the best dendrimer, **Hom2**, of (0.66, 0.34); making it an ideal saturated red dopant for sRGB gamut systems.

Ultimately, the dendronized materials containing red-emissive iridium(III) complexes designed and synthesized in this project proved to exhibit exceptional properties for solution processed devices. It is known that the devices fabricated thus far contain multiple flaws for which solutions are being investigated. From the perspective of future investigation of these materials, the first step will be to fabricate new devices once the problems involving fabrication have been resolved. While the photophysical properties of these materials are exciting, a complete conclusion on the materials cannot be made until the device fabrication has been corrected.

All organic light emitting diodes described within this document utilize a single dopant and emit with a single colour. The red-emitting dendrimeric materials synthesized herein are also being considered for use as co-dopants to produce single emissive layer OLEDs with white emission. By blending a small amount of the red-emitting dendrimers or poly(dendrimer) with a blue emitting material it is possible to achieve white light emission. At present the progress of these experiments are being hindered by the same fabrication difficulties that plagued the single colour OLEDs, however, it is still promising for future investigations.

One insight gained by the project was that the effectiveness of both dendrimers and poly(dendrimer)s is heavily impacted by their topology. For example, increasing the tether length in the green-emitting poly(dendrimer)s, **PD<sub>B</sub>** and **PD<sub>C</sub>**, decreased the effectiveness of the dendrons at inhibiting non-radiative decay through intra-chain, interchromophore interactions causing decreased photoluminescence quantum yields. At the same time **PD<sub>C</sub>** was shown to result in unusually high outcoupling efficiencies which are believed to result from alignment which is at least in part due to the shape of the polymer. For the red-emitting materials the dendrimer **Hom1** exhibited far better photoluminescence quantum yields in the neat film than the remaining dendrimers suggesting that when the dendrons are in reasonably close proximity to one another they are more effective at separating the emissive chromophores. This is supported by the isolated dendrons of **Het2** being ineffective at imbuing solubility or inhibiting interchromophore interactions. While some general observations were noted throughout this project, our understanding of the effects of moiety size and shape within these dendrimeric systems is far from complete.

In an attempt to expand our understanding of the poly(dendrimer) systems, two monomers were designed with branched tether units. It was hypothesized that these monomers would greatly alter the shape of the final poly(dendrimer) with an overall increase in rigidity which may result in less available non-radiative decay pathways through vibration/rotation. The hypothetical targets are shown in Figure 5.1 and remain interesting targets to develop our understanding.

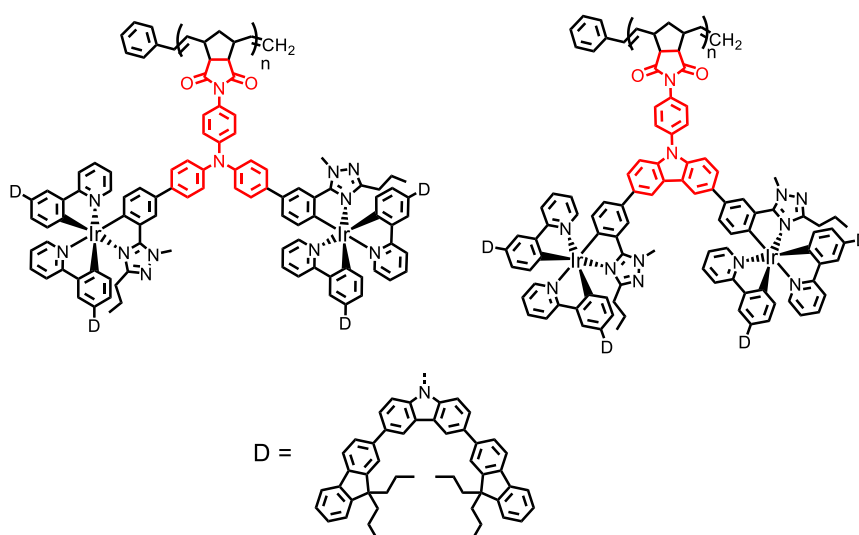
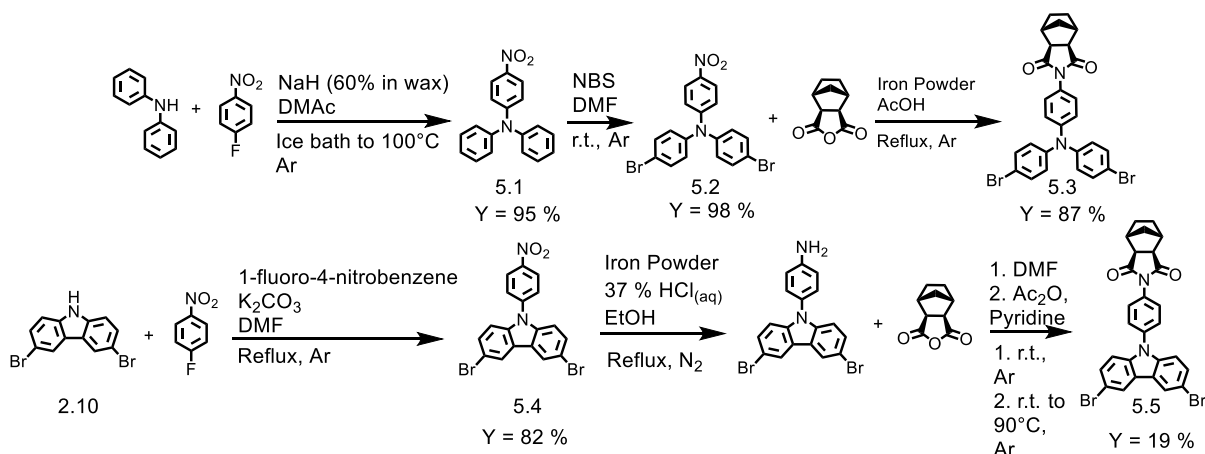


Figure 6.1: Structure of proposed poly(dendrimer)s with branched tether moieties. The branched tethers are shown in red.

Some progress was made towards the poly(dendrimer)s shown in Figure 6.1. The completed synthetic steps are shown in Scheme 6.1 and the details can be found in the experimental chapter 5. In addition to the proposed structures of Figure 6.1, the intermediates shown in Scheme 6.1 could be functionalized for many purposes such as OLED hosts, organic photovoltaics or organic explosive sensors. Progress towards these targets was postponed indefinitely as a result of the exciting results generated by the red-emitting dendrimer series which was given priority.



Scheme 6.1: Synthetic progress towards proposed poly(dendrimer)s with branched tether moieties.

While Figure 6.1 displays two examples of how the shape of dendrimeric materials can influence their properties, there are many other relatively simple routes that could be investigated. Considering how successful the red-emitting dendrimers and poly(dendrimer)s presented here appear to be, the most obvious extension would be substituting the carbazolyl-dendrons with another type or a higher generation. Ultimately, there are many available pathways through which dendrimers and poly(dendrimer)s could be expanded upon in the future as a synthetic approach for developing highly efficient, solution processable organic light-emitting diodes.

## References

---

- 1 M. Luckiesh, *Artificial Light Its Influence upon Civilization*, 2006.
- 2 S. Hofmann, M. Thomschke, B. Lüssem and K. Leo, *Opt. Express*, 2011, **19**, A1250–A1264.
- 3 Y. Iwao, H. Nobukazu, N. Makoto, I. Ayaka, M. Yoshihiro, Y. Nobuhide, N. Kazumasa, K. Jiro, Y. Akira and U. Tetsuo, *SID Symp. Dig. Tech. Pap.*, 2012, **38**, 1753–1756.
- 4 I. E. Agency, *Light's Labour's Lost- Policies for Energy-Efficient Lighting*, IEA, 2006.
- 5 *World Energy Outlook 2016*, Organisation for Economic Co-operation and Development.
- 6 N. Thejokalyani and S. J. Dhoble, *Renew. Sustain. Energy Rev.*, 2014, **32**, 448–467.
- 7 S. Reineke, F. Lindner, G. Schwartz, N. Seidler, K. Walzer, B. Lüssem and K. Leo, *Nature*, 2009, **459**, 234.
- 8 L. Zhou, H.-Y. Xiang, S. Shen, Y.-Q. Li, J.-D. Chen, H.-J. Xie, I. A. Goldthorpe, L.-S. Chen, S.-T. Lee and J.-X. Tang, *ACS Nano*, 2014, **8**, 12796–12805.
- 9 H. Mike, W. M. S. and B. J. J., *SID Symp. Dig. Tech. Pap.*, 2017, **48**, 187–190.
- 10 F. Zhao and D. Ma, *Mater. Chem. Front.*, 2017, **1**, 1933–1950.
- 11 D. B. Judd, *Color in business, science and industry.*, New York : Wiley, New York, 1952.
- 12 J. N. Tinsley, M. I. Molodtsov, R. Prevedel, D. Wartmann, J. Espigulé-Pons, M. Lauwers and A. Vaziri, 2016, **7**, 12172.
- 13 M. Wong, *AP via US Today*, 2006.
- 14 H.-W. Chen, J.-H. Lee, B.-Y. Lin, S. Chen and S.-T. Wu, *Light Sci. & Appl.*, 2018, **7**, 17168.
- 15 W. C. O'Mara, *Liquid Crystal Flat Panel Displays Manufacturing Science & Technology / by William C. O'Mara.*, Boston, MA : Springer US, Boston, MA, 1993.
- 16 D. Barnes, *Dig. Tech. Pap. - SID Int. Symp.*, 2013, **44**, 26–27.
- 17 D. Han, Y. Khan, J. Ting, S. M. King, N. Yaacobi- Gross, M. J. Humphries, C. J. Newsome and A. C. Arias, *Adv. Mater.*, **29**, 1606206.
- 18 J. H. Koo, S. Jeong, H. J. Shim, D. Son, J. Kim, D. C. Kim, S. Choi, J.-I. Hong and D.-H. Kim, *ACS Nano*, 2017, **11**, 10032–10041.
- 19 H. Soonkwang, J. Changhoon, S. Sangmoo, K. Jungchul, L. Jino, K. Dohyung, J.

- Seokhee, N. Hyunchul, L. Jaedo, Y. Wonjae, P. Seungchul, T. Yoonheung, R. Joungho, K. Changdong, A. Byungchul and Y. Sangdeog, *SID Symp. Dig. Tech. Pap.*, 2014, **45**, 334–337.
- 20 N. Li, S. Oida, G. S. Tulevski, S.-J. Han, J. B. Hannon, D. K. Sadana and T.-C. Chen, *Nat. Commun.*, 2013, **4**, 2294.
- 21 C. Jinkoo, L. Joohyeon, C. Junho, P. Chanyoung, H. Jaekook, C. Hokyoon and K. S. Soo, *SID Symp. Dig. Tech. Pap.*, 2012, **41**, 148–151.
- 22 B. Geffroy, P. le Roy and C. Prat, *Polym. Int.*, 2006, **55**, 572–582.
- 23 W. Kim, S. Kwon, S.-M. Lee, J. Y. Kim, Y. Han, E. Kim, K. C. Choi, S. Park and B.-C. Park, *Org. Electron.*, 2013, **14**, 3007–3013.
- 24 J.-L. Bredas, *Mater. Horizons*, 2014, **1**, 17–19.
- 25 W. Y. Liang, *Phys. Educ.*, 1970, **5**, 226.
- 26 C. Ulbricht, B. Beyer, C. Friebe, A. Winter and U. S. Schubert, *Adv. Mater.*, 2009, **21**, 4418–4441.
- 27 Y. Kawamura, K. Goushi, J. Brooks, J. J. Brown, H. Sasabe and C. Adachi, *Appl. Phys. Lett.*, 2005, **86**, 71104.
- 28 S. Kappaun, C. Slugovc and E. List, *Int. J. Mol. Sci.*, 2008, **9**, 1527–1547.
- 29 S. R. Forrest, *Nature*, 2004, **428**, 911–918.
- 30 A. R. Duggal, in *Conference on Lasers and Electro-Optics/Quantum Electronics and Laser Science Conference and Photonic Applications Systems Technologies*, Optical Society of America, San Jose, California , 2008, p. CMR1.
- 31 T. Tsujimura, in *OLED Displays*, John Wiley & Sons, Inc., 2012, pp. 1–4.
- 32 C. W. Tang and S. A. VanSlyke, *Appl. Phys. Lett.*, 1987, **51**, 913–915.
- 33 J. H. Burroughes, D. D. C. Bradley, A. R. Brown, R. N. Marks, K. Mackay, R. H. Friend, P. L. Burns and A. B. Holmes, *Nature*, 1990, **347**, 539.
- 34 S. S. Lee, T. J. Song and S. M. Cho, *Mater. Sci. Eng. B*, 2002, **95**, 24–28.
- 35 K. S. Yook and J. Y. Lee, *J. Ind. Eng. Chem.*, 2010, **16**, 181–184.
- 36 D. Lian, Z. Deqiang, W. Kongwu, H. Xiuqi, W. Liduo and Q. Yong, *Adv. Funct. Mater.*, 2011, **21**, 3540–3545.
- 37 M. Zhu, J. Zou, S. Hu, C. Li, C. Yang, H. Wu, J. Qin, Y. Cao, B. W. D’Andrade, S. R. Forrest, J. Kido, K. Hongawa, K. Okuyama, K. Nagai, B. W. D’Andrade, R. J. Holmes, S. R. Forrest, Y. Sun, N. C. Giebink, H. Kanno, B. Ma, M. E. Thompson, S. R. Forrest, G. Schwartz, M. Pfeiffer, S. Reineke, K. Walzer, K. Leo, S. Reineke, F. Lindner, G. Schwartz, N. Seidler, K. Walzer, B. Luessem, K. Leo, H. Sasabe, J. Takamatsu, T. Motoyama, S. Watanabe, G. Wagenblast, N. Langer, O. Molt, E.

Fuchs, C. Lennartz, J. Kido, Q. Wang, J. Ding, D. Ma, Y. Cheng, L. Wang, X. Jing, F. Wang, Q. Wang, J. Ding, D. Ma, Y. Cheng, L. Wang, F. Wang, K. Zhang, Z. Chen, C. Yang, Y. Tao, Y. Zou, J. Qin, Y. Cao, X. Gong, W. Ma, J. C. Ostrowski, G. C. Bazan, D. Moses, A. J. Heeger, J. X. Jiang, Y. H. Xu, W. Yang, R. Guan, Z. Q. Liu, H. Y. Zhen, Y. Cao, H. Wu, F. Huang, Y. Mo, W. Yang, D. Wang, J. Peng, Y. Cao, H. Wu, G. Zhou, J. Zou, C.-L. Ho, W.-Y. Wong, W. Yang, J. Peng, Y. Cao, H. B. Wu, J. H. Zou, F. Liu, L. Wang, A. Mikhailovsky, G. C. Bazan, W. Yang, Y. Cao, H. Wu, L. Ying, W. Yang, Y. Cao, N. Rehmman, C. Ulbricht, A. Köhnen, P. Zacharias, M. C. Gather, D. Hertel, E. Holder, K. Meerholz, U. S. Schubert, P. Zacharias, M. Gather, M. Rojahn, O. Nuyken, K. Meerholz, S. Gong, Y. Chen, C. Yang, C. Zhong, J. Qin, D. Ma, F. Huang, P.-I. Shih, C.-F. Shu, Y. Chi, A. K. Y. Jen, J.-H. Jou, M.-F. Hsu, W.-B. Wang, C.-L. Chin, Y.-C. Chung, C.-T. Chen, J.-J. Shyue, S.-M. Shen, M.-H. Wu, W.-C. Chang, C.-P. Liu, S.-Z. Chen, H.-Y. Chen, J. Ding, J. Lü, Y. Cheng, Z. Xie, L. Wang, X. Jing, F. Wang, S.-C. Lo, P. L. Burn, B. Liang, L. Wang, Y. H. Xu, H. H. Shi, Y. Cao, J. Ding, J. Gao, Y. Cheng, Z. Xie, L. Wang, D. Ma, X. Jing, F. Wang, G. Zhou, W.-Y. Wong, B. Yao, Z. Xie, L. Wang, J. Ding, B. Wang, Z. Yue, B. Yao, Z. Xie, Y. Cheng, L. Wang, X. Jing, F. Wang, T. Qin, J. Ding, L. Wang, M. Baumgarten, G. Zhou, K. Müllen, S.-C. Lo, R. E. Harding, C. P. Shipley, S. G. Stevenson, P. L. Burn, I. D. W. Samuel, A. Li, Y. Li, W. Cai, G. Zhou, Z. Chen, H. Wu, W.-Y. Wong, W. Yang, J. Peng, Y. Cao, N. Miyaura, A. Suzuki, A. B. Tamayo, B. D. Alleyne, P. I. Djurovich, S. Lamansky, I. Tsyba, N. N. Ho, R. Bau, M. E. Thompson, F. Huang, Y.-H. Niu, Y. Zhang, J.-W. Ka, M. S. Liu, A. K. Y. Jen, Y. Zhang, F. Huang, Y. Chi, A. K. Y. Jen, Y. Xu, R. Yang, J. Peng, A. A. Mikhailovsky, Y. Cao, T.-Q. Nguyen, G. C. Bazan, A. J. Campbell, D. D. C. Bradley, H. Antoniadis, H. Wu, J. Zou, D. An, F. Liu, W. Yang, J. Peng, A. Mikhailovsky, G. C. Bazan, Y. Cao, Y. Tao, Q. Wang, C. Yang, C. Zhong, J. Qin and D. Ma, *J. Mater. Chem.*, 2012, **22**, 361–366.

38 K. E. Linton, A. L. Fisher, C. Pearson, M. A. Fox, L.-O. Palsson, M. R. Bryce and M. C. Petty, *J. Mater. Chem.*, 2012, **22**, 11816–11825.

39 S. A. Holgate, *Understanding Solid State Physics*, CRC Press, Boca Raton, 2009.

40 P. I. Djurovich, E. I. Mayo, S. R. Forrest and M. E. Thompson, *Org. Electron.*, 2009, **10**, 515–520.

41 B. W. D'Andrade, S. Datta, S. R. Forrest, P. Djurovich, E. Polikarpov and M. E. Thompson, *Org. Electron.*, 2005, **6**, 11–20.

42 P. Stallinga, *Adv. Mater.*, **23**, 3356–3362.



- 43 A. A. Bakulin, A. Rao, V. G. Pavelyev, P. H. M. van Loosdrecht, M. S. Pshenichnikov, D. Niedzialek, J. Cornil, D. Beljonne and R. H. Friend, *Science* (80-), 2012, **335**, 1340–1344.
- 44 H. S. Nalwa, *Electronic and Photonic Properties*, Standford Scientific Corporation, Los Angeles, 2001.
- 45 R. Noriega, J. Rivnay, K. Vandewal, F. P. V Koch, N. Stingelin, P. Smith, M. F. Toney and A. Salleo, *Nat. Mater.*, 2013, **12**, 1038.
- 46 A. J. Kronemeijer, E. Gili, M. Shahid, J. Rivnay, A. Salleo, M. Heeney and H. Sirringhaus, *Adv. Mater.*, **24**, 1558–1565.
- 47 K. Seki and K. Kanai, *Mol. Cryst. Liq. Cryst.*, 2006, **455**, 145–181.
- 48 S. Reineke, M. Thomschke, B. Lüssem and K. Leo, *Rev. Mod. Phys.*, 2013, **85**, 1245–1293.
- 49 S. R. Forrest, D. D. C. Bradley and M. E. Thompson, *Adv. Mater.*, **15**, 1043–1048.
- 50 S. Nowy, B. C. Krummacher, J. Frischeisen, N. A. Reinke and W. Brütting, *J. Appl. Phys.*, 2008, **104**, 123109.
- 51 S.-Y. Kim and J.-J. Kim, *Org. Electron.*, 2010, **11**, 1010–1015.
- 52 C. Adachi, M. A. Baldo, M. E. Thompson and S. R. Forrest, *J. Appl. Phys.*, 2001, **90**, 5048–5051.
- 53 H. P.A., W. S., W. J.A.E., S. I. and B. W.L., *Adv. Mater.*, 2002, **14**, 1393–1396.
- 54 H. Benisty, H. De Neve and C. Weisbuch, *IEEE J. Quantum Electron.*, 1998, **34**, 1632–1643.
- 55 H. Raether, in *Surface plasmons on smooth and rough surfaces and on gratings*, Springer, 1988, pp. 4–39.
- 56 M. J. Jurow, C. Mayr, T. D. Schmidt, T. Lampe, P. I. Djurovich, W. Brütting and M. E. Thompson, *Nat. Mater.*, 2015, **15**, 85.
- 57 A. Graf, P. Liehm, C. Murawski, S. Hofmann, K. Leo and M. C. Gather, *J. Mater. Chem. C*, 2014, **2**, 10298–10304.
- 58 C.-Y. Lu, M. Jiao, W.-K. Lee, C.-Y. Chen, W.-L. Tsai, C.-Y. Lin and C.-C. Wu, *Adv. Funct. Mater.*, 2016, **26**, n/a-n/a.
- 59 T.-W. Koh, J. A. Spechler, K. M. Lee, C. B. Arnold and B. P. Rand, *ACS Photonics*, 2015, **2**, 1366–1372.
- 60 G. H. Lee, M. G. Han, D.-S. Leem, S.-J. Lim, S. Yun, K.-H. Lee, X. Bulliard, K.-B. Park, T. Yagi, Y. S. Choi, Y. W. Jin and S. Lee, *J. Phys. Chem. C*, 2016, **120**, 10176–10184.
- 61 J. R. Lakowicz, Ed., *Principles of Fluorescence Spectroscopy*, Springer US, Boston,

MA, 2006.

- 62 J. M. Younker and K. D. Dobbs, *J. Phys. Chem. C*, 2013, **117**, 25714–25723.
- 63 K. Goushi, K. Yoshida, K. Sato and C. Adachi, *Nat. Photonics*, 2012, **6**, 253.
- 64 X. Yang, G. Zhou and W.-Y. Wong, *Chem. Soc. Rev.*, 2015, **44**, 8484–8575.
- 65 H. Yersin, A. F. Rausch, R. Czerwieniec, T. Hofbeck and T. Fischer, *Coord. Chem. Rev.*, 2011, **255**, 2622–2652.
- 66 Y. You and S. Y. Park, *Dalt. Trans.*, 2009, 1267–1282.
- 67 A. F. Rausch, H. H. H. Homeier and H. Yersin, in *Photophysics of Organometallics*, ed. A. J. Lees, Springer Berlin Heidelberg, Berlin, Heidelberg, 2010, pp. 193–235.
- 68 M. K. Etherington, J. Gibson, H. F. Higginbotham, T. J. Penfold and A. P. Monkman, *Nat. Commun.*, 2016, **7**, 13680.
- 69 P. L. dos Santos, J. S. Ward, M. R. Bryce and A. P. Monkman, *J. Phys. Chem. Lett.*, 2016, **7**, 3341–3346.
- 70 T. Ogiwara, Y. Wakikawa and T. Ikoma, *J. Phys. Chem. A*, 2015, **119**, 3415–3418.
- 71 P. Qiming, O. Ablikim, Z. Ming and L. Feng, *Angew. Chemie Int. Ed.*, 2015, **54**, 7091–7095.
- 72 R. Tao, J. Qiao, G. Zhang, L. Duan, L. Wang and Y. Qiu, *J. Phys. Chem. C*, 2012, **116**, 11658–11664.
- 73 R. J. Holmes, S. R. Forrest, T. Sajoto, A. Tamayo, P. I. Djurovich, M. E. Thompson, J. Brooks, Y. J. Tung, B. W. D'Andrade, M. S. Weaver, R. C. Kwong and J. J. Brown, *Appl. Phys. Lett.*, 2005, **87**, 243503–243507.
- 74 G. Kim, J. Yun, S. Song, S. Park, C. D. Sunesh, H. Kim, H. Chae, J. Lee and Y. Choe, *Surf. Interface Anal.*, 44, 1479–1482.
- 75 A. Buckley, *Organic Light-Emitting Diodes (OLEDs): Materials, Devices and Applications*, Elsevier B.V., 2013.
- 76 D. C. H. M. D. Bertolucci, *Symmetry and Spectroscopy*, Oxford University Press, Oxford, 1978.
- 77 T. Sajoto, P. I. Djurovich, A. Tamayo, M. Yousufuddin, R. Bau, M. E. Thompson, R. J. Holmes and S. R. Forrest, *Inorg. Chem.*, 2005, **44**, 7992–8003.
- 78 L. Flamigni, A. Barbieri, C. Sabatini, B. Ventura and F. Barigelletti, in *Photochemistry and Photophysics of Coordination Compounds II*, eds. V. Balzani and S. Campagna, Springer Berlin Heidelberg, Berlin, Heidelberg, 2007, p. 148.
- 79 C.-Y. Kuei, W.-L. Tsai, B. Tong, M. Jiao, W.-K. Lee, Y. Chi, C.-C. Wu, S.-H. Liu, G.-H. Lee and P.-T. Chou, *Adv. Mater.*, 2016, n/a-n/a.
- 80 D. Chen, K. Li, X. Guan, G. Cheng, C. Yang and C.-M. Che, *Organometallics*, 2017,

**36**, 1331–1344.

- 81 I. M. Dixon, J.-P. Collin, J.-P. Sauvage, L. Flamigni, S. Encinas and F. Barigelletti, *Chem. Soc. Rev.*, 2000, **29**, 385–391.
- 82 Y. You and S. Y. Park, *J. Am. Chem. Soc.*, 2005, **127**, 12438–12439.
- 83 S. Kesarkar, W. Mróz, M. Penconi, M. Pasini, S. Destri, M. Cazzaniga, D. Ceresoli, P. R. Mussini, C. Baldoli, U. Giovanella and A. Bossi, *Angew. Chemie Int. Ed.*, 2016, **55**, 2714–2718.
- 84 M. Kasha, *Discuss. Faraday Soc.*, 1950, **9**, 14–19.
- 85 S. Ikawa, S. Yagi, T. Maeda, H. Nakazumi, H. Fujiwara and Y. Sakurai, *Dye. Pigment.*, 2012, **95**, 695–705.
- 86 X. Ren, D. J. Giesen, M. Rajeswaran and M. Madaras, *Organometallics*, 2009, **28**, 6079–6089.
- 87 P. L. Burn, S. -C. Lo and I. D. W. Samuel, *Adv. Mater.*, **19**, 1675–1688.
- 88 J. C. Ribierre, A. Ruseckas, K. Knights, S. V Staton, N. Cumpstey, P. L. Burn and I. D. W. Samuel, *Phys. Rev. Lett.*, 2008, **100**, 17402.
- 89 S. Reineke, K. Walzer and K. Leo, *Phys. Rev. B*, 2007, **75**, 125328.
- 90 F. Xu, H. U. Kim, J.-H. Kim, B. J. Jung, A. C. Grimsdale and D.-H. Hwang, *Prog. Polym. Sci.*
- 91 W. E. Howard, *Sci. Am.*, 2004, 76–81.
- 92 E. Holder, B. M. W. Langeveld and U. S. Schubert, *Adv. Mater.*, **17**, 1109–1121.
- 93 F. Xu, H. U. Kim, J.-H. Kim, B. J. Jung, A. C. Grimsdale and D.-H. Hwang, *Prog. Polym. Sci.*, 2015, **47**, 92–121.
- 94 K. S. Yook and J. Y. Lee, *Adv. Mater.*, **26**, 4218–4233.
- 95 B. M. T., I. M., O. J. and W. W., *Adv. Mater.*, 2000, **12**, 1737–1750.
- 96 C. Sekine, Y. Tsubata, T. Yamada, M. Kitano and S. Doi, *Sci. Technol. Adv. Mater.*, 2014, **15**, 34203.
- 97 J. W. Levell, W.-Y. Lai, R. J. Borthwick, P. L. Burn, S.-C. Lo and I. D. W. Samuel, *New J. Chem.*, 2012, **36**, 407–413.
- 98 Z. Hongyu, J. Changyun, Y. Wei, J. Jiaying, H. Fei and C. Yong, *Chem. – A Eur. J.*, 2005, **11**, 5007–5016.
- 99 S.-J. Liu, Q. Zhao, Y. Deng, Y.-J. Xia, J. Lin, Q.-L. Fan, L.-H. Wang and W. Huang, *J. Phys. Chem. C*, 2007, **111**, 1166–1175.
- 100 X. Chen, J.-L. Liao, Y. Liang, M. O. Ahmed, H.-E. Tseng and S.-A. Chen, *J. Am. Chem. Soc.*, 2003, **125**, 636–637.
- 101 G. L. Schulz, X. Chen, S.-A. Chen and S. Holdcroft, *Macromolecules*, 2006, **39**,

9157–9165.

- 102 Y. Tao, C. Yang and J. Qin, *Chem. Soc. Rev.*, 2011, **40**, 2943–2970.
- 103 T.-F. Guo, S.-C. Chang, Y. Yang, R. C. Kwong and M. E. Thompson, *Org. Electron.*, 2000, **1**, 15–20.
- 104 N. R. Evans, L. Sudha Devi, C. S. K. Mak, S. E. Watkins, S. I. Pascu, A. Köhler, R. H. Friend, C. K. Williams and A. B. Holmes, *J. Am. Chem. Soc.*, 2006, **128**, 6647–6656.
- 105 M. Sudhakar, P. I. Djurovich, T. E. Hogen-Esch and M. E. Thompson, *J. Am. Chem. Soc.*, 2003, **125**, 7796–7797.
- 106 S. Gong, C. Yang and J. Qin, *Chem. Soc. Rev.*, 2012, **41**, 4797–4807.
- 107 K. Zhang, Z. Chen, Y. Zou, S. Gong, C. Yang, J. Qin and Y. Cao, *Chem. Mater.*, 2009, **21**, 3306–3314.
- 108 W.-Y. Lai, M. N. Balfour, J. W. Levell, A. K. Bansal, P. L. Burn, S.-C. Lo and I. D. W. Samuel, *Macromolecules. (Washington, DC, U. S.)*, 2012, **45**, 2963–2971.
- 109 S. Tokito, M. Suzuki, F. Sato, M. Kamachi and K. Shirane, *Org. Electron.*, 2003, **4**, 105–111.
- 110 H. Yersin, 2008, 329.
- 111 K. A. Knights, S. G. Stevenson, C. P. Shipley, S.-C. Lo, S. Olsen, R. E. Harding, S. Gambino, P. L. Burn and I. D. W. Samuel, *J. Mater. Chem.*, 2008, **18**, 2121–2130.
- 112 S. C. Lo, E. B. Namdas, P. L. Burn and I. D. W. Samuel, *Macromolecules*, 2003, **36**, 9721–9730.
- 113 W.-Y. Lai, J. W. Levell, M. N. Balfour, P. L. Burn, S.-C. Lo and I. D. W. Samuel, *Polym. Chem.*, 2012, **3**, 734–740.
- 114 X. Zhifu and M. J.S., *Acta Polym.*, 2003, **45**, 83–87.
- 115 B. P. L., L. S.-C. and S. I. D. W., *Adv. Mater.*, 2007, **19**, 1675–1688.
- 116 T. Qin, J. Ding, L. Wang, M. Baumgarten, G. Zhou and K. Müllen, *J. Am. Chem. Soc.*, 2009, **131**, 14329–14336.
- 117 G. Zhou, W. Wong and X. Yang, *Chem. – An Asian J.*, **6**, 1706–1727.
- 118 J. M. Lupton, I. D. W. Samuel, R. Beavington, M. J. Frampton, P. L. Burn and H. Bässler, *Phys. Rev. B*, 2001, **63**, 155206.
- 119 S. Gambino, S. G. Stevenson, K. A. Knights, P. L. Burn and I. D. W. Samuel, *Adv. Funct. Mater.*, 2009, **19**, 317–323.
- 120 S. Gambino, S. Lo, Z. Liu, P. L. Burn and I. D. W. Samuel, *Adv. Funct. Mater.*, **22**, 157–165.
- 121 W. Tian, Q. Qi, B. Song, C. Yi, W. Jiang, X. Cui, W. Shen, B. Huang and Y. Sun, *J.*

- Mater. Chem. C*, 2014.
- 122 J. Li and D. Liu, *J. Mater. Chem.*, 2009, **19**, 7584–7591.
- 123 L. B., W. L., X. Y. H., S. H. H. and C. Y., *Adv. Funct. Mater.*, 2007, **17**, 3580–3589.
- 124 J. Ding, J. Gao, Y. Cheng, Z. Xie, L. Wang, D. Ma, X. Jing and F. Wang, *Adv. Funct. Mater.*, 2006, **16**, 575–581.
- 125 M. Zhu, Y. Li, S. Hu, C. Li, C. Yang, H. Wu, J. Qin and Y. Cao, *Chem. Commun.*, 2012, **48**, 2695–2697.
- 126 S. Madhusudan, H. H. M., D. Parul and J. G. E., *Adv. Mater.*, 2009, **22**, 673–685.
- 127 J. P. Gunning, J. W. Levell, M. F. Wyatt, P. L. Burn, J. Robertson and I. D. W. Samuel, *Polym. Chem.*, 2010, **1**, 730–738.
- 128 A. D. Schlüter and J. P. Rabe, *Angew. Chem. Int. Ed.*, 2000, **39**, 864–883.
- 129 S. Salah-Eddine, F. Holger and H. Rainer, *Angew. Chem. Int. Ed.*, 2002, **41**, 1329–1334.
- 130 W. Wu, L. Huang, Y. Fu, C. Ye, J. Qin and Z. Li, *Chinese Sci. Bull.*, 2013, **58**, 2753–2761.
- 131 A. Chakrabarti, A. Juilfs, R. Filler and B. K. Mandal, *Solid State Ionics*, 2010, **181**, 982–986.
- 132 M. A. Quadir and R. Haag, *J. Control. Release*, 2012, **161**, 484–495.
- 133 H. Jin, Y. Xu, Z. Shen, D. Zou, D. Wang, W. Zhang, X. Fan and Q. Zhou, *Macromolecules*, 2010, **43**, 8468–8478.
- 134 X. Xiong and Y. Chen, *Eur. Polym. J.*, 2012, **48**, 569–579.
- 135 S. M. Grayson and J. M. J. Fréchet, *Macromolecules*, 2001, **34**, 6542–6544.
- 136 A. J. Boydston, T. W. Holcombe, D. A. Unruh, J. M. J. Fréchet and R. H. Grubbs, *J. Am. Chem. Soc.*, 2009, **131**, 5388–5389.
- 137 K. O. Kim and T.-L. Choi, *ACS Macro Lett.*, 2012, **1**, 445–448.
- 138 K. O. Kim and T.-L. Choi, *Macromolecules*, 2013, **46**, 5905–5914.
- 139 B. Helms, J. L. Mynar, C. J. Hawker and J. M. J. Fréchet, *J. Am. Chem. Soc.*, 2004, **126**, 15020–15021.
- 140 W.-Y. Lai, J. W. Levell, A. C. Jackson, S.-C. Lo, P. V Bernhardt, I. D. W. Samuel and P. L. Burn, *Macromolecules. (Washington, DC, U. S.)*, 2010, **43**, 6986–6994.
- 141 J. W. Levell, S. Zhang, W. Y. Lai, S. C. Lo, P. L. Burn and I. D. W. Samuel, *Opt. Express*, 2012, **20**, A213–A218.
- 142 R. D. Jansen-van Vuuren, *Unpubl. Work*, 2017.
- 143 W.-Y. Lai, M. N. Balfour, J. W. Levell, A. K. Bansal, P. L. Burn, S.-C. Lo and I. D. W. Samuel, *Macromolecules*, 2012, **45**, 2963–2971.

- 144 T. Lampe, T. D. Schmidt, M. J. Jurow, P. I. Djurovich, M. E. Thompson and W. Brütting, *Chem. Mater.*, 2016, **28**, 712–715.
- 145 K.-H. Kim, S. Lee, C.-K. Moon, S.-Y. Kim, Y.-S. Park, J.-H. Lee, J. Woo Lee, J. Huh, Y. You and J.-J. Kim, *Nat Commun*, 2014, **5**.
- 146 M. Flämmich, M. C. Gather, N. Danz, D. Michaelis, A. H. Bräuer, K. Meerholz and A. Tünnermann, *Org. Electron.*, 2010, **11**, 1039–1046.
- 147 J.-S. Kim, P. K. H. Ho, N. C. Greenham and R. H. Friend, *J. Appl. Phys.*, 2000, **88**, 1073–1081.
- 148 G. M. C. and B. D. D. C., *Adv. Funct. Mater.*, 2007, **17**, 479–485.
- 149 Y. H. Lee, A. Fuyuhiko, J. M. Harrowfield, Y. Kim, A. N. Sobolev and S. Hayami, *Eur. J. Inorg. Chem.*, 2013, **2013**, 5862–5870.
- 150 P. S. van Heerden, B. C. B. Bezuidenhoudt and D. Ferreira, *J. Chem. Soc. Perkin Trans. 1*, 1997, 1141–1146.
- 151 H. C. Cheng, P. P. Y. Chen and Y. O. Su, *Dalt. Trans.*, 2014, **43**, 1424–1433.
- 152 Z. Huang, B. Wang, Q. Zhang, S. Xiang, X. Lv, L. Ma, B. Yang, Y. Gao and L. Wang, *Dye. Pigment.*, 2017, **140**, 328–336.
- 153 F. Gallou, R. Haenggi, H. Hirt, W. Marterer, F. Schaefer and M. Seeger-Weibel, *Tetrahedron Lett.*, 2008, **49**, 5024–5027.
- 154 C. J. F. Du, H. Hart and K. K. D. Ng, *J. Org. Chem.*, 1986, **51**, 3162–3165.
- 155 T.-H. Kwon, H. S. Cho, M. K. Kim, J.-W. Kim, J.-J. Kim, K. H. Lee, S. J. Park, I.-S. Shin, H. Kim, D. M. Shin, Y. K. Chung and J.-I. Hong, *Organometallics*, 2005, **24**, 1578–1585.
- 156 C.-H. Fan, P. Sun, T.-H. Su and C.-H. Cheng, *Adv. Mater.*, 2011, **23**, 2981–2985.
- 157 T. Giridhar, T.-H. Han, W. Cho, C. Saravanan, T.-W. Lee and S.-H. Jin, *Chem. – A Eur. J.*, 2014, **20**, 8260–8264.
- 158 S. V Ryabukhin, D. M. Volochnyuk, A. S. Plaskon, V. S. Naumchik and A. A. Tolmachev, *Synthesis (Stuttg.)*, 2007, **2007**, 1214–1224.
- 159 C.-S. Jia, Z. Zhang, S.-J. Tu and G.-W. Wang, *Org. Biomol. Chem.*, 2006, **4**, 104–110.
- 160 K.-H. Kim, C.-K. Moon, J.-H. Lee, S.-Y. Kim and J.-J. Kim, *Adv. Mater.*, 2014, n/a–n/a.
- 161 E. Baranoff, H. J. Bolink, F. De Angelis, S. Fantacci, D. Di Censo, K. Djellab, M. Grätzel and M. K. Nazeeruddin, *Dalt. Trans.*, 2010, **39**, 8914.
- 162 E. Baranoff, S. Suárez, P. Bugnon, C. Barolo, R. Buscaino, R. Scopelliti, L. Zuppiroli, M. Graetzel and M. K. Nazeeruddin, *Inorg. Chem.*, 2008, **47**, 6575–6577.

- 163 J. Us, M. Fernandez-Hern, C.-H. Yang, J. I. Beltr, V. Lemaur, F. Polo, R. Fr€e, J. Er^  
Ome Cornil, L. De Cola, J. M. Fernandez-Hernandez, C.-H. Yang, J. I. Beltran, V.  
Lemaur, F. Polo, R. Frohlich, J. Cornil and L. De Cola, 2011, **133**, 10543–10558.
- 164 G. Longhi, E. Castiglioni, J. Koshoubu, G. Mazzeo and S. Abbate, *Chirality*, 2016,  
**28**, 696–707.
- 165 F. J. Coughlin, M. S. Westrol, K. D. Oyler, N. Byrne, C. Kraml, E. Zysman-Colman,  
M. S. Lowry and S. Bernhard, *Inorg. Chem.*, 2008, **47**, 2039–2048.
- 166 T. Yasuda, T. Shimizu, F. Liu, G. Ungar and T. Kato, *J. Am. Chem. Soc.*, 2011, **133**,  
13437–13444.
- 167 N. Matsuo, *Bull. Chem. Soc. Jpn.*, 1974, **47**, 767–768.
- 168 F. O. Garces, K. A. King and R. J. Watts, *Inorg. Chem.*, 1988, **27**, 3464–3471.
- 169 † Sergey Lamansky, † Peter Djurovich, † Drew Murphy, † Feras Abdel-Razzaq, †  
Hae-Eun Lee, ‡ Chihaya Adachi, ‡,§ Paul E. Burrows, \*,‡ and Stephen R. Forrest  
and † Mark E. Thompson\*, 2001.
- 170 M. Graf, M. Thesen, H. Kruger, P. Mayer and K. Sunkel, *Inorg. Chem. Commun.*,  
2009, **12**, 701–703.
- 171 E. Baranoff, B. F. E. Curchod, J. Frey, R. Scopelliti, F. Kessler, I. Tavernelli, U.  
Rothlisberger, M. Gratzel and M. K. Nazeeruddin, *Inorg. Chem.*, 2012, **51**, 215–224.
- 172 Y. Tamura, Y. Hisamatsu, S. Kumar, T. Itoh, K. Sato, R. Kuroda and S. Aoki, *Inorg.*  
*Chem.*, 2017, **56**, 812–833.
- 173 A. B. Tamayo, B. D. Alleyne, P. I. Djurovich, S. Lamansky, I. Tsyba, N. N. Ho, R.  
Bau and M. E. Thompson, *J. Am. Chem. Soc.*, 2003, **125**, 7377–7387.
- 174 M. J. A., C. A. J., S. P. E., N. Andrew, D. T. A., B. P. L. and G. I. R., *Adv. Mater.*  
*Interfaces*, 2016, **3**, 1600184.
- 175 P. Spellane, R. J. Watts and A. Vogler, *Inorg. Chem.*, 1993, **32**, 5633–5636.
- 176 M. Schulze, A. Steffen and F. Wurthner, *Angew. Chemie Int. Ed.*, 2015, **54**, 1570–  
1573.
- 177 R. Tao, J. Qiao, G. Zhang, L. Duan, C. Chen, L. Wang and Y. Qiu, *J. Mater. Chem.*  
*C*, 2013, **1**, 6446–6454.
- 178 R. E. Harding, S.-C. Lo, P. L. Burn and I. D. W. Samuel, *Org. Electron.*, 2008, **9**,  
377–384.
- 179 C.-H. Yang, M. Mauro, F. Polo, S. Watanabe, I. Muenster, R. Frohlich and L. De  
Cola, *Chem. Mater.*, 2012, **24**, 3684–3695.
- 180 S. Takayasu, T. Suzuki and K. Shinozaki, *J. Phys. Chem. B*, 2013, **117**, 9449–9456.
- 181 G. Zhou, W.-Y. Wong, B. Yao, Z. Xie and L. Wang, *Angew. Chemie Int. Ed.*, 2007,

- 46**, 1149–1151.
- 182 Y.-L. Tung, P.-C. Wu, C.-S. Liu, Y. Chi, J.-K. Yu, Y.-H. Hu, P.-T. Chou, S.-M. Peng, G.-H. Lee, Y. Tao, A. J. Carty, C.-F. Shu and F.-I. Wu, *Organometallics*, 2004, **23**, 3745–3748.
- 183 A. Tsuboyama, H. Iwawaki, M. Furugori, T. Mukaide, J. Kamatani, S. Igawa, T. Moriyama, S. Miura, T. Takiguchi, S. Okada, M. Hoshino and K. Ueno, *J. Am. Chem. Soc.*, 2003, **125**, 12971–12979.
- 184 M. Sugawara, D. Seo-Young Choi and D. Wood, *Signal Process. Mag. IEEE*, 2014, **31**, 170–174.
- 185 F.-M. Hwang, H.-Y. Chen, P.-S. Chen, C.-S. Liu, Y. Chi, C.-F. Shu, F.-I. Wu, P.-T. Chou, S.-M. Peng and G.-H. Lee, *Inorg. Chem.*, 2005, **44**, 1344–1353.
- 186 L. Zhao, S. Wang, J. Lu, J. Ding and L. Wang, *J. Mater. Chem. C*, 2017, **5**, 9753–9760.
- 187 W. L. F. Armarego and C. L. L. Chai, Butterworth-Heinemann, Oxford, 2009, pp. 1–60.
- 188 N. C. Greenham, I. D. W. Samuel, G. R. Hayes, R. T. Phillips, Y. A. R. R. Kessener, S. C. Moratti, A. B. Holmes and R. H. Friend, *Chem. Phys. Lett.*, 1995, **241**, 89–96.
- 189 S.-O. Kim, Q. Zhao, K. Thangaraju, J. J. Kim, Y.-H. Kim and S.-K. Kwon, *Dye. Pigment.*, 2011, **90**, 139–145.
- 190 Y. You, C.-G. An, D.-S. Lee, J.-J. Kim and S. Y. Park, *J. Mater. Chem.*, 2006, **16**, 4706–4713.
- 191 S.-C. Lo, R. N. Bera, R. E. Harding, P. L. Burn and I. D. W. Samuel, *Adv. Funct. Mater.*, 2008, **18**, 3080–3090.
- 192 A. Kamal, M. Kashi Reddy, T. B. Shaik, Rajender, Y. V. V Srikanth, V. Santhosh Reddy, G. Bharath Kumar and S. V Kalivendi, *Eur. J. Med. Chem.*, 2012, **50**, 9–17.
- 193 H. Bonin, D. Delbrayelle, P. Demonchaux and E. Gras, *Chem. Commun.*, 2010, **46**, 2677–2679.
- 194 F. Leroux, T. U. Hutschenreuter, C. Charrière, R. Scopelliti and R. W. Hartmann, *Helv. Chim. Acta*, 2003, **86**, 2671–2686.
- 195 R. D. Jansen-van Vuuren, 2011.
- 196 Z. Du, W. Chen, M. Qiu, Y. S. Chen, N. Wang, T. Wang, M. Sun, D. Yu, R. Yang, C. X. Li, B. Kan, M. M. Li and Y. S. Chen, *Phys. Chem. Chem. Phys.*, 2015, **17**, 17391–17398.
- 197 M. V. Peters, R. S. Stoll, A. Kühn and S. Hecht, *Angew. Chemie Int. Ed.*, 2008, **47**, 5968–5972.



- 198 S-C. Lo, E. B. Namdas, P. L. Burn, and I. D. W. Samuel, *Macromolecules*, 2003, **36** (26), 9721–9730.
- 199 Isis Innovation Limited, UK; The University Court of the University of St Andrews ., 2004, 32 pp.
- 200 S. S. Y. Chen, 2012.
- 201 S.-C. Lee, G. A. Williams and G. D. Brown, *Phytochemistry*, 1999, **52**, 537–540.
- 202 K. A. Knights, S. G. Stevenson, C. P. Shipley, S.-C. Lo, S. Olsen, R. E. Harding, S. Gambino, P. L. Burn and I. D. W. Samuel, *J. Mater. Chem.*, 2008, **18**, 2121.
- 203 C. M. Counciller, C. C. Eichman, B. C. Wray and J. P. Stambuli, *Org. Lett.*, 2008, **10**, 1021–1023.
- 204 C. A. Fleckenstein and H. Plenio, *J. Org. Chem.*, 2008, **73**, 3236–3244.
- 205 W.-Y. Lee, T. Kurosawa, S.-T. Lin, T. Higashihara, M. Ueda and W.-C. Chen, *Chem. Mater.*, 2011, **23**, 4487–4497.
- 206 C. V. Reddy, J. V Kingston and J. G. Verkade, *J. Org. Chem.*, 2008, **73**, 3047–3062.
- 207 S.-T. Huang, D.-J. Liaw, L.-G. Hsieh, C.-C. Chang, M.-K. Leung, K.-L. Wang, W.-T. Chen, K.-R. Lee, J.-Y. Lai, L.-H. Chan and C.-T. Chen, *J. Polym. Sci. Part A Polym. Chem.*, 2009, **47**, 6231–6245.
- 208 E. Ishow, A. Brosseau, G. Clavier, K. Nakatani, R. B. Pansu, J.-J. Vachon, P. Tauc, D. Chauvat, C. R. Mendonça and E. Piovesan, *J. Am. Chem. Soc.*, 2007, **129**, 8970–8971.
- 209 A. Kulasi, H. Yi and A. Iraqi, *J. Polym. Sci. Part A Polym. Chem.*, 2007, **45**, 5957–5967.